UNIVERSITY OF AMSTERDAM

UvA-DARE (Digital Academic Repository)

Radiological imaging characteristics of thrombus and infarct core in acute ischemic stroke and their association with clinical outcome

Tolhuisen, M.L.

[Link to publication](#)

Citation for published version (APA):
Tolhuisen, M. L. (2022). *Radiological imaging characteristics of thrombus and infarct core in acute ischemic stroke and their association with clinical outcome*.

Radiological imaging characteristics of thrombus and infarct core in acute ischemic stroke and their association with clinical outcome

Manon Tolhuisen

Radiological imaging characteristics of thrombus and infarct core in acute ischemic stroke and their association with clinical outcome

Manon L. Tolhuisen

Radiological imaging characteristics of thrombus and infarct core in acute ischemic stroke and their association with clinical outcome.

Funded by Hartstichting

This thesis was printed on 100% recycled paper

Radiological imaging characteristics of thrombus and infarct core in acute ischemic stroke and their association with clinical outcome.

ACADEMISCH PROEFSCHRIFT

ter verkrijging van de graad van doctor

aan de Universiteit van Amsterdam

op gezag van de Rector Magnificus

prof. dr. ir. P.P.C.C. Verbeek

ten overstaan van een door het College voor Promoties ingestelde commissie,

in het openbaar te verdedigen in de Agnietenkapel

op donderdag 24 november 2022, te 13.00 uur

door Manon Louise Tolhuisen

geboren te Almere

Contents

Part II: infarct core

Chapter 1

General introduction
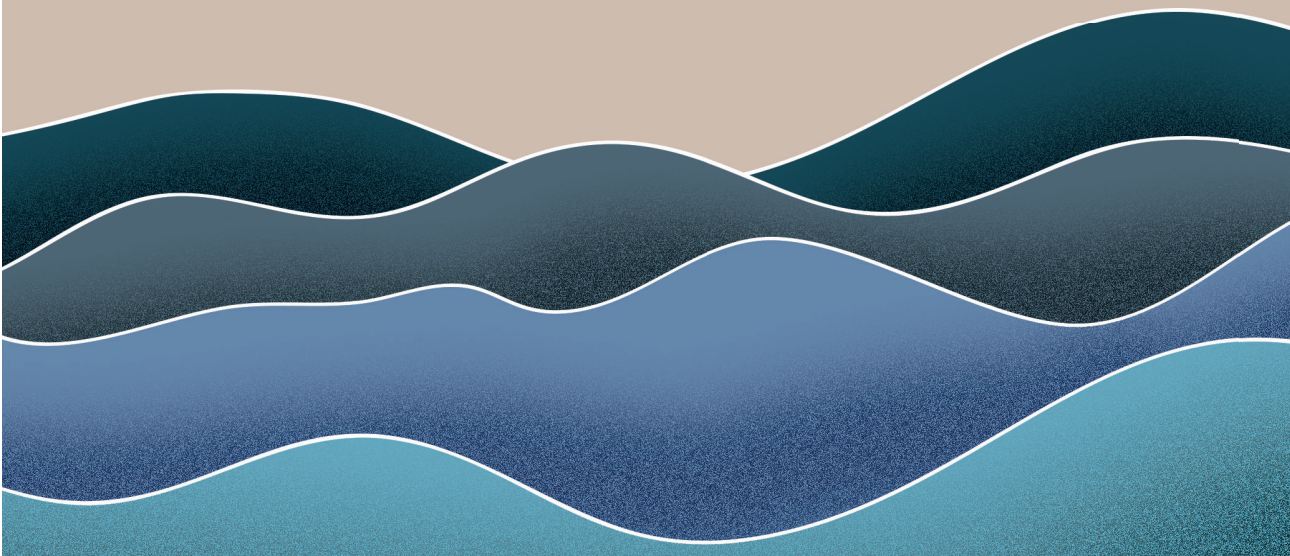
Acute ischemic stroke

Acute ischemic stroke (AIS) is caused by the occlusion of an intracranial artery by a thrombus, blocking the blood supply to regions of the brain distal to the occlusion. It has a high burden on an individual and society level due to its high prevalence and accompanying morbidity and mortality [1]. In the year 2020, over 30.000 people were hospitalized in the Netherlands. From 1980 to 2020 the incidence increased by 156% [2]. Currently, approximately one-third of patients who experience AIS remain functionally dependent [3]. Another third does not survive the first three months after stroke onset.

In the western world poor lifestyle, including smoking, poor diet, alcohol abuse, and lack of exercise, leads to an increased risk for AIS [4],[5]. This poor lifestyle is often accompanied by abdominal obesity, hypertension, diabetes mellitus, and high cholesterol, which are all associated with AIS [2],[5],[6]. Due to longer exposure to these risk factors, the chance for AIS increases over time[6].

Given the brain's low capacity for storing nutrients and oxygen and its high metabolism, deprivation of blood supply quickly leads to tissue death [7],[8]. Initially, a small infarct core originates and additional tissue is put at risk (penumbra). If reperfusion of tissue fails, neuron cells within the penumbra turn necrotic, increasing the infarct core size, and more tissue is put at risk. The fast depravation of neuron cells leads to sudden neural deficits, including numb feeling or weakness of one side of the body, confusion, and difficulty speaking [9].

Diagnosis and treatment

Standard AIS treatment includes the intravenous administration of alteplase (IVT) within 4.5 hours and endovascular treatment (EVT) within 6 hours after stroke onset, up to 24 hours in selected patients [10],[11]. Alteplase is a thrombolytic agent that lyses fibrin, which is the backbone of the thrombus. EVT consists of introducing a catheter in the vasculature (often within the femoral artery at the groin) and propagating it through the vasculature until the thrombus is reached. A

stent retriever is placed and unfolded into the thrombus, capturing the thrombus within the stent, and allowing retraction of the thrombus from the vasculature. Another option is to place a relatively wide bore distal access catheter against the proximal surface of the thrombus and directly aspirate the thrombus (contact-aspiration technique). The combination of these techniques is also commonly used.

The primary aim of AIS treatment is fast recanalization of the occluded artery. Within the Netherlands, when AIS is suspected, the patient is often brought to the nearest hospital where medical imaging is acquired. First, a non-contrast computed tomography (NCCT) is acquired to differentiate from hemorrhagic stroke. Next, a CT angiography (CTA) is acquired to locate the occlusion. If the patient is eligible, administration of IVT is proceeded. If the occlusion is within the proximal anterior cerebral vasculature and the patient is first presented at a primary stroke center, the patient needs to be transferred to an intervention center in order to receive EVT [12].

Acute ischemic stroke research

In 2015, multiple randomized controlled trials, pooled in the HERMES collaboration and including the Dutch MR CLEAN trial, showed that EVT in addition to best medical management more than doubled the odds for improved functional outcome in patients with an occlusion in the anterior cerebral vasculature [13]. Nonetheless, still many patients do not recover after EVT, even when complete reperfusion has been achieved. Therefore more insight into predictors of outcomes after reperfusion therapy is urgently needed to aid in treatment decisions. Thus researchers focus on improving the understanding of the relation between AIS pathogenesis and treatment efficacy.

Gaining knowledge of the relation between image characteristics and clinical outcomes could help understand the chance of treatment success. Medical images can provide information on the length, location, density, and composition of thrombi and infarct lesions [14]. Previous studies have already shown that measurements of the thrombus architecture on medical images are associated with treatment outcome. For example, Riedel et al. [15]. showed that patients with thrombi longer

than 8 mm have a low chance of recanalization after IVT. Santos et al. [16] showed that residual flow through thrombi can be quantified on CT images and introduced thrombus perviousness as a thrombus image biomarker. Thrombus perviousness is defined by the thrombus intensity difference between CTA and NCCT. The studies of Santos et al. showed that thrombus perviousness is associated with a higher chance for recanalization, improved functional outcome, and lower infarct volume [17],[15]. Another study has shown that a low clot burden score is associated with a lower chance of recanalization [15],[18].

Other studies have focused on the relation between the ischemic lesion and functional outcome. For example, follow-up infarct volume showed a negative relation with functional outcome [19],[20]. Ernst et al. [21] has shown that accounting for the location of lesions strengthens the association between the lesion volume and functional outcome.

Aim and thesis outline

The goal of this thesis was to extend our knowledge of the relation between thrombus and infarct core imaging characteristics and clinical outcome in patients with AIS. This thesis is divided into three parts. The first part includes studies focusing on thrombus image characteristics and the second part includes studies focusing on follow-up infarct volume. The last part concludes this thesis with a general discussion, summary in both English and Dutch, list of abbreviations, portfolio, list of publications, 'dankwoord', and information about the author.

Thrombus imaging characteristics

In the first part, we focus on the association between thrombus image characteristics and treatment outcome.

In **chapter 2**, we study the effect of NCCT slice thickness on the assessment of thrombus density and perviousness to gain knowledge on a possible bias that is introduced when the image quality is reduced. Previously, thrombus density and perviousness measurements have only been performed on thin-slice CT images. However, only thick-slice NCCT images are generally available for patients

enrolled in AIS studies. Consequently, a large number of patients is excluded. If the effect of slice thickness on the measured thrombus density and perviousness appears minimal, future studies that study these characteristics could discard the exclusion criterion for thick-slice CT images, resulting in larger study populations.

Directly after the finalization of the MR CLEAN trial, 16 Dutch intervention hospitals started the MR CLEAN Registry, which was a prospective, observational study including patients treated with EVT [3]. The MR CLEAN Registry provides a large study population that was treated within daily clinical practice. Since the treatment of these patients was not subjected to strict randomized controlled trial protocols, the MR CLEAN Registry allows us to study a population that better represents the 'normal' AIS population compared to populations included in previous AIS studies. Therefore, in **chapter 3**, we study the relation between thrombus image characteristics and clinical outcome of patients enrolled in the MR CLEAN Registry.

In **chapter 4** we study the relation between thrombus perviousness and AIS treatment success based on the HERMES population. Due to the pooling of multiple randomized controlled trials, the HERMES collaboration allows us to study a large population of patients with AIS and compare the results from patients who only received best medical management, with results from patients who additionally received EVT.

A previous study has shown that patients who are first admitted to a primary stroke center and then transferred to a comprehensive stroke center have longer onset to treatment times compared to patients who are directly transferred to a comprehensive stroke center [12]. For the transferred patients, the start of treatment was delayed by 30 minutes. The results of the study also showed that transfer patients had lower chance of good functional outcome. The start of the treatment in primary stroke centers might be delayed because the radiologists are less experienced in recognizing AIS. In **chapter 5**, we propose a machine learning based thrombus detection tool for NCCT images that could aid less experienced radiologists in recognizing AIS. The results from the tool are compared with two expert neuroradiologists.

Finally, the thrombus structure is non-static, but changes over time depending on the thrombus composition and surrounding environment. For example, in a low pressure environment, red blood cells can accumulate causing growth of the thrombus [22],[23]. On the other hand, a thrombus shrinks over time due to clot contraction and natural lysis [24],[25]. It is unknown if these processes affect thrombus imaging characteristics in the early time window. Therefore, in **chapter 6,** we study the influence of onset to imaging time on radiological thrombus characteristics.

Follow-up infarct volume

In the second part, we focus on the association between infarct imaging characteristics and clinical outcome.

In the first chapter, **chapter 7**, we study the value of a machine learning based approach for the automated segmentation of infarct lesions on follow-up NCCT images (FIV). The manual delineation of infarct lesions is very time consuming, labor-intensive and introduces user-dependency. It is therefore not feasible to obtain lesion delineations within daily clinical practice. Moreover, study image datasets in AIS studies are growing and time spent on data analyses is increasing. An automated infarct segmentation tool would support fast user-independent delineation of infarct lesions.

In a previous study, performed by Ernst et al. [21], it was shown that the association between FIV measured on NCCT images and functional outcome is strengthened if lesion location is taken into account. Diffusion weighted imaging (DWI) has the highest sensitivity for infarction and is therefore more appropriate in the assessment of infarct lesions [26],[27]. In c**hapter 8** we study the added value of the infarct location in the prediction of functional outcome. Within this study FIV and location are assessed on follow-up DWI images.

Finally, in **chapter 9** we hypothesize that infarct lesions on DWI images include additional prognostic information. Follow-up infarct volume is only moderately associated with functional outcome [19]. An earlier study showed that textural features extracted from lesions are associated with clinical outcome [28]. Also, the

shape of lesions assessed on admission DWI has been associated with FIV [29]. These results motivate us to investigate if DWI images contain other biomarkers than volume that can improve models in the prediction of functional outcome. We will compare the performance of three machine learning models, based on FIV alone, features extracted by a convolutional autoencoder and based on radiomics features.

References

[1]   V. Saini, L. Guada, and D. R. Yavagal, "Global Epidemiology of Stroke and Access to Acute Ischemic Stroke Interventions," *Neurology* 2021, vol. 97, pp. S6–S16, doi:10.1212/WNL.0000000000012781

[2]   Y. Koop, R. H. Wimmers, M. L. Bots, and I. Vaartjes, "Basiscijfers herseninfarct," 2022. [Online]. Available: https://www.hartenvaatcijfers.nl/jaarcijfers/basiscijfers-herseninfarct-f596c. [Accessed: 13-Jul-2022].

[3]   I. G. H. Jansen, M. J. H. L. Mulder, and R. J. B. Goldhoorn, "Endovascular treatment for acute ischaemic stroke in routine clinical practice: Prospective, observational cohort study (MR CLEAN Registry)," *BMJ* 2018, vol. 360, doi:10.1136/bmj.k949

[4]   V. L. Feigin *et al.*, "Global, regional, and national burden of stroke and its risk factors, 1990-2019: A systematic analysis for the Global Burden of Disease Study 2019," *Lancet Neurol.* 2021, vol. 20, no. 10, pp. 1–26, doi: 10.1016/ S1474-4422(21)00252-0

[5]   M. J. O'Donnell *et al.*, "Risk factors for ischaemic and intracerebral haemorrhagic stroke in 22 countries (the INTERSTROKE study): A case-control study," *Lancet* 2010, vol. 376, no. 9735, pp. 112–123, doi: 10.1016/S0140-6736(10)60834-3

[6]   A. Kisialiou *et al.*, "Risk factors and acute ischemic stroke subtypes," J. *Neurol. Sci.* 2014, vol. 339, no. 1–2, pp. 41–46, doi:10.1016/j.jns.2014.01.014

[7]   C. Desai and A. Hays Shapshak, "Cerebral Ischemia," Cerebral Ischemia, 2022. [Online]. Available: https://www.ncbi.nlm.nih.gov/books/NBK560510/. [Accessed: 05-Feb-2022].

[8]   J. L. Saver, "Time is brain - Quantified," *Stroke* 2006, vol. 37, no. 1, pp. 263–266, doi: doi:10.1161/01.STR.0000196957.55928.ab

[9]   W. J. Powers *et al.*, "2018 Guidelines for the Early Management of Patients With Acute Ischemic Stroke: A Guideline for Healthcare Professionals From the American Heart Association/American Stroke Association" *Stroke* 2018, vol. 49, no. 3. doi:10.1161/STR.0000000000000158

[10]   W. J. Powers *et al.,* "Guidelines for the early management of patients with acute ischemic stroke: 2019 update to the 2018 guidelines for the early management of acute ischemic stroke a guideline for healthcare professionals from the American Heart Association/American" *Stroke* 2019, vol. 50, no. 12, doi: 10.1161/STR.0000000000000211

[11]   G. Turc *et al.*, "European Stroke Organisation (ESO) - European Society for Minimally Invasive Neurological Therapy (ESMINT) Guidelines on Mechanical Thrombectomy in Acute Ischemic Stroke," *J. Neurointerv. Surg.* 2019, pp. 1–30, doi:10.1136/neurintsurg-2018-014569

[12]   E. Venema *et al.*, "Effect of Interhospital Transfer on Endovascular Treatment for Acute Ischemic Stroke," *Stroke* 2019, pp. 923–930, doi:10.1161/strokeaha.118.024091

[13]   M. Goyal *et al.*, "Endovascular thrombectomy after large-vessel ischaemic stroke: A meta-analysis of individual patient data from five randomised trials," *Lancet* 2016, vol. 387, no. 10029, pp. 1723–1731, doi:10.1016/S0140-6736(16)00163-X

[14]   W. Brinjikji *et al.*, "Correlation of imaging and histopathology of thrombi in acute ischemic stroke with etiology and outcome: A systematic review," *J. Neurointerv. Surg* 2017., vol. 9, no. 6, pp. 529–534, doi:10.1136/neurintsurg-2016-012391

[15]   C. H. Riedel, P. Zimmermann, U. Jensen-Kondering, R. Stingele, G. Deuschl, and O. Jansen, "The Importance of Size," *Stroke* 2011, vol. 42, no. 6, pp. 1775 LP – 1777, doi:10.1161/STROKEAHA.110.609693

[16]   E. M. M. Santos *et al.*, "Observer variability of absolute and relative thrombus density measurements in patients with acute ischemic stroke," *Neuroradiology* 2016, vol. 58, no. 2, pp. 133–139, doi:10.1007/s00234-015-1607-4

[17]   E. M. M. Santos *et al.*, "Thrombus Permeability Is Associated with Improved Functional Outcome and Recanalization in Patients with Ischemic Stroke," *Stroke* 2016, vol. 47, no. 3, pp. 732–741, doi: 10.1161/STROKEAHA.115.011187

[18]   K. M. Treurniet et al., "Clot Burden Score on Baseline Computerized Tomographic Angiography and Intra-Arterial Treatment Effect in Acute Ischemic Stroke," Stroke, vol. 47, 2016.

[19]   A. M. M. Boers et al., "Association of follow-up infarct volume with functional outcome in acute ischemic stroke: a pooled analysis of seven randomized trials," J. Neurointerv. Surg., p. neurintsurg-2017-013724, 2018.

[20]   J. Yoo et al., "Thrombus Volume as a Predictor of Nonrecanalization After Intravenous Thrombolysis in Acute Stroke," Stroke, vol. 49, no. 9, pp. 2108–2115, 2018.

[21]   M. Ernst et al., "Association of Computed Tomography Ischemic Lesion Location with Functional Outcome in Acute Large Vessel Occlusion Ischemic Stroke," Stroke, vol. 48, no. 9, pp. 2426–2433, 2017.

[22]   S. F. De Meyer et al., "Analyses of thrombi in acute ischemic stroke: A consensus statement on current knowledge and future directions," Int. J. Stroke, vol. 12, no. 6, pp. 606–614, 2017.

[23]   E. M. Qazi et al., "Thrombus Characteristics Are Related to Collaterals and Angioarchitecture in Acute Stroke.," Can. J. Neurol. Sci., vol. 42, no. 6, pp. 381–8, 2015.

[24]   D. B. Cines et al., "Clot contraction: Compression of erythrocytes into tightly packed polyhedra and redistribution of platelets and fibrin," Blood, vol. 123, no. 10, pp. 1596–1603, 2014.

[25]   I. B. Kovacs and J. Yamamoto, "Spontaneous thrombolysis: A forgotten determinant of life or death," Clin. Appl. Thromb., vol. 12, no. 3, pp. 358–363, 2006.

[26]   S. J. Warach et al., "Acute Stroke Imaging Research Roadmap III Imaging Selection and Outcomes in Acute Stroke Reperfusion Clinical Trials: Consensus Recommendations and Further Research Priorities," Stroke, vol. 47, no. 5, pp. 1389–1398, 2016.

[27]   S. Rudkin, R. Cerejo, A. Tayal, and M. F. Goldberg, "Imaging of Acute Ischemic Stroke," Emerg. Radiol., pp. 1–13, 2018.

[28]   H. Wang, J. Lin, L. Zheng, J. Zhao, B. Song, and Y. Dai, "Texture analysis based on ADC maps and T2-FLAIR images for the assessment of the severity and prognosis of ischaemic stroke," Clin. Imaging, vol. 67, no. March, pp. 152–159, 2020.

[29]   C. Frindel et al., "Validity of Shape as a Predictive Biomarker of Final Infarct Volume in Acute Ischemic Stroke," Stroke, vol. 46, no. 4, pp. 976–981, 2015.

Part I - thrombus
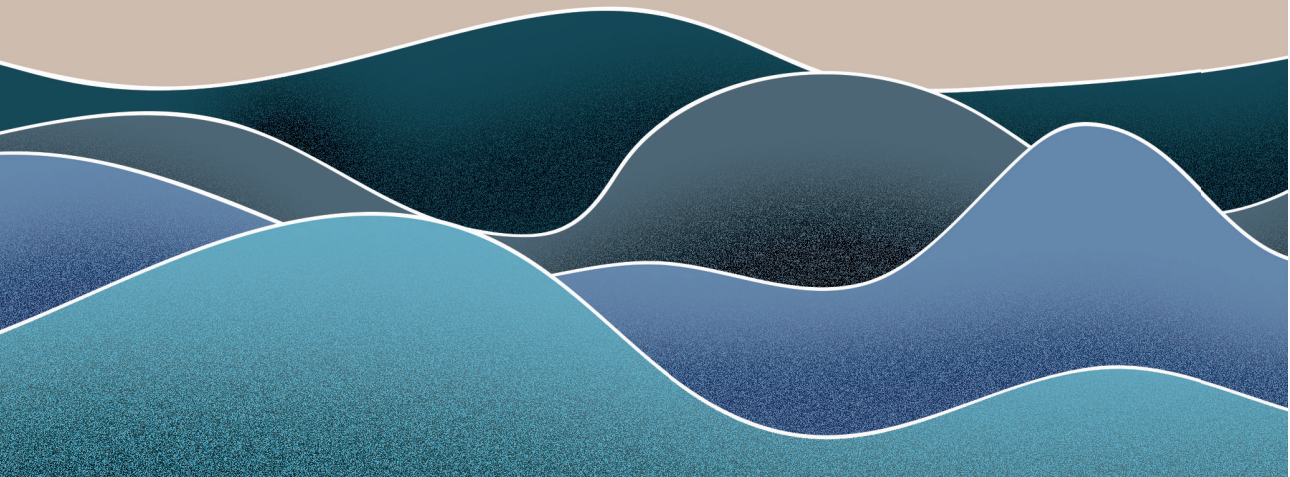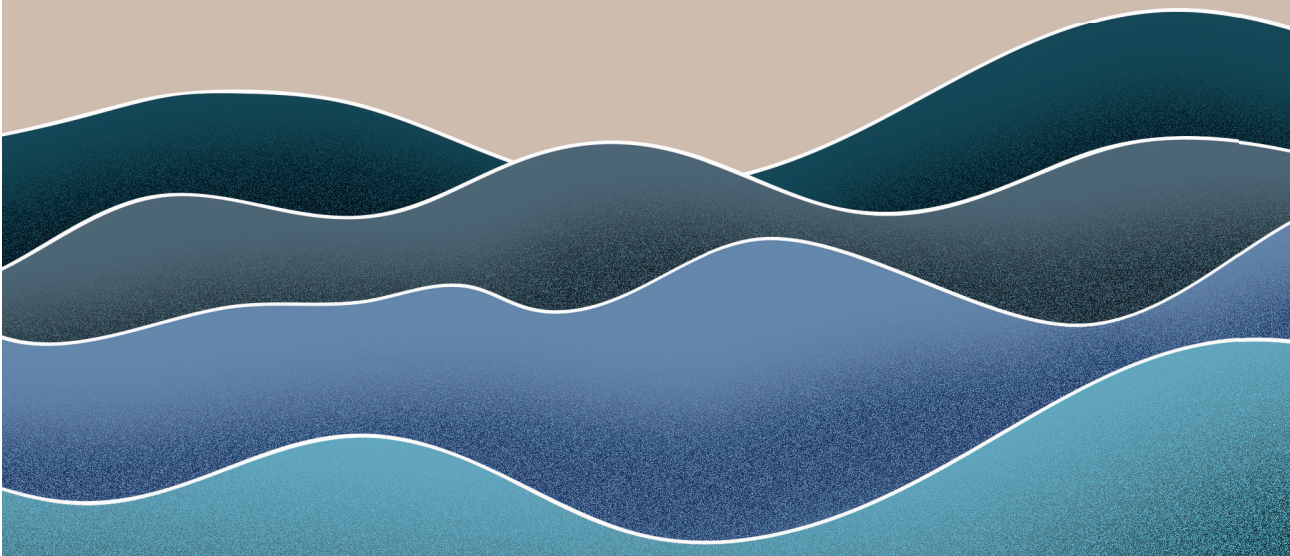
Chapter 2
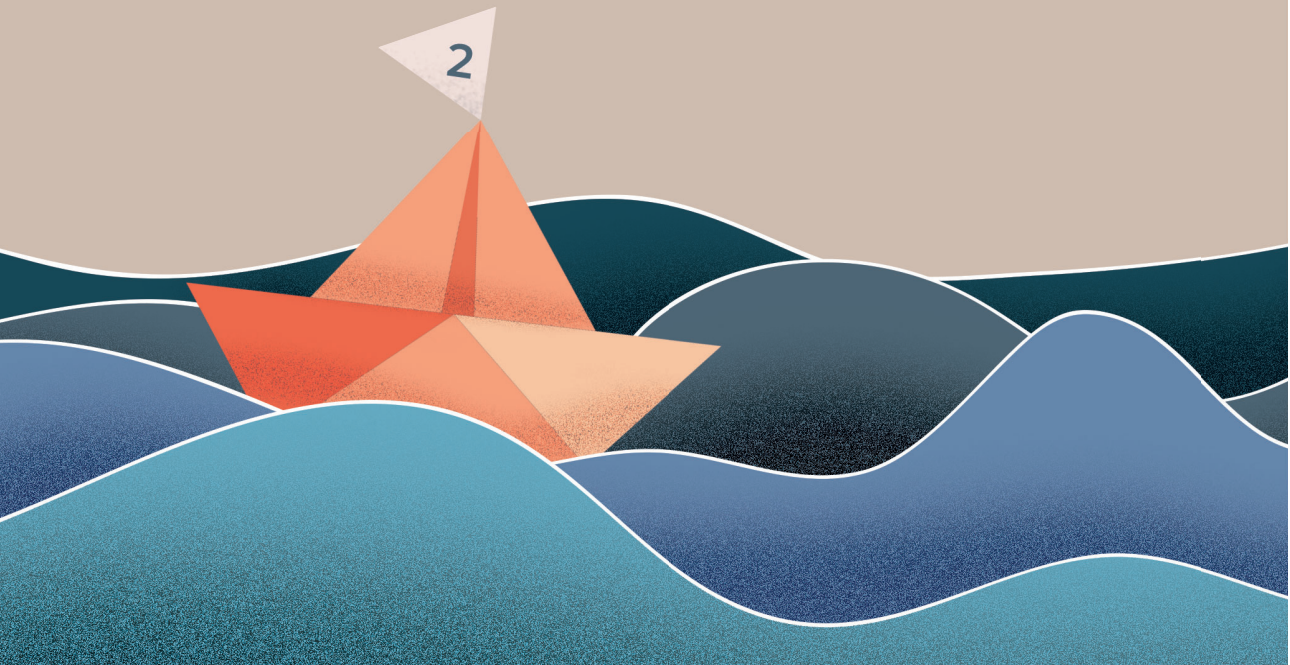
The effect of non-contrast CT slice thickness on thrombus density and perviousness assessment

M.L. Tolhuisen, J. Enthoven, E.M.M. Santos, W.J. Niessen, L.F.M. Beenen, D.W.J. Dippel, A. van der Lugt, W.H. van Zwam, Y.B.W.E.M. Roos, R.J. van Oostenbrugge, C.B.L.M. Majoie, and H.A. Marquering

Abstract

Background— It is expected that thrombus density and perviousness measurements are dependent on CT slice thickness because density values are blurred in thicker slices. This study quantifies the effect of slice thickness on thrombus density and perviousness measurements.

Methods— Thrombus density and perviousness measurements were performed in 50 patients for varying slice thicknesses, using a manual and semi-automated technique. Linear regression was performed to determine the dependence of density measurements on slice thickness. Paired t-tests were used to test for differences in density and perviousness measures for varying slice thickness.

Results— Thrombus density decreased for increasing slice thickness with approximately 2 HU per mm. Perviousness measurements were significantly higher for thick slice compared to thin slice NCCT.

Conclusion— Thick slice NCCT scans result in an underestimation of thrombus density and overestimation of thrombus perviousness.

Introduction

Stroke has a major impact on society as it is one of the leading causes of death worldwide [1]. In 87% of all cases, stroke is caused by a thrombus that occludes an intracranial vessel (ischemic stroke) [2]. As a patient loses around 1.9 million neurons each minute, fast treatment to restore blood flow is crucial [3].

For the past years, research has focused on improving treatment for ischemic stroke. This resulted in endovascular treatment (EVT) as an addition to the standard treatment after it showed increased functional outcome in several randomized clinical trials [4]. Nonetheless, patient outcome is still poor and further research is focusing on patient-specific treatment selection, for example based on thrombus characteristics. It has been suggested that thrombus density measurements provide information on thrombus architecture and is a potential predictor for treatment effect [5]. In addition, Santos et al. [6],[7] showed that

thrombus permeability was associated with a higher recanalization rate and better functional outcome, after both EVT and IV-tPA.

Because the measurement of permeability requires dynamic imaging, the definition of thrombus perviousness was introduced as a measure to estimate thrombus permeability [6]. Perviousness is defined as the difference in thrombus voxel intensities, comparing CT angiography (CTA) to non-contrast CT (NCCT) [6]. In this assessment, imaging quality may be a limiting factor. Preferably, the assessment should be performed on low noise, high resolution, and thin slice images. In current clinical practice, thick slice NCCT images are commonly used because of lower noise levels and lower demand on storage capacity. CTA images have higher contrast to noise ratio and are therefore commonly stored as thin slices (approximately 1 mm thick). Because of averaging, which is applied to generate thick slice images, the signal of small-scale structures such as thrombi may be reduced. Kim et al. [8] showed reduced sensitivity and specificity for thrombus detection on thick slice NCCT compared to thin slice NCCT. In this study, we aim to quantify the effect of slice thickness on thrombus density and perviousness measurements.

Materials and methods

Patient selection

We included 50 consecutive patients from the Multicenter Randomized Clinical trial of Endovascular treatment of ischemic stroke in the Netherlands (MR CLEAN) cohort with thin-slice (≤ 2.5 mm) NCCT and CTA scans that were performed within 30 minutes on the same scanner.

Slice reconstruction

Thick(er) slice images were reconstructed by taking the average over multiple thin slices for each voxel location. For a given slice thickness, multiple approaches can be followed to generate such an image. For example, if a new image is generated with twice as thick slice thickness, one can combine slices 1

and 2 or slices 2 and 3. Figure 2.1 illustrates how multiple approaches can be followed for thick slice reconstructions out of thin slices. First, all scans were supersampled to an initial slice thickness of 0.45 mm. Then, different reconstructions were created for given slice thicknesses. The resulted slice thicknesses ranged from 0.45 mm to 4.95 mm with an increment of 0.45 mm. The CTA slice thickness was kept at 0.45 mm.
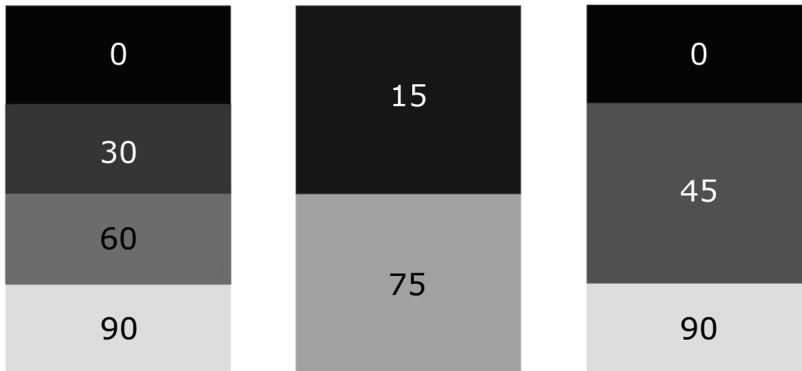
Figure 2.1 *Illustration of the slice reconstruction that is used to increase slice thickness. The numbers in the layers show examples of densities. This figure shows two examples in which a scan with a slice thickness twice as large as the original (Left) was created. The example in the (Middle) shows the results when slices 1 and 2 and slices 3 and 4 were combined. The second example (Right) shows the results when slices 2 and 3 are combined to generate an image with a thicker slice.*

Density and pervious measurements

Thrombus density measurements were initially performed on the original thin slice NCCT and CTA by a single expert observer, using both manual and semi-automated thrombus perviousness measurements described in [6] and [9]. First, Elastix® [10] was used for rigid image registration to align the NCCT and CTA for each patient. For the manual density measurement, a spherical region of interest (ROI) with a radius of 1 mm was placed in the proximal, middle, and distal part of the thrombus. The semi-automated perviousness measurements followed multiple steps. First, 2 ROIs were placed proximal and distal to the thrombus and symmetrically on the contralateral side. A coarse centerline of the contralateral

vessel between the proximal and distal ROIs was determined using a minimum cost path calculation on the CTA image, filtered with a tuned Frangi's vesselness filter [11], [12]. Then, the vessel contour was obtained from this coarse centerline using a graph-cut segmentation technique with kernel regression [12]. The initial coarse centerline was corrected to be the center of mass of this segmented vessel contour and the radius along the fine centerline was determined. Finally, based on symmetry, the fine centerline was projected onto the occluded vessel using 3D B-spline registration to optimize alignments. The same kernel regression segmentation technique was used on the CTA to segment the occluded vessel, guided by the aligned centerline. Due to a drop in intensity at the location of the thrombus, the radius of the segmented lumen decreases significantly. At the site of the thrombus, the vessel contours were replaced with the contralateral radius contours, thereby creating a shape prior. Within the shape prior, a combination of region growing segmentation and mathematical morphologies is used to obtain the final thrombus segmentation.

To assess thrombus perviousness, we used the thrombus attenuation increase (TAI), which is defined as the thrombus attenuation difference between CTA and NCCT measurements. The thrombus density measurements were obtained using the newly reconstructed NCCT images for all slice thicknesses. The density and perviousness measures for all slice thicknesses were compared to the original, thin slice, density and perviousness measurements.

Statistical Analysis

The mean and standard deviation of the difference in density measurements was calculated for each slice thickness. To investigate a potential correlation between thrombus density and slice thickness, a linear regression model was used based on the mean thrombus density for all patients. A paired t-test was used to investigate whether a significant difference in density and perviousness measurements was present, comparing the thin slice measurements to the measurements with the reconstructed scans with increased slice thicknesses.

All analyses were performed using IBM® SPSS® Statistics software, version 24 (IBM Corp., Armonk, NY).

Results

Linear regression showed that the thrombus density values significantly decreased with increasing slice thickness. For each mm increase in slice thickness, the density measures decreased by 2.9 and 2.2 HU (both $p < 0.001$), for the manual measurements and the full thrombus segmentation respectively. Figure 2.2 shows the manual thrombus density measurements in 50 patients for varying slice thicknesses. The density measurements as assessed by the full thrombus segmentation are shown in Figure 2.3.

The paired t-test showed that there was a significant increase ($p<0.001$) in thrombus perviousness measures for increasing slice thickness, comparing the thin slice measurements with the measurement for NCCT with 0.9 mm slice thickness. Figure 2.4 and Figure 2.5 show the results of the perviousness measurements in 50 patients for varying slice thicknesses, measured with the ROIs and full thrombus segmentation respectively.
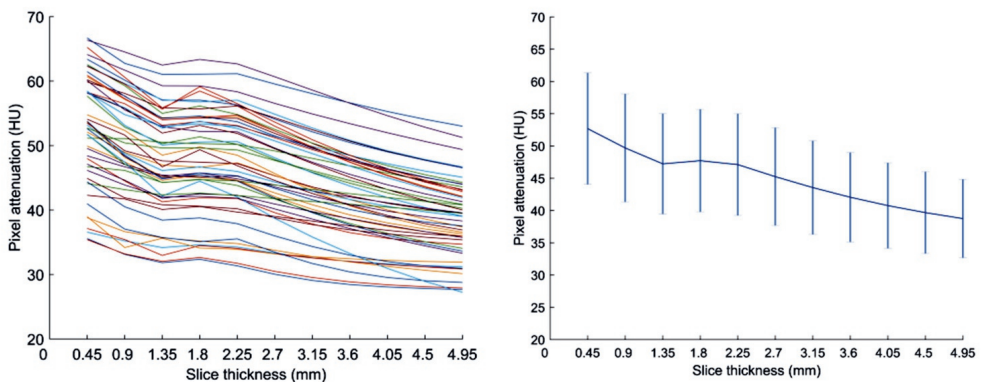
Figure 2.2 (Left) NCCT thrombus density measurements for varying slice thickness for 50 patients manually measured with ROIs; (Right) NCCT mean thrombus density for varying slice thickness measured with ROIs
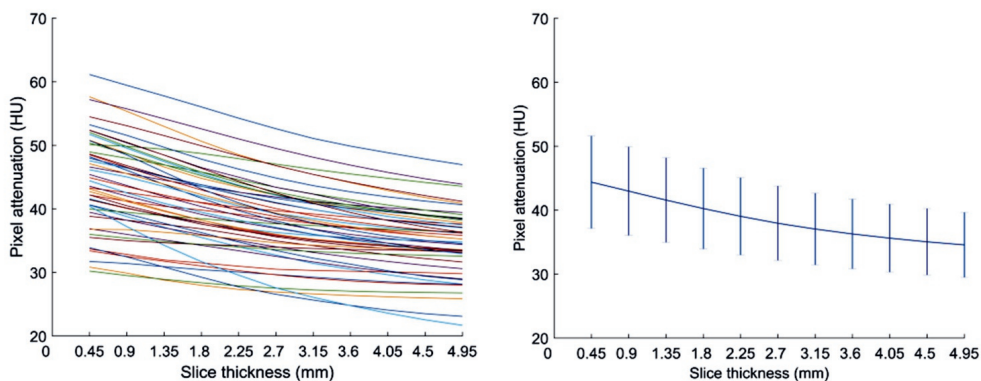
Figure 2.3 *(Left) NCCT thrombus density measurements for varying slice thickness for 50 patients measured with the full thrombus segmentation; (Right) NCCT mean attenuation decrease over slice thickness measured with the full thrombus segmentation*
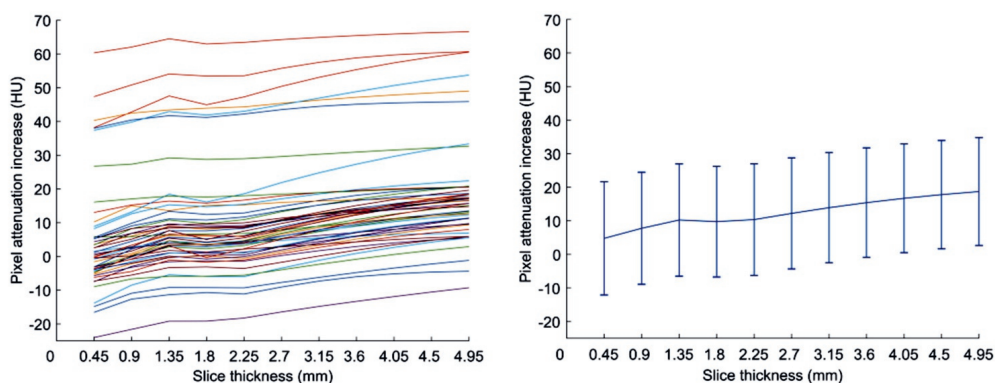
Figure 2.4 *(Left) Thrombus attenuation increase for varying slice thickness for 50 patients manually measured with ROIs; (Right) Mean attenuation increase over slice thickness measured with the ROIs*
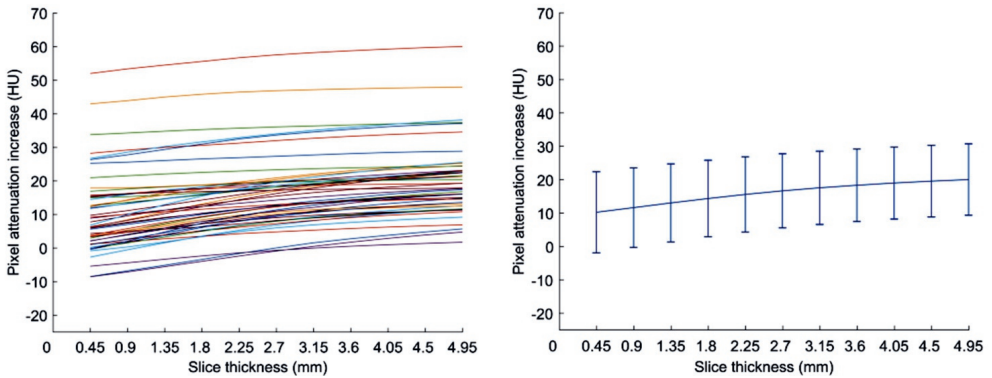
Figure 2.5 *(Left) Thrombus attenuation increase for varying slice thickness for 50 patients measured with the full thrombus segmentation; (Right) Mean attenuation increase over slice thickness measured with the full thrombus segmentation*

Discussion

In this study, it was shown that there was a significant decrease in thrombus density measures with increasing CT slice thickness. As a result, perviousness measures increased with increasing NCCT slice thickness.

Thrombus characteristics, such as thrombus density and perviousness, may be used as treatment selection parameters or predictive parameters for treatment success and functional outcome for patients with ischemic stroke in the future [5-7]. While data storage will become a major challenge in the medical imaging field, it is important to know the consequences of data reduction [11]. This study showed that the increase of NCCT slice thickness resulted in reduced thrombus density and increased perviousness measurement values. Therefore, previous associations made between thrombus perviousness and favorable prognostics cannot be extrapolated for thick slice NCCT measurements, as they may lead to the overestimation of favorable prognostics.

The results showed differences between the thrombus density and perviousness measurements, performed with the manual annotation compared to the semi-automated thrombus segmentation. Less variation was visible in the thrombus density and perviousness measurements between patients and the effect

of increased slice thickness appeared less for the semi-automated full thrombus segmentation. This was expected because a larger volume of density values is included in this technique, which makes it less susceptible to noise.

The placement of ROIs in imaging data is easily applicable and can already be applied in daily clinical practice. However, it was shown that the full thrombus segmentation is less sensitive to slice thickness. Also, Santos et al. [12] showed a stronger association between thrombus perviousness and functional outcome and recanalization, based on full segmented thrombi measurements.

The linear regression showed an inverse relation between slice thickness and density measurements. This suggests that a correction for slice thickness could result in a more accurate density measurement.

A limitation of this study is that we did not correct for confounders. It could be possible that factors such as scanner manufacturer, reconstruction, size of the thrombus, or filtering algorithms have influenced our results.

This study only used thrombus density and perviousness measurements from a single observer. Thereby, we did not take inter-observer variability into account. However, Santos et al. [9],[13] already showed reasonable inter-observer variability for both measurement techniques.

The increase in slice thickness creates a blurring effect in the z-direction. As a result, the decrease in density of the thrombus in the CT image is dependent on the orientation and fraction of the vessels present within the slice.

The longitudinal partial volume effect will be more apparent in thicker slices. Based on a phantom study, Monnin et al. [14] suggested that the optimal slice thickness is 75% of object width. As the average diameter of the M1 segment is 2.3 ± 0.3 mm and the vessel diameters are expected to decrease distally, this suggests a maximal slice thickness of approximately 1.7 mm [15]. However, we also see a reduction of thrombus densities with slice thickness between 0.45 and 1.7 mm.

Conclusion

This study showed that increasing NCCT slice thickness results in a decreasing thrombus density and an increase in thrombus perviousness assessment.

References

[1]   H. Wang, M. Naghavi, C. Allen, R.M. Barber, Z.A. Bhutta, A. Carter, *et al.* "Global, regional, and national life expectancy, all-cause mortality, and cause-specific mortality for 249 causes of death, 1980-2015: a systematic analysis for the Global Burden of Disease Study 2015," *Lancet* 2016, vol. 388, no. 10053, pp. 1459-1544. doi: 10.1016/S0140-6736(16)31012-1

[2]   American Heart Association, "Ischemic stroke," 2017 *[Online]* Available: http://www.strokeassociation.org/STROKEORG/AboutStroke/TypesofStroke/IschemicClots/Ischemic-Strokes-Clots_UCM_310939_Article.jsp#.WSRFoevyhhE.

[3]   J.L. Saver, "Time is brain–Quantified." *Stroke* 2006, vol. 37, pp. 263–266. doi: 10.1161/01.STR.0000196957.55928.ab

[4]   M. Goyal, B.K. Menon, W.H. van Zwam, D.W. Dippel, P.J. Mitchell, A.M. Demchuk *et al.* "Endovascular thrombectomy after large-vessel ischaemic stroke: A meta-analysis of individual patient data from five randomised trials." *Lancet 2016*, vol. 387, pp. 1723–1731. doi: 10.1016/S0140-6736(16)00163-X

[5]   P. Moftakhar, J.D. English, D.L. Cooke, W.T. Kim, C. Stout, W.S. Smith *et al.*, "Density of Thrombus on Admission CT Predicts Revascularization Efficacy in Large Vessel Occlusion Acute Ischemic Stroke," *Stroke 2013*, vol. 44, pp. 243-246. doi: 10.1161/STROKEAHA.112.674127

[6]   E.M.M. Santos, H.A. Marquering, M.D. den Blanken, O.A. Berkhemer, A.M.M. Boers, A.J. Yoo *et al.*, "Thrombus permeability Is Associated with Improved Functional Outcome and Recanalization in Patients with Ischemic Stroke," *Stroke 2016*, vol. 47, no. 3, pp. 732-741. doi: 10.1161/STROKEAHA.115.011187

[7]   E.M.M. Santos, J.W. Dankbaar, K.M. Treurniet, A.D. Horsch, Y.B. Roos, L.J. Kappelle *et al.,* "Permeable Thrombi Are Associated With Higher Intravenous Recombinant Tissue-Type Plasminogen Activator Treatment Success in Patients With Acute Ischemic Stroke," *Stroke*, vol. 47, no. 8, p. 2058 LP-2065, Jul. 2016. doi: 10.1161/STROKEAHA.116.013306

[8]   K.Y. Eung, S.K. Lee, D.J. Kim, S.H. Suh, J. Kim, J.H. Heo *et al.*, "Detection of thrombus in acute ischemic stroke: value of thin-section noncontrast-computed

tomography," *Stroke 2005*, vol. 36, no. 12, pp. 2745-2747. doi:
10.1161/01.STR.0000185720.03803.41

[9]   E.M.M. Santos, H.A. Marquering, O.A. Berkhemer, W.H. van Zwam, A. van
der Lugt, C.B. Majoie *et al.*, "Development and validation of intracranial thrombus
segmentation on CT angiography in patients with acute ischemic stroke,"*PLoS One
2014*, vol. 9, no. 7. doi: 10.1371/journal.pone.0101985

[10]   S. Klein, M. Staring, K. Murphy, M.A. Viergever, and J.P.W. Pluim, "Elastix:
A toolbox for intensity-based medical image registration," *IEEE Trans. Med.
Imaging 2010*, vol. 29, no. 1, pp. 196-205. doi: 10.1109/TMI.2009.2035616

[11]   D. Reinsel, J. Gantz, and J. Rydning, "Data Age 2025: The Evolution of
Data to Life-Critical Don't Focus on Big Data; Focus on the Data That's Big -
Sponsored by Seagate," IDC White Paper, November 2018, *[Online]* Available:
http://www.seagate.com/www-content/our-story/trends/files/Seagate-WP-
DataAge2025-March-2017.pdf

[12]   E.M.M. Santos, W.J. Niessen, A.J. Yoo, and O.A. Berkhemer, "Automated
Entire Thrombus Density Measurements for Robust and Comprehensive Thrombus
Characterization in Patients with Acute Ischemic Stroke," *PLoS One 2016*, vol. 11,
no. 1, pp. 1-16. doi: 10.1371/journal.pone.0145641

[13]   E.M.M. Santos, W.J. Niessen, A.J. Yoo, O.A. Berkhemer, L.F. Beenen,
C.B. Majoie *et al.* "Observer variability of absolute and relative thrombus density
measurements in patients with acute ischemic stroke," *Neuroradiology 2016*, vol.
58, no. 2, pp. 133-139. doi: 10.1007/s00234-015-1607-4

[14]   P. Monnin, N. Sfameni, A. Gianoli, and S. Ding, "Optimal slice thickness for
object detection with longitudinal partial volume effects in computed tomography,"
J. Appl. Clin. Med. Phys. 2017, vol. 18, pp. 251-259. doi: 10.1002/acm2.12005

[15]   R. Peter, B.J. Emmer, A.C.G.M. van Es, and T. van Walsum, "Quantitative
Analysis of Geometry and Lateral Symmetry of Proximal Middle Cerebral Artery," *J.
Stroke Cerebrovasc. Dis. 2017*, vol. 26, no. 10, pp. 2427-2434. doi:
10.1016/j.jstrokecerebrovasdis.2017.05.039

Chapter 3
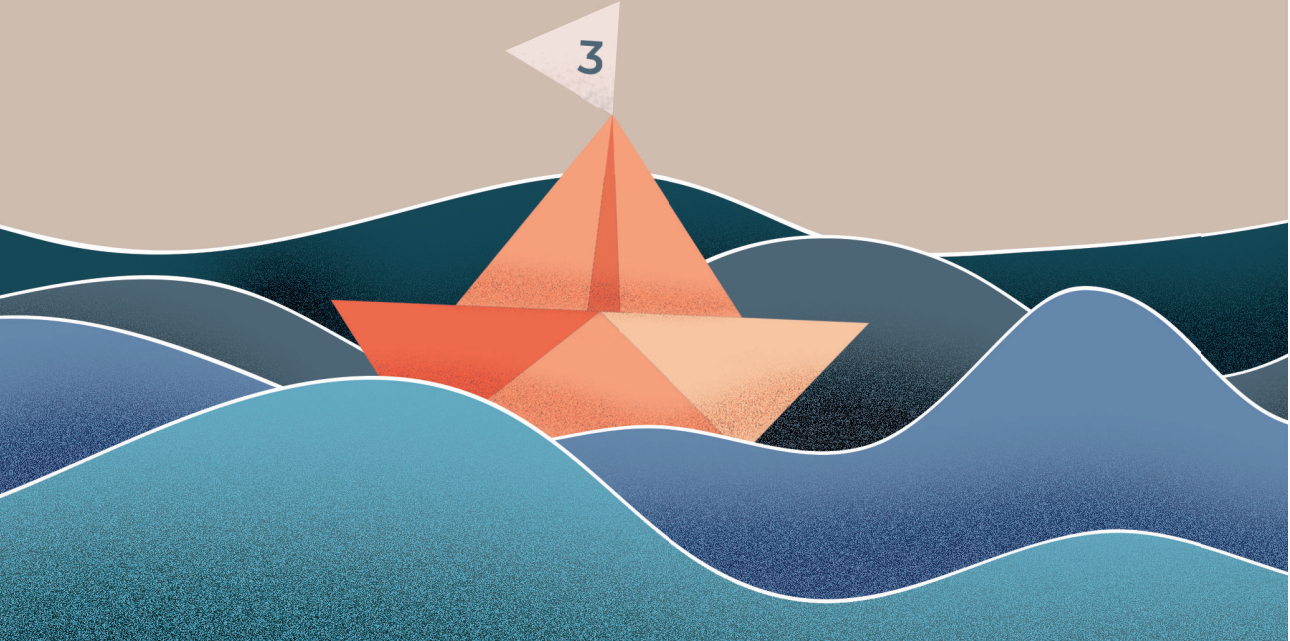
Influence of onset to imaging time on radiological thrombus characteristics in acute ischemic stroke

M.L. Tolhuisen*, M. Kappelhof*, B.G. Dutra, I.G.H. Jansen, V. Guglielmi, D.W.J. Dippel, W.H. van Zwam, R.J. van Oostenbrugge, A. van der Lugt, Y.B.W.E.M. Roos, C.B.L.M. Majoie, M.W.A. Caan, H.A. Marquering, on behalf of the MR CLEAN Registry Investigators
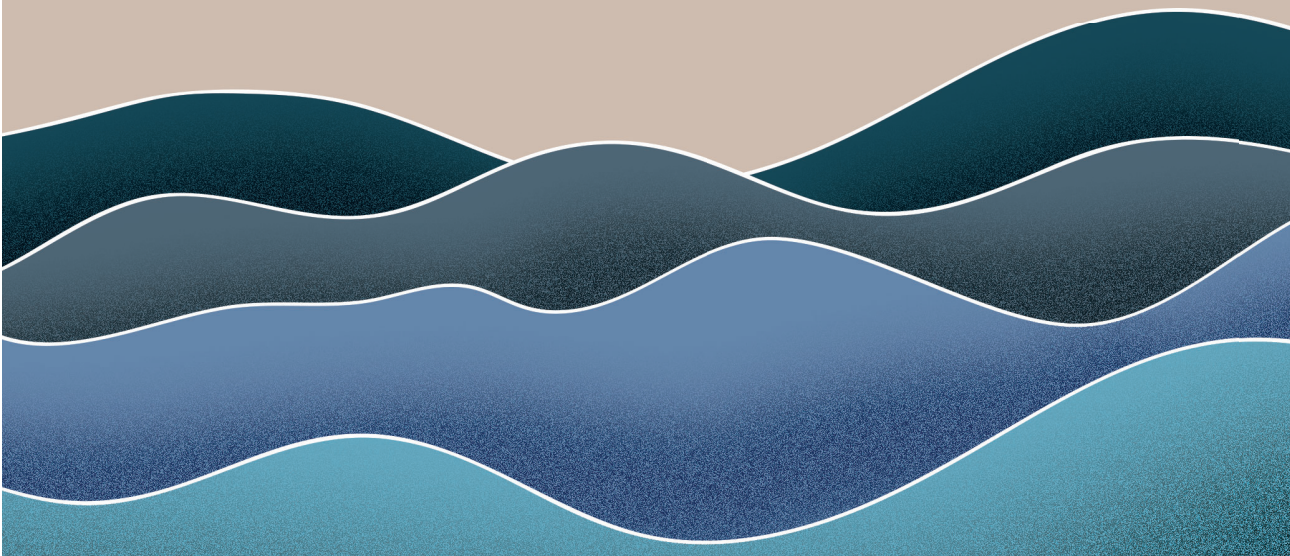
Abstract

Background— Radiological thrombus characteristics are associated with patient outcomes and treatment success after acute ischemic stroke. These characteristics could be expected to undergo time-dependent changes due to factors influencing thrombus architecture like blood stasis, clot contraction, and natural thrombolysis. We investigated whether stroke onset-to-imaging time was associated with thrombus length, perviousness, and density in the MR CLEAN Registry population.

Methods— We included 245 patients with M1-segment occlusions and thin-slice baseline CT imaging from the MR CLEAN Registry, a nationwide multicenter registry of patients who underwent endovascular treatment for acute ischemic stroke within 6.5 h of onset in the Netherlands. We used multivariable linear regression to investigate the effect of stroke onset-to-imaging time (per 5 min) on thrombus length (in mm), perviousness, and density (both in Hounsfield Units). In the first model, we adjusted for age, sex, intravenous thrombolysis, antiplatelet use, and history of atrial fibrillation. In a second model, we additionally adjusted for observed vs. non-observed stroke onset, CT-angiography collateral score, direct presentation at a thrombectomy-capable center vs. transfer, and stroke etiology. We performed exploratory subgroup analyses for intravenous thrombolysis administration, observed vs. non-observed stroke onset, direct presentation vs. transfer, and stroke etiology.

Results— Median stroke onset-to-imaging time was 83 (interquartile range 53–141) min. Onset to imaging time was not associated with thrombus length nor perviousness (β 0.002; 95% CI –0.004 to 0.007 and β −0.002; 95% CI −0.015 to 0.011 per 5min, respectively) and was weakly associated with thrombus density in the fully adjusted model (adjusted β 0.100; 95% CI 0.005–0.196 HU per 5min). The subgroup analyses showed no heterogeneity of these findings in any of the subgroups, except for a significantly positive relation between onset-to-imaging time and thrombus density in patients transferred from a primary stroke center (adjusted β 0.18; 95% CI 0.022–0.35).

Conclusion— In our population of acute ischemic stroke patients, we found no clear association between onset-to-imaging time and radiological thrombus characteristics. This suggests that elapsed time from stroke onset plays a limited role in the interpretation of radiological thrombus characteristics and their effect on treatment results, at least in the early time window.

Introduction

Radiological thrombus characteristics are among the few biomarkers that are associated with acute ischemic stroke (AIS) treatment success. Thrombus perviousness, reflecting the extent to which intravenous contrast permeates into a thrombus, was shown to be strongly associated with higher recanalization rates and treatment success of intravenous alteplase (IVT) [1],[2]. Thrombus length was reported to negatively affect success rates of both IVT and endovascular treatment (EVT) [3], [4], although no effect on EVT outcomes was found in some other studies [5], [6]. Higher thrombus density is related to higher recanalization rates after IVT and EVT [7], [8].

Thrombus characteristics may vary over time. For example, stasis in low-pressure systems can cause thrombus growth over time by the accumulation of red blood cells in low-density fibrin networks [9]. In contrast, time may allow for natural thrombolysis or IVT to reduce the size of the clot [10–13]. In addition, if a patient has good collaterals, decreased blood stasis was reported to limit thrombus growth distal to the clot and improve thrombus exposure to alteplase [14], [15]. Clot contraction may also reduce thrombus length, increase thrombus density, and decrease perviousness [16], [17].

Dynamic behavior of thrombi may influence the success of stroke treatment. For example, patients with a prolonged time to AIS treatment and favorable thrombus dynamics may show alteplase-induced or even spontaneous recanalization. This effect has been observed in patients transferred from primary hospitals to comprehensive stroke centers for EVT [18]. Alternatively, if the thrombus grows before treatment, the chance of recanalization with IVT reduces, and endovascular procedure time increases [3], [4]. Moreover, if radiological thrombus characteristics

change over time, the elapsed time between the moment of measurement and the start of stroke treatment may affect the association between these values and stroke treatment outcomes.

Despite these possibly relevant effects, the effects of time on thrombus characteristics have been understudied. We therefore aimed to assess the relation between stroke onset to imaging time and thrombus length, perviousness, and density using data from a large national registry.

Methods

Study population

This study includes patients from the Multicenter Randomized Clinical trial of Endovascular Treatment for Acute ischemic stroke in the Netherlands (MR CLEAN) Registry (part I) [19] between March 2014 and June 2016. The MR CLEAN Registry is a nationwide, prospective, observational, multicenter study at 16 comprehensive stroke centers in the Netherlands, including all patients who underwent EVT for AIS since the completion of the MR CLEAN trial [20]. IVT was administered before EVT if patients were eligible. The central medical ethics committee of the Erasmus Medical Center Rotterdam, the Netherlands, granted permission (MEC-2014–235) to perform the study as a registry. Source data of this study are available in anonymized form upon reasonable request to the corresponding author.

Inclusion criteria for the current study were: M1 occlusion; age ≥18 years; groin puncture within 6.5 h after stroke onset; and treatment in an MR CLEAN trial center. Only patients with thin-slice (≤2.5mm) CT-angiography (CTA) and non-contrast CT (NCCT) images that were acquired on the same scanner no longer than 30 min apart were included. We used the images acquired at the first point in time. For patients who were transferred from a primary stroke center we used the primary center's radiological images if they were available and of sufficient quality. Otherwise, we used the images acquired at the comprehensive stroke center. Patients were excluded if images contained excessive noise, artifacts, poor

contrast opacification on CTA, or uncorrectable registration errors. Patients with calcified thrombi were excluded as well since the high attenuation of these thrombi can cause streak and partial volume artifacts.

Image Analysis

Measurements of radiological thrombus characteristics were performed in ITK-SNAP (www.itksnap.org) [19] by two neuroradiologists (B.G.D. and H.A.) [4]. The NCCT and CTA images for each patient were co-registered with rigid registration, using Elastix R® [21], such that thrombus measurements could be performed in both modalities simultaneously. If the alignment of the CTA and NCCT was suboptimal, we performed manual registration.

Thrombus length was measured manually using the ITK-SNAP ruler function [22]. If contrast pick-up distal to the thrombus was not seen on CTA, the hyperdense artery sign on NCCT was used as a reference point for the distal thrombus end. If the thrombus extended into two arterial branches, the longest thrombus length was included as measurement. Thrombus perviousness and density were computed from three regions of interests (ROIs). On the co-registered NCCT and CTA images, three spherical ROIs with a 1mm radius were placed in the proximal, middle, and distal parts of the thrombus. Thrombus density was defined as the mean density of these ROIs on NCCT, in Hounsfield Units (HU). Thrombus perviousness was computed by subtracting the mean density of the ROIs on NCCT from the mean density of the ROIs on CTA, resulting in the average thrombus attenuation increase in HU (thrombus perviousness = $\rho CTA - \rho NCCT$).

Collateral score [23], occlusion location, and the Alberta Stroke Program Early CT Score were assessed on baseline CTA and NCCT by the MR CLEAN Registry core laboratory [19].

Statistical Analysis

The dependent variables were thrombus length (mm), perviousness, and density (HU). The independent variable of interest was time from symptom onset or last seen well to imaging per 5 min. Imaging time was defined as the acquisition time of the NCCT images. Baseline characteristics were summarized appropriately

to the type of data. Comparisons were made by one-way ANOVA, Kruskal-Wallis, Mann-Whitney-U, or Fisher's exact-test appropriate to the type of data. Visual representations of the data were made with scatter and bar plots.

Univariable and multivariable linear regression were used to assess the association between onset to imaging time and thrombus length, perviousness, and density, resulting in beta coefficients (β) with 95% confidence intervals (95% CI). The multivariable models were adjusted for the following baseline pre-specified variables: age, sex, history of atrial fibrillation, IVT administration, and antiplatelets. Model 2 was additionally adjusted for: observed stroke vs. non-observed stroke, CTA collateral score, transfer or direct presentation at a comprehensive stroke center, and stroke etiology according to the modified Trial of ORG 10172 in Acute Stroke Treatment (TOAST) criteria (cardio-embolic vs. large artery atherosclerosis vs. unknown). The TOAST criteria were scored for a previous study on our data set [15]. Because thrombus length and perviousness showed a right-skewed distribution, they were log-transformed for the regression analyses (Supplementary Figure 1).

Exploratory sensitivity analyses were performed by comparing the results of univariable models for different subgroups: (a) patients with observed stroke onset vs. patients without observed stroke onset (using last-seen-well time as onset time), (b) patients with vs. without IVT administration prior to EVT, (c) patients with collateral score 0–1 vs. patients with CS 2–3, (d) transfer patients vs. direct presentation to a comprehensive stroke center, (e) patients with different stroke etiologies: cardioembolic stroke, large-artery atherosclerotic stroke and stroke with an undetermined origin.

Missing data in the main and secondary variables of interest were imputed using multiple imputation for regression analyses only, based on relevant covariates and outcomes. A two-sided p-value of 0.05 was considered significant. Statistical analyses were performed with Stata/SE 14.2 (StataCorp, TX).

Results

The total MR CLEAN Registry part I population consisted of 1,627 patients, of whom 825 had an M1 occlusion. We included 245 patients in the current study (Supplementary Figure 2 and Table 3.1). Of these, 90 patients were transferred from a primary to a comprehensive center for EVT. We measured radiological thrombus characteristics on images acquired in the primary center for 44 of these patients. Baseline characteristics of our study population were similar to the overall MR CLEAN Registry population with an M1 occlusion except for a lower frequency of patients transferred from a primary stroke center [90/245 (36%) vs. 441/825 (53%), p < 0.01]. The median time from stroke onset to imaging was 83 (IQR 53–141) min. Median thrombus length was 12 (IQR 9–16) mm, median perviousness was 5 (IQR 0.1–11) HU, and median density was 52 (IQR 46–58) HU (Figures 3.1A–D). Figures 3.1E–G show the values of onset to imaging time in relation to thrombus length, thrombus perviousness, and thrombus density for all patients.

The regression coefficients of the association of onset-to-imaging time and thrombus length, perviousness, or density are presented in Table 3.2. None of these associations were statistically significant, except for a positive association for thrombus density in the adjusted Model 2 (β 0.10; 95% CI 0.005–0.20 HU/5min, Table 3.2). The sensitivity analyses showed no statistically significant associations for thrombus length, perviousness, or density in any of the subgroups (Supplementary Tables 1–4 and Supplementary Figures 3–7), except for a significantly positive relation between onset-to-imaging time and thrombus density in patients transferred for EVT from a primary stroke center (n = 90) in the adjusted Model 2 only (β 0.18; 95%CI 0.022–0.35 HU/5min, Supplementary Table 4). Patients who were transferred from a primary center had longer median onset to imaging times (median 137min, IQR 65–181) than those presented directly to a comprehensive center (median 69min, IQR 48–103, p < 0.01). In addition, among IVT-treated transferred patients (n = 77), median onset-to-imaging times were shorter among patients whose thrombus characteristics were measured on images acquired in the primary stroke center (n = 36; 67 min, IQR 56–100), as compared to the comprehensive stroke center (n = 41, 175 min, IQR 138–197; p < 0.01).

Nonetheless, the longer time for IVT to work did not affect the association between onset-to-imaging time and thrombus characteristics (Supplementary Table 4).

Table 3.1: *Baseline characteristics of patients included in the current study, compared to all MR CLEAN Registry patients with an M1 occlusion.*

	Current study (n=245)	MR CLEAN Registry patients with M1 occlusion (n=825)	P
Baseline clinical variables (data known in [n])			
Age, median (IQR)	69 (61-80)	72 (61-80)	0.57
Sex (male), n(%)	127 (52)	423 (51)	0.89
NIHSS baseline, median (IQR)	15 (11-20) [243]	16 (11-19) [811]	0.85
SBP (mmHG), median (IQR)	148 (130-162) [238]	150 (131-165) [803]	0.29
Medical history, n. (%)			
Diabetes mellitus	45 (19) [242]	151 (18) [820]	0.93
..Previous stroke	37 (15) [242]	152 (19) [820]	0.29
Atrial fibrillation	48 (20) [240]	195 (24) [812]	0.22
Pre-stroke mRS, n (%)			0.45
0-2	204 (85) [240]	707 (86) [814]	
≥3	36 (15) [240]	107 (14) [814]	
Workflow (data known in [n])			
Observed onset time, n (%)	187 (76)	618 (75)	0.67
Intravenous alteplase, n (%)	188 (77)	637 (78)	0.86
Transferred from primary stroke center*, n (%)	90 (36)	441 (53)	<0.01
Time from onset to presentation at first hospital, minutes, median (IQR)	55 (40-92) [200]	55 (39-93) [640]	0.87
Time from onset to imaging$^\$$, minutes, median (IQR)	83 (53-141)	69 (51-106) [733]	0.62

(Continued)

Table 3.1: Continued

Imaging variable (data known in [n])			
ASPECTS subgroups, n (%)			0.47
0-4	9 (4)	46 (6)	
5-7	56 (23)	186 (23)	
8-10	180 (73)	571 (71)	
Collateral score, n (%) [known in]			0.95
0	16 (7) [240]	48 (6)	
1	72 (30) [240]	252 (31)	
2	97 (40) [240]	323 (40)	
3	55 (23) [240]	179 (22)	
Extracranial carotid tandem lesion#	28 (11) [192]	136 (16) [689]	
Thrombus length, mm, median (IQR)	12 (9-16)	NA	NA
NCCT thrombus density, HU, median (IQR)	52 (46-58)	NA	NA
Thrombus perviousness, attenuation increase, HU, median (IQR)	5 (0.1-11)	NA3	NA

ASPECTS, Alberta Stroke Program Early CT Score; CTA, CT-angiography; IQR, interquartile range; HU, Hounsfield Units; mRS, modified Rankin Scale; NA, not applicable; NCCT, non-contrast CT, NIHSS, National Institutes of Health Stroke Scale; SBP, systolic blood pressure. If no [known in] number is shown, data were available for all included patients.

*Images from the primary stroke center were used in 44/90 transfer patients (49%).

$In current study sample: time of imaging used for measurements. In all Registry M1 occlusion patients: time of first acquired imaging.

#Tandem lesion was defined as an atherosclerotic occlusion, high-grade stenosis, or dissection ipsilateral to the intracranial occlusion, as assessed on baseline CT angiography.

Influence of onset to imaging time on thrombus characteristics
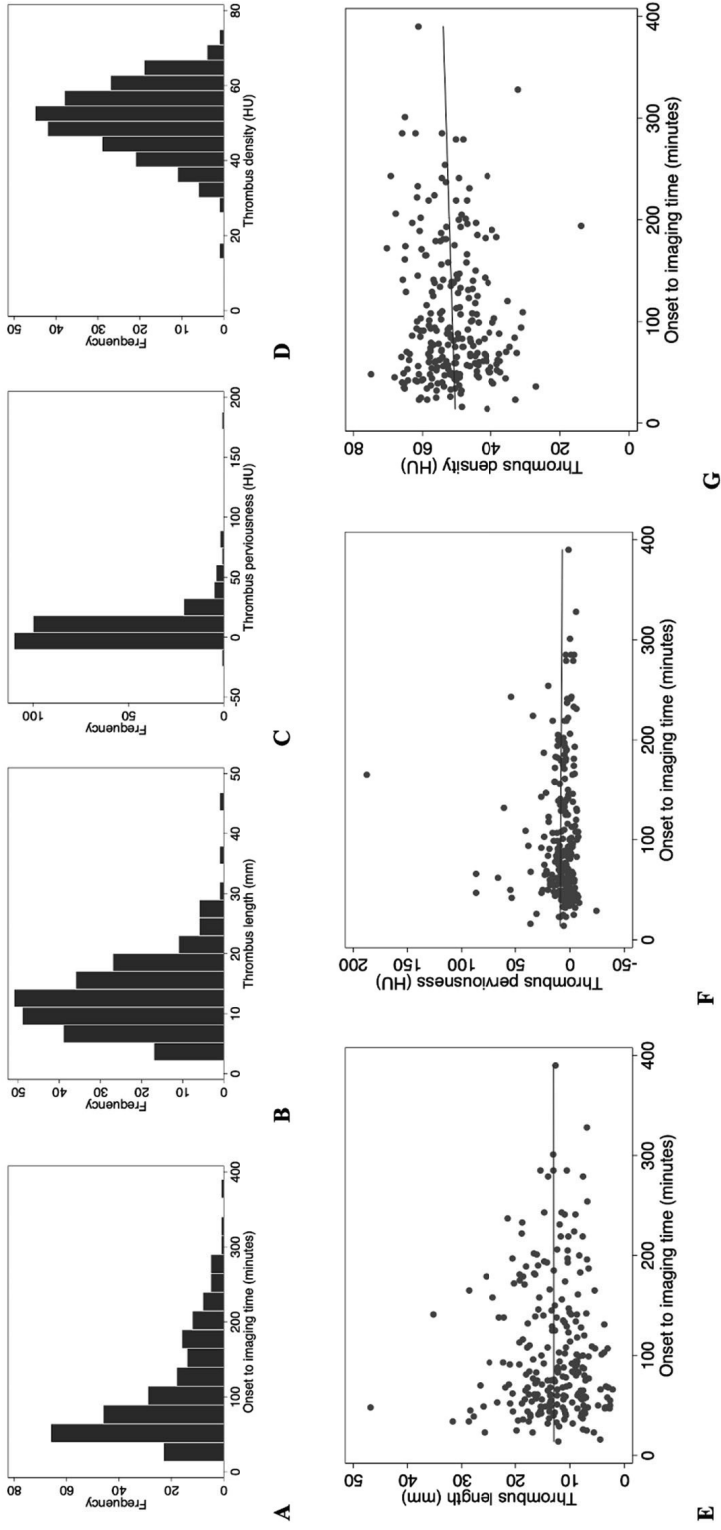
Figure 3.1: Scatter and box plots of image characteristics. (A) Time from symptom onset to imaging distribution, (B) thrombus length histogram, (C) thrombus perviousness histogram, (D) thrombus density histogram, (E) onset to imaging time versus thrombus length, (F) onset to imaging time versus perviousness, (G) onset to imaging time versus non-contrast CT density. HU, Hounsfield Units; mm, millimeter.

Table 3.2: beta coefficients of the effect of time from stroke onset to CT imaging (per 5 minutes) on thrombus characteristics.

	Model 0 Unadjusted		Model 1 Adjusted for pre-specified variables *		Model 2 Adjusted for pre-specified variables* + variables of interest#	
Outcome variable						
	β	95% CI	β	95% CI	β	95% CI
Thrombus length	0.002	-0.002 to 0.007	0.003	-0.002 to 0.008	0.002	-0.004 to 0.007
Perviousness	-0.005	-0.012 to 0.011	-0.001	-0.012 to 0.012	-0.002	-0.015 to 0.011
Thrombus density	0.046	-0.036 to 0.129	0.047	-0.035 to 0.120	0.100	0.005 to 0.196

CI, confidence interval; ICA-T, internal carotid artery terminus.

*pre-specified variables: age, sex, and history of atrial fibrillation.

#variables of interest: observed stroke onset, intravenous alteplase, CTA collateral score, direct presentation at thrombectomy-capable center or transfer, stroke etiology (cardio-embolic versus large artery atherosclerosis versus unknown).

DISCUSSION

Our study showed no association between stroke-onset to imaging time and thrombus length, density and perviousness, suggesting that within the critical time window of treatment no observable changes occur. Thrombus density may slightly increase over time, which was visible in our data in patients transferred from a primary stroke center. Transferred patients had a longer median onset to imaging time, possibly allowing for a higher density difference to develop. This density increase could be caused by the contraction of the thrombus resulting in the compression of erythrocytes in a densely packed structure, though may also have been a chance finding [17]. Overall, however, the effects of thrombus contraction [16], [17], thrombus growth [9], and endogenous or alteplase-induced thrombolysis [10–13] seem to balance each other out in the time window we observed.

Only a small number of studies have been reported that focus on the influence of time on thrombus image characteristics. Qazi et al. [24] included onset to imaging time for the analysis of thrombus characteristics in patients with AIS. They

have studied the relation between collateral status and thrombus length. Similar to our study, onset-to-imaging time did not influence thrombus length. Also, Pikija et al. [25] have studied the relation of time with thrombus density. In contrast to our results, their results showed a drop in thrombus density within a 5-h time window for onset to imaging time. Finally, Haridy et al. [26] reported no association between the presence of a hyperdense artery sign (HAS) or relative thrombus density and onset to imaging time within a 24 h time window. Unfortunately, they did not specifically study the relation of time with thrombus density or perviousness. Therefore, we cannot directly compare our results with their study.

Since the assessment of the radiological thrombus characteristics addressed in this study is not part of current treatment decision making in clinical practice and is not included in the national or international stroke guidelines [27], our results do not give rise to changes in the standard clinical care for AIS. For research on radiological thrombus characteristics in relation to stroke treatment outcomes, our results indicate that the elapsed time from symptom onset is of limited influence on the values of these characteristics, and as such would not have to be taken into account in the time window that we investigated.

Our study has limitations. First, a selective group of patients was included. Our study population contained patients who underwent EVT and therefore included severe cases of stroke only. All patients were treated within a short time window since the onset to hospital time is relatively low due to the small surface area and high hospital density of the Netherlands [19], [28]. In addition, it is expected that the treatment window for EVT will be extended in the future, and onset to imaging time will be prolonged. Increased variation in time from stroke onset may make changes in radiological thrombus characteristics more pronounced [29]. In the overall Registry population, the proportion of transfer patients was higher than in our study sample. This may have contributed to our shorter median onset to imaging time: thin-slice CT scans are less often available for transferred patients, which was one of our inclusion criteria. Second, the dynamic behavior of thrombus size could not be assessed in a controlled environment; we combined data of a heterogeneous group of patients. To reduce the variability, we only selected

patients with an occlusion of the M1, though this resulted in a relatively small sample size. Third, thrombus measurements were performed on single-phase CTA. As such, results are dependent on the phase of the CTA. In case of stasis of blood flow and early CTA san timing, the contrast may not reach the exact proximal location of the thrombus, and contrast may not have reached the distal part of the thrombus. This may have resulted in an overestimation of thrombus length and lower perviousness values. Future implementation of multiphase CTA may resolve that issue [30]. Fourth, we tried to assess the dynamic behavior of thrombi on imaging made at a single point in time. Ideally, thrombus measurements would be performed at two moments in time in the same patient, to address individual rates of thrombus growth or shrinkage. By comparing thrombus characteristics in a large group of patients with varying onset-to-imaging times, we expected other factors influencing thrombus length to be approximately evenly distributed. Fifth, thrombi may be older than the duration of stroke symptoms, and hence be more organized than what one would expect based on the time from stroke onset to imaging. Cardiac thrombi for example may form and age in the heart, break loose, and embolize to cause a stroke [31], [32]. However, our results did not vary between stroke etiology subgroups. Sixth, apparent trends in the subgroup analyses may not have translated to statistically significant regression results due to the small number of patients in the subgroups. However, our effect estimates were close to zero and any trends found in the data visualization may have occurred due to chance. Finally, because we only included patients with an M1-occlusion to improve data homogeneity, we could not assess differences in thrombus location and length. Thrombi may contract over time in all directions, instead of only in length, thereby decreasing in diameter and embolizing to a more distal location. Further research with more observations in distal occlusion locations could focus on the association between onset-to-imaging time and the distance from the carotid terminus to the proximal thrombus border.

3

Conclusion

Our results did not show a clear association between onset to imaging time and radiological thrombus characteristics for AIS patients within the observed time window. Only thrombus density slightly increased with longer onset to imaging time intervals due to inter-hospital transfer. There was no association between time and thrombus perviousness or length. This suggests that elapsed time from stroke onset plays a limited role in the interpretation of radiological thrombus characteristics and their effect on treatment results, at least in the relatively short time window observed in this study.

References

[1]   E.M.M. Santos, J.W. Dankbaar, K.M. Treurniet, A.D. Horsch, Y.B. Roos, L.J. Kappelle, *et al.* "Permeable thrombi are associated with higher intravenous recombinant tissue-type plasminogen activator treatment success in patients with acute ischemic stroke." *Stroke.* 2016, vol. 47, pp. 2058–65. doi: 10.1161/STROKEAHA.116.013306

[2]   E.M.M. Santos, H.A. Marquering, M.D. den Blanken, O.A. Berkhemer, A.M.M. Boers, A.J. Yoo, *et al.* "Thrombus permeability is associated with improved functional outcome and recanalization in patients with ischemic stroke." *Stroke.* 2016, vol. 47, pp. 732–41. doi: 10.1161/STROKEAHA.115.011187

[3]   C.H. Riedel, P. Zimmermann, U. Jensen-Kondering, R. Stingele, G. Deuschl, O. Jansen, "The importance of size: successful recanalization by intravenous thrombolysis in acute anterior stroke depends on thrombus length." *Stroke.* 2011, vol. 42, pp.1775–7. doi: 10.1161/STROKEAHA.110.609693

[4]   B.G. Dutra, M.L. Tolhuisen, C.B.R.H. Alves, K.M. Treurniet, M. Kappelhof, A.J. Yoo, *et al.* "Thrombus imaging characteristics and outcomes in acute ischemic stroke patients undergoing endovascular treatment." *Stroke.* 2019, vol. 50, pp. 2057– 64. doi: 10.1161/STROKEAHA.118.024247

[5]   C. Weisstanner, P.P. Gratz, G. Schroth, R.K. Verma, A. Köchl, S. Jung, *et al.* "Thrombus imaging in acute stroke: correlation of thrombus length on

susceptibility-weighted imaging with endovascular reperfusion success." *Eur Radiol.* 2014, vol. 24 pp. 1735–41. doi: 10.1007/s00330-014-3200-3

[6]   F. Seker, J. Pfaff, M. Wolf, S. Schönenberger, S. Nagel, C. Herweh, *et al.* "Impact of thrombus length on recanalization and clinical outcome following mechanical thrombectomy in acute ischemic stroke." *J Neurointerv Surg.* 2017, vol. 9, pp. 937– 9. doi: 10.1136/neurintsurg-2016-012591

[7]   P. Moftakhar, J.D. English, D.L. Cooke, W.T. Kim, C. Stout, W.S. Smith, *et al.* "Density of thrombus on admission CT predicts revascularization efficacy in large vessel occlusion acute ischemic stroke." *Stroke.* 2013, vol. 44, pp. 243– 6. doi: 10.1161/STROKEAHA.112.674127

[8]   M. Mokin, S. Morr, S.K. Natarajan, N. Lin, K.V. Sneyder, L.N. Hopkins, *et al.* "Thrombus density predicts successful recanalization with Solitaire stent retriever thrombectomy in acute ischemic stroke." *J Neurointerv Surg.* 2015, vol. 7, pp. 104–7. doi: 10.1136/neurintsurg-2013-011017

[9]   S.F. de Meyer, T. Andersson, B. Baxter, M. Bendszus, P. Brouwer, W. Brinjikji, *et al.* "Analyses of thrombi in acute ischemic stroke: a consensus statement on current knowledge and future directions." *Int J Stroke.* 2017, vol. 12, pp. 606– 14. doi: 10.1177/1747493017709671

[10]   F. Docagne, J. Parcq, R. Lijnen, C. Ali, D. Vivien. "Understanding the functions of endogenous and exogenous tissue-type plasminogen activator during stroke." *Stroke.* 2015, vol. 46, pp. 314–20. doi: 10.1161/STROKEAHA.114.006698

[11]   J. Zhu, Y. Wan, H. Xu, Y. Wu, B. Hu, H. Jin. "The role of endogenous tissue-type plasminogen activator in neuronal survival after ischemic stroke: friend or foe?" *Cell Mol Life Sci.* 2019, vol. 76, pp. 1489–506. doi: 10.1007/s00018-019-03005-8

[12]   I.B. Kovacs, J. Yamamoto. "Spontaneous thrombolysis: a forgotten determinant of life or death." *Clin Appl Thromb.* 2006, vol. 12, pp. 358– 63. doi: 10.1177/1076029606291410

[13]   J. Minnerup, C. Kleinschnitz. "Visualization of clot composition in ischemic stroke: do we get what we see?" *Stroke.* 2011, vol. 42, pp. 1193–4. doi: 10.1161/STROKEAHA.110.612150

3

[14]   H.C. Alves, K.M. Treurniet, B.G. Dutra, I.G.H. Jansen, A.M.M. Boers, E.M.M. Santos, *et al.* "Associations between collateral status and thrombus characteristics and their impact in anterior circulation stroke." *Stroke.* 2018, vol. 49, pp. 391– 6. doi: 10.1161/STROKEAHA.117.019509

[15]   X. Ding, S. Yan, R. Zhang, M. Lou, Y. Zhou, S. Zhang. "Slow collateral flow is associated with thrombus extension in patients with acute large-artery occlusion." *Am J Neuroradiol.* 2018, vol. 39, pp. 1088–92. doi: 10.3174/ajnr.A5614

[16]   V. Tutwiler V, A.D. Peshkova, I.A. Andrianova, D.R. Khasanova, J.W. Weisel, R.I. Litvinov. "Contraction of blood clots is impaired in acute ischemic stroke." *Arterioscler Thromb Vasc Biol.* 2017, vol. 37, pp. 271–9. doi: 10.1161/ATVBAHA.116.308622

[17]   D.B. Cines, T. Lebedeva, C. Nagaswami, V. Hayes, W. Massefski, R.I. Litvinov, *et al.* "Clot contraction: compression of erythrocytes into tightly packed polyhedra and redistribution of platelets and fibrin." *Blood.* 2014, vol. 123, pp. 1596– 603. doi: 10.1182/blood-2013-08-523860

[18]   H. Kassem-Moussa, C. Graffagnino. "Nonocclusion and spontaneous recanalization rates in acute ischemic stroke." *Arch Neurol.* 2002, vol. 59, pp. 1870. doi: 10.1001/archneur.59.12.1870

[19]   I.G.H. Jansen, J.H.L.M. Mulder, R.J.B. Goldhoorn. "Endovascular treatment for acute ischaemic stroke in routine clinical practice: prospective, observational cohort study (MR CLEAN Registry)." *BMJ.* 2018, vol.360m pp. k949. doi: 10.1136/bmj.k949

[20]   O.A. Berkhemer, P.S.S. Fransen, D. Beumer, L.A. van den Berg, H.F. Lingsma, A.J. Yoo, *et al.* "A randomized trial of intraarterial treatment for acute ischemic stroke." *NEngl JMed.* 2014, vol. 372, pp.11–20. doi: 10.1056/NEJMoa1411587

[21]   S. Klein, M. Staring, K. Murphy, M.A. Viergever, J.P.W. Pluim. "Elastix: a toolbox for intensity-based medical image registration." *IEEE Trans Med Imaging.* 2010, vol. 29, pp.196–205. doi: 10.1109/TMI.2009.2035616

[22]   P.A. Yushkevich, J. Piven, H.C. Hazlett, R.G. Smith, S. Ho, J.C. Gee, *et al.* "User-guided 3D active contour segmentation of anatomical structures: significantly

improved efficiency and reliability." *Neuroimage.* 2006, vol. 31, pp.1116– 28. doi: 10.1016/j.neuroimage.2006.01.015

[23]   I.Y.L. Tan, A.M. Demchuk, J. Hopyan, L. Zhang, D. Gladstone, K. Wong, *et al.* "CT angiography clot burden score and collateral score: correlation with clinical and radiologic outcomes in acute middle cerebral artery infarct." *AJNR.* 2009 vol. 30, pp. 525–31. doi: 10.3174/ajnr.A1408

[24]   E.M. Qazi, S.I. Sohn, S. Mishra, M.A. Almekhlafi, M. Eesa, C.D. d'Esterre, *et al.* "Thrombus characteristics are related to collaterals and angioarchitecture in acute stroke." *Can J Neurol Sci.* 2015, vol. 42, pp. 381–8. doi: 10.1017/cjn.2015.291

[25]   S. Pikija, J. Magdic, V. Trkulja, P. Underkreuter, J.S. Mutzenbach, H.F. Novak, *et al.* "Intracranial thrombus morphology and composition undergoes time-dependent changes in acute ischemic stroke: a CT densitometry study." *Int J Mol Sci.* 2016, vol. 17, pp. 1–12. doi: 10.3390/ijms17111959

[26]   J. Haridy, L. Churilov, P. Mitchell, R. Dowling, B. Yan. "Is there association between hyperdense middle cerebral artery sign on CT scan and time from stroke onset within the first 24-hours?" *BMC Neurol.* 2015, vol. 15, pp. 1– 6. doi: 10.1186/s12883-015-0358-5

[27]   W.J. Powers, A.A. Rabinstein, T. Ackerson, O.M. Adeoye, N.C. Bambakidis, K. Becker, *et al.* "Guidelines for the early management of patients with acute ischemic stroke: 2019 update to the 2018 guidelines for the early management of acute ischemic stroke a guideline for healthcare professionals from the American Heart Association/American Stroke A." *Stroke.* 2019, vol. 50, pp. e344– 418. doi: 10.1161/STR.0000000000000211

[28]   M. Goyal, B.K. Menon, W.H. van Zwam, D.W.J. Dippel, P.J. Mitchell, A.M. Demchuk, *et al.* "Endovascular thrombectomy after large-vessel ischaemic stroke: a meta-analysis of individual patient data from five randomised trials." *Lancet.* 2016, vol. 387, pp. 1723–31. doi: 10.1016/S0140-6736(16)00163-X

[29]   K. Kirchhof, T. Welzel, C. Mecke, S. Zoubaa, K. Sartor. "Differentiation of white, mixed, and red thrombi: value of CT in estimation of the prognosis of

3

thrombolysis phantom study." *Radiology.* 2003, vol. 228, pp. 126– 30. doi: 10.1148/radiol.2273020530

[30]   E.M.M. Santos, C.D. d'Esterre, K.M. Treurniet, W.J. Niessen, M. Najm, M. Goyal, *et al.* "Added value of multiphase CTA imaging for thrombus perviousness assessment." *Neuroradiology.* 2018, vol. 60, pp. 71–9. doi: 10.1007/s00234-017-1907-y

[31]   J.H. Heo, H.S. Nam, Y.D. Kim, J.K. Choi, B.M. Kim, D.J. Kim, *et al.* "Pathophysiologic and therapeutic perspectives based on thrombus histology in stroke. J Stroke." 2020, vol. 22, pp. 64–75. doi: 10.5853/jos.2019.03440

[32]   V. Guglielmi, N.E. LeCouffe, S.M. Zinkstok, K.C.J. Compagne, R. Eker, K.M. Treurniet, *et al.* "Collateral circulation and outcome in atherosclerotic versus cardioembolic cerebral large vessel occlusion." *Stroke.* 2019, vol. 50, pp. 3360–8. doi: 10.1161/STROKEAHA.119.026299

Supplementary materials:

3

Chapter 4
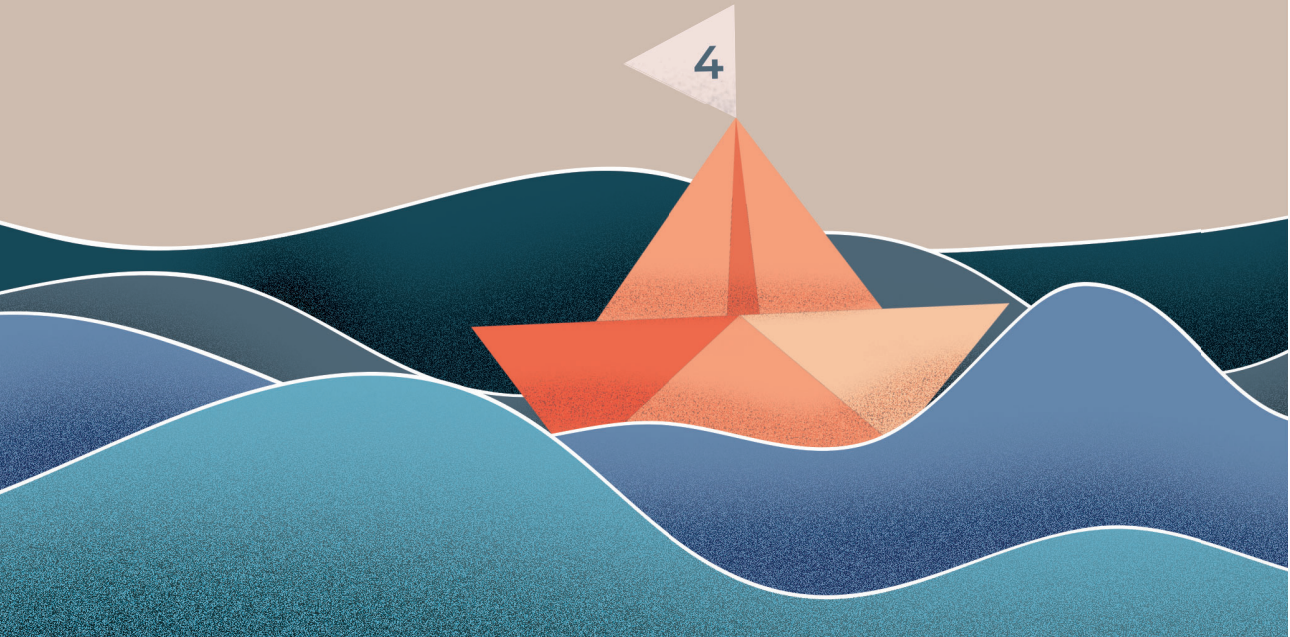
Thrombus imaging characteristics and outcome in acute ischemic stroke patients undergoing endovascular treatment

B.G. Dutra*, M.L. Tolhuisen*, H.C.B.R. Alves, K.M. Treurniet, M. Kappelhof, A.J. Yoo, I.G.H. Jansen, D.W.J. Dippel, W.H. van Zwam, R.J. van Oostenbrugge, A.J. de Rocha, H.F. Lingsma, A. van der Lugt, Y.B.W.E.M. Roos, H.A. Marquering and C.B.L.M. Majoie on behalf of the MR CLEAN Registry Investigators

Abstract

Background— Thrombus imaging characteristics have been reported to be useful to predict functional outcome and reperfusion in acute ischemic stroke. However, conflicting data about this subject exist in patients undergoing endovascular treatment. Therefore, we aimed to evaluate whether thrombus imaging characteristics assessed on computed tomography are associated with outcomes in patients with acute ischemic stroke treated by endovascular treatment.

Methods— The MR CLEAN (Multicenter Randomized Clinical Trial of Endovascular Treatment for Acute Ischemic Stroke in the Netherlands) Registry is an ongoing, prospective, and observational study in all centers performing endovascular treatment in the Netherlands. We evaluated associations of thrombus imaging characteristics with the functional outcome (modified Rankin Scale at 90 days), mortality, reperfusion, duration of endovascular treatment, and symptomatic intracranial hemorrhage using univariable and multivariable regression models. Thrombus characteristics included location, clot burden score (CBS), length, relative and absolute attenuation, perviousness, and distance from the internal carotid artery terminus to the thrombus. All characteristics were assessed on thin-slice (≤2.5 mm) non-contrast computed tomography and computed tomography angiography, acquired within 30 minutes from each other.

Results— In total, 408 patients were analyzed. Thrombi with a distal location, higher CBS, and shorter length were associated with better functional outcome (adjusted common odds ratio, 3.3; 95% CI, 2.0 to 5.3 for distal M1 occlusion compared with internal carotid artery occlusion; adjusted common odds ratio, 1.15; 95% CI, 1.07 to 1.24 per CBS point; and adjusted common odds ratio, 0.96; 95% CI, 0.94 to 0.99 per mm, respectively) and reduced duration of endovascular procedure (adjusted coefficient B, −14.7; 95% CI, −24.2 to −5.1 for distal M1 occlusion compared with internal carotid artery occlusion; adjusted coefficient B, −8.5; 95% CI, −14.5 to −2.4 per CBS point; and adjusted coefficient B, 7.3; 95% CI, 2.9 to 11.8 per mm, respectively). Thrombus perviousness was associated with better functional outcome (adjusted common odds ratio, 1.01; 95% CI, 1.00 to 1.02 per Hounsfield

units increase). Distal thrombi were associated with successful reperfusion (adjusted odds ratio, 2.6; 95% CI, 1.4 to 4.9 for proximal M1 occlusion compared with internal carotid artery occlusion).

Conclusion— Distal location, higher CBS, and shorter length are associated with better functional outcome and faster endovascular procedure. Distal thrombus is strongly associated with successful reperfusion, and a pervious thrombus is associated with better functional outcome.

Introduction

Thrombus location is the only thrombus imaging characteristic currently evaluated in the assessment of patients with acute ischemic stroke (AIS) in daily practice [1,2]. However, recent studies have reported other thrombus imaging characteristics that may be useful for predicting functional outcome and reperfusion in AIS [3–6]. Associations between thrombus imaging characteristics and these outcomes have been evaluated primarily in patients undergoing intravenous thrombolysis (IVT) [3],[6–9]. Conflicting data exist about the associations between thrombus characteristics and outcomes after endovascular treatment (EVT) of AIS.

Because EVT has emerged as the mainstay of treatment for AIS because of proximal intracranial occlusions, the identification of imaging biomarkers that predict EVT outcomes would be highly relevant to acute stroke management. The present study aims to evaluate the associations between thrombus imaging characteristics and outcomes in patients undergoing EVT in the MR CLEAN (Multicenter Randomized Clinical Trial of Endovascular Treatment for Acute Ischemic Stroke in the Netherlands) Registry.

Materials and methods

Patient selection

The MR CLEAN Registry is an ongoing, prospective, observational, multicenter study at 16 intervention hospitals in the Netherlands. It includes all patients with AIS who underwent EVT since the completion of the MR CLEAN trial in March

2014. Patients were treated with IVT before EVT if eligible. The central medical ethics committee of the Erasmus Medical Centre Rotterdam, the Netherlands, evaluated the study protocol and granted permission (MEC-2014–235) to perform the study as a registry [10]. For the purpose of this analysis, we used the following inclusion criteria: intracranial proximal occlusion in the anterior arterial circulation; age ≥18 years; groin puncture within 6.5 hours after stroke onset; and treatment in an MR CLEAN trial center. The current study reports on patients registered in the MR CLEAN Registry between March 2014 and June 2016. Source data of this study are available from the corresponding author on reasonable request.

Image analysis

Patients underwent the MR CLEAN Registry imaging protocol (Methods I in the online-only Data Supplement). We included patients with available thin-slice (≤2.5 mm) baseline non-contrast computed tomography (NCCT) and computed tomography angiography (CTA), acquired within 30 minutes from each other. All baseline NCCT and CTA scans were automatically aligned using rigid registration with Elastix software.[11] In case of suboptimal alignment, adjustments were performed by manual rigid registration, with Mevislab (by Dr. Dutra). Scans with uncorrectable registration errors, artifacts, excessive noise, or poor contrast opacification on CTA were excluded. To prevent bone artifacts that might interfere with the thrombus attenuation measurements, we excluded patients with an intracranial arterial occlusion restricted to the petrous, cavernous, and clinoid segments of the internal carotid artery (ICA). Calcified thrombi were also excluded because of their higher attenuation values (related to calcium composition) compared with the attenuation values of non-calcified thrombi, and because calcification produces streak and partial volume artifacts, which can cause overestimation of the thrombus size.

We evaluated the following thrombus imaging characteristics: location, clot burden score (CBS), absolute and relative attenuation, perviousness, length, and distance from the ICA terminus to the thrombus (DT). The observers were blinded for all clinical data except for symptom side. The assessments of thrombus imaging

characteristics are detailed in the online-only Data Supplement (Methods II and Figures I and II in the online-only Data Supplement).

Outcome measures

The primary outcome was defined as the modified Rankin Scale (mRS) score at 90 days. The mRS is a 7-point scale ranging from 0 (no symptoms) to 6 (death). Secondary outcomes were good functional outcome (score of 0 to 2 on the mRS), mortality at 90 days, reperfusion status assessed on digital subtraction angiography according to the extended Thrombolysis in Cerebral Infarction (eTICI) score,[12] duration of EVT, and symptomatic intracranial hemorrhage (sICH). The eTICI score was assessed by the MR CLEAN Registry imaging core lab, based on the degree of reperfusion in the downstream territory of the original occlusion on digital subtraction angiography. The eTICI score ranges from 0 (no reperfusion or antegrade flow beyond occlusion site) to 3 (complete reperfusion), including a 2C category (90% to 99% reperfusion) [12],[13]. Successful reperfusion status was defined as eTICI scores of 2b, 2c, or 3.

Duration of EVT was determined in patients who underwent an actual thrombectomy, and this outcome was measured from artery puncture (time zero) to the time that successful reperfusion was achieved or to the end of procedure if no successful reperfusion was achieved. The following patients were not considered in the assessments of duration of EVT: no target occlusion depicted on digital subtraction angiography (recanalization of primary occlusion on the first run), or unreachable target occlusion (i.e. due to vascular tortuosity, stenosis, or occlusion of the carotid artery).

Statistical analysis

Subject characteristics

We present the baseline clinical and imaging characteristics of our study population and of the full published MR CLEAN Registry data set [10] using median and interquartile range (IQR) for continuous variables and frequencies and

percentages for categorical variables. A correlation chart was performed to summarize the data about the distribution of each thrombus imaging characteristic, and to investigate whether thrombus imaging characteristics are correlated to each other, using the Spearman correlation coefficient for non-normally distributed data and the Pearson correlation coefficient for normally distributed data.

Associations between thrombus imaging characteristics and outcomes

Univariable and multivariable regression models were used to evaluate the association between thrombus imaging characteristics and outcomes. Ordinal logistic regression was used to assess the associations between thrombus characteristics and mRS as primary outcome measurement, resulting in an unadjusted and adjusted common odds ratio (common OR and adjusted common OR, respectively) for a 1-step shift towards better functional outcome. Unadjusted and adjusted binary logistic regression models were used to assess the associations with good functional outcome, successful reperfusion, mortality, and sICH as secondary outcomes. Unadjusted and adjusted linear regressions were performed to evaluate the associations with a duration of EVT as a secondary outcome measurement. We adjusted for age, pre-stroke mRS, time from stroke onset to artery puncture, IVT, diabetes mellitus, previous myocardial infarction, previous stroke, hypertension, and atrial fibrillation. Use of anticoagulants and antiplatelet agents was added to the adjustments for the analyses with reperfusion status, duration of EVT, and sICH as outcome measurements. In developing the multivariable model, we did not consider Alberta Stroke Program Early CT Score, baseline National Institutes of Health Stroke Scale score, and collaterals as potential confounders because we assumed they were in the causal pathway between thrombus and outcomes, as the following: proximal arterial thrombi (low CBS, short DT, and longer thrombus length) are hypothesized to cause impaired collateral filling [14],[15] and greater areas of hypodensity on NCCT, consequently leading to a lower Alberta Stroke Program Early CT Score, higher severity stroke score scale (National Institutes of Health Stroke Scale score), [16] poorer functional

outcome and higher chances of sICH. Interaction terms between primary treatment modalities and thrombus burden (CBS and length) were performed for the achieved outcomes.

All statistical analyses were performed using R (R Foundation for Statistical Computing, version 3.5.1). For the regression analyses, missing data were imputed using multiple imputation [17]. Missing mRS scores at 90 days or mRS scores of 0–5 assessed at <30 days from stroke were imputed. We performed multiple imputation using the variables listed in the online-only Data Supplement (Table I in the online-only Data Supplement).

Results

Subject characteristics

Overall, 408 patients were included in our analysis (Figure 4.1). The median age was 70 years (IQR, 59 to 80), 54% (n=222) were male, and the median National Institutes of Health Stroke Scale score was 16 (IQR, 11 to 20). Of all patients eligible for EVT, 87% (n=356/408) underwent EVT with thrombus retrieval, and the most used primary treatment modality was the stent retriever (75%). The median duration of EVT was 62 minutes (IQR, 44 to 90 minutes). Thrombus location was the most commonly distal M1 (36%) followed by ICA (25%), and proximal M1 (24%). CBS of 8 to 10 was observed in 29% of patients (n=102/353). Median values of thrombus length, DT, absolute attenuation, relative attenuation, and perviousness were 12.7 mm (IQR, 8.7 to 17.9 mm), 8.3 mm (IQR, 0 to 14.4 mm), 51.8 Hounsfield units (HU; IQR 45 to 58 HU), 1.33 (IQR, 1.19 to 1.52), and 5 HU (–0.2 to 12.3 HU). IVT was administered in 77% of patients (n=314). Baseline characteristics in our cohort were similar to the full MR CLEAN Registry data set [10] (Table 4.1).

Results of data distribution and correlation analyses among thrombus characteristics are detailed in the online-only Data Supplement (Figure III in the online-only Data Supplement). Longer thrombi were statistically correlated with shorter DT, more proximal location, lower CBS, lower perviousness, and higher

absolute attenuation (correlation coefficients of –0.44, –0.45, –0.53, –0.23, and +0.35, respectively).
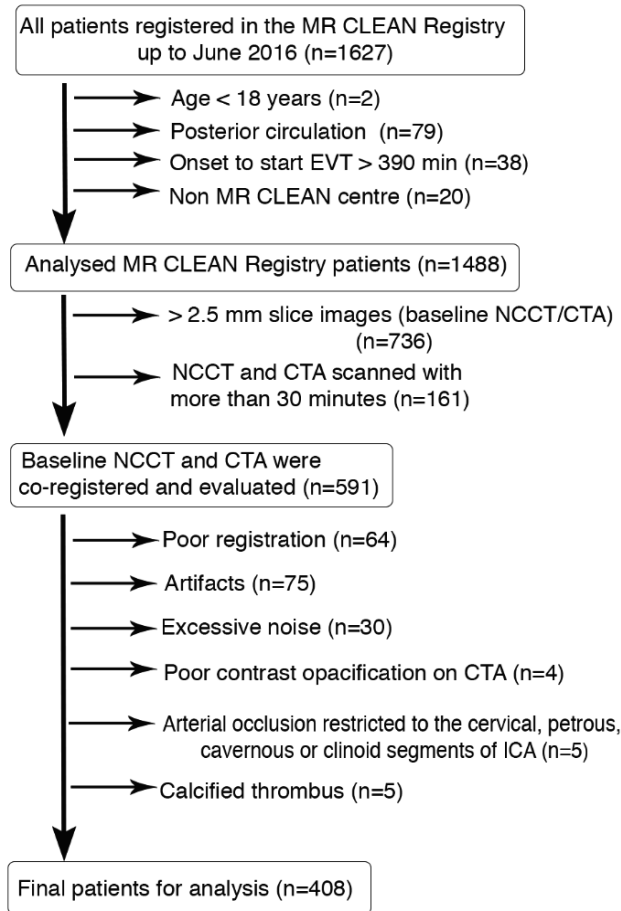
Figure 4.1: *Flow chart of the patient selection process. CTA indicates angiography tomography; EVT, endovascular treatment; ICA, internal carotid artery; MR CLEAN, Multicenter Randomized Clinical Trial of Endovascular Treatment for Acute Ischemic Stroke in the Netherlands; and NCCT, non-contrast computed tomography.*

Associations between thrombus image characteristics and outcomes

Primary outcome

More distal thrombus location and higher CBS values were significantly associated with improved functional outcome in the unadjusted and adjusted models. Thrombus located in the distal M1 segment had an increased odds of having improved functional outcome compared to ICA thrombus (adjusted common OR, 3.27; 95% CI, 2.03 to 5.29). Unadjusted and adjusted common ORs per point CBS were 1.12 (95% CI, 1.04 to 1.20) and 1.15 (95% CI, 1.07 to 1.24). A longer thrombus was associated with a reduced likelihood of improved functional out-come (adjusted common OR, 0.96; 95% CI, 0.94 to 0.99 per mm). An increased chance of improved functional outcome was observed in a more pervious thrombus (adjusted common OR, 1.01; 95% CI, 1.00 to 1.02 per HU increase) in the adjusted analyses (Table 4.2).

Secondary outcomes

Favorable functional outcome (mRS score of 0 to 2)

Favorable functional outcome was observed in 38% of patients (n=155). Associations between thrombus imaging characteristics and dichotomized functional outcome (mRS score of 0 to 2) were similar to the primary functional outcome analyses, as listed in Table 4.2. A statistically significant interaction was observed between CBS and primary EVT modality. For higher CBS, patients treated with stent-retriever had increased chances of having favorable functional outcome compared with other EVT modalities (Figure IV in the online-only Data Supplement). No statistically significant interaction was observed between thrombus length and primary treatment modality.

Mortality at 90 days

Death at 90 days was observed in 26.2% of patients (n=107). This outcome was significantly associated with more proximally located thrombi (adjusted OR [aOR], 0.29; 95% CI, 0.14 to 0.61 for proximal M1 thrombi compared with ICA

occlusions), lower CBS (aOR, 0.85; 95% CI, 0.77 to 0.95), and longer thrombus length (aOR, 1.04; 95% CI, 1.01 to 1.07), as detailed in Table 4.2.

Reperfusion status

In patients who underwent thrombectomy, successful reperfusion was achieved in 60% (n=215/356). Only site of occlusion was significantly associated with successful reperfusion (Table 4.3). Proximal and distal M1 thrombi were associated with an increased likelihood of successful reperfusion compared with ICA thrombi (aOR, 2.60; 95% CI, 1.42 to 4.97 for proximal M1 thrombi and aOR, 1.96; 95% CI, 1.14 to 3.44 for distal M1 thrombi). No significant associations were observed between reperfusion and thrombus location in M2 or other segments. However, a trend towards an increased chance of successful reperfusion with a more distal thrombus location was observed.

Duration of endovascular procedure

Duration of EVT was significantly associated with thrombus location, CBS, and thrombus length (Table 4.3). Endovascular procedure was 14 to 15 minutes faster for distal M1 occlusions compared with ICA occlusions (adjusted coefficient B, −14.7; 95% CI, −24.2 to −5.1). For each 1 mm increase in thrombus length, there was an increase of ≈7 to 8 minutes in EVT duration (adjusted coefficient B, 7.3; 95% CI, 2.9 to 11.8). An increase of 1 point in CBS was associated with a reduction of ≈8 to 9 minutes of the duration of EVT (adjusted coefficient B, −8.5; 95% CI, −14.5 to −2.4).

Symptomatic intracranial hemorrhage

No significant associations were observed between thrombus imaging characteristics and sICH (Table 4.3).

Table 4.1: *Baseline characteristics of the Registry subgroup included in our study and of the MR CLEAN Registry dataset*

	MR CLEAN Registry subgroup included (n=408)	Full MR CLEAN Registry database (n=1488)
Baseline clinical variables		
Age, median (IQR)	70 (59–80); (n=408)	71 (60 to 80); (n=1488)
Sex (men), n. (%)	222 (54.4); (n=408)	794 (53.3); (n=1488)
NIHSS baseline, median (IQR)	16 (11 to 20); (n=398)	16 (11 to 20); (n=1458)
SBP (mm Hg), median (IQR)	149 (131 to 163); (n=397)	150 (125 to 175); (n=1446)
DBP (mm Hg), median (IQR)	80 (70 to 90); (n=396)	80 (70 to 91); (n=1439)
Medical history, n (%)		
Diabetes	75 (18.6); (n=404)	255 (17.2); (n=1479)
Hypertension	202 (50.4); (n=401)	745 (50.7); (n=1469)
Dyslipidemia	116 (29.1); (n=398)	431 (29.9); (n=1401)
Current smoking	97 (24); (n=404)	338 (22.9); (n=1474)
Previous stroke	63 (15.6); (n=404)	249 (16.8); (n=1479)
Previous myocardial infarction	73 (18.4); (n=397)	228 (15.6); (n=1459)
Previous atrial fibrillation	84 (20.9); (n=401)	327 (22.3); (n=1466)
Anticoagulation	131 (33); (n=395)	493 (33.6); (n=1457)
Pre-stroke modified Rankin Scale score, n (%)		
0	253/397 (63.7)	991/1461 (67.8)
1	52/397 (13.1)	189/1461 (12.9)
2	36/397 (9.1)	110/1461 (7.5)
≥ 3	56/397 (14.1)	171/1461 (11.7)
Pre-stroke modified Rankin Scale score, n (%)		
0	253/397 (63.7)	991/1461 (67.8)
1	52/397 (13.1)	189/1461 (12.9)
2	36/397 (9.1)	110/1461 (7.5)
≥ 3	56/397 (14.1)	171/1461 (11.7)

4

(Continued)

Table 4.1: *Continued*

	MR CLEAN Registry subgroup included (n=408)	Full MR CLEAN Registry database (n=1488)
Imaging variables		
ASPECTS subgroups, n (%)		
0-4	23/408 (5.6)	93/1488 (6.5)
5-7	101/408 (24.7)	341/1488 (24)
8-10	284/408 (69.6)	989/1488 (69.5)
Collateral score, n (%)		
0% filling of the occluded territory	32/397 (8.1)	97/1381 (7)
>0% and ≤50% filling of the occluded territory	127/397 (32.0)	461/1381 (33.3)
>50% and <100% filling of the occluded territory	158/397 (39.8)	535/1381 (38.7)
100% filling of the occluded territory	80/397 (20.2)	282/1381 (20.9)
Thrombus location, n (%);		
ICA	101/407 (24.8)	395/1422 (27.8)
Proximal M1	97/407 (23.8)	364/1422 (25.6)
Distal M1	148/407 (36.4)	462/1422 (32.4)
M2	51/407 (12.5)	175/1422 (12.3)
M3	4/407 (1.0)	9/1422 (0.6)
A1/A2	6/407 (1.4)	6/1422 (0.4)
Clot burden score, n (%);		
0-4	97/353 (27.5)	371/1238 (30)
5-7	154/353 (43.6)	510/1238 (41.2)
8-10	102/353 (28.9)	537/1238 (28.8)
DT, median (IQR)	8.3 (0 to 14.4)	NA
Thrombus length (mm), median (IQR)	12.75 (8.7 to 17.9); (n=408)	NA

(Continued)

Table 4.1: Continued

	MR CLEAN Registry subgroup included (n=408)	Full MR CLEAN Registry database (n=1488)
Imaging variables		
Thrombus absolute attenuation (HU), median (IQR)	51.8 (45 to 58); (n=408)	NA
Treatment variables		
Intravenous thrombolysis, n. (%)	314/408 (77)	1161/1488 (78.0)
Time to artery puncture, median (IQR)–minutes;	195 (150 to 251); (n=408)	208 (160 to 265); (n=1488)
Performed procedure, n. (%)		
EVT with thrombus retrieval	356/408 (87.3)	1280/1488 (86)
Target occlusion not accessible	21/408 (5.1)	80/1488 (5.4)
No target occlusion depicted on DSA	27/408 (6.6)	119/1488 (8)
Other (procedure ended before attempt)	4/408 (1)	80/1488 (5.4)
Primary treatment modality, n (%)	334/356 (93.8)	1220/1280 (95.3)
Stent retriever	252/334 (75.4)	969/1280 (79.4)
Aspiration device	65/334 (19.4)	207/1280 (17)
Local delivery of the thrombolytic agent	4/334 (1.2)	10/1280 (0.8)
Different approach	13/334 (3.8)	34/1220 (2.8)
Duration of EVT – median (IQR)–minutes;	62 (44 to 90); (n=319)	64 (40 to 90); (n=1331)

A1/A2 indicates occlusions in segment A1 or A2 of the anterior cerebral artery; ASPECTS, Alberta Stroke Program Early CT Score; DBP, diastolic blood pressure; DSA, digital subtraction angiography; DT, distance from the internal carotid artery terminus to the thrombus; EVT, endovascular treatment; HU, Hounsfield units; ICA, internal carotid artery; IQR, interquartile range; M1, segment M1 of the middle cerebral artery; M2, segment M2 of the middle cerebral artery; M3, segment M3 of the middle cerebral artery; MR CLEAN, Multicenter Randomized Clinical Trial of Endovascular Treatment for Acute Ischemic Stroke in the Netherlands; NA, not available; NIHSS, National Institutes of Health Stroke Scale; and SBP, systolic blood pressure.

Table 4.2: *Associations of Thrombus Imaging Characteristics With Functional Outcome (modified Rankin Scale) and Mortality at 90 days*

	Functional Outcome (mRS)							
	Ordinal Regression (Shift to Better Outcome)				Binary Regression (Good Outcome, mRS Score of 0-2)			
	Unadjusted Model		Adjusted Model*		Unadjusted Model		Adjusted Model	
	OR	95% CI	aOR	95% CI	B	95% CI	B	95% CI
Site of occlusion								
ICA	1 (Reference)		1 (Reference)		1 (Reference)		1 (Reference)	
Proximal M1	1.97†	1.20 to 3.24†	2.44†	1.44 to 4.13†	1.88†	1.03-3.41†	2.35†	1.21-4.57†
Distal M1	2.44†	1.55 to 3.86†	3.27†	2.03 to 5.29†	2.26†	1.30-3.89†	3.17†	1.72-5.85†
M2	1.52	0.82 to 2.82	2.13†	1.11 to 4.09†	1.49	0.72-3.08	2.29†	1.02-5.14†
Other‡	2.01	0.52 to 7.81	3.91	0.96 to 15.84	2.05	0.43-9.78	2.98	0.47-18.85
CBS	1.12†	1.04 to 1.20†	1.15†	1.07 to 1.24†	1.12†	1.03-1.21†	1.16†	1.06-1.28†
DT	1.00	0.98 to 1.02	1.01	0.99 to 1.03	1.00	0.98-1.02	1.01	0.99-1.04
Length	0.98	0.96 to 1.00	0.96†	0.94 to 0.99†	0.98	0.96-1.01	0.96†	0.93-0.99†
Perviousness	1.01	0.99 to 1.02	1.01†	1.00 to 1.02†	1.01	0.99-1.02	1.01	0.99-1.02
Absolute attenuation	1.02	0.99 to 1.03	1.01	0.98 to 1.02†	1.02	1.00-1.04	1.01	0.98-1.04
Relative attenuation	1.01	0.99 to 1.03	1.00	0.98 to 1.02	1.66	0.85-3.24	1.72	0.82-3.60

(Continued)

Table 4.2: *Continued*

	Mortality at 90 days			
	Binary regression (death)			
	Unadjusted Model		Adjusted Model*	
	OR	95% CI	aOR	95% CI
Site of occlusion				
ICA	1 (Reference)		1 (Reference)	
Proximal M1	0.44†	0.24—0.84†	0.29†	0.14—0.61†
Distal M1	0.35†	0.19—0.61†	0.19†	0.09—0.38†
M2	0.79	0.38—1.59	0.52	0.21—1.23
Other‡	0.63	0.08—3.11	0.21	0.01—2.30
CBS	0.91†	0.83—0.99†	0.85†	0.77—0.95†
DT	1.00	0.98—1.02	0.98	0.95—1.01
Length	1.01	0.98—1.04	1.04†	1.01—1.07†
Perviousness	1.00	0.99—1.01	0.99	0.98—1.01
Absolute attenuation	0.98	0.96—1.01	1.00	0.97—1.03
Relative attenuation	1.27	0.62—2.62	1.64	0.72—3.73

acOR indicates adjusted common odds ratio; aOR, adjusted odds ratio; CBS, clot burden score; cOR, common odds ratio; distal M1, distal M1 segment of middle cerebral artery; DT, distance from the internal carotid artery terminus to the thrombus; ICA, internal carotid artery; M2, M2 segment of middle cerebral artery; mRS, modified Rankin Scale at 90 d; proximal M1, proximal M1 segment of middle cerebral artery; and OR, odds ratio.

*Adjusted for: age; pre-stroke mRS; intravenous thrombolysis; time from onset to groin puncture; previous history of stroke, atrial fibrillation, hypertension, diabetes mellitus, and myocardial infarction.

†P value <0.05.

‡M3 segment of middle cerebral artery or anterior cerebral artery.

Table 4.3: Associations of Thrombus Imaging Characteristics With successful Reperfusion, Duration of EVT and sICH

	Functional Outcome (mRS)				Duration of EVT			
	Binary Regression				Linear Regression			
	Unadjusted Model		Adjusted Model*		Unadjusted Model		Adjusted Model*	
	OR	95% CI	aOR	95% CI	B	95% CI	B	95% CI
	Site of occlusion							
ICA	1 (Reference)		1 (Reference)		1 (Reference)		1(Reference)	
Proximal M1	2.37†	1.35 to 4.25†	2.60†	1.42 to 4.97†	-14.58†	-19.9 to -4.3†	-14.62†	-25.1 to -4.1†
Distal M1	1.87†	1.12 to 3.13†	1.96†	1.14 to 3.44†	-15.17†	-24.6 to -6.3†	-14.68†	-24.2 to -5.1†
M2	1.34	0.68 to 2.65	1.55	0.74 to 3.32	-16.58†	-29.9 to -3.2†	-10.86	-24.3 to 2.6
Other‡	1.47	0.30 to 7.79	0.87	0.13 to 5.63	-31.58†	-60.6 to -2.6†	-21.32	-52.8 to 10.2
CBS	1.05	0.97 to 1.13	1.05	0.97 to 1.14	-9.18†	-15.0 to -3.3†	-8.47†	-14.5 to -2.4†
DT	0.98	0.96 to 1.01	0.98	0.95 to 1.01	-4.57	-10.3 to 1.2	-3.17	-9.0 to 2.7
Length	0.98	0.96 to 1.01	0.97	0.94 to 1.01	8.20†	3.7 to 12.7†	7.33†	2.9 to 11.8†
Perviousness	0.99	0.98 to 1.01	0.99	0.98 to 1.01	-1.22	-4.1 to 1.7	-0.61	-3.6 to 2.4
Absolute attenuation	1.01	0.98 to 1.03	1.00	0.98 to 1.02	4.62	-0.2 to 9.6	3.25	-1.8 to 8.3
Relative attenuation	1.31	0.67 to 2.57	1.35	0.65 to 2.79	0.27	-4.0 to 4.6	0.86	-3.6 to 5.3

(Continued)

Table 4.3: *Continued*

	sICH			
	Binary regression			
	Unadjusted Model		Adjusted Model*	
	OR	95% CI	aOR	95% CI
Site of occlusion				
ICA	1 (Reference)		1 (Reference)	
Proximal M1	0.45	0.13—1.43	0.33	0.09—1.20
Distal M1	0.43†	0.15—1.25	0.32	0.10—1.02†
M2	0.42	0.08—2.00	0.38	0.07—1.98
Other‡	0.00	NA	0.00	NA
CBS	0.95	0.79—1.13†	0.92	0.76—1.12†
DT	098	0.91—1.06	0.99	0.90—1.08
Length	1.03	0.98—1.09	1.04	0.98—1.10
Perviousness	1.13	0.92—1.39	1.16	0.94—1.43
Absolute attenuation	1.01	0.99—1.03	1.01	0.99—1.03
Relative attenuation	0.91	0.21—4.04	0.84	0.16—4.25

aOR indicates adjusted odds ratio; B, regression coefficient B; CBS, clot burden score; distal M1, distal M1 segment of middle cerebral artery; DT, distance from the internal carotid artery terminus to the thrombus; EVT, endovascular treatment; ICA, internal carotid artery; M2, M2 segment of middle cerebral artery; proximal M1, proximal M1 segment of middle cerebral artery; OR, odds ratio; and sICH, symptomatic intracerebral hemorrhage.

*Adjusted for: age; pre-stroke mRS; intravenous thrombolysis; time from onset to groin puncture; use of anticoagulants and antiplatelet agents; previous history of stroke, atrial fibrillation, hypertension, diabetes mellitus, and myocardial infarction.

†P value <0.05.

‡M3 segment of middle cerebral artery or anterior cerebral artery.

functional

Discussion

In the MR CLEAN Registry, thrombus imaging characteristics are associated with outcomes after EVT. A lower thrombus burden (i.e. distal occlusion, shorter thrombus length, and higher CBS value) was associated with better functional outcome and faster endovascular procedure. A more pervious thrombus was also

associated with favorable functional outcome. Only site of thrombus occlusion was significantly associated with reperfusion, in which a distal thrombus had a higher chance of successful reperfusion. We also demonstrated that a shorter thrombus is more likely to have a distal location, higher CBS, increased perviousness, and lower attenuation.

Associations of thrombus imaging characteristics with functional outcome and recanalization are well-described in patients treated with IVT, in whom failed recanalization and worse functional outcome were associated with low CBS, proximal thrombus location, longer thrombus length, and lower perviousness [3],[6],[8],[9]. However, conflicting data about thrombus imaging characteristics and outcomes are observed in EVT. In accordance with our study, thrombi with a more distal location, shorter length, and higher CBS have been reported to be associated with improved functional outcome in patients who underwent EVT [6],[18–20]. Conversely, some studies reported no association between functional outcome and thrombus length after EVT, however, they included only MCA thrombi [21],[22]. In accordance with our study, longer endovascular procedural time has been associated with longer thrombus length [18]. The associations of thrombus characteristics with functional outcome and duration of EVT could be related to 2 possible mechanisms: (1) As demonstrated in our study, longer thrombi had a lower CBS and a more proximal location, and by virtue of their larger thrombus volume may simply be more difficult to retrieve, requiring more attempts and prolonging the procedural time, as shown previously [18],[23] and (2) ICA and proximal M1 occlusions may result in decreased collateral flow via the anterior cerebral artery pial vessels [14],[15] or lead to greater stroke volume because of the involvement of the lenticulostriate vessels, consequently leading to a higher NIHHS score and poor functional outcome [16],[24].

Conflicting data about the association of thrombus attenuation and perviousness with outcomes have been reported. Some studies have reported that successful reperfusion after EVT is more likely in hyperdense thrombi.[25],[26] However, other reports, as well as the 2 largest published cohorts of thrombus attenuation assessments, are in line with our findings, showing that thrombus

attenuation was not associated with reperfusion,[6],[21],[27],[28] functional outcome, duration of EVT and sICH.[21] Different results about thrombus attenuation assessment might be because of variability in hematocrit levels, vessel calcification, and time of CT scan acquisition.[29] Further studies need to be performed before concluding that thrombus density is a not predictor of successful reperfusion and to evaluate the utility of this parameter in thrombectomy planning.

Thrombus perviousness has been associated with successful recanalization and improved functional outcome after IVT.[3],[5],[19] We observed an association between improved functional outcome and more pervious thrombi, yet no significant association was observed between thrombus perviousness and reperfusion after EVT. Likewise, despite a trend towards an increased chance of successful reperfusion with a more distal thrombus location, we observed no significant association between reperfusion and thrombus located in M2 or more distal segment. The absence of a significant effect of both thrombus perviousness and thrombus located in M2 or more distal segment on reperfusion may share an explanation since pervious thrombus, and more distal thrombus location was reported to be associated with one another [3], as demonstrated in our study. Thrombi located in the M2 or M3 segments, and therefore, more pervious thrombi, are technically more difficult to reach during EVT because of their distal location and the smaller diameter of these MCA segments.[30],[31] Moreover, the use of IVT before EVT might increase the chance of thrombus fragility and thrombus migration especially in more pervious thrombi, leading to a higher frequency of clot inaccessibility by EVT, or thrombus fragmentation and thereby decreased eTICI scores.[32] Conversely, some studies have reported that IVT softens thrombi and thereby facilitates EVT.[33] Given that more pervious thrombi may be more sensitive to IVT, this effect may increase the chance of reperfusion after EVT.[19] All these together might provide an explanation for the neutral effect of thrombus perviousness or distal location on reperfusion after EVT. However, further research is needed on this topic.

Our study has limitations. Many patients were excluded because of the absence of thin-section NCCT or CTA, pro- longed time between the scanned NCCT and

4

CTA (>30 minutes), poorly co-registered scans and poor image quality. This might be explained by the fact the MRCLEAN Registry is a multicenter study, and not all centers saved or performed thin-slice NCCT/CTA, especially primary stroke centers. However, despite excluding a considerable number of patients, our study population is the largest sample to date about thrombus imaging characteristics in AIS treated by EVT, and it was a reliable sample of the entire MR CLEAN Registry, demonstrating similar baseline characteristics. An additional limitation is the use of CTA to assess CBS and thrombus length, which may be influenced by the backflow of a poor collateral circulation. However, overestimated CBS and length may strengthen the prognostic value of these thrombus characteristics because poor collaterals are known to be associated with poor outcomes.[4],[18] For a more reliable measurement, dynamic CTA imaging might be a valuable alternative. Furthermore, accurate measurements of thrombus length are limited in curved or branched arteries. Although thrombus volume has been described to be a more accurate measure for thrombus burden, irrespective of angioarchitecture and col-laterals, we think thrombus length and CBS are reasonable quantitative parameters for thrombus burden, and they might be more feasible in clinical practice in terms of rapidity and ease of use.[18],[22] Differences in operator techniques, thrombectomy devices,[10] imaging parameters across institutions, may have led to distinct clot-retriever interactions and might have interfered with thrombus imaging assessments. However, this aspect of the study makes it more generalizable to real-world clinical practice. In our population, stent-retriever was by far the most performed modality, which may be a bias in the statistical analyses because of the unbalanced variation of EVT modalities. Our study does not account for operator differences. Further studies need to be done analyzing this operator and device variables. Finally, our data were gathered in routine clinical practice. Registries, in general, are prone to missing and incorrect values. However, all data were verified by our study coordinators and missing values were imputed.

Conclusion

Imaging characteristics related to thrombus burden are associated with functional outcome and duration of endovascular procedure after thrombectomy for AIS. Distal site of occlusion, shorter thrombi, and higher CBS is associated with better functional outcome and faster endovascular procedure. Site of occlusion is strongly associated with reperfusion status, and pervious thrombus is associated with favorable functional outcome.

References

[1]   W.J. Powers, A.A. Rabinstein, T. Ackerson *et al.*, "Guidelines for the early management of patients with acute ischemic stroke: a guideline for healthcare professionals from the American Heart Association/ American Stroke Association," *Stroke* 2018. vol 49, pp. e46-e110. doi: 10.1161/STR 0000000000000158.

[2]   O.A. Berkhemer, P.S. Fransen, D. Beumer *et al.* ;MR CLEAN Investigators. "A randomized trial of intraarterial treatment for acute ischemic stroke," *N Engl J Med* 2015. vol. 372. pp. 11–20. doi: 10.1056/NEJMoa1411587.

[3]   E.M. Santos, H.A. Marquering, M.D. den Blanken *et al.*; MR CLEAN Investigators. "Thrombus permeability is associated with improved functional outcome and recanalization in patients with ischemic stroke". *Stroke* 2016. vol: 47, pp. 732–741. doi: 10.1161/STROKEAHA.115.011187.

[4]   K.M. Treurniet, A.J. Yoo, O.A. Berkhemer *et al.*; MR CLEAN Investigators. "Clot burden score on baseline computerized tomographic angiography and intra-arterial treatment effect in acute ischemic stroke." *Stroke* 2016. Vol. 47, pp. 2972–2978. doi: 10.1161/STROKEAHA.116.014565.

[5]   S.M. Mishra, J. Dykeman, T.T. Sajobi *et al.* "Early reperfusion rates with IV tPA are determined by CTA clot characteristics," *AJNR Am J Neuroradiol.* 2014, vol. 35, pp. 2265–2272. doi: 10.3174/ajnr.A4048

[6]   J. Borst, O.A. Berkhemer, E.M.M. Santos *et al.*; MR CLEAN Investigators. "Value of thrombus CT characteristics in patients with acute ischemic stroke." *AJNR Am J Neuroradiol.* 2017, vol. 38, pp. 1758–1764. doi: 10.3174/ajnr.A5331

[7]   C.H. Riedel, P. Zimmermann, U. Jensen-Kondering *et al.* "The importance of size: successful recanalization by intravenous thrombolysis in acute anterior stroke depends on thrombus length," *Stroke* 2011. Vol. 42, pp. 1775–1777. doi: 10.1161/STROKEAHA.110.609693

[8]   V. Rohan, J. Baxa, R. Tupy *et al.* "Length of occlusion predicts recanalization and outcome after intravenous thrombolysis in middle cerebral artery stroke," *Stroke* 2014, vol. 45, pp.2010–2017. doi: 10.1161/STROKEAHA.114.005731

[9]   A. Murphy, S.P. Symons, J. Hopyan and R.I. Aviv, "Factors influencing clinically meaningful recanalization after IV-rtPA in acute ischemic stroke," *AJNR Am J Neuroradiol.* 2013, vol. 34, pp.146–152. doi: 10.3174/ajnr.A3169

[10]   I.G.H. Jansen, M.J.H.L. Mulder, R.B. Goldhoorn *et al.*; MR CLEAN Registry Investigators. "Endovascular treatment for acute ischaemic stroke in routine clinical practice: prospective, observational cohort study (MR CLEAN Registry)," *BMJ* 2018. vol. 360, pp. k949. doi: 10.1136/bmj.k949

[11]   S. Klein, M. Staring, K. Murphy *et al.* "Elastix: a toolbox for intensity-based medical image registration," *IEEE Trans Med Imaging* 2010, vol. 29, pp. 196–205. doi: 10.1109/TMI.2009.2035616

[12]   E.A. Noser, H.M. Shaltoni, C.E. Hall *et al.* "Aggressive mechanical clot disruption: a safe adjunct to thrombolytic therapy in acute stroke?" *Stroke.* 2005, vol. 36, pp. 292–296, doi: 10.1161/01.STR.0000152331.93770.18

[13]   A.M. Spiotta, D. Fiorella, A.S. Arthur *et al.* "The semiotics of distal thrombectomy : towards a TICI score for the target vessel." *J Neurointerv Surg.* 2019, vol. 11, pp. 213–214. doi: 10.1136/neurintsurg-2018-014353

[14]   H.C. Alves, K.M. Treurniet KM, B.G. Dutra BG *et al.*; MR CLEAN trial Investigators. "Associations between collateral status and thrombus characteristics and their impact in anterior circulation stroke," *Stroke* 2018, vol. 49, pp. 391–396. doi: 10.1161/STROKEAHA.117.019509

[15]   E.M. Qazi, S.I. Sohn, S. Mishra *et al.* "Thrombus characteristics are related to collaterals and angioarchitecture in acute stroke," *Can J Neurol Sci.* 2015, vol. 42, pp. 381–388. doi: 10.1017/cjn.2015.291

[16]   V. Puetz, I. Dzialowski, M.D. Hill *et al*.; Calgary CTA Study Group. "Intracranial thrombus extent predicts clinical outcome, final infarct size and hemorrhagic transformation in ischemic stroke: the clot burden score," *Int J Stroke* 2008, vol. 3, pp. 230–236. doi: 10.1111/j.1747-4949.2008.00221.x

[17]   A.R. Donders, G.J. van der Heijden, T. Stijnen and K.G. Moons, "Review: a gentle introduction to imputation of missing values." *J Clin Epidemiol.* 2006, vol. 59, pp.1087–1091. doi: 10.1016/j.jclinepi.2006.01.014

[18]   A.J. Yoo, P. Khatri, J. Mocco *et al.;* THERAPY Trial Investigators. "Impact of thrombus length on outcomes after intra-arterial aspiration thrombectomy in the THERAPY trial," *Stroke* 2017, vol. 48, pp.1895–1900. doi: 10.1161/STROKEAHA.116.016253

[19]   E.M. Santos, J.W. Dankbaar, K.M. Treurniet *et al*.; DUST Investigators. "Permeable thrombi are associ- ated with higher intravenous recombinant tissue-type plasminogen activator treatment success in patients with acute ischemic stroke," *Stroke* 2016, vol. 47, pp.2058–2065. doi: 10.1161/STROKEAHA.116.013306

[20]   B.K. Menon, F.S. Al-Ajlan, M. Najm *et al.* "Association of clinical, imaging, and thrombus characteristics with recanalization of visible intracranial occlusion in patients with acute ischemic stroke," *JAMA Neurol.* 2018, vol. 320, pp. 1017–1026. doi: 10.1001/jama.2018.12498

[21]   Spiotta AM, Vargas J, Hawk H, Turner R, Chaudry MI, Battenhouse H, *et al.* Hounsfield unit value and clot length in the acutely occluded vessel and time required to achieve thrombectomy, complications and outcome. J Neurointerv Surg. 2014;6:423–427. doi: 10.1136/ neurintsurg-2013-010765

[22]   F. Seker, J. Pfaff, M. Wolf *et al.* "Impact of thrombus length on recanalization and clinical outcome following mechanical thrombectomy in acute ischemic stroke," *J Neurointerv Surg.* 2017, vol.9, pp. 937–939. doi: 10.1136/neurintsurg-2016-012591

[23]   J.H. Baek, J. Yoo, D. Song, Y.D. Kim *et al.* "Predictive value of thrombus volume for recanalization in stent retriever thrombectomy," *Sci Rep.* 2017, vol. 7, pp.15938. doi: 10.1038/s41598-017-16274-9

4

[24]   I.Y. Tan, A.M. Demchuk, J. Hopyan *et al.* "CT angiography clot burden score and collateral score: correlation with clinical and radiologic outcomes in acute middle cerebral artery infarct," *AJNR Am J Neuroradiol.* 2009, vol. 30, pp. 525–531. doi: 10.3174/ajnr.A1408

[25]   M. Mokin, S. Morr, S.K. Natarajan *et al.* "Thrombus density predicts successful recanalization with solitaire stent retriever thrombectomy in acute ischemic stroke," *J Neurointerv Surg.* 2015, vol. 7, pp. 104–107. doi: 10.1136/neurintsurg-2013-011017

[26]   M.T. Froehler, S. Tateshima, G. Duckwiler *et al.*; UCLA Stroke Investigators. The hyperdense vessel sign on CT predicts successful recanalization with the merci device in acute ischemic stroke. *J Neurointerv Surg.* 2013, vol. 5, pp. 289–293. doi: 10.1136/neurintsurg-2012-010313

[27]   M. Jagani, D.F. Kallmes and W. Brinjikji, "Correlation between clot density and recanalization success or stroke etiology in acute ischemic stroke patients*,"* *Interv Neuroradiol.* 2017, vol. 23, pp. 274–278. doi: 10.1177/1591019917694478

[28]   U. Yilmaz, C. Roth, W. Reith, P. Papanagiotou "Thrombus attenuation does not predict angiographic results of mechanical thrombectomy with stent retrievers," *AJNR Am J Neuroradiol.* 2013, vol. 34, pp. 2184–2186. doi: 10.3174/ajnr.A3565

[29]   V. Polito, R. La Piana, M. Del Pilar Cortes and D. Tampieri "Assessment of clot length with multiphase CT angiography in patients with acute ischemic stroke," *Neuroradiol J.* 2017, vol. 30, pp. 593–599. doi: 10.1177/ 1971400917736928

[30]   J.M. Coutinho, D.S. Liebeskind, L.A. Slater *et al.* "Mechanical thrombectomy for isolated M2 occlusions: a post hoc analysis of the STAR, SWIFT, and SWIFT PRIME studies." *AJNR Am J Neuroradiol.* 2016, vol. 37, pp. 667–672. doi: 10.3174/ajnr.A4591

[31]   K. Compagne, P. van der Sluijs, I. van den Wijngaard *et al.* "The role of dominant caliber M2 segment occlusion in ischemic stroke," *Stroke* 2019, vol. 50, pp.419–427. doi: 10.1161/STROKEAHA.118.023117

[32]   J. Kaesmacher, C. Maegerlein, M. Kaesmacher *et al.* "Thrombus migration in the middle cerebral artery: incidence, imaging signs, and impact on success of

endovascular thrombectomy," *J. Am. Heart Assoc.* 2017, vol. 6(2), pp. e005149. doi: https://doi.org/10.1161/JAHA.116.005149

[33]   T. Pfefferkorn, M. Holtmannspötter, M. Patzig *et al.* "Preceding intravenous thrombolysis facilitates endovascular mechanical recanalization in large intracranial artery occlusion," *Int J Stroke* 2012, vol. 7, pp. 14–18. doi: 10.1111/j.1747-4949.2011.00639.x

Supplementary materials:
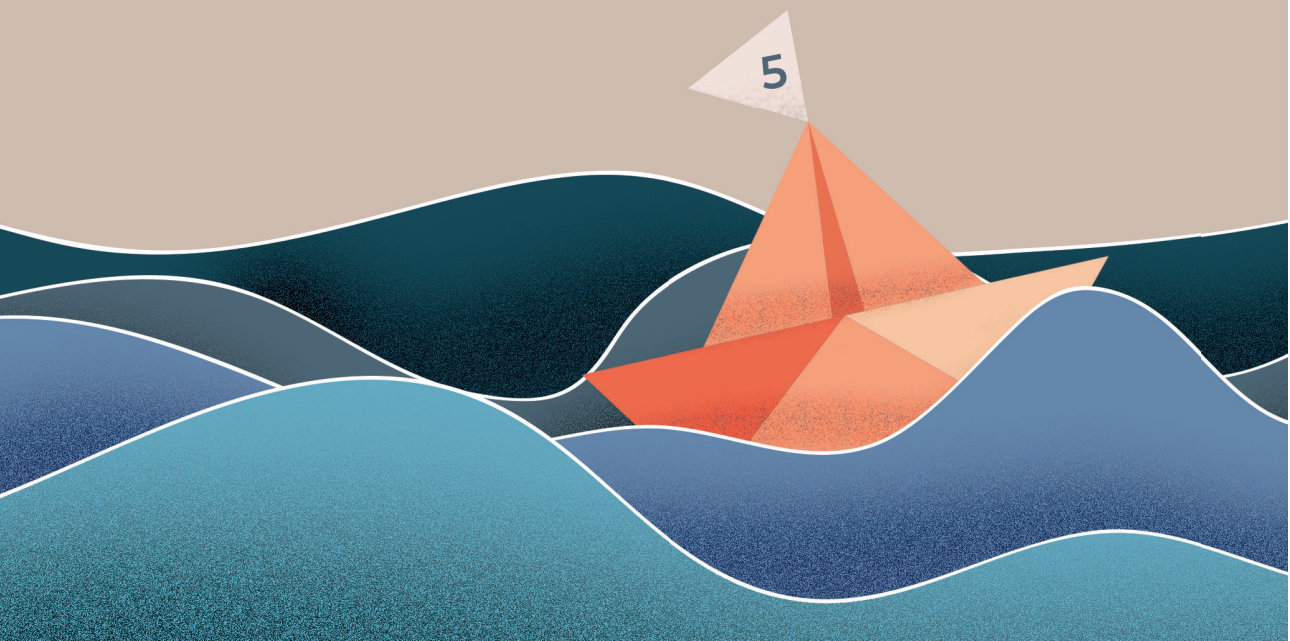
4

Chapter 5

Endovascular treatment effect diminishes with increasing thrombus perviousness: Pooled data from 7 trials on acute ischemic stroke

M. Kappelhof, M.L. Tolhuisen, K.M. Treurniet, B.G. Dutra, H. Alves, G. Zhang, S. Brown, K.W. Muir, A. Dávalos, Y.B.W.E.M. Roos, J.L. Saver, A.M. Demchuck, T.G. Jovin, S. Bracard, B.C.V. Campbell, A. van der Lugt, F. Guilleman, P. White, M.D. Hill, D.W.J. Dippel, P.J. Mitchell, M. Goyal, H.A. Marquering, C.B.L.M. Majoie, on behalf of the HERMES collaborators

Abstract

Background— Thrombus perviousness estimates residual flow along a thrombus in acute ischemic stroke, based on radiological images, and may influence the benefit of endovascular treatment for acute ischemic stroke. We aimed to investigate potential endovascular treatment (EVT) effect modification by thrombus perviousness.

Methods— We included 443 patients with thin slice imaging available, out of 1766 patients from the pooled HERMES (Highly Effective Reperfusion Evaluated in Multiple Endovascular Stroke trials) data set of 7 randomized trials on EVT in the early window (most within 8 hours). Control arm patients (n=233) received intravenous alteplase if eligible (212/233; 91%). Intervention arm patients (n=210) received additional EVT (prior alteplase in 178/210; 85%). Perviousness was quantified by thrombus attenuation increase on admission computed tomography angiography compared with non-contrast computed tomography. Multivariable regression analyses were performed including multiplicative interaction terms between thrombus attenuation increase and treatment allocation. In case of significant interaction, subgroup analyses by treatment arm were performed. Our primary outcome was 90-day functional outcome (modified Rankin Scale score), resulting in an adjusted common odds ratio for a one-step shift towards improved outcome. Secondary outcomes were mortality, successful reperfusion (extended Thrombolysis in Cerebral Infarction score, 2B–3), and follow-up infarct volume (in mL).

Results— Increased perviousness was associated with improved functional outcome. After adding a multiplicative term of thrombus attenuation increase and treatment allocation, model fit improved significantly (P=0.03), indicating interaction between perviousness and EVT benefit. Control arm patients showed significantly better outcomes with increased perviousness (adjusted common odds ratio, 1.2 [95% CI, 1.1–1.3]). In the EVT arm, no significant association was found (adjusted common odds ratio, 1.0 [95% CI, 0.9–1.1]), and perviousness was not significantly associated with successful reperfusion. Follow-up infarct volume (12% [95% CI, 7.0–17] per 5 Hounsfield units) and chance of mortality (adjusted odds ratio, 0.83

[95% CI, 0.70–0.97]) decreased with higher thrombus attenuation increase in the overall population, without significant treatment interaction.

Conclusion— Our study suggests that the benefit of best medical care including alteplase, compared with additional EVT, increases in patients with more pervious thrombi

Introduction

In acute ischemic stroke, thrombi are often assumed to completely occlude vessels, blocking all flow like a cork on a bottle of wine. However, some thrombi are permeable, allowing for residual flow into and through them.[1–3] Thrombus perviousness estimates residual flow through thrombi based on routine non-contrast CT (NCCT) and single-phase CT angiography (CTA).[4],[5] Perviousness was associated with improved outcomes and recanalization rates after intravenous alteplase. [4] For endovascular treatment (EVT) however, reported effects of perviousness vary considerably.[6],[7]

The current standard treatment of acute ischemic stroke due to anterior circulation large vessel occlusions consists of alteplase if patients are eligible, followed by EVT.[8],[9] Although EVT has greatly improved outcomes, even after EVT more than half of the patients remain permanently disabled or die after their stroke.[9] The added benefit of intravenous alteplase is investigated in several recently completed and ongoing randomized trials.[10] Alteplase benefit may vary case-by-case: large proximal occlusions are known to show little benefit,[11] while 10% of EVT-eligible patients recanalize with alteplase before initiation of EVT.[12] Selecting the treatment with the highest chance of benefit (alteplase, EVT, neither, or both) is, therefore, expedient and could enable a more targeted and effective use of treatment modalities.

Currently, no radiological thrombus characteristics other than occlusion location are used in acute ischemic stroke decision-making.[8] The possible association of thrombus perviousness with alteplase treatment success, either alone or combined with EVT, could play a role in improving stroke treatment selection.[4],[5] To assess the role of perviousness, a large data set is needed, enabling separate analysis of

treatment approaches. We aimed to investigate the effect of thrombus perviousness on EVT results in the HERMES trial (Highly Effective Reperfusion Evaluated in Multiple Endovascular Stroke) pooled data set of 7 large randomized trials on EVT for stroke.[9],[13–19]

Methods

Patients

The HERMES collaboration pooled individual patient data from 7 randomized controlled trials on EVT in acute ischemic stroke of the anterior circulation, [9],[13–19] totaling 1766 patients included between December 2010 and December 2014. Inclusion criteria of the individual trials were reported previously.[13–19] Pooling protocol, study selection, risk of bias, individual patient data acquisition, and data checks are described in the original pooling report.[9] Control arm patients received best medical care, including alteplase if eligible. The intervention arm consisted of additional EVT.

Patients were included in the current study if thin-slice (≤2.5 mm) NCCT and CT angiography (CTA) images were available (n=690). We excluded patients if NCCT and CTA images were on different scanners (n=11), or >30 minutes apart (n=40). We excluded patients with scans that did not cover the intracranial area of interest (n=33), were of insufficient quality (n=93; beam hardening: n=50, movement artifacts: n=32, contrast present on NCCT: n=6, scatter artifacts: n=4, and venous phase CTA: n=1), or with incorrigible registration errors (n=76). Thrombi located too close to bone (n=6), partial occlusions (n=4), narrow and distal thrombi (n=3), and bilateral middle cerebral artery thrombi (n=1) were excluded. The remaining 443 patients were included in the final analysis (Figure 5.1). The HERMES data used for this study are available via the VISTA-Endovascular repository. We followed the PRISMA-IPD guideline for study execution and reporting (Methods in the Data Supplement).

Thrombus perviousness Measurements

NCCT and CTA images were co-registered using rigid registration with Elastix.[20] Thrombus perviousness was quantified by measuring thrombus attenuation increase (TAI) between NCCT and CTA images as described previously.[4] For image selection and ROI placement, open-source software ITK-SNAP was used.[21]
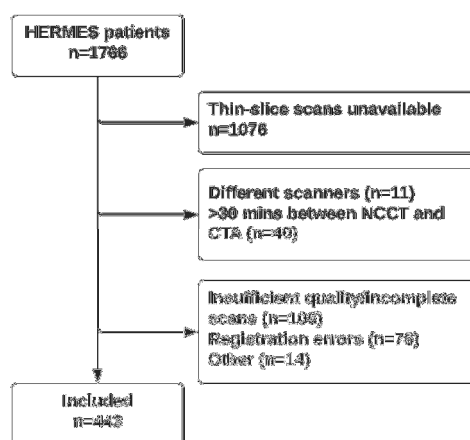
Figure 5.1: *Patient inclusion flowchart. Other includes too close to bone (n=6), only atrial occlusion (n=4), too narrow thrombus (n=3), bilateral middle cerebral artery thrombus (n=1), CTA indicates computed tomographic angiography; HERMES, Highly Effective Reperfusion Evaluated in Multiple endovascular Stroke and NCCT, non-contrast computed tomography*

Thrombus attenuation was measured manually by placing 3 spherical ROIs with a radius of one millimeter in the proximal, middle, and distal parts of the thrombus (Figure 5.2). The average density (ρ in Hounsfield units [HU]) of all ROIs was calculated for NCCT and CTA (ρNCCT and ρCTA). TAI was calculated according to: TAI=ρCTA–ρNCCT.[5]

Measurements were performed by one of 3 trained raters (Drs. Kappelhof, Dutra, and Alves).[22] Raters were blinded for occlusion location, clinical information, and measured attenuation values. Training was done with 25 cases from the MR CLEAN Registry.[23] Scan acquisition characteristics including NCCT

and CTA slice thickness difference (CTA slice thickness minus NCCT slice thickness), [24] scanner brand, and scanner kVp were recorded for all included patients.
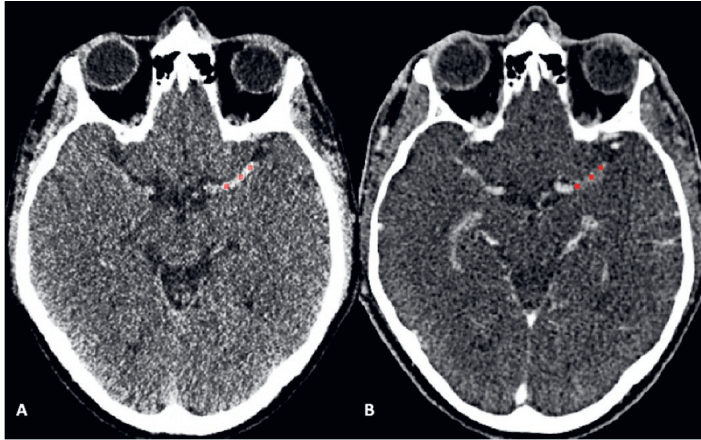
Figure 5.2: Three regions of interest (red) are placed in a left middle cerebral artery thrombus on non-contrast computed tomography (CT; A) and CT angiography (B). To calculate thrombus attenuation increase as a measure for perviousness, the density (in Hounsfield Units) in each region of interest is measured. Subsequently, the average non-contrast CT attenuation value is deducted from the average CT angiography value.

Outcome measures

Our primary outcome was functional outcome (ordinal modified Rankin Scale [mRS]) at 90 days. The mRS score ranges from 0 to 6, with 0 indicating complete functional independence, and 6 indicating death. Secondary outcome measures were dichotomized functional outcome (mRS score, 0–2 versus 3–6 indicating functional independence; mRS score, 5–6 versus 0–4 indicating poor outcome), mortality, successful reperfusion (extended Thrombolysis in Cerebral Infarction score grade, 2B–3) after EVT (intervention arm patients only), and follow-up infarct volume (FIV) in mL as measured on follow-up NCCT.[25]

Statistical Analysis

Statistical analyses were pre-specified in a statistical analysis plan (Methods in the Data Supplement). Baseline clinical, imaging, and follow-up variables were

compared with the overall HERMES population and between every quartile of TAI. One-way ANOVA was used to assess differences in normally distributed numerical variables, Kruskal-Wallis and Mann-Whitney U tests for non-normal numerical variables, and Fisher exact tests for categorical variables.

TAI outliers (n=11) were identified with the outlier labeling rule with a multiplier of 2.2, marking them as outliers if their difference with the median was ≥2.2× the interquartile range (IQR).[26] For 10 patients (2%), one marker was adjusted due to erroneous placement outside the vessel or thrombus. All remaining outliers (n=4, 1%) were attributable to short pervious thrombi, random noise, or slice thickness differences between NCCT and CTA, and were included in the final analysis.

Univariable and multivariable ordinal logistic regression were used in the primary outcome variable analysis (mRS shift). Univariable and multivariable binary logistic regression was used for dichotomized outcome variables. Associations between TAI and FIV were tested with linear regression. Because FIV showed a right-skewed distribution, log-trans- formation was performed. Associations between TAI and outcomes are reported per 5 HU.

Regression analyses were adjusted for age, baseline National Institutes of Health Stroke Scale score, intravenous alteplase, occlusion location, diabetes, stroke onset to randomization time, slice thickness difference between NCCT and CTA, and included random effects for allocated study and scanner brand. Unadjusted and adjusted (common) odds ratios (u[c]OR and a[c]OR) were reported with 95% CI. We added an interaction term between TAI and allocated treatment in separate, subsequent models. For successful reperfusion as outcome measure, an additional regression model included an interaction term between TAI and alteplase treatment. If treatment interaction was significant, subgroup analyses were performed. Exploratory subgroup analyses were performed using unadjusted and adjusted ordinal logistic regression for EVT effect per quartile of TAI, for the primary outcome only.

Statistical analyses were performed with R version 3.5.2 (R Foundation for Statistical Computing, Vienna, Austria). The significance level was set at $P<0.05$.

Results

Median age was 67 years (IQR, 59–76), median baseline National Institutes of Health Stroke Scale score was 18 (interquartile range, 14–21), and 53% of patients were male (Table 5.1). In comparison to the overall HERMES population, mRS scores, occurrence of sICH, and FIV were slightly higher. Intravenous alteplase was administered to 91% of the patients in the control arm and 85% of the patients in the intervention arm.

TAI showed a slightly right-skewed distribution with a mean of 4.5 HU (SD, 12.7) and median 3.2 HU (IQR, −4.3 to 11.4; Figure I in the Data Supplement). Baseline characteristics did not significantly differ between TAI quartiles (Table I in the Data Supplement). TAI values did not differ between patients with and without extracranial carotid tandem lesions (P=0.47). Scan acquisition details are discussed in Results in the Data Supplement.

Primary Outcomes

Ninety-day mRS was available for 438 of 443 patients. Higher TAI corresponded to lower mRS (P<0.01; Figure 5.3). There was significant interaction between TAI and allocated treatment (P for interaction, 0.03; Table 5.2). In the control arm, TAI was associated with improved outcomes (acOR, 1.22 [95% CI, 1.11–1.33]). In the intervention arm, no significant effect was found (acOR, 0.99 [95% CI, 0.88–1.11]). These results were consistent in an exploratory analysis of alteplase-treated patients (390/443, 88%; Table III in the Data Supplement). Analysis per TAI quartile showed a non-significant benefit of EVT in the highest quartile (Table IV in the Data Supplement).

Table 5.1: *Baseline and follow-up Characteristics*

	Current study (n=443)	HERMES total (n=1766)	p
Baseline clinical characteristics (data known in [n])			
Age, median (IQR)	67 (59-76) [442]	68 (57-76) [1761]	0.26
Sex (male), n(%)	236 (53) [442]	929 (53) [1762]	0.78
Left hemisphere stroke, n(%)	198 (51) [389]	652 (51) [1275]	0.95
Baseline NIHSS, median (IQR)	18 (14-21) [440]	17 (13-21) [1751]	0.13
Treatment allocation, n(%)			
Intervention	210 (48) [442]	871 (49) [1764]	0.38
Control	232 (53) [442]	893 (51) [1764]	0.38
Intravenous alteplase, n(%)			
Intervention	179 (85) [210]	763 (88) [871]	0.23
Control	211 (91) [232]	809 (91) [893]	0.90
Onset to randomization time (min), median (IQR)	189 (148-252) [441]	183 (140-245) [1756]	0.62
Atrial fibrillation, n(%)	117 (30) [390]	424 (33) [1286]	0.14
Diabetes mellitus, n(5)	74 (17) [442]	287 (16) [1756]	0.82
Hypertension	238 (54) [442]	988 (56) [1757]	0.25
Imaging (data known in [n])			
Occlusion location			
ICA	92 (21) [443]	442 (27) [1648]	0.80
M1	331 (75) [443]	1073 (65) [1648]	0.80
M2	19 (4.3) [443]	131 (7.9) [1648]	0.80
Other	1 (0.2) [443]	2 (0.1) [1648	0.80

(Continued)

5

Table 5.1: Continued

	Current study (n=443)	HERMES total (n=1766)	P
Imaging (data known in [n])			
Carotid tandem location, n(%)			
Intervention	18 (8.6) [210]	122 (7.4) [1648]	0.71
Control	17 (7.2) [232]	122 (7.4) [1648]	0.71
NCCT thrombus density (HU), median (IQR)	55 (48-62) [443]	NA	
Follow-up (data known in [n])			
mRS at 90 days, n(%)			
0	27 (6) [438]	156 (9) [1743]	0.04*
1	51 (12) [438]	244 (14) [1743]	
2	68 (16) [438]	282 (16) [1743]	
3	91 (21) [438]	274 (16) [1743]	
4	89 (20) [438]	356 (20) [1743]	
5	38 (9) [438]	150 (9) [1743]	
Mortality (mRS 6), n(%)	74 (17) [440]	281 (16) [1754]	0.84
Post-EVT eTICI score 2B-3, n(%)	134 (74) [180]	548 (74) [745]	0.74
sICH, n(%)	22 (5) [389]	63 (4) [1729]	0.01*
Follow-up infarct volume (mL), median (IQR)	51 (17-125) [425]	41 (14-120) [1665]	0.01*

eTICI indicates extended Thrombolysis in Cerebral Infarction score; EVT, endovascular treatment; HERMES, Highly Effective Reperfusion Evaluated in Multiple Endovascular Stroke; HU, Hounsfield units; ICA, internal carotid artery; IQR, interquartile range; M1, segment 1 of medial cerebral artery; M2, segment 2 of medial cerebral artery; mRS, modified Rankin Scale; NA, not available; NCCT, non-contrast computed tomography; NIHSS, National Institutes of Health Stroke Scale; and sICH, symptomatic intracranial hemorrhage.

*Statistical significance (P<0.05).
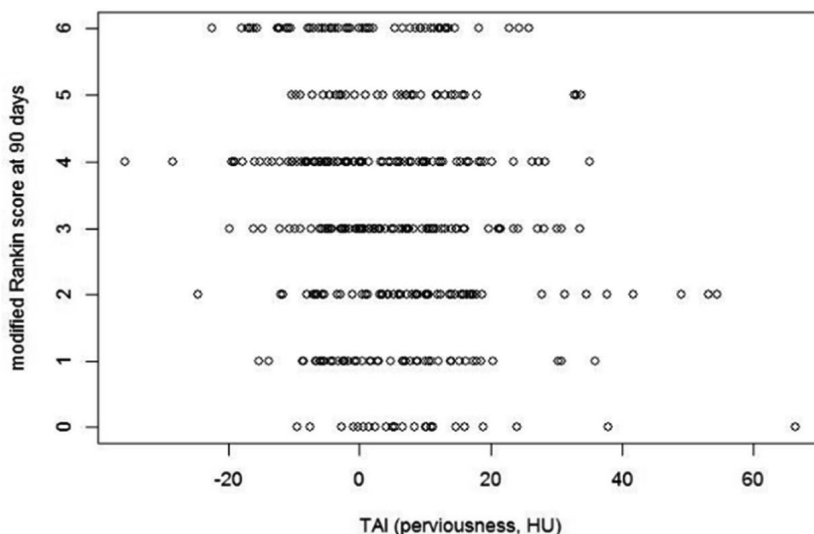
Figure 5.3: *Thrombus attenuation increase (TAI) values varied per modified Rankin Scale (mRS) score (P>0.001)*

Secondary Outcomes

Functional Independence

In the control arm, patients with 90-day mRS score of 0 to 2 (n=59/231; 26%) had more pervious thrombi than patients with mRS score of 3 to 6 (median, 8.5 [IQR, 1.1– 17.4]) versus 1.2 [IQR, –4.9 to 9.4], P≤0.01, respectively). In the intervention arm, TAI values did not significantly differ between patients with mRS score of 0 to 2 and mRS score of 3 to 6 (Figure II in the Data Supplement).

Interaction between TAI and allocated treatment was significant (P=0.046). Subgroup analysis showed a significant positive association between TAI and functional independence in the control arm, but not in the intervention arm (Table 2). Figure 5.4 shows the adjusted probability of functional independence plotted against TAI, for intervention and control arm patients. Treatment effect of EVT in addition to best medical care (alteplase if eligible) decreases with higher TAI, although there is no point where the CIs are separated. Unadjusted results are presented in Figure III in the Data Supplement.

Table 5.2: *aOR for the effect of TAI (per 5 HU) on outcomes*

Outcome measure	aOR[#] (95% CI)*	Interaction with EVT	aOR[#] per arm (95% CI)
Ordinal mRS	1.10 (1.03-1.18) †	p=0.03†	Control: 1.22 (1.04-1.19)*
			Intervention: 0.96 (0.85-1.08)
mRS 0-2	1.15 (1.05-1.27) †	p=0.05†	Control: 1.33 (1.14-1.56)*
			Intervention: 1.04 (0.90-1.21)
mRS 5-6	0.92 (0.83-1.02)	p=0.03†	Control: 0.82 (0.70-0.95)*
			Intervention: 1.07 (0.90-1.27)
Mortality	0.85 (0.75-0.97) †	p=0.58	NA
Final infarct volume (effect ratio)	0.91 (0.86-0.95) †	p=0.11‡	Control: 0.87 (0.82-0.93)*
			Intervention: 0.97 (0.89-1.05)
Intervention arm only: Successful reperfusion	0.95 (0.79-1.14)	Interaction with IV alteplase: p=0.47	NA

Unadjusted results shown in Table II in the Data Supplement. Control arm: intravenous alteplase if eligible (n=232), intervention arm: additional EVT (n=210). aOR indicates adjusted odds ratio; CTA, computed tomography angiography; EVT, endovascular treatment; HU, Hounsfield units; mRS, modified Rankin Scale; NA, not applicable/available; NCCT, non-contrast computed tomography; and TAI, thrombus attenuation increase.

*Adjusted for age (y), baseline NIHSS, alteplase, occlusion location, diabetes, stroke onset to randomization time, NCCT-CTA slice thickness difference; and including random effects for study and scanner brand.

†Statistical significance (P<0.05).

‡Exploratory analysis in model with non-significant treatment interaction

mRS score of 5 to 6 and Mortality

Higher TAI was associated with a lower chance of poor outcome in the control arm (P for interaction 0.03; Table 5.2). Greater TAI also corresponded to a smaller chance of mortality in the overall population (aOR, 0.85 [95% CI, 0.75–0.97]), but treatment interaction was not significant (P=0.58).

Figure 5.4: Probability of functional independence (90-d modified Rankin Scale [mRS] score, 0-2) vs thrombus attenuation increase (TAI)
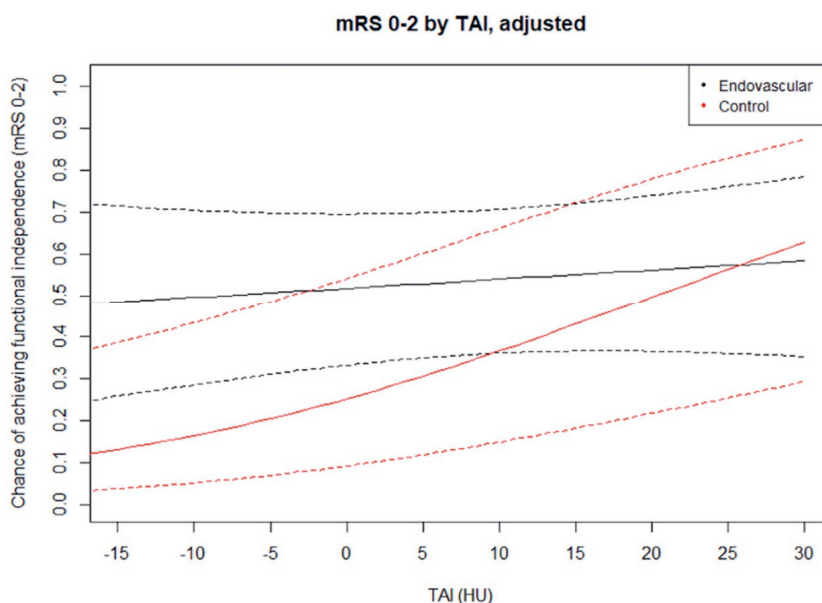
Results are adjusted for pre-specified variables: age, baseline National Institutes of Health Stroke Scale, alteplase, occlusion location, diabetes, stroke onset to randomization time, and non-contrast computed tomography-computed tomography angiography slice thickness difference. Control arm: best medical care (intravenous alteplase if eligible; n=232). Intervention arm: endovascular treatment in addition to best medical care (n=210).

Successful Endovascular Reperfusion

eTICI scores were available for 180/210 intervention arm patients (86%). Successful reperfusion was reached in 134/180 cases (74%). We found no significant effect of TAI on reperfusion (Table 5.2). Interaction between TAI and alteplase was not significant for successful reperfusion (P=0.47)—although only 31 patients (15%) in the intervention arm did not receive intravenous alteplase. Post-EVT eTICI scores were known in 26 of them (12% of all intervention arm patients).

Follow-up Infarct Volume

A 5 HU increase in TAI was associated with a 9% decrease in FIV (95% CI, 14%–5%). Interaction between TAI and treatment arm was not significant (P=0.11; Table 5.2; Figure IV in the Data Supplement).

Discussion

The benefit of EVT as an addition to alteplase diminishes in patients with more pervious thrombi, due to improved outcomes with increasing perviousness in patients receiving alteplase alone. Increased thrombus perviousness was associated with improved functional outcome in HERMES control arm patients, who, in a high proportion, were treated with intravenous alteplase. No significant effect of perviousness on functional outcome was found in patients included in the intervention arm, who received EVT in addition to best medical care. Results of associations with secondary outcomes were similar. No value for perviousness was observed where better outcomes were associated with withholding EVT, though the association with functional outcome was more pronounced in the higher perviousness quartiles.

Our findings generally agree with previous studies showing increased recanalization rates and improved outcomes in patients with more pervious thrombi after intravenous alteplase treatment.[4],[5],[7],[27–29] These studies, however, compared intravenous alteplase to conservative treatment only [4] or found no interaction with EVT, possibly due to lower patient numbers.[5] Improved target vessel recanalization for pervious thrombi seems to lead to improved outcomes after intravenous alteplase, [28] on average leaving less opportunity for EVT to give additional benefit. On the association between perviousness and EVT, results vary: in contrast to our results, a recent study in EVT-treated patients reported a significantly positive association between perviousness and functional outcome in the adjusted analyses.[7] Perviousness was reported to be associated with higher chances of first-pass success of aspiration thrombectomy.[30]

Previous studies have dichotomized TAI, to classify thrombi into pervious and non-pervious.[4],[5] The optimal cut-off value varied between studies and data sets.

However, these values were subsequently used by other study groups without testing validity in their data.[31] Therefore, and since dichotomization was not necessary for our research question, we did not dichotomize TAI. Following this reasoning, the TAI values in the per-quartile analysis should be interpreted with care. Though interesting, the subgroup analysis is not meaningfully powered with ≈110 patients per group: TAI cutoff values may not be applicable to other data sets.

The observed effect of perviousness may be partly explained by thrombus histopathology. A study on thrombi retrieved during EVT showed a positive correlation between perviousness and fibrin/platelet fractions.[31] However, conflicting results exist: a recent study reported opposite results.[32] RBC-rich thrombi were found to be more responsive to thrombolytic therapy.[33] In relation to EVT, fibrin-rich thrombi were associated with longer intervention times and a higher chance of secondary embolisms.[34] Thrombus perviousness may also be associated with stroke cause, though published results on this topic are inconsistent.[35],[36]

Interestingly, we observed some negative values for TAI. Slice thickness differences between NCCT and CTA could affect density measurements due to partial volume effect.[24] Minor co-registration errors could minimally offset marker placement in NCCT or CTA. Random (Gaussian) noise could affect HU values on either NCCT or CTA. These factors unlikely affect TAI measurement validity: random noise and small co-registration flaws are likely random, we adjusted for slice thickness differences, and our results are reproducible in studies using the same methods.[4],[7] An effect of differences in scanner voltage on HU values was not supported by our data.

Limitations

We excluded patients due to unavailable thin-slice imaging. Alternative methods like the qualitative assessment of residual flow is possible using thick-slice NCCT, but less precise.[24] Almost all centers acquire thin-slice imaging initially but do not store such images: perviousness could be measured for many more patients if thin-slice imaging is preserved, and a practical, fast, (automatic) measurement method is available.

5

In our sample, we had no information on alteplase administration before scan acquisition. In patients receiving thrombolysis before transfer to an EVT-performing center, alteplase may have been started before scan acquisition, already exposing some thrombi to alteplase. The effects of alteplase administration on thrombus perviousness are currently unknown. Patients may have recanalized and recovered after alteplase and before randomization, leading to a possible inclusion bias, though start of EVT was not delayed by waiting for the effect of alteplase (except for REVASCAT, n=206/1766).[17] These patients may have had more pervious thrombi; thereby the current study may under-represent patients with very pervious thrombi and underestimate the effect of perviousness. Likewise, we did not know the time from alteplase administration to CTA acquisition. Thrombus perviousness might increase if alteplase has had more time to act on the thrombus.

Our data consisted of pooled data from multiple trials. We cannot exclude an uneven distribution of the number of included patients per trial. However, since part of the imaging was requested from trials individually, and scanning protocols were heterogeneous, we are reasonably sure that patients from each trial were included. In addition, we included a random effect for allocated study in all adjusted regression analyses.

Technical aspects of image acquisition can influence TAI measurements. Slice thickness of the images we used varied from 0.6 to 2.5 mm. Thicker slices give a lower measured density on NCCT due to volume averaging with surrounding brain tissue.[24] In addition, CTA scan timing can influence TAI, by slightly differing scanning phase. Dynamic or multiphase CTA incorporates the time dimension by making CTA scans at multiple time points after contrast injection, which can avoid the issue of scanning too early after contrast bolus.[37]

Difficult delineation of thrombi can hamper measurements. The distal thrombus border is hard to discern in case of poor collaterals on CTA and an isodense thrombus on NCCT. However, this occurred only in nine patients in our data set. Measurement in dynamic CTA may show the distal thrombus border more accurately in patients with poor collateral flow.[37]

Finally, it is important to note that although we found significant treatment interaction and decreasing additional benefit of EVT with increasing perviousness, we did not find a TAI value where control arm patients did significantly better than intervention arm patients. Thus, our results do not provide definitive evidence to withhold treatment based on a certain value of perviousness.

Further research could focus on combinations of thrombus characteristics, like perviousness, length, and location, in relation to alteplase and EVT response. Small-volume, short, pervious, distal M2-thrombi may benefit from alteplase, whereas proximal, large-volume, long, impervious ICA terminus occlusions may not. Larger thrombi may respond better to intravenous tenecteplase.[38] Additionally, the effect of perviousness on outcomes of combined alteplase and EVT versus direct EVT only, or on EVT device outcomes could be studied further. In the future, thrombus perviousness may support patient selection for alteplase alone, combined alteplase and EVT, or EVT alone, and support endovascular treatment modality choice.

Conclusions

In patients treated in the control arm of HERMES, of whom most were treated with alteplase, increased thrombus perviousness was associated with improved functional outcome, decreased mortality, and reduced infarct volume. We found no significant association among patients allocated to the EVT-arm. The benefit of EVT as an addition to best medical care including alteplase diminishes in patients with more pervious thrombi, due to improved outcomes with increasing perviousness in patients receiving alteplase alone—though no value for perviousness was observed where withholding EVT was associated with better outcomes.

References

[1]   R.S. Voronov, T.J. Stalker, L.F. Brass, S.L. Diamond. "Simulation of intra-thrombus fluid and solute transport using in vivo clot structures with single

platelet resolution." *Ann Biomed Eng.* 2013, vol. 41, pp. 1297–1307. doi: 10.1007/s10439-013-0764-z

[2]   N. Laurens, P. Koolwijk, M.P. de Maat. "Fibrin structure and wound healing." *J Thromb Haemost.* 2006, vol. 4, pp. 932–939. doi: 10.1111/j.1538-7836.2006.01861.x

[3]   L.F. Brass, K.M. Wannemacher, P. Ma, T.J. Stalker. "Regulating thrombus growth and stability to achieve optimal response to injury." *J Thromb Haemost.* 2011, vol. 9, pp. 66–75. doi: 10.1111/j.1538-7836.2011.04364.x

[4]   E.M. Santos, J.W. Dankbaar, K.M. Treurniet, A.D. Horsch, Y.B. Roos, L.J. Kappelle, W.J. Niessen, C.B. Majoie, B. Velthuis, H.A. Marquering; DUST Investigators. "Permeable thrombi are associated with higher intravenous recombinant tissue-type plasminogen activator treatment success in patients with acute ischemic stroke." *Stroke.* 2016, vol. 47, pp. 2058–2065. doi: 10.1161/ STROKEAHA.116.013306

[5]   E.M. Santos, H.A. Marquering, M.D. den Blanken, O.A. Berkhemer, A.M. Boers, A.J. Yoo, L.F. Beenen, K.M. Treurniet, C. Wismans, K. van Noort, *et al.* "MR CLEAN Investigators. Thrombus permeability is associated with improved functional outcome and recanalization in patients with ischemic stroke." *Stroke.* 2016, vol. 47, pp. 732–741. doi: 10.1161/STROKEAHA.115.011187

[6]   J. Borst, O.A. Berkhemer, E.M.M. Santos, A.J. Yoo, M. den Blanken, Y.B.W.E.M. Roos, E. van Bavel, W.H. van Zwam, R.J. van Oostenbrugge, H.F. Lingsma, *et al.*;MR CLEAN investigators. "Value of thrombus CT characteristics in patients with acute ischemic stroke." *AJNR Am J Neuroradiol.* 2017, vol. 38, pp. 1758–1764. doi: 10.3174/ajnr.A5331

[7]   B.G. Dutra, M.L. Tolhuisen, H.C.B.R. Alves, K.M. Treurniet, M. Kappelhof, A.J. Yoo, I.G.H. Jansen, D.W.J. Dippel, W.H. van Zwam, R.J. van Oostenbrugge, *et al.*; MR CLEAN Registry Investigators†. "Thrombus imaging characteristics and out- comes in acute ischemic stroke patients undergoing endovascular treatment." *Stroke.* 2019, vol. 50, pp. 2057–2064. doi: 10.1161/STROKEAHA.118.024247

[8]   W.J. Powers, A.A. Rabinstein, T. Ackerson, O.M. Adeoye, N.C. Bambakidis, K. Becker, J. Biller, M. Brown, B.M. Demaerschalk, B. Hoh, *et al.*

"American Heart Association Stroke Council. 2018 Guidelines for the early management of patients with acute ischemic stroke: a guideline for healthcare professionals from the American Heart Association/American Stroke Association." *Stroke.* 2018, vol. 49, pp. e46–e110. doi: 10.1161/STR.0000000000000158

[9]   M. Goyal, B.K. Menon, W.H. van Zwam, D.W. Dippel, P.J. Mitchell, A.M. Demchuk, A. Dávalos, C.B. Majoie, A. van der Lugt, M.A. de Miquel, *et al.* HERMES collaborators. "Endovascular thrombectomy after large-vessel ischaemic stroke: a meta-analysis of individual patient data from five randomised trials." *Lancet.* 2016, vol. 387, pp. 1723–1731. doi: 10.1016/S0140-6736(16)00163-X

[10]   P. Yang, Y. Zhang, L. Zhang, Y. Zhang, K.M. Treurniet, W. Chen, Y. Peng, H. Han, J. Wang, S. Wang, *et al.* DIRECT-MT Investigators. "Endovascular thrombectomy with or without intravenous alteplase in acute stroke." *N Engl J Med.* 2020, vol. 382, pp.1981–1993. doi: 10.1056/NEJMoa2001123

[11]   D.A. de Silva, C. Brekenfeld, M. Ebinger, S. Christensen, P.A. Barber, K.S. Butcher, C.R. Levi, M.W. Parsons, C.F. Bladin, G.A. Donnan, *et al.* Echoplanar Imaging Thrombolytic Evaluation Trial (EPITHET) Investigators. "The benefits of intravenous thrombolysis relate to the site of baseline arterial occlusion in the Echoplanar Imaging Thrombolytic Evaluation Trial (EPITHET)." *Stroke.* 2010, vol. 41, pp. 295–299. doi: 10.1161/STROKEAHA.109.562827

[12]   L. Mueller, F. Pult, J. Meisterernst, M.R. Heldner, M.L. Mono, R. Kurmann, M. Buehlmann, U. Fischer, H.P. Mattle, M. Arnold, *et al.* "Impact of intravenous thrombolysis on recanalization rates in patients with stroke treated with bridging therapy." *Eur J Neurol.* 2017, vol. 24, pp. 1016–1021. doi: 10.1111/ene.13330

[13]   J.L. Saver, M. Goyal, A. Bonafe, H.C. Diener, E.I. Levy, V.M. Pereira, G.W. Albers, C. Cognard, D.J. Cohen, W. Hacke, *et al.* SWIFT PRIME Investigators. "Stent-retriever thrombectomy after intravenous t-PA vs. t-PA alone in stroke." *N Engl J Med.* 2015, vol. 372, pp. 2285–2295. doi: 10.1056/NEJMoa1415061

[14]   M. Goyal, A.M. Demchuk, B.K. Menon, M. Eesa, J.L. Rempel, J. Thornton, D. Roy, T.G. Jovin, R.A. Willinsky, B.L. Sapkota, *et al*; ESCAPE Trial Investigators. "Randomized assessment of rapid endovascular treatment of ischemic stroke." *N Engl J Med.* 2015, vol. 372, pp. 1019–1030. doi: 10.1056/NEJMoa1414905

5

[15]   O.A. Berkhemer, P.S. Fransen, D. Beumer, L.A. van den Berg, H.F. Lingsma, A.J. Yoo, W.J. Schonewille, J.A. Vos, P.J. Nederkoorn, M.J. Wermer, *et al*. MR CLEAN Investigators. "A randomized trial of intra-arterial treatment for acute ischemic stroke." *N Engl J Med.* 2015, vol.372, pp. 11–20. doi: 10.1056/NEJMoa1411587

[16]   B.C. Campbell, P.J. Mitchell, T.J. Kleinig, H.M. Dewey, L. Churilov, N. Yassi, B. Yan, R.J. Dowling, M.W. Parsons, T.J. Oxley, *et al.*; EXTEND-IA Investigators. "Endovascular therapy for ischemic stroke with perfusion-imaging selection." *N Engl J Med.* 2015, vol. 372, pp. 1009–1018. doi: 10.1056/NEJMoa1414792

[17]   T.G. Jovin, A. Chamorro, E. Cobo, M.A. de Miquel, C.A. Molina, A. Rovira, L. San Román, J. Serena, S. Abilleira, M. Ribó, *et al.*; REVASCAT Trial Investigators. "Thrombectomy within 8 hours after symptom onset in ischemic stroke." *N Engl J Med.* 2015, vol. 372, pp. 2296–2306. doi: 10.1056/NEJMoa1503780

[18]   K.W. Muir, G.A. Ford, C.M. Messow, I. Ford, A. Murray, A. Clifton, M.M. Brown, J. Madigan, R. Lenthall, F. Robertson, *et al.*; PISTE Investigators. "Endovascular therapy for acute ischaemic stroke: the Pragmatic Ischaemic Stroke Thrombectomy Evaluation (PISTE) randomised, controlled trial." *J Neurol Neurosurg Psychiatry*. 2017, vol. 88, pp. 38–44. doi: 10.1136/jnnp-2016-314117

[19]   S. Bracard, X. Ducrocq, J.L. Mas, M. Soudant, C. Oppenheim, T. Moulin, F. Guillemin; THRACE investigators. "Mechanical thrombectomy after intra- venous alteplase versus alteplase alone after stroke (THRACE): a randomised controlled trial." *Lancet Neurol.* 2016, vol. 15, pp. 1138–1147. doi: 10.1016/ S1474-4422(16)30177-6

[20]   S. Klein, M. Staring, K. Murphy, M.A. Viergever, J.P. Pluim. "elastix: a toolbox for intensity-based medical image registration." *IEEE Trans Med Imaging.* 2010, vol. 29, pp. 196–205. doi: 10.1109/TMI.2009.2035616

[21]   P.A. Yushkevich, J. Piven, H.C. Hazlett, R.G. Smith, S. Ho, J.C. Gee, G. Gerig "User-guided 3D active contour segmentation of anatomical structures:

significantly improved efficiency and reliability." *Neuroimage.* 2006, vol. 31, pp. 1116– 1128. doi: 10.1016/j.neuroimage.2006.01.015

[22]   E.M. Santos, A.J. Yoo, L.F. Beenen, O.A. Berkhemer, M.D. den Blanken, C. Wismans, W.J. Niessen, C.B. Majoie, H.A. Marquering; MR CLEAN investigators. "Observer variability of absolute and relative thrombus density measurements in patients with acute ischemic stroke." *Neuroradiology.* 2016, vol. 58, pp. 133–139. doi: 10.1007/s00234-015-1607-4

[23]   I.G.H. Jansen, M.J.H.L. Mulder, R.B. Goldhoorn; MR CLEAN Registry investigators. "Endovascular treatment for acute ischaemic stroke in routine clinical practice: prospective, observational cohort study (MR CLEAN Registry)." *BMJ.* 2018, vol. 360, pp. k949. doi: 10.1136/bmj.k949

[24]   M.L. Tolhuisen, J. Enthoven, E.M.M. Santos, W.J. Niessen, L.F.M. Beenen, D.W.J. Dippel, A. van der Lugt, W.H. van Zwam, Y.B.W.E.M. Roos, R.J. van Oostenbrugge, *et al.* "The effect of non-contrast CT slice thickness on thrombus density and perviousness assessment." *Lect Notes Comput Sci.* 2017, vol. 10555, pp. 105–115. doi: 10.1007/978-3-319-67564-0_17

[25]   A.M.M. Boers, I.G.H. Jansen, L.F.M. Beenen, T.G. Devlin, L. San Roman, J.H. Heo, M. Ribó, S. Brown, M.A. Almekhlafi, D.S. Liebeskind, *et al.* "Association of follow-up infarct volume with functional outcome in acute ischemic stroke: a pooled analysis of seven randomized trials." *J Neurointerv Surg.* 2018, vol. 10, pp. 1137–1142. doi: 10.1136/neurintsurg-2017-013724

[26]   D.C. Hoaglin, B. Iglewicz. "Fine-tuning some resistant rules for outlier labeling." *J Am Stat Assoc.* 1987, vol. 82, pp. 1147–1149.

[27]   S.M. Mishra, J. Dykeman, T.T. Sajobi, A. Trivedi, M. Almekhlafi, S.I. Sohn, S. Bal, E. Qazi, A. Calleja, M. Eesa, *et al.* "Early reperfusion rates with IV tPA are deter- mined by CTA clot characteristics." *AJNR Am J Neuroradiol.* 2014, vol. 35, pp. 2265– 2272. doi: 10.3174/ajnr.A4048

[28]   B.K. Menon, F.S. Al-Ajlan, M. Najm, J. Puig, M. Castellanos, D. Dowlatshahi, A. Calleja, S.I. Sohn, S.H. Ahn, A. Poppe, *et al.*; INTERRSeCT Study Investigators. "Association of clinical, imaging, and thrombus characteristics with

5

recanalization of visible intracranial occlusion in patients with acute ischemic stroke." *JAMA.* 2018, vol. 320, pp. 1017–1026. doi: 10.1001/jama.2018.12498

[29]   A.B. Bilgic, R. Gocmen, E.M. Arsava, M.A. Topcuoglu. "The effect of clot volume and permeability on response to intravenous tissue plasminogen activator in acute ischemic stroke." *J Stroke Cerebrovasc Dis.* 2020, vol. 29, pp. 104541. doi: 10.1016/j.jstrokecerebrovasdis.2019.104541

[30]   M. Mokin, M. Waqas, J. Fifi, R. de Leacy, D. Fiorella, E.I. Levy, K. Snyder, R. Hanel, K. Woodward, I. Chaudry, *et al.* "Clot perviousness is associated with first pass success of aspiration thrombectomy in the COMPASS trial." *J Neurointerv Surg.* 2021, vol. 13, pp. 509–514. doi: 10.1136/neurintsurg-2020-016434

[31]   M. Berndt, B. Friedrich, C. Maegerlein, S. Moench, D. Hedderich, M. Lehm, C. Zimmer, A. Straeter, H. Poppert, S. Wunderlich, *et al.* "Thrombus permeability in admission computed tomographic imaging indicates stroke pathogenesis based on thrombus histology." *Stroke.* 2018, vol. 49, pp. 2674–2682. doi: 10.1161/STROKEAHA.118.021873

[32]   J.C. Benson, S.T. Fitzgerald, R. Kadirvel, C. Johnson, D. Dai, D. Karen, D.F. Kallmes, W. Brinjikji. "Clot permeability and histopathology: is a clot's perviousness on CT imaging correlated with its histologic composition?" *J Neurointerv Surg.* 2020, vol. 12, pp. 38–42. doi: 10.1136/neurintsurg-2019-014979

[33]   J. Puig, S. Pedraza, A. Demchuk, J. Daunis-I-Estadella, H. Termes, G. Blasco, G. Soria, I. Boada, S. Remollo, J. Baños, *et al.* "Quantification of thrombus hounsfield units on non-contrast CT predicts stroke subtype and early recanalization after intravenous recombinant tissue plasminogen activator." *AJNR Am J Neuroradiol.* 2012, vol. 33, pp. 90–96. doi: 10.3174/ajnr.A2878

[34]   P.B. Sporns, U. Hanning, W. Schwindt, A. Velasco, B. Buerke, C. Cnyrim, J. Minnerup, W. Heindel, A. Jeibmann, T. Niederstadt. "Ischemic stroke: histological thrombus composition and pre-interventional CT attenuation are associated with intervention time and rate of secondary embolism." *Cerebrovasc Dis.* 2017, vol. 44, pp. 344–350. doi: 10.1159/000481578

[35]   N. Boodt, K.C.J. Compagne, B.G. Dutra, N. Samuels, M.L. Tolhuisen, H.C.B.R. Alves, M. Kappelhof, G.J. Lycklama À Nijeholt, H.A. Marquering, C.B.L.M. Majoie, *et al.*; Coinvestigators MR CLEAN Registry. "Stroke etiology and thrombus computed tomography characteristics in patients with acute ischemic stroke: a MR CLEAN registry substudy." *Stroke.* 2020, vol. 51, pp. 1727–1735. doi: 10.1161/STROKEAHA.119.027749

[36]   A. Kufner, H. Erdur, M. Endres, C.H. Nolte, M. Scheel, L. Schlemm. "Association between thrombus perviousness assessed on computed tomography and stroke cause." *Stroke.* 2020, vol. 51, pp. 3613–3622. doi: 10.1161/STROKEAHA.120.031148

[37]   E.M.M. Santos, C.D. d'Esterre, K.M. Treurniet, W.J. Niessen, M. Najm, M. Goyal, A.M. Demchuk, C.B. Majoie, B.K. Menon, H.A. Marquering; PRove-IT investigators. "Added value of multiphase CTA imaging for thrombus perviousness assessment." *Neuroradiology.* 2018, vol. 60, pp. 71–79. doi: 10.1007/s00234-017-1907-y

[38]   B.C.V. Campbell, P.J. Mitchell, L. Churilov, N. Yassi, T.J. Kleinig, R.J. Dowling, B. Yan, S.J. Bush, H.M. Dewey, V. Thijs, *et al.*; EXTEND-IA TNK Investigators. "Tenecteplase versus alteplase before thrombectomy for ischemic stroke." *N Engl J Med.* 2018, vol. 378, pp. 1573–1582. doi: 10.1056/NEJMoa1716405
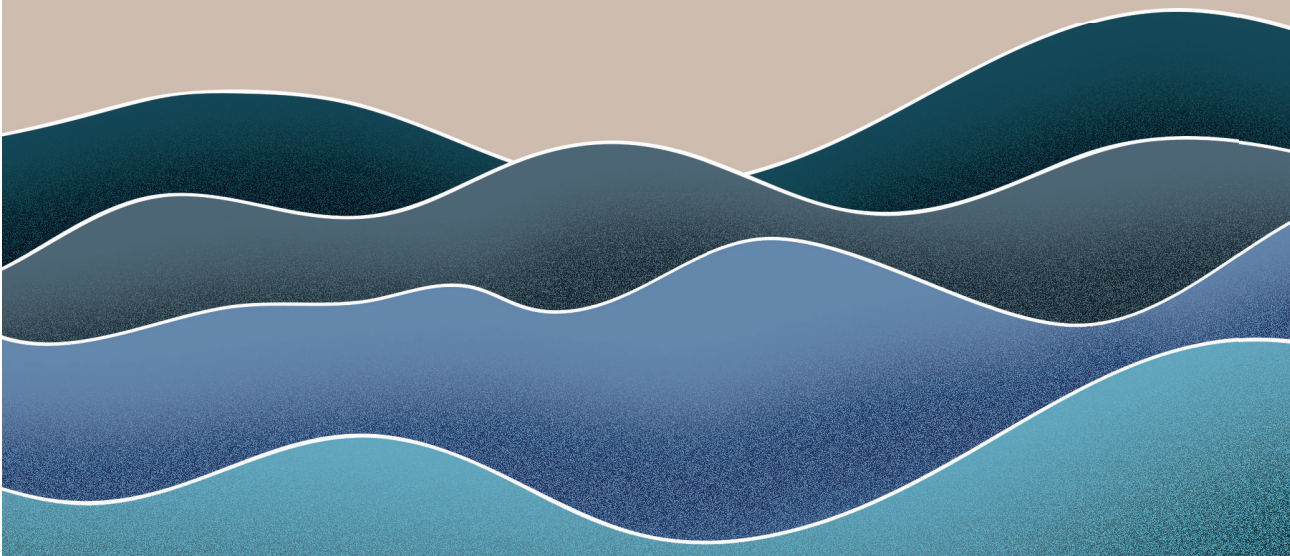
5

Supplementary materials:

Chapter 6
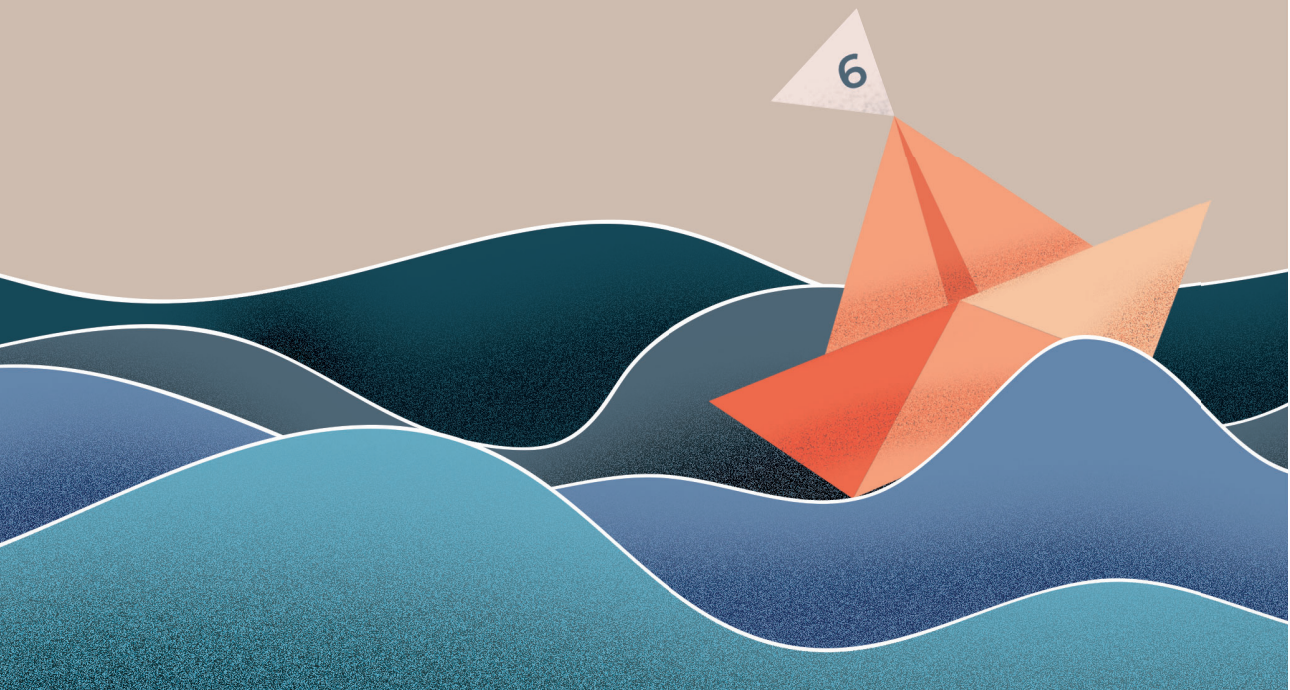
A convolutional neural network for anterior intra-arterial thrombus detection and segmentation on non-contrast computed tomography of patients with acute ischemic stroke

M.L. Tolhuisen, E. Ponomareva, A.M.M. Boers, I.G. H. Jansen, M.S. Koopman, R. Sales Barros, O.A. Berkhemer, W.H. van Zwam, A. van der Lugt, C.B.L.M. Majoie and H.A. Marquering

Abstract

Background— The aim of this study was to develop a convolutional neural network (CNN) that automatically detects and segments intra-arterial thrombi on baseline non-contrast computed tomography (NCCT) scans.

Methods— We retrospectively collected computed tomography (CT)-scans of patients with an anterior circulation large vessel occlusion (LVO) from the Multicenter Randomized Clinical Trial of Endovascular Treatment for Acute Ischemic Stroke in the Netherlands trial, both for training (n = 86) and validation (n = 43). For testing, we included patients with (n = 58) and without (n = 45) an LVO from our comprehensive stroke center. Ground truth was established by consensus between two experts using both CT angiography and NCCT. We evaluated the CNN for correct identification of a thrombus, its location and thrombus segmentation and compared these with the results of a neurologist in training and expert neuroradiologist.

Results— Sensitivity of the CNN thrombus detection was 0.86, vs. 0.95 and 0.79 for the neuroradiologists. Specificity was 0.65 for the network vs. 0.58 and 0.82 for the neuroradiologists. The CNN correctly identified the location of the thrombus in 79% of the cases, compared to 81% and 77% for the neuroradiologists.

Conclusion— The sensitivity and specificity for thrombus identification and the rate for correct thrombus location assessment by the CNN were similar to those of expert neuroradiologists.

Introduction

The outcome of patients with an acute ischemic stroke (AIS) caused by a large vessel occlusion (LVO) of the anterior circulation has been significantly improved since the introduction of endovascular treatment (EVT) [1],[2]. However, the number of patients that reach a favorable functional outcome after treatment is still low [2]. Reducing the time to treatment is currently the main goal in optimizing the treatment of AIS [3-5].

Fast recognition of the occluding thrombus is key in diagnosis and treatment selection. Patients with symptoms of AIS are most commonly brought to the nearest primary stroke center [6],[7]. In most hospitals, computed tomography (CT) is the modality of choice for AIS diagnosis because of its speed and broad availability at emergency rooms [8]. A non-contrast CT (NCCT) is initially acquired to exclude hemorrhagic stroke. An intra-arterial thrombus might already be recognized on NCCT by a hyperdense artery sign (HAS) [9-11]. An additional CT angiography (CTA) is normally used to determine the location of the occlusion and to evaluate the accessibility to the thrombus with EVT. If the stroke is caused by an LVO, patients might need to be transferred to a comprehensive stroke center to receive EVT. Consequently, if an LVO is missed by the radiologist, a patient might be withheld from EVT and not receive appropriate treatment.

Furthermore, a delay in diagnosis and assessment of treatment eligibility reduces the chance of favorable outcome [12-14]. In many primary stroke centers, radiologists are less familiar with the detection of thrombus. Moreover, specialized neuroradiologists are often limitedly available during non-office hours. The automated detection and segmentation of thrombus on baseline NCCT images has the potential to reduce time to treatment and improve appropriate treatment selection.

Convolutional neural networks (CNN) have shown high potential for the automated analysis of medical images. They have been applied with high performance for multiple segmentation tasks, including brain lesion and vessel segmentation [15-18]. The aim of this study was to assess the accuracy of a CNN for (1) identification of intra-arterial thrombus in NCCT of the brain, (2) thrombus location assessment, and (3) thrombus segmentation on baseline NCCT images.

Materials and Methods

Patient Selection and Data Sets

For training and validation of the CNN we used baseline NCCT from the Multicenter Randomized Clinical Trial of Endovascular Treatment for Acute

Ischemic Stroke in the Netherlands (MR CLEAN) trial. MR CLEAN included patients from the Dutch stroke treatment centers with an LVO in the anterior circulation confirmed by CTA [19]. The training and validation set consisted of 86 and 43 NCCT images of stroke patients, respectively. The training and validation set were randomly selected and separated, such that the optimization of the hyperparameters was not influenced by the validation set and the accuracy assessment was performed solely on unseen data. We used the validation set to evaluate network performance during the optimization process.

The accuracy of the trained CNNs was assessed using a test set, which consisted of 58 NCCT scans with a proven LVO and 45 NCCT scans from patients with stroke mimics. For testing, we included patients with AIS or stroke mimics from our comprehensive stroke center. The imaging protocol of our test data was similar to the imaging protocol of the MR CLEAN trial [19]. The study was conducted in accordance with the Declaration of Helsinki. The medical ethical committee of each participating center approved the MR CLEAN trial (MEC-2010-041) and written informed consent was obtained for each participant. For the additional test set, the center's medical ethical committee approved the use of the anonymized datasets in this study and informed consent was waived (W19_255 # 19.307).

We only included scans with a slice thickness less than 2.5 mm and with a maximum time difference between NCCT and CTA of 30 min. We excluded scans with artifacts, excessive noise, and poor contrast enhancement. We also excluded scans of stroke patients with migration of the thrombus between NCCT and CTA acquisition.

Pre-processing

All scans were registered to an atlas so that the NCCT and CTA for each patient were aligned and the voxel dimensions were equal for all scans. The registration ensured that the midplane of the brain coincided with the y-z plane halfway the x-direction. As a result, the hemispheres were symmetrically oriented. For the registration we used ELASTIX ® software [20].

For each patient, we obtained a brain mask using a region growing approach: First, we considered all voxels with intensity value above 160 Hounsfield units (HU) as skull. We filled all foramina within the skull by a morphological dilatation with a 7 mm radius. A seed with a 7 mm radius was placed at the center of gravity of the segmented skull to segment the brain with region growing. The region expanded until the border of the skull was reached. To assure that calcified arteries were included in the mask, we performed an additional closing operation that filled all holes that existed after the region growing step. For the brain mask, all segmentations within slices below the foramen magnum were excluded. The location of the foramen magnum was considered the first slice with a brain segmentation area below 900 mm^2 below the slice with the largest segmented brain area.

CNN design

The thrombus detection was based on two observations: (1) the asymmetry between the hemispheres and (2) the HAS of the thrombus on NCCT images. Therefore, we developed two CNNs: an asymmetry detection network and a HAS detection network. Both networks were patch-based. The asymmetry detection network consisted of two parallel convolutional pathways, one for each hemisphere. The output of both pathways was combined and fed to the fully connected layers. The HAS network consisted of a single convolutional pathway. Patch size was 24×24×24 voxels, corresponding to 12×12×12 mm.

Both networks had a design similar to AlexNet [21] and consisted of five 3D convolutional layers with a $5 \times 5 \times 5$ dimension followed by a Rectified Linear Unit (ReLU) layer (see Figure 6.1). Within the first three layers, we decreased the dimension of the feature maps and increased the number of feature maps by a factor two for each layer. Subsequently, we decreased the number of feature maps by half within each subsequent layer. To reduce the chance for overfitting, we added an additional dropout after the first fully connected layer. We used the default settings of the pytorch library, which is 0.5 for fully connected layers.

The fully connected part of both networks consisted of two fully connected layers followed by ReLU. The input of the fully connected part of the HAS detection network consisted of a single output from the convolutional layers. For the asymmetry detection network, we concatenated the output from the two parallel convolutional pathways before feeding it to the fully connected layers. We added an additional dropout after the first fully connected layer. The CNNs were trained and validated separately. During training, we alternated thrombus patches with non-thrombus patches for input so that the number of thrombus and non-thrombus was balanced. Because the thrombus is very small, we only required a small number of non-thrombus patches to balance the data. As it is possible to extract an abundant number of non-thrombus patches from a single scan, we did not need additional scans to extract negative patches. During the training process, the hyperparameters of the CNN were optimized for correctly discriminating thrombus patches from non-thrombus patches.

Ground truth

Ground truth thrombus segmentations in the MR CLEAN data have been previously obtained in a study performed by Santos et al. [22]. The ground truth thrombus segmentations for the test set were established by joint reading of two experts with >5 years of experience. Because the thrombus location is more apparent for the human eye on CTA images, we used the combination of CTA with the NCCT images to determine the ground truth thrombus location. The thrombus segmentations were performed using ITK-SNAP [23].
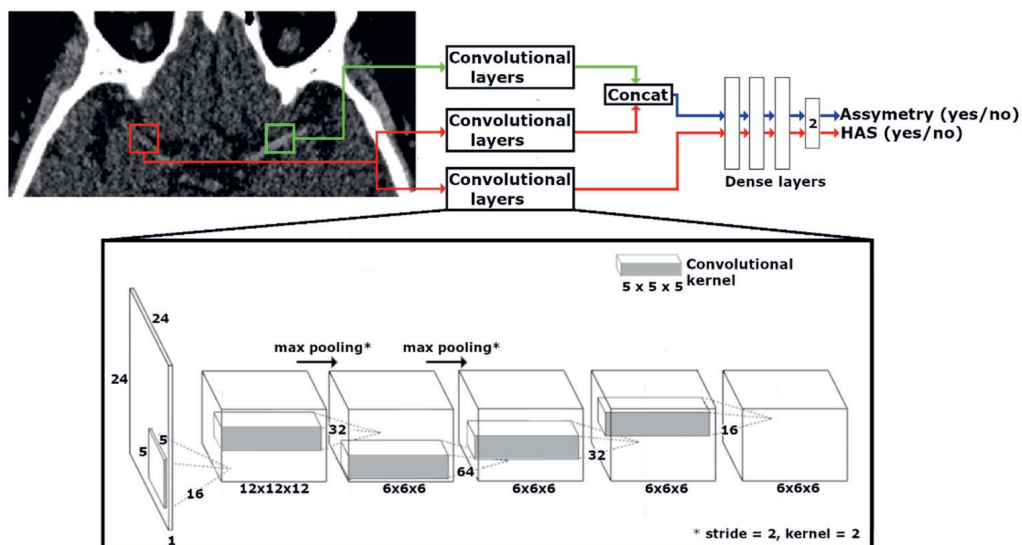
Figure 6.1 *Convolutional neural networks (CNN) architectures for the asymmetry and hyperdense artery sign (HAS) detection network. Both networks have similar architectures. The convolutional layers consist of 5 convolutional layers with max pool layers after the first two convolutions. The asymmetry detection network concatenates the output of the convolutional layer from left and right patch pair, before passing through the dense layers. Dimensions of the feature maps and convolutional kernels are shown at the borders. The number of filters is shown at the forward pass for each convolutional kernel.*

Classification pipeline

To speed up processing, we performed the thrombus segmentation in two steps. For each scan, we first performed a coarse segmentation by feeding both networks with non-overlapping patches. If both networks or only the HAS detection network classified a patch within the scan as "thrombus present", we performed an additional voxel-wise segmentation for that specific patch by the same networks. Therefore, the number of patches per scan to be processed by the networks was reduced.

Network evaluation

We evaluated the CNN for the correct identification of a thrombus, thrombus location assessment and thrombus segmentations. An expert neuroradiologist with >15 years of experience (expert 1) and a neuroradiologist in training with >4 years of experience (expert 2) performed the same task on the same test set independently: the experts evaluated the scans for presence of a thrombus and performed manual segmentations of the thrombus if they assumed the presence of a thrombus in the scan. The neuroradiologists were blinded for any clinical information and were not aware of the ratio of non-thrombus versus thrombus scans. We compared the results from the CNN with those of the experts.

We assessed the sensitivity, specificity and precision for the detection of a thrombus within a NCCT scan. A thrombus was considered as "present" if at least one voxel within the NCCT scan was classified as "thrombus". The thrombus location was considered correct if at least a single voxel of the segmentation overlapped with the ground truth segmentation. Sensitivity was defined as the ratio of thrombi correctly found "present" by the CNN or neuroradiologists and the total number of scans with truly present thrombi according to the ground truth. Specificity was defined as the ratio of thrombi correctly found "absent" by the CNN or neuroradiologists and the total number of scans with absent thrombi according to the ground truth. The accuracy of the thrombus location assessment was defined as the percentage of scans with correct thrombus location. To evaluate the thrombus segmentation of the CNN and both neuroradiologists we assessed the agreement of the thrombus volume and mean density by the computation of the two-way intraclass correlation coefficient (ICC) agreement using the 'irr' library from R CRAN repository [24] for thrombus volume and mean density in HU. The ICC of the thrombus volume assessment was computed for all patients within the test set with a proven thrombus. If a thrombus was not correctly detected, we set the volume to zero. For the ICC of the mean thrombus density, we only included the thrombus density measurements for patients with a proven thrombus for which the CNN and both neuroradiologists correctly detected the thrombus. We additionally

created scatter and Bland–Altman plots to study the relation between the measurements made by network or neuroradiologists and the ground truth.

Results

The sensitivity of the CNN thrombus detection was 0.86, vs. 0.95 and 0.79 for neuroradiologist 1 and 2 respectively (Table 6.1). Specificity was 0.65 for the network vs. 0.58 and 0.82 for the neuroradiologists. Precision was 0.75, 0.74 and 0.81 for the CNN, neuroradiologist 1 and neuroradiologist 2, respectively. The CNN correctly identified the location of the thrombus in 79% of the cases, compared to 81% and 77% for the neuroradiologists. An example of the results is given in Figure 6.2. The agreement in thrombus volume was fair (ICC: 0.49) for the CNN, poor for neuroradiologist 1 (ICC: 0.37) and fair for neuroradiologist 2 (ICC: 0.55). For the thrombus density, the ICC was poor (ICC: 0.14) for the CNN and fair for neuroradiologist 1 and 2 (ICC: 0.45 and ICC: 0.40, respectively). The scatter and Bland–Altman plots for the segmented thrombus volumes and for the thrombus density are shown in Figures 6.3 and 6.4, respectively. The scatter plots show the relation of the thrombus volumes and densities that were computed from the

6
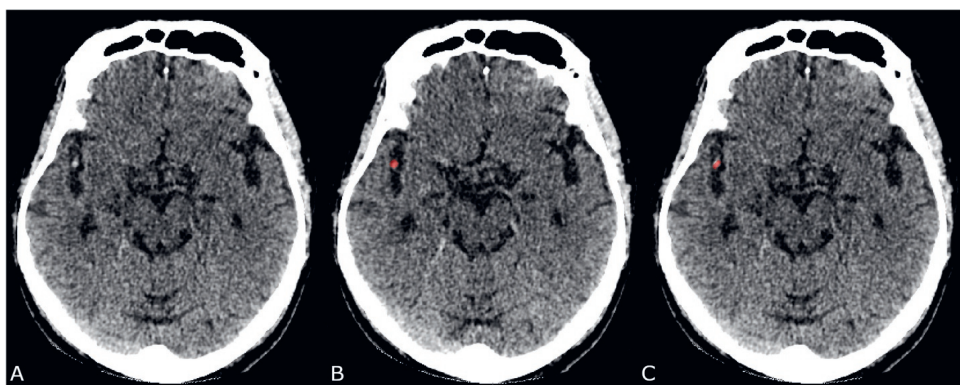
Figure 6.2: *An example of the segmentation results. (A) Original non-contrast computed tomography (NCCT); (B) Segmentation made by one of the neuroradiologists; (C) Segmentation acquired by the CNN*

thrombus segmentations by one of the neuroradiologists or CNN and those of the ground truth. The diagonal line within the scatter plots, represents the perfect match of the results between the neuroradiologists or CNN and ground truth. The Bland–Altman plots show the difference in measurements, comparing the results of the neuroradiologists or CNN with the ground truth. The mean and standard deviation of the differences are also shown within the plots, represented as bias and limits of agreements. The exact values of the bias and limits of agreements for thrombus volume and density, together with the other results are shown in Table 6.1.

Table 6.1. *Test results from the CNN, neuroradiologist 1 and neuroradiologist 2. The table shows sensitivity, specificity, correct thrombus location assessment rate and the intraclass correlation coefficient (ICC) with bias and limits of agreements (LoA) for both thrombus volume and density.*

	CNN	Neuroradiologist 1	Neuroradiologist 2
Sensitivity	0.86	0.93	0.78
Specificity	0.69	0.60	0.88
Precision	0.75	0.74	0.82
Correct thrombus location	0.79	0.81	0.77
Thrombus volume			
ICC	0.49	0.37	0.55
	95% CI: 0.27 to 0.66	95% CI: 0.42 to 0.75	95% CI: 0.29 to 0.72
Bias (mm^3)	73	-58.6	-91.5
LoA (mm^3)	-447/593	-427/309	-453/269
Thrombus density			
ICC	0.14	0.45	0.40
	95% CI: 0.12 to 0.41	95% CI: 0.07 to 0.70	95% CI: 0.07 to 0.64
Bias (mm^3)	-4.6	3.8	2.8
LoA (mm^3)	-18/9	-7/14	-7/13
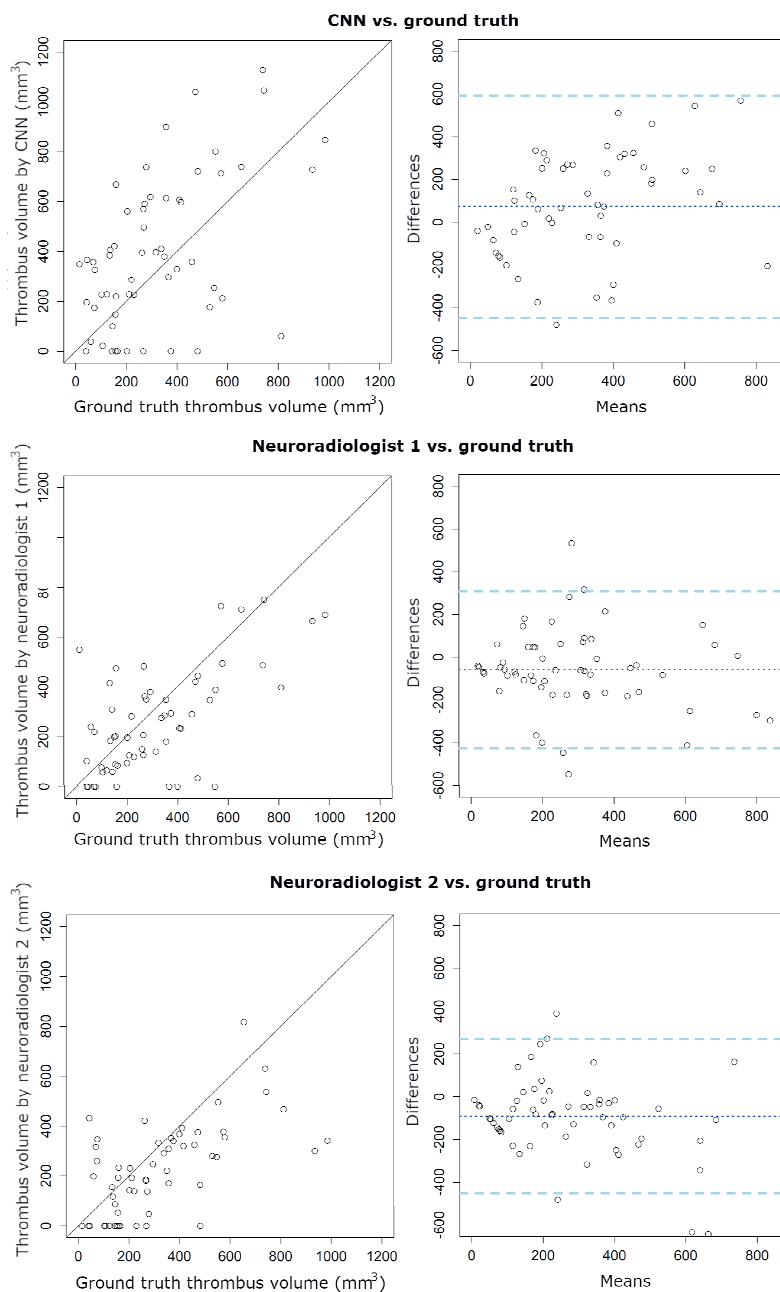
Figure 6.3: *Scatter (Left) and Bland–Altman plots (Right) for thrombus volumes. The dotted line and dashed lines within the Bland–Altman plot represent the bias and limits of agreements, respectively*
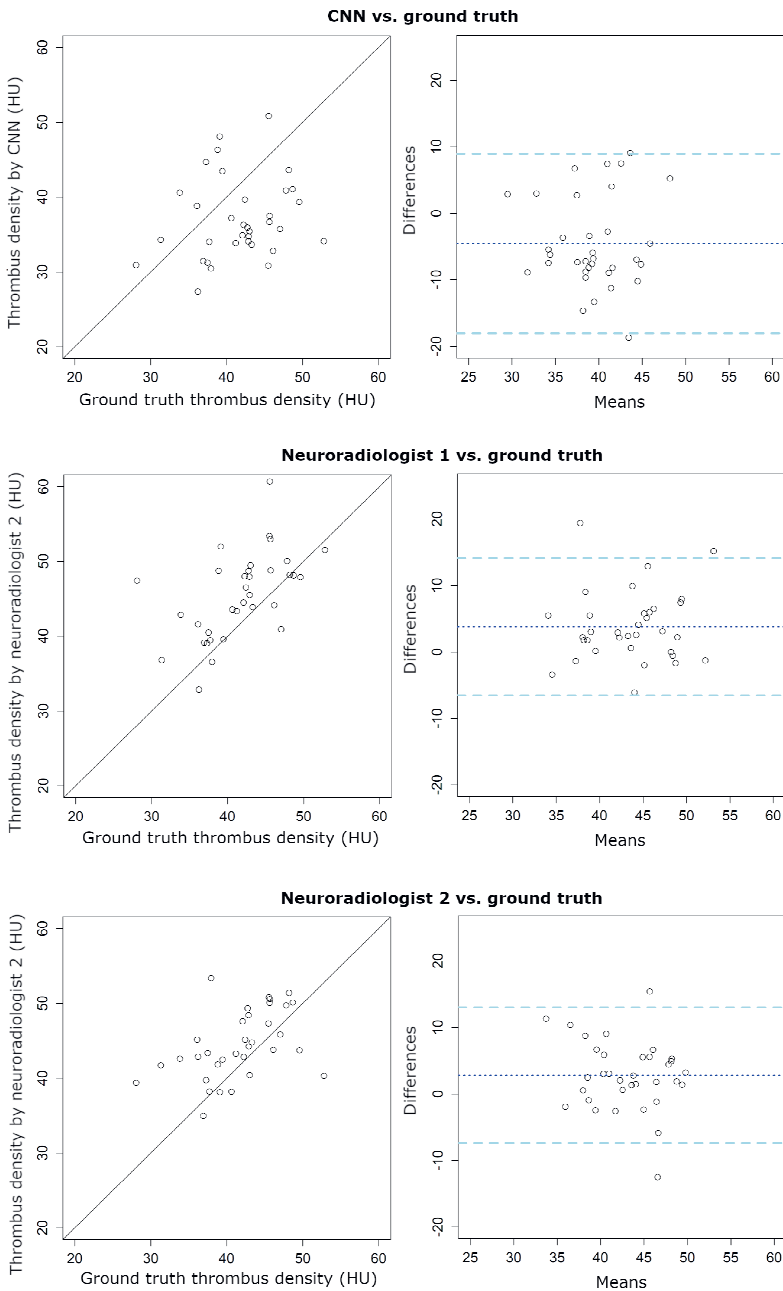
Figure 6.4: *Scatter (Left) and Bland–Altman (Right) plots for thrombus density. The dotted line and dashed lines within the Bland–Altman plot represent the bias and limits of agreements, respectively*

Discussion

We have implemented and evaluated a CNN-based thrombus detection and segmentation approach on baseline NCCT image data. The accuracy was similar to expert neuroradiologists.

Of the two neuroradiologists who evaluated the images, one had highest sensitivity for thrombus identification and thrombus location assessment, while the other had the highest specificity for thrombus detection. In all cases, the network scored second best. The network performed better on sensitivity than specificity, which means that the network is better at detecting true positives than true negatives.

The thrombus volumetric agreement, represented by the ICC, of the segmentations of the network was similar to the agreement amongst the neuroradiologists. However, the agreement of the thrombus density as determined with the network was poor and less accurate than the density agreements of the neuroradiologists. This suggests that, even though the thrombus volume was similar, the thrombus was not segmented at the exact same location as the ground truth segmentation. Moreover, the Bland–Altman plots for the CNN show that the segmentation generated by the CNN generally caused an overestimation of the thrombus volume and underestimation of the thrombus density. The segmentations of both neuroradiologists generally underestimated the thrombus volume and overestimated the thrombus density. Overall, the results suggest that our network is less suitable for exact thrombus segmentation and should mainly be used for thrombus detection.

6

The evaluation of correct thrombus segmentation is challenging because of class imbalance. A common segmentation evaluation is the DICE coefficient, which quantifies the overlap between ground truth and segmentation [25]. However, because the number of background voxels is substantially larger than the number of thrombus voxels the DICE score will be strongly penalized for false positives. Because thrombus volume and density have been associated with treatment outcome [26],[27], we have decided that these parameters were more appropriate evaluation parameters.

Before the presented CNN was established, we evaluated multiple CNN architectures. Hereby, we varied patch size, learning rate, batch size, dropout rate and inclusion of batch normalization. In the end, the presented CNN architecture performed best in discriminating thrombus from non-thrombus patches.

There are a few studies that describe the detection of LVO. Murray et al. published an extensive systematic review in which they summarized the available tools for LVO detection [28]. However, most of these methods do not point out where the thrombus is located. Machine learning methods, such as random forest learning and support vector machines, are used to detect LVO based on the Alberta stroke program early CT score or the detection of diffusion-perfusion mismatch from CT perfusion images. The use of these so-called black-box LVO detection is suboptimal since radiologists have to search for the thrombus location themselves after the detection of the LVO. Moreover, previous approaches detect thrombi in CTA images only, whereas the availability of contrast-enhanced imaging is suboptimal in off-hours situations [29],[30].

Lisowska et al. [31] presented a thrombus segmentation method with a similar approach. Their network performs thrombus detection based on asymmetry in NCCT images. Their network resulted in a high area under the receiver operating characteristic curve, but low precision-sensitivity area under the curve (AUC). Concretely, the network showed high performance for balanced data, but low performance in unbalanced data. This makes their network less suitable for the segmentation of entire scans.

In addition to the approach presented by Lisowska et al. we combined asymmetry detection with HAS detection. Moreover, the presented architecture of our CNNs was based on AlexNet [21], which is a well-known and validated architecture for image recognition tasks. Because our results were obtained by the joined result of both CNN's, we were not able to create an AUC similar to Lisowska et al. and directly compare the results. More specifically, since the two CNN's each have their own threshold, these two thresholds would result in a 3D type of AUC. To compare our results, we computed the Youden's J statistic for our results and made an estimation of this statistic from the AUC presented by Lisowska et al.

From this we were able to conclude that our network outperformed their network. More details on this comparison can be found within the Supplementary Materials (Analysis S1).

The presented CNN has the potential to be used in clinical practice to support non-experts in thrombus detection on baseline NCCT. The detection of thrombus on NCCT has several benefits. First, it can speed up the clinical workup, as NCCT is always performed first. When the thrombus is clearly detected on NCCT, the patient can be immediately sent to a comprehensive stroke center and the intervention team can already be informed before CTA imaging is performed and analyzed. In addition, it could be beneficial for smaller community hospitals, which operate in less developed settings to detect LVOs, without the need for an additional CTA.

The CNN could be incorporated within the current workflow. The application of our network requires registration and pre-processing steps as described in the methods section. With the appropriate hardware typical analysis time is less than 2 min.

Still, the presented results showed that in about 15% of patients the thrombus is missed and approximately 35% of the detected thrombi are actually false positives. Therefore, this network is not yet accurate enough to replace experts and should be considered a support tool. Moreover, in current practice, all patients with a clinical suspicion of an LVO, require a CTA. Before such a CNN could be integrated within daily clinical practice, its value should be assessed in a prospective study to determine if the use of the CNN advances correct thrombus detection, faster treatment and reduction in workload of expert neuroradiologists.

The future availability of accurate thrombus volume segmentation may support the analysis of thrombus image characteristics in large image data sets present in randomized controlled trials. Thrombus density, perviousness and volume have previously been associated with functional outcome and recanalization [26],[27],[32]. Currently, thrombus image characteristics are analyzed using semi-manual annotation, which is tedious, time-consuming and is prone to observer variability. This makes analysis of large number of images less feasible. In

6

contrast, automated segmentation allows for fast segmentation and thrombus biomarker extraction.

Automated accurate thrombus volume segmentation may also support machine learning approaches for the extraction of histological information, based on thrombus image characteristics. For example, Liebeskind et al. [33] showed that thrombus density might characterize thrombi as blood-cell rich or fibrin-rich, indicating whether a thrombus would be susceptible to intravenous thrombolysis. In future work, the CNN could be fed with histological information in combination with the segmentation and location of the thrombus to train for thrombus histology information extraction from imaging data alone.

This study suffers some limitations. First, the sample size of this study was limited. CNN networks require large number of samples to obtain a good accuracy. The more samples are included for training, the more generalizable the CNN will be, since it will be trained on a larger variation of thrombus cases. Since our main goal was to evaluate the accuracy of a tool for thrombus detection and the thrombus segmentations were merely evaluated for exploration for potential future work, we think that the current training dataset is sufficient enough for this proof of concept. We thereby kept track of the training and validation accuracy to prevent from overfitting.

Second, the number of experts that were included to determine the accuracy of manual detection was low. To accurately assess the performance of manual detection for clinical practice, readings by more observers would be required.

Third, the non-thrombus patches used within our training data were obtained from images of patients with an LVO. We made the assumption that the pixel values of patches with no thrombus pixels were comparable to patches that would be sampled from scans acquired from patients with stroke mimics. A limitation of this assumption is that we did not take any parenchymal and/or vascular changes into account that could have been caused by the occlusion.

Finally, we only included patients with anterior circulation LVOs. Future research should extend the task to identifying posterior circulation LVOs and more distal occlusions.

Conclusions

We have proposed a CNN for the detection and segmentation of thrombus in the anterior intra-arterial vasculature on NCCT in order to provide a tool for less experienced radiologists for the fast detection of AIS. The accuracy of thrombus detection is similar to expert neuroradiologists. Therefore, the presented CNN is a promising tool to be included in future clinical workflows. However, the sensitivity and specificity are currently too low to exclude CTA imaging in the workup of patients suspected with an LVO.

Moreover, the results of the thrombus segmentations showed a low volumetric agreement, similar to expert neuroradiologists, and low thrombus density agreement with ground truth. Therefore, the presented network is less suitable for exact thrombus segmentation.

References

[1]   M. Goyal, B.K. Menon, W.H. van Zwam, D.W. Dippel, P.J. Mitchell, A.M. Demchuk *et al.* "Endovascular thrombectomy after large-vessel ischaemic stroke: A meta-analysis of individual patient data from five randomised trials." *Lancet 2016*, vol. 387,pp. 1723–1731. doi:10.1016/S0140-6736(16)00163-X.

[2]   I.G.H. Jansen, M.J.H.L. Mulder, R.J.B. Goldhoorn *et al.* "Endovascular treatment for acute ischaemic stroke in routine clinical practice: Prospective, observational cohort study (MR CLEAN Registry). *BMJ* 2018,vol. 360, pp. k949. doi: 10.1136/bmj.k949.

[3]   J.L. Saver, "Time is brain–Quantified." *Stroke* 2006, vol. 37, pp. 263–266. doi: 10.1161/01.STR.0000196957.55928.ab

[4]   A.J. Yoo, B. Pulli, R.G. Gonzalez, "Imaging-based treatment selection for intravenous and intra-arterial stroke therapies: A comprehensive review." *Expert Rev. Cardiovasc. Ther.* 2011, vol. 9, pp. 857–876. doi: 10.1586/erc.11.56

[5]   E. Venema, M.J.H.L. Mulder, B. Roozenbeek, J.P. Broderick, S.D. Yeatts, P. Khatri, *et al.* "Selection of patients for intra-arterial treatment for acute ischaemic

6

stroke: Development and validation of a clinical decision tool in two randomised trials." *BMJ* 2017, vol. 357, pp. j1710. doi:10.1136/bmj.j1710.

[6]   M. Ismail, X. Armoiry, N. Tau, F. Zhu, U. Sadeh-Gonik, M. Piotin, *et al.* "Mothership versus drip and ship for thrombectomy in patients who had an acute stroke: A systematic review and meta-analysis." *J. Neuro-Interventional Surg.* 2019, vol. 11, pp. 11–19. doi:10.1136/neurintsurg-2018-014249

[7]   M.S. Milne, J.K. Holodinsky, M.D. Hill, A. Nygren, C. Qiu, M. Goyal, *et al.* "Drip 'n Ship Versus Mothership for Endovascular Treatment." *Stroke* 2017, 48, 791–794. doi:10.1161/STROKEAHA.116.015321

[8]   R.E. Latchaw, M.J. Alberts, M.H. Lev, J.J. Connors, R.E. Harbaugh, R.T. Higashida *et al.* "Recommendations for Imaging of Acute Ischemic Stroke." *Stroke* 2009, vol. 40, pp. 3646–3678. doi: 10.1161/STROKEAHA.108.192616

[9]   C. Koo, E. Teasdale, K.W. Muir, "What constitutes a true hyperdense middle cerebral artery sign?" *Cerebrovasc. Dis.* 2000, vol. 10, pp. 419–423.

[10]   G. Mair, E.V. Boyd, F.M. Chappell, R. von Kummer, R.I. Lindley, P. Sandercock *et al.* "Sensitivity and specificity of the hyperdense artery sign for arterial obstruction in acute ischemic stroke." *Stroke* 2015, vol. 46, pp. 102–107. doi: 10.1161/STROKEAHA.114.007036

[11]   J.M. Niesten, I.C. van der Schaaf, L. Van Dam, A. Vink, J.A. Vos, W.J. Schonewille *et al.* "Histopathologic composition of cerebral thrombi of acute stroke patients is correlated with stroke subtype and thrombus attenuation." *PLoS ONE* 2014, vol. 9, pp. 12–14. doi: 10.1371/journal.pone.0088882.

[12]   E. Venema, A.E. Groot, H.F. Lingsma, W. Hinsenveld, K.M. Treurniet, V. Chalos *et al.* "Effect of Interhospital Transfer on Endovascular Treatment for Acute Ischemic Stroke." *Stroke* 2019, vol. 50, pp. 923–930. doi:10.1161/STROKEAHA.118.024091

[13]   R. Gupta, A. Horev, T. Nguyen, *et al.* "Higher volume endovascular stroke centers have faster times to treatment, higher reperfusion rates and higher rates of good clinical outcomes." *J. NeuroInterventional Surg.* 2013, vol. 5, pp. 294–297. doi: 10.1136/neurintsurg-2011-010245.

[14]   N. Kamal, S. Sheng, Y. Xian, *et al.* "Delays in Door-to-Needle Times and Their Impact on Treatment Time and Outcomes in Get with the Guidelines-Stroke." *Stroke* 2017, vol. 48, pp. 946–954. doi: 10.1161/STROKEAHA.116.015712.

[15]   G. Litjens, T. Kooi, B.E. Bejnordi, *et al.* "A survey on deep learning in medical image analysis." *Med. Image Anal.* 2017, vol. 42, pp. 60–88. doi:10.1016/j.media.2017.07.005

[16]   R. Zhang, L. Zhao, W. Lou, J. Abrigo, V.C.T. Mok, W.C.W. Chu *et al.* "Automatic Segmentation of Acute Ischemic Stroke From DWI Using 3-D Fully Convolutional DenseNets." *IEEE Trans. Med. Imaging* 2018, vol. 37, pp. 2149–2160. doi: 10.1109/TMI.2018.2821244

[17]   G. Tetteh, V. Efremov, N.D. Forkert, M. Schneider, J. Kirschke, B. Weber, *et al.* "DeepVesselNet: Vessel Segmentation, Centerline Prediction, and Bifurcation Detection in 3-D Angiographic Volumes." *arXiv* 2018, arXiv:1803.09340

[18]   K. Kamnitsas, C. Ledig, V.F.J. Newcombe, J.P. Simpson, A.D. Kane, D.K. Menon *et al.* "Efficient multi-scale 3D CNN with fully connected CRF for accurate brain lesion segmentation." *Med. Image Anal.* 2017, vol. 36, pp. 61–78, doi: 10.1016/j.media.2016.10.004

[19]   O.A. Berkhemer, P.S. Fransen, D. Beumer, L.A.V.D. Berg, H.F. Lingsma, A.J. Yoo *et al.* "A Randomized Trial of Intraarterial Treatment for Acute Ischemic Stroke." *N. Engl. J. Med.* 2014, vol. 372, pp. 11-20, doi: 10.1056/NEJMoa1411587

[20]   S. Klein, M. Staring, K. Murphy, M. Viergever and J. Pluim, "Elastix: A toolbox for intensity-based medical image registration." *IEEE Trans. Med. Imaging* 2010, vol. 29, pp. 196–205. doi: 10.1109/TMI.2009.2035616.

[21]   A. Krizhevsky, I. Sutskever and G.E. Hinton, "ImageNet Classification with Deep Conventional Neural Networks." *Adv. Neural Inf. Process. Syst.* 2012, vol. 1, pp. 1097-1105, doi: 10.1145/3065386

[22]   E. Santos, W. Niessen, A.J. Yoo *et al.* "Automated Entire Thrombus Density Measurements for Robust and Comprehensive Thrombus Characterization in Patients with Acute Ischemic Stroke." *PLoS ONE* 2016, vol. 11, pp. 1–16. doi: 10.1371/journal.pone.0145641

6

[23]   P.A. Yushkevich, J. Piven, H.C. Hazlett, *et al.* "User-guided 3D active contour segmentation of anatomical structures: Significantly improved efficiency and reliability." *Neuroimage* 2006, vol. 31, pp. 1116–1128. doi:10.1016/j.neuroimage.2006.01.015

[24]   M. Garner and J. Lemon, _irr: Various Coefficients of Interrater Reliability and Agreement._ R package version 0.84.1 IFPS 2019, Available online: https://CRAN.R-project.prd/package=irr (accessed on 29 May 2020).

[25]   A.A. Taha and A. Hanbury,"Metrics for evaluating 3D medical image segmentation: Analysis, selection, and tool." *BMC Med. Imaging* 2015, vol. 15, pp. 29. doi: 10.1186/s12880-015-0068-x

[26]   J. Yoo, J.H. Baek, H. Park, D. Song, Kim, K.; Hwang, I.G.; Kim, Y.D.; Kim, S.H.; Lee, H.S.; Ahn, S.H.; *et al*. "Thrombus Volume as a Predictor of Nonrecanalization After Intravenous Thrombolysis in Acute Stroke." *Stroke* 2018, vol. 49, pp. 2108–2115, doi: 10.1161/STROKEAHA.118.021864.

[27]   P. Moftakhar, J.D. English, D.L. Cooke, *et al.* "Density of Thrombus on Admission CT Predicts Revascularization Efficacy in Large Vessel Occlusion Acute Ischemic Stroke." *Stroke* 2013, vol. 44, pp. 243–246, doi: 10.1161/STROKEAHA.112.674127

[28]   N.M. Murray, M. Unberath, G.D. Hager, F.K. Hui, "Artificial intelligence to diagnose ischemic stroke and identify large vessel occlusions: A systematic review." *J. NeuroInterventional Surg.* 2020, vol. 12, pp. 156–164, doi: 10.1136/neurintsurg-2019-015135

[29]   A. Chatterjee, N.R. Somayaji, I.M. Kabakis, "Abstract WMP16: Artificial Intelligence Detection of Cerebrovascular Large Vessel Occlusion–Nine Month, 650 Patient Evaluation of the Diagnostic Accuracy and Performance of the Viz.ai LVO Algorithm." *Int Stroke Conf* 2019 Moderated Poster Abstracts Session Title: Acute Neuroimaging Moderated Poster Tour; Honolulu, Hawaï 10-12 February 2019, Stroke, vol. 50, Suppl_1, doi: 10.1161/str.50.suppl_1.WMP16

[30]   C. Barreira, M. Bouslama, J. Lim, A. Al-Bayati, Y. Saleem, *et al.* "E-108 Aladin study: Automated large artery occlusion detection in stroke imaging study –

a multicenter analysis*." J. NeuroInterventional Surg.* 2018, vol. 10 (Suppl. 2), doi: https://doi.org/10.1161/str.49.suppl_1.WP61.

[31]   A. Lisowska, E. Beveridge, K. Muir, I. Poole, "Thrombus Detection in CT Brain Scans using a Convolutional Neural Network. In Proceedings of the 10th International Joint Conference on Biomedical Engineering Systems and Technologies(BIOSTEC 2017)", Porto, Portugal, 21–23 February 2017; pp. 24–33.

[32]   E. Santos, J. Dankbaar, K.M. Treurniet, A. Horsch, Y. Roos *et al.* "Permeable Thrombi Are Associated With Higher Intravenous Recombinant Tissue-Type Plasminogen Activator Treatment Success in Patients With Acute Ischemic Stroke" *Stroke* 2016, vol. 47, pp. 2058–2065, doi: 10.1161/STROKEAHA.116.013306
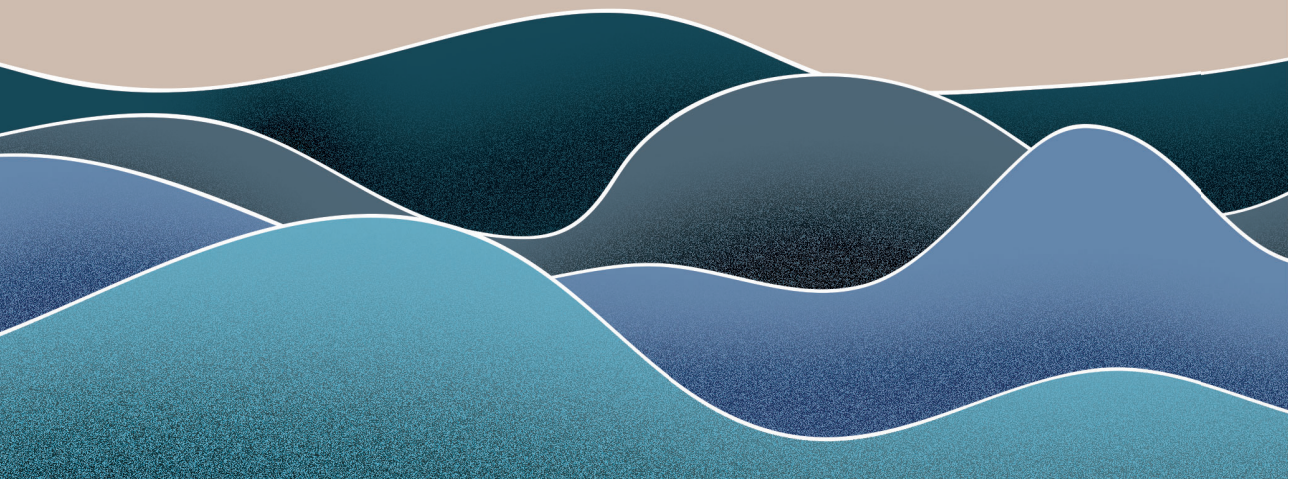
[33]   D.S. Liebeskind, N. Sanossian, W.H. Yong, S. Starkman, M.P. Tsang, A.L. *et al.* "CT and MRI early vessel signs reflect clot composition in acute stroke" *Stroke* 2011, vol. 42, pp. 1237-1243, doi: 10.1161/STROKEAHA.110.605576
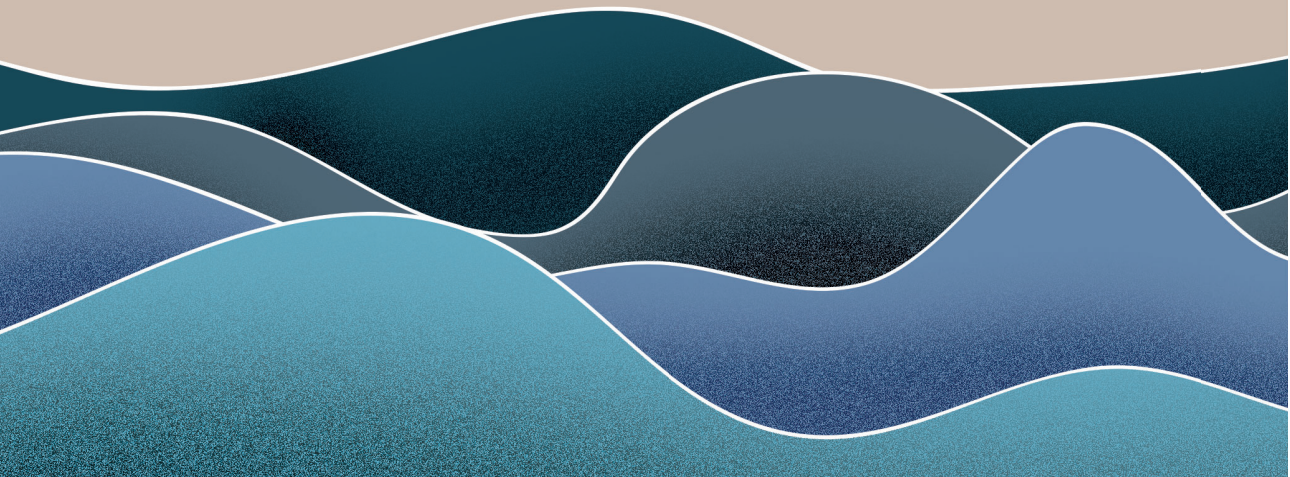
Supplementary materials:

6

# Part II - infarct core

Chapter 7

Automatic segmentation of cerebral infarcts in follow-up computed tomography images with convolutional neural networks

R. Sales Barros, M.L. Tolhuisen, A.M.M. Boers, I.G.H. Jansen, E. Ponomareva, D.W.J. Dippel, A. van der Lugt, R.J. van Oostenbrugge, W.H. van Zwam, O.A. Berkhemer, M. Goyal, A.M. Demchuk, B.K. Menon, P. Mitchell, M.D. Hill, T.G. Jovin, A. Davalos, B.C. V. Campbell, J.L. Saver, Y.B.W.E.M. Roos, K.W. Muir, P. White, S. Bracard, F. Guillemin, S. Delgado Olabarriaga, C.B. L. M. Majoie and H.A. Marquering

7
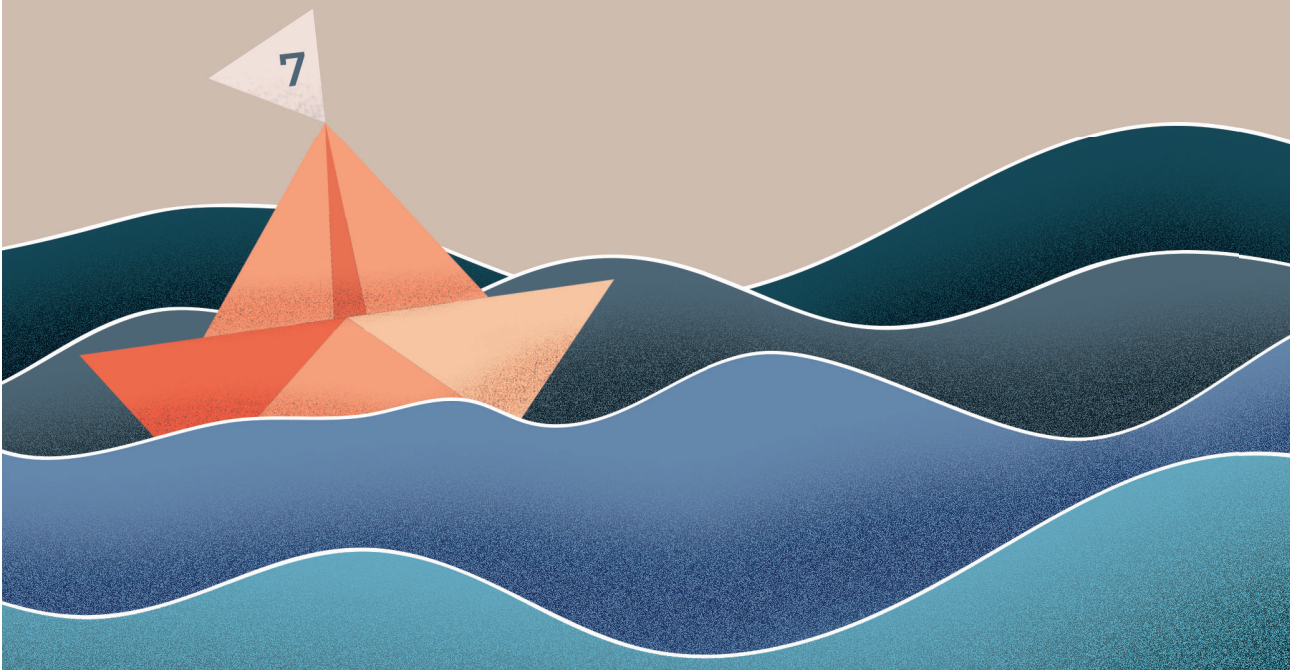
Abstract

Background—Infarct volume is a valuable outcome measure in treatment trials of acute ischemic stroke and is strongly associated with functional outcome. Its manual volumetric assessment is, however, too demanding to be implemented in clinical practice. The aim of this study is to assess the value of convolutional neural networks (CNNs) in the automatic segmentation of infarct volume in follow-up CT images in a large population of patients with acute ischemic stroke.

Methods—We included CT images of 1026 patients from a large pooling of patients with acute ischemic stroke. A reference standard for the infarct segmentation was generated by manual delineation. We introduce three CNN models for the segmentation of subtle, intermediate, and severe hypodense lesions. The fully automated infarct segmentation was defined as the combination of the results of these three CNNs. The results of the three-CNNs approach were compared with the results from a single-CNN approach and with the reference standard segmentations.

Results—The median infarct volume was 48 mL (IQR 15–125 ml). Comparison between the volumes of the three-CNNs approach and manually delineated infarct volumes showed excellent agreement, with an intraclass correlation coefficient (ICC) of 0.88. Even better agreement was found for severe and intermediate hypodense infarcts, with ICCs of 0.98 and 0.93, respectively. Although the number of patients used for training in the single-CNN approach was much larger, the accuracy of the three-CNNs approach strongly outperformed the single-CNN approach, which had an ICC of 0.34.

Conclusion—Convolutional neural networks are valuable and accurate in the quantitative assessment of infarct volumes, for both subtle and severe hypodense infarcts in follow-up CT images. Our proposed three-CNNs approach strongly outperforms a more straightforward single-CNN approach.

Introduction

Measuring the volume of infarcts on non-contrast computed tomography (NCCT) scans provides a quantitative assessment of infarcted brain tissue resulting from ischemic stroke. Follow- up infarct volume measured after 24 hours from onset [1] is a valuable predictor of functional outcome. Infarct volume has been suggested as a surrogate endpoint for classic patient outcome scales in multiple randomized controlled trials.[2] By combining infarct volume with infarct location, a more precise prediction of patient outcome can be achieved.[3]

The reference standard for infarct segmentation is manual delineation by medical experts. However, manual delineation has several disadvantages as it is time-demanding, subjective, prone to errors, and costly.[4] Accordingly, manual delineation does not work well in large cohort studies.

Convolutional neural networks (CNNs) have outperformed many existing image analysis methods for image classification and image segmentation. CNNs have produced good segmentation results in multiple medical imaging domains, including segmentation of ischemic stroke lesions in magnetic resonance images of the brain.[5–7] In this study, we evaluated the usefulness of CNNs for automatic segmentation of infarcted brain tissue in follow-up NCCT scans from patients with an acute ischemic stroke.

Materials and Methods

Image data

We used anonymized image data from the HERMES collaboration.[8] This collaboration combined clinical and image data from seven clinical trials that investigated the efficacy of endovascular therapy in patients with acute ischemic stroke. Central medical ethics committees and research boards of each participating hospital approved each trial and the use of anonymized image data in this retrospective study. All patients, or their legal representatives, provided written informed consent.

We used image data only from patients with follow-up NCCT acquired between 12 hours and 2 weeks after stroke onset and for whom a reference infarct segmentation was available. A total of 1026 patients had follow-up NCCT imaging acquired within the selected time window and with an available reference segmentation. Thin-slice image data were reconstructed into scans with 5 mm slice thickness.

Reference segmentations

The reference infarct segmentation on the follow-up NCCT scans was manually delineated by one of two experienced observers, as described by Boers et al.[9] In short, infarcts were identified as hypodense areas. Infarcted tissue in the ipsilateral hemisphere with characteristics of an old infarct were excluded from the reference segmentation. NCCT scans of patients who underwent decompressive hemicraniectomy were excluded. Parenchymal hemorrhages within or adjacent to the infarcted area were included in the reference segmentation. A standard window width of 30 Hounsfield units (HU) and center level of 35 HU were used to limit variation between observers. If multiple follow-up images were available, reference segmentation was performed in the latest acquired scan. The manual segmentations were checked by one of three expert radiologists and, when necessary, corrections were made.

Preprocessing

To exclude trivial voxels that were of no interest, such as air or skull, we used automatic methods for intracranial region and cerebrospinal fluid (CSF) segmentation. First, we excluded all voxels outside the brain using an intracranial region segmentation. Subsequently, we also discarded all voxels selected by the CSF segmentation. All discarded voxels were neither used to train the CNN nor used for accuracy testing of the CNN.

The intracranial region segmentation uses the size range of the foramina of the skull, as reported by Berge et al. [10], and typical HU values of the skull. This segmentation was performed according to the following steps:

- A threshold-based segmentation was performed to segment bones. We considered everything with intensity >160 HU as bone.
- A morphological dilatation with a 7 mm radius was used to close all foramina of the skull except the foramen magnum.
- The center of gravity of the segmented bone was used as a seed for a region growing inside the skull.
- A morphological dilatation with a 7 mm radius was applied to the region growing result to bring the segmented intracranial region close to the skull border.
- The foramen magnum was detected by evaluation of the segmented area in each individual slice from top to bottom. The foramen magnum slice was determined as the first slice with a segmented area <900 mm² after the slice with the maximum segmented area. All voxels below the foramen magnum slice were excluded from the segmentation.

The CSF segmentation was performed by selecting the voxels around the centroid of the segmented intracranial region as seeds for region growing. All voxels within a maximum distance of 15 mm from this centroid and with density values between −5 and 13 HU were used as seeds. The lower and upper thresholds of this region growing were also −5 and 13 HU.

We used a previously presented method for automated intra-cranial hemorrhage segmentation [11] to exclude the parenchymal hemorrhages of the CNN- based infarct segmentation. These hemorrhage voxels were not used to train the CNN. However, for infarct volume accuracy testing, any area that was classified as hemorrhage was added to the infarct segmentation.

CNN-based infarct segmentation

The CNN architecture used in this study was developed in-house. Its hyperparameters were optimized for segmentation of a single foreground structure in head NCCT scans, which in this case was the infarcted brain tissue. Previously, the same CNN architecture was successfully used for intracranial hemorrhage segmentation.[11] This CNN architecture determines the probability of the voxel at

7

the center of an image patch being foreground (infarcted tissue) or background (any other tissue). This probability was subsequently dichotomized using a cut-off value, which was optimized with the data in the validation set.

The CNN architecture has two convolutional layers followed by two fully connected dense layers. Each dense layer has 256 nodes. The size of the input patch was 19×19×3 voxels; 19×19 voxels in the axial plane and three slices high. Each slice of the input patch was processed as a different image channel. After each convolutional layer, there is a max-pooling layer with a 2×2 kernel and a 2×2 stride. The first convolutional layer has 64 feature maps and the second has 128 feature maps. Both convolutional layers have kernels with size 5×5.

The hypodensity of the infarcted tissue in NCCT scans is related to breakdown of cells and its fluid content. As shown in Figure 7.1, the infarcted areas in the three NCCT scans have different HU values. In Figure 7.1, we also show the distribution of the average HU values of the infarct reference segmentations. In our population, the HU value distribution depicted three peaks, which we named subtle, intermediate, and severe hypodense infarcts. Because of this observation, we trained three CNNs. Each of these CNNs was trained to classify a different hypodensity distribution of infarcted brain tissue. We grouped all patients according to the hypodensity of the delineated infarct. We used the average HU value of the infarction for this grouping. The average infarct intensity was computed after excluding the hemorrhage voxels of the reference segmentation. The thresholds that define each infarction class were (14, 22) HU for severe, (22, 32) HU for intermediate, and (32, 44) HU for subtle.

We used 570 randomly selected scans to train the three CNNs. We augmented the number of training infarct patches by flipping along the sagittal plane and by rotation. No data augmentation was applied to the non-infarct patches. We used an additional 60 scans to optimize the cut-off value for generating binary segmentations, 20 scans for each CNN. The union of the results of these three CNNs and the result of the intracranial hemorrhage segmentation was considered to be the automated generated infarct segmentation. The remaining 396 scans were used to test segmentation performance.
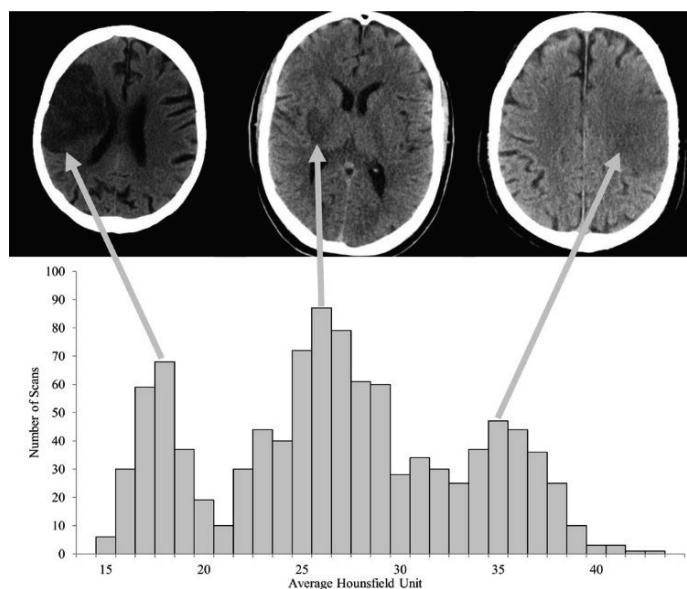
Figure 7.1: Histogram of average infarct intensities of the manually delineated infarcts. The left CT image at the top displays a relatively old infarct with a severe hypodensity; in the middle, an intermediate old infarct is shown; and the image on the right shows a relatively young infarct with a subtle hypodensity.

For comparison, we also trained a single CNN architecture for the segmentation of all types of infarction. The same methodology and data were used for this single CNN approach and the three-CNNs approach.

We used the Dice coefficient as an accuracy measure of the infarct segmentation performance in the test set. We calculated the intraclass correlation coefficients (ICCs) to compare the reference and the automatically generated infarct volumes. ICCs were interpreted according to the American Psychological Association al. [12] :<0.4 is poor; ≥0.4 to <0.6 is fair, ≥0.6 to <0.75 is good, and ≥0.75 is excellent. We opted not to compare our approach with U-Net or Mask R-CNN architectures. Both these architectures are more extensive than the proposed architecture and, in a straightforward approach, their input would be an entire NCCT slice. Since we used 5 mm reconstructions, and not all slices from a NCCT scan have infarction, we did not expect a satisfactory segmentation given the

limited number of NCCT slices with infarcted brain tissue that would be used as training samples.

Results

The median infarct volume was 48 (IQR 15–125) mL overall, with 29 (IQR 11–86), 46 (IQR 18–101), and 89 (IQR 35–210) mL for patients with a subtle, intermediate, and severe hypodense infarct, respectively.

The comparison between manually delineated infarct volumes and the volumes from the three-CNNs approach showed an excellent agreement with an ICC of 0.88. Even better agreement was observed for severe and intermediate hypodense infarcts with ICCs of 0.98 and 0.93, respectively. Agreement was good for subtle
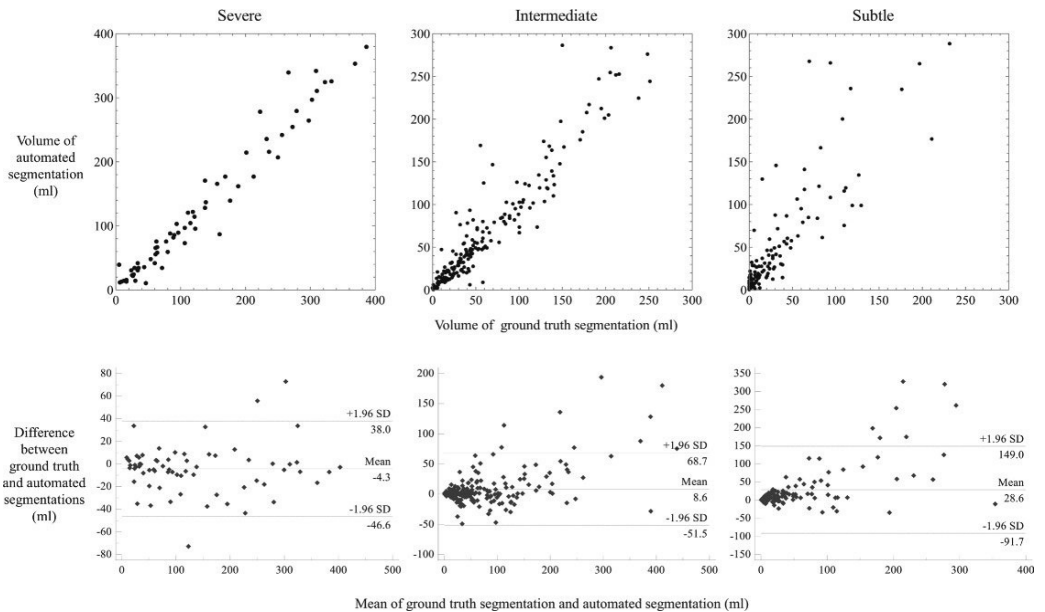
Figure 7.2: *Top: Comparison of the infarct volume of the results from the three-CNNs approach (y axis) with the reference to infarct volume (x axis). Bottom: Bland-Altman plots of the infarct volumes. The difference in the volume determination is given along the y axis, and the average of the automated and reference infarct volume is depicted along the x axis. The different columns show separate severe, intermediate, and subtle hypodensity infarcts.*

Table 7.1: *Results of automated infarct segmentation for severe, intermediate, and subtle hypodense infarcts and the average over the whole test dataset for the three-CNNs approach. For comparison with the accuracy of the single CNN approach.*

	ICC	Dice	Test set size
Three-CNNS approach			
Severe	0.98	0.78±0.09	67
Intermediate	0.93	0.61±0.21	204
Subtle	0.66	0.37±0.26	125
All infarctions	0.88	0.57±0.26	396
Single CNN approach			
All infarctions	0.34	0.18±0.23	396

*CNN, convolutional neural network; ICC, intraclass correlation coefficient*

hypodense infarcts, with an ICC of 0.66. In Figure 7.2, the agreement between the infarct volumes is shown. Agreement of the single CNN approach was poor, with an ICC of 0.34.

The average Dice coefficient achieved by the three-CNNs approach was 0.57±0.26. The average Dice coefficients for each category were 0.78±0.09, 0.61±0.21, and 0.37±0.26, for the severe, intermediate, and subtle hypodense infarcts, respectively. The method based on a single CNN achieved an average Dice coefficient of 0.18±0.23. Table 7.1 shows a summary of the segmentation performance measures. In Figure 7.3, we show some sample results from the three-CNNs approach.

Discussion

We have shown that CNNs are valuable in the automated cerebral infarct segmentation in follow-up CT images of patients with acute ischemic stroke, with excellent agreement with volumetric assessments of expert observers. Owing to the wide variety of the severity of hypodensities, we proposed using the combination of three CNNs, which strongly outperformed a single CNN approach.

Infarct location and infarct volume have been strongly associated with outcome of patients with ischemic stroke in several studies.[3],[13] Reliably segmenting
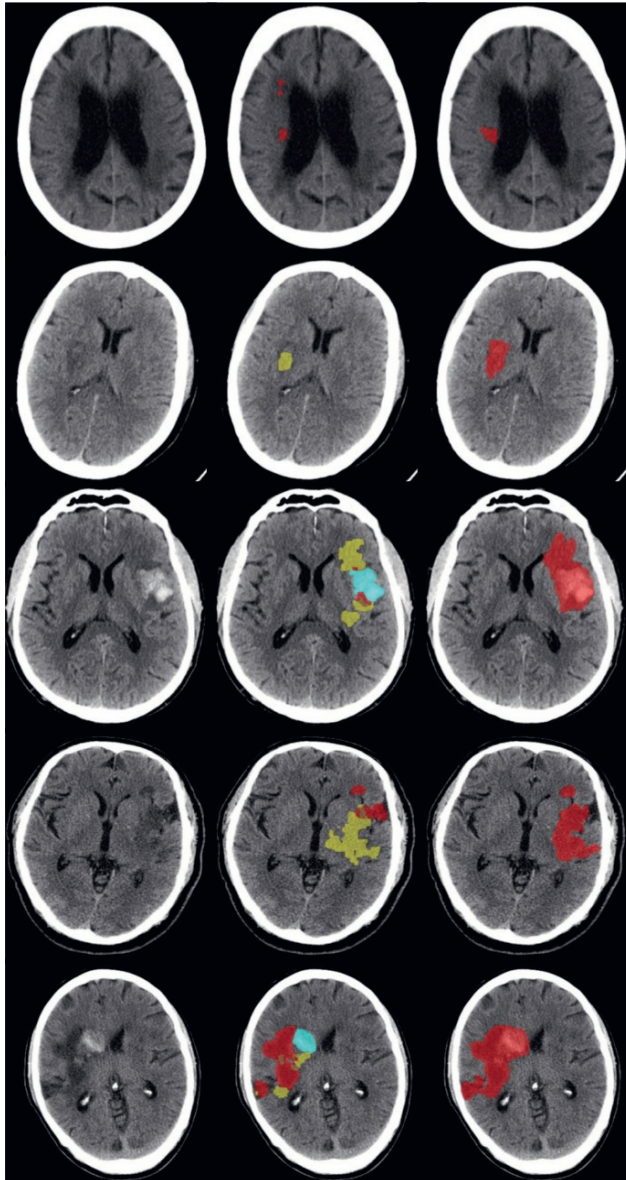
Figure 7.3: Sample results. From left to right we have input image, union of the segmentation results, and reference segmentation. For simplicity, in the center column we rendered the hemorrhages (blue) over the subtle infarcts (yellow), subtle infarcts over standard infarcts (orange), and standard infarcts over severe infarcts (red). The Dice coefficients from top to bottom were 0.10, 0.26, 0.40, 0.55, and 0.70. In the left column the original images are shown. The right shows the merged segmentations

cerebral infarcts is challenging because of pathophysiological heterogeneity, presence of pre-existing pathologies such as old infarcts, leukoaraiosis, atrophy, intrinsic differences in attenuation of grey and white matter, and hemorrhagic transformation. Thus, to be able to develop robust automated methods for cerebral infarct segmentation, heterogeneous image data are required. The proposed method was evaluated in a large cohort of patients from seven multicenter randomized trials enrolling in multiple countries. The follow-up NCCT scans used in our study also had a (pragmatically) wide range of follow-up time after stroke onset, ranging from 12 hours to 2 weeks. Despite these variations, the proposed approach based on three different CNNs produced accurate cerebral infarct segmentations. The volume of these segmentations had good or excellent correlation with the reference infarct volume. We have shown that accuracy for old, severe hypodense infarcts was higher than for subtle hypodense infarcts. Note that, although we presented the results in a selective manner, exactly the same procedure was applied for the infarct segmentations in all the three different infarct categories.

A number of previous studies on automatic infarct core segmentation in various image modalities have been presented. Multiple CNN-based techniques have been introduced recently. On baseline CT perfusion, state-of-the-art infarct segmentation was obtained by a CNN architecture proposed by Liu et al., [14] achieving an average Dice coefficient of 0.51 ± 0.31. On MRI the CNN architecture proposed by Kamnitsas et al. [6] reported an average Dice coefficient of 0.66 ± 0.24. Maier et al7 tested several methods with different types of MR images. Their best reported result was achieved by a CNN with an average Dice coefficient of 0.73 ± 0.18. The current state-of-the-art method for infarct segmentation on MR images is the CNN proposed by Zhang et al., [5] which achieved an average Dice coefficient of 0.79 in a test set with 90 images. Although good segmentation results were achieved in CT perfusion and MR images, NCCT scans are still the predominant method for assessment of follow-up infarct in patients with ischemic stroke. Therefore, we focused on using NCCT as input for the proposed cerebral infarct segmentation method.

7

On NCCT scans, two semi-automated methods are available for infarct segmentation. The semi-automated method by Bardera et al. [15] was evaluated with 18 patients and reported a Pearson's correlation coefficient of 0.98 and 0.97 compared with the manual segmentations from two different observers. The semi-automated method by Kuang et al. [16] was evaluated with 16 patients and reported an average Dice coefficient of 0.76±0.10. By contrast, our method is both fully automated, which avoids the variability introduced by the user inputs, and has been tested on a far larger number of patients.

Other fully automated methods for infarct segmentation on NCCT are available. The method by Boers et al. [17] reported an average Dice coefficient of 0.74±0.13 in a test set with 34 images. The average onset to follow-up scanning time in the study by Boers et al. was 4.1±2.3 days. The average Dice coefficient between human observers in the study by Boers et al. was 0.84 ranging from 0.63 to 0.94, which was somewhat higher than the agreement we achieved. However, it should be noted that the manual delineation was performed for old, hypodense infarcts only. The method by Vos et al. [18] reported an average Dice coefficient of 0.74±0.09 in a test set with 30 images. In the study by Vos et al, the average time between onset and scan acquisition was 3 days ranging between 2 and 5 days. More recently, the method by Gillebert et al. [19] was evaluated with 12 patients with ischemic stroke and reported Dice coefficients ranging from 0.27 to 0.71. The scans used to evaluate the method by Gillebert et al. had an average acquisition time after onset of 40 hours. Their method was evaluated in a limited set of selected images to illustrate different types of ischemic stroke lesions. In contrast with the methods of Boers et al., Vos et al., and Gillebert et al., our method has been thoroughly evaluated with a large and diverse test set.

The data used in our study included follow-up scans as early as 12 hours after stroke onset. Infarcts in these early follow-up scans might be subtle and harder to segment. Thus, it was expected that our method would achieve a lower accuracy in such scans. Moreover, the manual delineation in these scans is more difficult, resulting in more variation among experts. This may also strongly contribute to the lower agreement of the automated method with the reference standard. It some

cases (also in Figure 7.3), the network in charge of segmenting subtle infarcts overestimates the infarct region by including subtle hypodense areas which are not part of the infarction. Another common source of misclassifications by our proposed method is the inclusion of cerebral sulci in the results of the network trained to segment severe infarctions (Figure 7.3).

A major limitation is the highly selective nature of the HERMES population. All patients had anterior circulation stroke confirmed by CT angiography, mostly within 6 hours of onset. Patients were excluded from most studies if they had prior disability or low Alberta Stroke Program Early CT scores. As a result, many of the background abnormalities typical in populations with acute stroke were less prevalent in our population. Moreover, average age was around 69, and very elderly patients were under-represented. Despite variation among study populations, these still represent a much more homogeneous group than patients with stroke as a whole.

Overall, the proposed method achieved an excellent correlation with the reference infarct volume. This suggests that our method can be used in clinical trials, replacing tedious manual delineations. Its value in functional outcome prediction for patients with ischemic stroke and its value as a secondary outcome measure in treatment trials still has to be established.
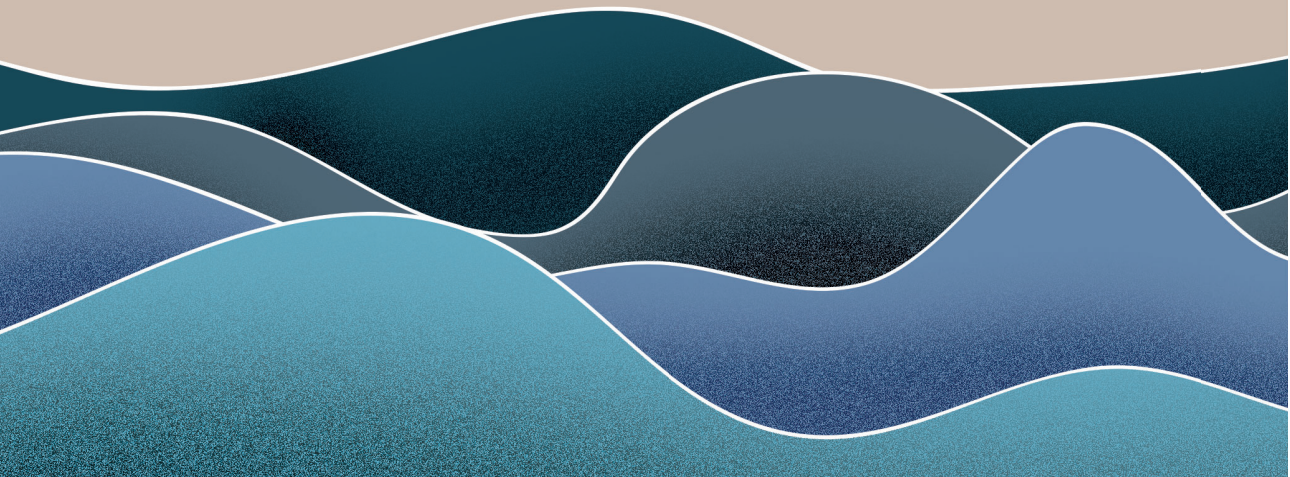
References

[1]   O.A. Berkhemer, S. Kamalian, R.G. González, *et al.* "Imaging biomarkers for intra-arterial stroke therapy." *Cardiovasc Eng Technol* 2013; vol. 4, pp. 339–51. doi: 10.1007/s13239-013-0148-4

[2]   S.J. Warach, M. Luby, G.W. Albers, *et al.* "Acute stroke imaging research roadmap III imaging selection and outcomes in acute stroke reperfusion clinical trials." *Stroke* 2016; vol. 47, pp. 1389–98. doi: 10.1161/STROKEAHA.115.012364

[3]   M. Ernst, A.M.M. Boers, A. Aigner, et al. " Association of computed tomography ischemic lesion location with functional outcome in acute large vessel occlusion ischemic stroke" . *Stroke 2017*; vol. 48, pp. 2426–33. doi: 10.1161/STROKEAHA.117.017513

7

[4]   S. Doyle, F. Forbes, A. Jaillard, "Sub-acute and Chronic Ischemic Stroke Lesion MRI Segmentation." In: Brainlesion: glioma, multiple sclerosis, stroke and traumatic brain injuries. *Springer International Publishing*, 2018; pp. 111–22. doi: 10.1007/978-3-319-75238-9_10

[5]   R. Zhang, L. Zhao, W. Lou, et al. "Automatic segmentation of acute ischemic stroke from DWI using 3-D fully convolutional DenseNets." *IEEE Trans Med Imaging* 2018; vol. 37, pp. 2149–60, doi: 10.1109/TMI.2018.2821244

[6]   K. Kamnitsas, C. Ledig, V.F.J. Newcombe, et al. "Efficient multi-scale 3D CNN with fully connected CRF for accurate brain lesion segmentation." *Med Image Anal,* 2017; vol.36, pp. 61–78. doi: 10.1016/j.media.2016.10.004

[7]   O. Maier, C. Schröder, N.D. Forkert, et al. "Classifiers for ischemic stroke lesion segmentation: a comparison study." *PLoS One* 2015; vol. 11, pp. e0149828 doi:10.1371/journal.pone.0145118

[8]   M. Goyal, B.K. Menon, W.H. van Zwam, et al. "Endovascular thrombectomy after large-vessel ischaemic stroke: a meta-analysis of individual patient data from five randomised trials." *The Lancet* 2016; vol.387, pp.1723–31. doi: 10.1016/S0140-6736(16)00163-X

[9]   A.M.M. Boers , Jansen IGH, Brown S, *et al.* "Mediation of the relationship between endovascular therapy and functional outcome by follow-up infarct volume in patients with acute ischemic stroke." *JAMA Neurol* 2019;76:194.

[10]   J.K. Berge, R.A. Bergman. "Variations in size and in symmetry of foramina of the human skull." *Clin Anat* 2001, vol. 14, pp. 406–13, doi: 10.1002/ca.1075

[11]   R.S. Barros, W.E. van der Steen, A.M.M. Boers, I. Zijlstra *et al.* "Automated segmentation of subarachnoid hemorrhages with convolutional neural networks" *Inf in Med Unl.* 2020, vol. 19, doi: 10.1016/j.imu.2020.100321

[12]   D.V. Cicchetti. "Guidlines, criteria, and rules of thumb for evaluating normed and standardized assessment instruments in psychology." *Psychol Assess* 1995, vol. 6, pp. 284–90, doi: 10.1037/1040-3590.6.4.284

[13]   A. Bivard, C. Levi, L. Lin, *et al.* "Validating a predictive model of acute advanced imaging biomarkers in ischemic stroke." *Stroke* 2017, vol. 48, pp. 645–50, doi: 10.1161/STROKEAHA.116.015143

[14]   L. Liu, S. Yang, L. Meng. "Multi-scale Deep Convolutional Neural Network for Stroke Lesions Segmentation on CT Images." In: Crimi A, Bakas S, Kuijf H, eds. Brain lesion: Glioma, Multiple Sclerosis, Stroke and Traumatic Brain Injuries. Cham: Springer International Publishing, 2019, pp. 283–91, doi: 10.1007/978-3-030-11723-8_28

[15]   A. Bardera, I. Boada, M. Feixas M, *et al.* "Semi-automated method for brain hematoma and edema quantification using computed tomography." *Comput Med Imaging Graph* 2009, vol. 33, pp. 304–11, doi: 10.1016/j.compmedimag.2009.02.001

[16]   H. Kuang, M. Najm, B.K. Menon. "Joint Segmentation of Intracerebral Hemorrhage and Infarct from Non-Contrast CT Images of Post-treatment Acute Ischemic Stroke Patients." In: Frangi AF, Schnabel JA, Davatzikos C, eds. Medical Image Computing and Computer Assisted Intervention - *MICCAI* 2018. . Springer International Publishing, 2018: vol.11072. pp. 681–8, doi: 10.1007/978-3-030-00931-1_78

[17]   A.M. Boers, H.A. Marquering, J.J. Jochem, *et al.* "Automated cerebral infarct volume measurement in follow-up noncontrast CT scans of patients with acute ischemic stroke." *AJNR Am J Neuroradiol* 2013, vol. 34, pp. 1522–7, doi: 10.3174/ajnr.A3463

[18]   P.C. Vos, N.A. Weaver, J.M. Biesbroek. "Automatic detection and segmentation of ischemic lesions in computed tomography images of stroke patients." In: *Medical imaging* 2013: computer-aided diagnosis. 8670, 2013.

[19]   C.R. Gillebert, G.W. Humphreys, D. Mantini. "Automated delineation of stroke lesions using brain CT images." *Neuroimage Clin* 2014, vol. 4, pp. 540–8, doi: 10.1016/j.nicl.2014.03.009

7

Chapter 8

Value of infarct location in the prediction of functional outcome in patients with an anterior large vessel occlusion: results from the HERMES study

M.L. Tolhuisen, M. Ernst, A.M.M. Boers, S. Brown, L.F.M. Beenen, F. Guillemin, Y.B.W.E.M. Roos, J.L. Saver, R. van Oostenbrugge, A.M. Demchuck, W. van Zwam, T.G. Jovin, O.A. Berkhemer, K.W. Muir, S. Bracard, B.C.V. Campbell, A. van der Lugt, P. White, M.D. Hill, D.W.J. Dippel, P.J. Mitchell, M. Goyal, M.W.A. Caan, H.A. Marquering, and C.B.L.M. Majoie, on behalf of the HERMES collaborators

8
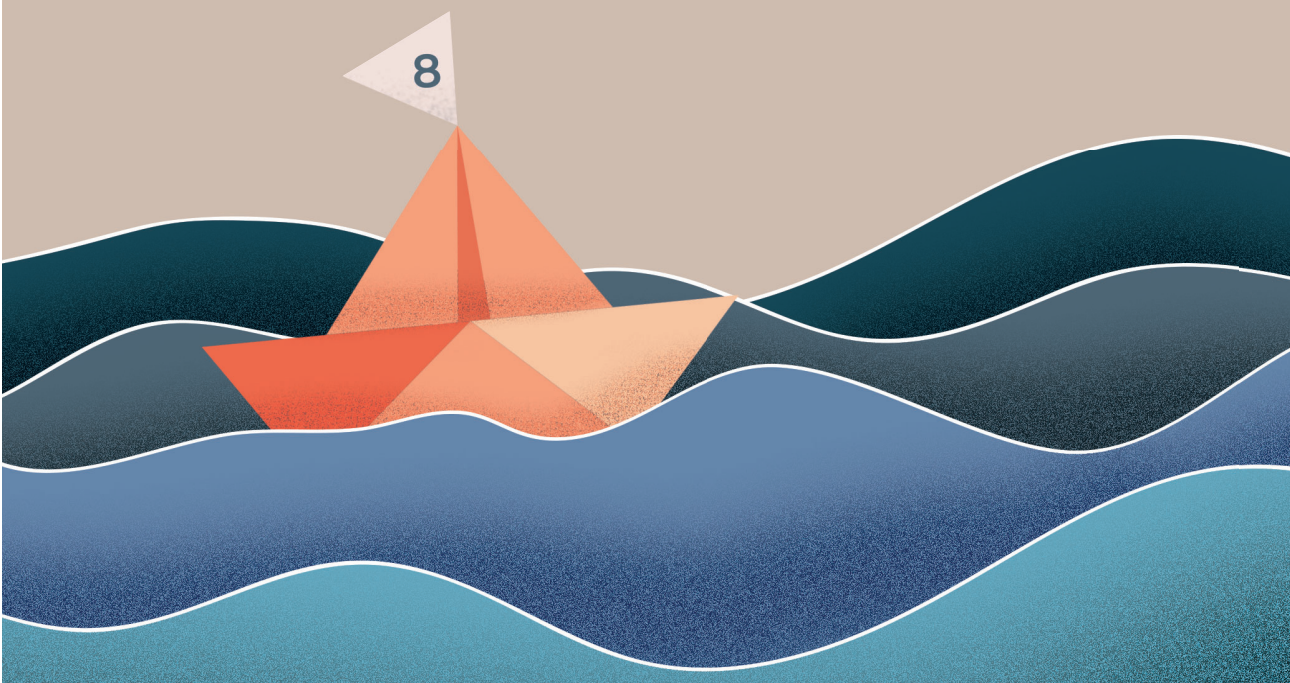
Abstract

Background— Follow-up infarct volume (FIV) is moderately associated with functional outcome. We hypothesized that accounting for infarct location would strengthen the association of FIV with functional outcome.

Methods— We included 252 patients from the HERMES collaboration with follow-up diffusion weighted imaging. Patients received endovascular treatment combined with best medical management (n = 52%) versus best medical management alone (n = 48%). FIV was quantified in low, moderate and high modified Rankin Scale (mRS)-relevant regions. We used binary logistic regression to study the relation between the total, high, moderate or low mRS-relevant FIVs and favorable outcome (mRS < 2) after 90 days. The strength of association was evaluated using the c-statistic.

Results— Small lesions only occupied high mRS-relevant brain regions. Lesions additionally occupied lower mRS-relevant brain regions if FIV expanded. Higher FIV was associated with a higher risk of unfavorable outcome, as were volumes of tissue with low, moderate and high mRS-relevance. In multivariable modeling, only the volume of high mRS-relevant infarct was significantly associated with favorable outcome. The c-statistic was highest (0.76) for the models that included high mRS-relevant FIV or the combination of high, moderate and low mRS-relevant FIV but was not significantly different from the model that included only total FIV (0.75).

Conclusion— This study confirms the association of FIV and unfavorable functional outcome but showed no strengthened association if lesion location was taken into account.

Introduction

Despite advances in treatment of acute ischemic stroke (AIS), many patients do not return to functional independence. Insight into the course of disease obtained by the prediction of functional outcome might help patient specific rehabilitation. For example, the patient and family could be informed on realistic expectations

about recovery, and rehabilitation therapy could be focused specifically on the patient's needs.

Follow-up infarct volume (FIV) is associated with functional outcome after AIS and has been suggested as a prognostic marker. However, FIV is only moderately associated with outcome: only 12% of functional outcome is explained by FIV [1]. Moreover, the association between the volume of infarcted tissue and functional outcome varies among lesion locations[2],[3],[4].

Infarcts that are located in highly modified Rankin Scale (mRS)-relevant regions negatively affect functional outcome, even when the lesion is small [2],[3],[4],[5]. Ernst et al. [2] and Sheth et al. [6] showed that the association between lesion volume and functional outcome, measured by mRS at 90 days, is stronger if lesion location is taken into account. In the study of Ernst et al., an increase in lesion volume in high mRS-relevant areas was associated with a higher risk of unfavorable outcome. In their study, lesion volume was quantified on 3 to 9 days follow-up (FU) non-contrast computed tomography (NCCT) images.

Diffusion weighted imaging (DWI) is the preferred modality for assessing infarcted tissue due to its high sensitivity, which reaches near 100% sensitivity within 6 h after stroke onset [7], [8]. We therefore aimed to study whether the association between FIV as depicted on FU DWI and functional outcome according to the mRS at 90 days is strengthened when lesion location is taken into account for patients with an anterior large vessel occlusion.

Materials and Methods

Patient population

We included patients from the HERMES collaboration with available FU DWI. The HERMES collaboration is a prospective meta-analysis of seven clinical randomized controlled trials (RCTs) that assessed the treatment efficacy of the combination of endovascular treatment (EVT) and best medical management including intravenous alteplase versus best medical management alone for patients with an occlusion within the proximal anterior circulation (ICA, M1 and M2

occlusions) [9]. In case patients were randomized for additional endovascular treatment, intravenous thrombolysis was administered within 4.5 h if eligible. Most trials allowed randomization for EVT within 6 h. The REVASCAT trial and the ESCAPE trial allowed randomization within 8 and 12 h respectively. Patients were excluded in case of poor FU DWI quality. Poor image quality scans included motion artefacts, noise or incomplete field of view. According to the trial protocols, if follow-up DWI was acquired, it was done at 24 h after treatment [10],[11],[12],[13],[14].

Each RCT in the HERMES collaboration was approved by the relevant national or local medical ethical committee. All medical images and reports were anonymized, and informed consent was obtained for each patient according to each trial protocol. Patients included in these trials consented for participation on the individual trials as well as additional research with the data.

Lesion segmentation and regions

For segmentation, an initial coarse delineation was obtained by labeling all voxels as infarct positive that differed in intensity by $\geq 20\%$ compared to the mirrored ROI at the contralateral side on trace DWI. Then, a subsequent manual adjustment was performed if needed by one of three expert neuroradiologists (WHvZ, LFMB or CM). Lesion segmentations also included areas with parenchymal hemorrhage within and adjacent to the infarct. In this study, hemorrhage was recognized on DWI as hypointense regions. If the patients received decompressive hemicraniectomy and no pre-surgical scan was available, only lesions within the theoretical boundary of the skull were included within the segmentation.

Each brain was divided into 66 anatomical regions using three different atlases. We used the Laboratory of Neuro Imaging Probabilistic Brain Atlas [15], which includes 56 mostly cortical regions. These regions were extended with internal capsule, corona radiata, thalamus, corpus callosum and middle cerebral peduncles, which are part of the John Hopkins University International Consortium DTI-based white matter atlases [16] and Harvard–Oxford cortical and subcortical atlases [17],[18],[19],[20]. The atlases were aligned to each DWI scan by affine and

additional B-spline registration with the use of the statistical parametric mapping 8 toolbox (http://www.fil.ion.ucl.ac.uk/spm/). The regions were classified as high, moderate and low relevance for mRS, similar as presented by Ernst et al.[2] and according to a previously presented strength of association by Cheng et al. [3] (see Figure 8.1). A voxel-based lesion mapping approach was used in which the impact of a brain region on functional outcome was represented by the Z-score acquired through a Brunner and Munzel Rank order test. Corresponding to these regions, total FIV was divided into sub-volumes categorized as being low, moderate and high mRS relevant.
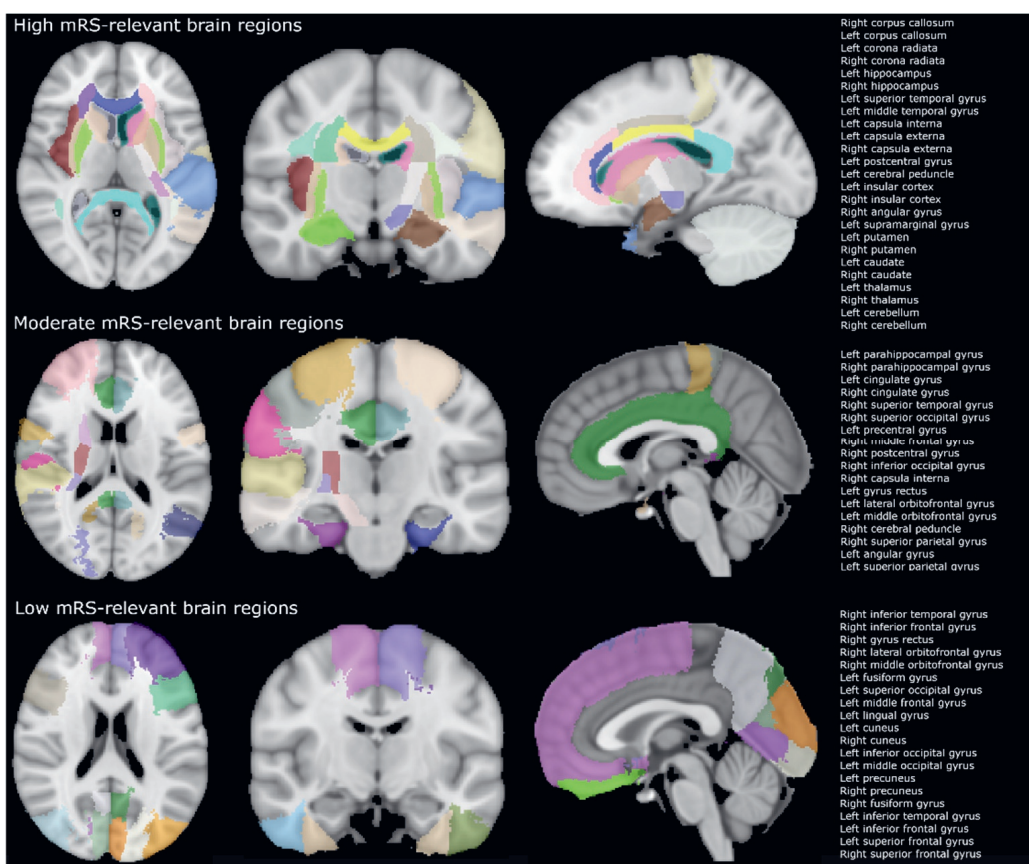
Figure 8.1: The division of brain regions according to high, moderate and low mRS relevance

Statistical analysis

Medians and interquartile ranges (IQR) are reported for all continuous variables. Frequencies (*n*) and percentages (%) are reported for all categorical and dichotomous variables. Odds ratios are presented per 10 mL of FIV with 95% confidence interval. We tested for a significance level of $p < 0.05$.

Primary outcome was a favorable functional outcome according to the modified Rankin Scale (mRS), defined as mRS ≤ 2, at 90 days after stroke onset. For the primary outcome, we performed unadjusted univariable and multivariable logistic regression analyses. The independent variables for the univariable models were total FIV and high, moderate and low mRS-relevant FIV in milliliter. The independent variables for the multivariable model were high, moderate and low mRS-relevant FIV in milliliter. For each analysis, we performed an additional adjusted multivariable regression analysis in which we adjusted for age, sex, diabetes mellitus, atrial fibrillation, previous stroke or pre-stroke mRS > 0, treatment allocation, occlusion site, time from stroke onset to treatment and the collateral score.

Secondary outcome was shift (on the mRS) towards better functional outcome at 90 days, for which we performed ordinal logistic regression. We performed univariable and multivariable regression analysis as per the models for the primary outcome.

To study the quality of the statistical models, we computed the c-statistic and the Akaike information criterion (AIC). For logistic regression, the c-statistic is the area under the curve (AUC) of the receiver operating characteristic (ROC). An ROC graphically represents the ability of a binary classifier to predict the correct diagnosis as its discrimination threshold varies. The AUC represents the probability of the classifier to correctly predict the outcome. For ordinal outcomes, a single ROC no longer exists. In this case, the c-statistic can be computed from the cumulative ROCs [21]. We used DeLong's test [21] to compare the different c-statistics. The AIC gives a measure of the relative quality of fit of the models: it tests how well a model fits the sampled data compared to the other models that were fitted on the same data.

Results

Within the HERMES collaboration 307 patients had available 24-h FU DWI. We excluded 55 patients due to poor FU DWI quality, resulting in a total population of 252 patients. Baseline and follow-up characteristics for the subpopulation of this study and the overall HERMES patient group are shown in Table 8.1. The median age of the study population was 69 years, and a small majority was female. Most patients (81%) had a pre-stroke mRS of 0. The occlusion location was most common within the M1 segment (72%) of the MCA, followed by the ICA-T (22%). Only a small number of patients had a M2 occlusion (6.1%). Within our study population, 52% received endovascular treatment, from which 46% also received IVT and 46% received IVT alone. The remaining 2% received neither IVT nor EVT and supportive care only. Favorable outcome at 90 days was reached in 53% of the study population. Figure 8.2 shows an example of the infarct segmentations on diffusion weighted MRI in areas with different mRS relevance. Figure 8.3 shows the infarct distribution for the study population for the axial, coronal and sagittal slice with the largest infarct probability. Lesions were most often present in the right lentiform nucleus.

Table 8.1: *Baseline and follow-up characteristics for our subpopulation and those of the HERMES dataset*

| Characteristic	Volume analysis subgroup (n=252) Mean ± SD (N) [Median] (IQR) or % (n/N)	HERMES (n=1764) Mean ± SD (N) [Median] (IQR) or % (n/N)
Age (years)	66 ± 14 (251) [69] (59, 76)	66 ± 14 (1761) [68] (57, 76)
Male gender	49% (124/252)	53% (929/1762)
NIHSS at baseline	17 ± 4.9 (251) [17] (13, 21)	17 ± 5.1 (1751) [17] (13, 21)
Diabetes mellitus	16% (40/251)	16% (287/1756)
Atrial fibrillation	44% (77/177)	33% (447/1351)
Prior stroke	11% (27/252)	11% (188/1751)

Continued

Table 8.1: *Continued*

| Characteristics	Volume analysis subgroup (n=252) Mean ± SD (N) [Median] (IQR) or % (n/N)	HERMES (n=1764) Mean ± SD (N) [Median] (IQR) or % (n/N)
Pre-stroke mRS		
0	81.4% (144/177)	83% (1057/1280)
1	16% (28/177)	13% (162/1280)
2+	2.8% (5/177)	4.8% (61/1280)
Occlusion location		
ICA-T	22% (55/246)	20.2% (350/1731)
M1	72% (176/246)	73.8% (1277/1731)
M2	6.1% (15/246)	6.0% (104/1731)
EVT allocation	52% (131/252)	49% (871/1764)
tPA delivered	93% (233/252)	89% (1572/1764)
Treatment		
EVT + tPA	46% (117/252)	43% (763/1764)
EVT only	5.6% (14/252)	6.1% (108/1764)
tPA only	46% (116/252)	46% (809/1764)
Best medical management	2.0% (5/252)	4.8% (84/1764)
Onset to randomization (min)	195 ± 97.6 (252) [180] (130.0,233.0)	202 ± 89 (1756) [183] (140.0,245.0)
NIHSS at baseline		
0-4	0.4% (1/251)	0.4% (7/1751)
5-15	42% (105/251)	37% (647/1751)
16-20	32% (81/251)	37% (655/1751)
21-42	26% (64/251)	25% (442/1751)
TICI 2b/3 (EVT treated subjects only)	84% (97/115)	75% (550/729)
Favorable outcome at 90 days	53% (133/249)	47%(462/978)
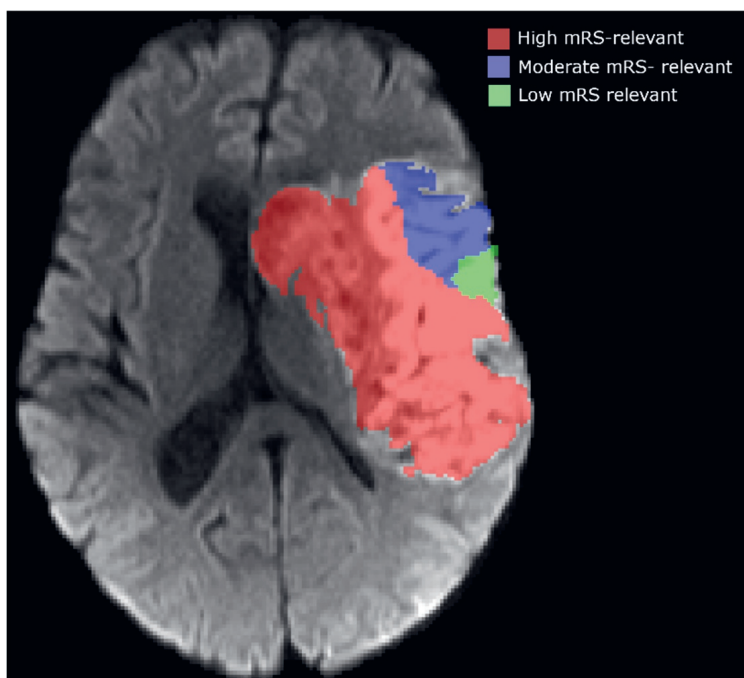
Figure 8.2: *An example of the infarct segmentations on diffusion weighted MRI in areas with different mRS-relevance*
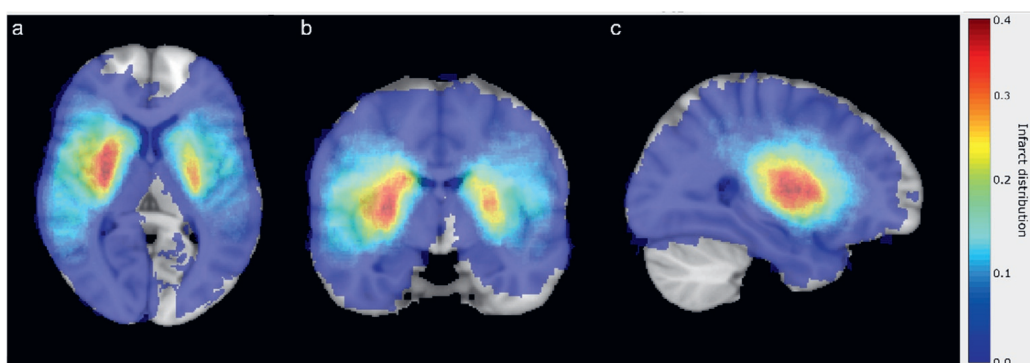

Figure 8.3: *Infarct distribution shown for the axial (a), coronal (b) and sagittal (c) slice with the largest infarct probability present.*

Figure 8.4 shows box plots for the FIV for the low, moderate, high mRS-relevant regions and total FIV in relation to mRS with corresponding standard deviations. The increase of FIV was associated with a higher risk of unfavorable outcome for all the different regions. Moreover, the variance in infarct volume increased with worsening outcome, especially for high and low mRS-relevant regions.
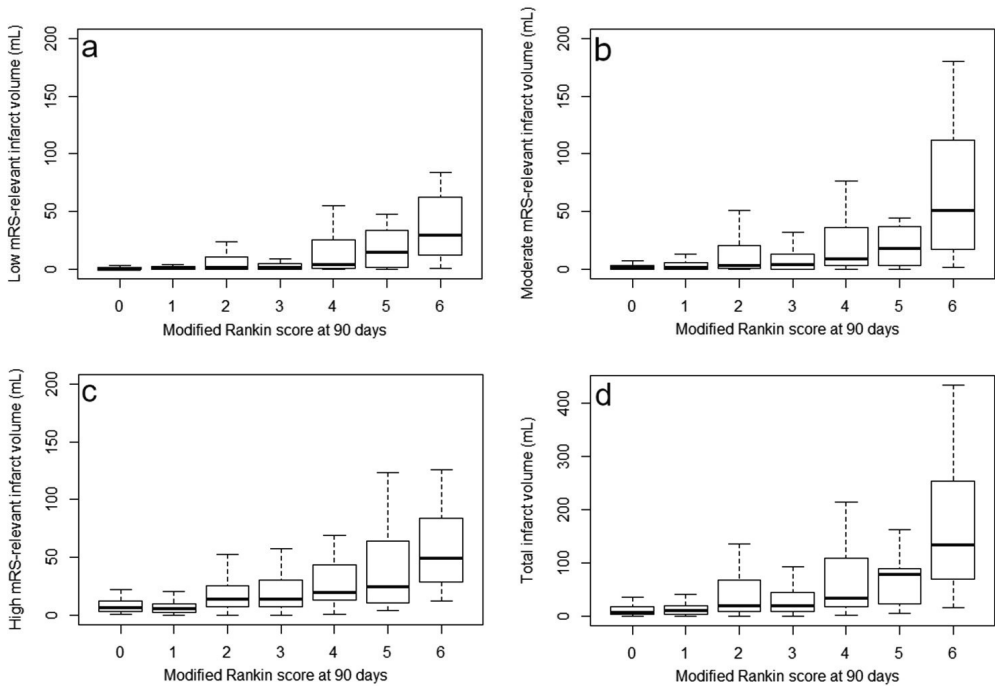
Figure 8.4: *Box plots showing the infarct volume distribution per mRS category for the low (a), moderate (b) and high (c) mRS-relevant infarct regions and the total infarct volume (d).*

Figure 8.5 shows the lesion volume for low, moderate and high mRS-relevant brain regions per patient. In patients with small total FIV, only high mRS-relevant brain regions were affected. With increasing total FIV, the lesions additionally occupied moderate mRS and subsequently low mRS-relevant brain regions.
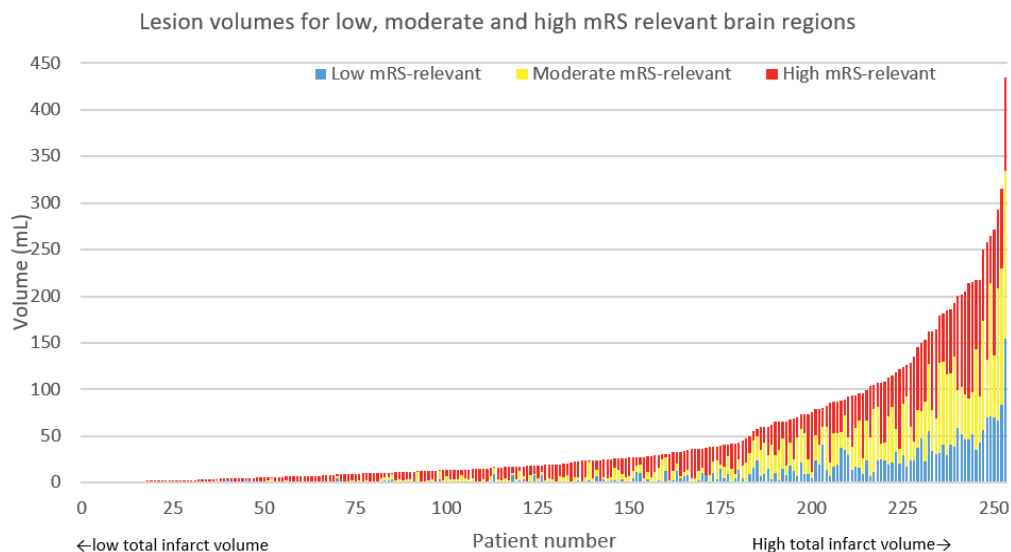
Figure 8.5: Lesion volume distribution classified as low, moderate and high mRS-relevant. Total lesion volume increases along the x-axis. Each bar represents a single subject.

Results for the logistic regression models and ordinal logistic regression are presented in Table 8.2. For the univariable logistic models (models 1 to 4), all volume measures were significantly associated with favorable mRS. The odds ratio was highest for total FIV and lowest for low mRS-relevant region FIV. For the multivariable model (model 5), only high mRS-relevant region FIV was significantly associated with favorable mRS. Similar results were obtained for the ordinal logistic regression model. Results after adjustments were comparable to the unadjusted analyses.

For the univariable logistic regression models, the AIC was lowest for the model that included high mRS-relevant FIV. The model including high mRS-relevant FIV was a better fit to the data than the multivariable model. For the ordinal logistic regression models, AIC was lowest for the model that included total FIV.

Only small differences were seen in the c-statistic for the different models. For the logistic model, the c-statistic was highest for the model that included high mRS-relevant FIV. However, according to DeLong's test, there was no significant difference between the c-statistic of the total FIV model (model 1) and the c-

statistic for the high mRS-relevant FIV model (model 2). For the ordinal logistic regression models, the c-statistic was highest for both the model that included total FIV (model 6) and the high mRS-relevant FIV model (model 7).

Table 8.2: *Associations between the total follow-up infarct lesion volume and the follow-up infarct lesion volume divided in high, moderate and low mRS-relevant regions and favourable mRS at 90 days*

		OR (95% CI)	AIC	c-stat	aOR (95% CI)
Logistic regression (Favorable outcome, mRS≤)					
Univariable					
Model 1	Total FIV	0.83 (0.77, 0.89)	300	0.75	0.78 (0.70, 0.86)
Model 2	High mRS-relevant FIV	0.62 (0.53, 0.74)	295	0.76	0.53 (0.42, 0.67)
Model 3	Moderate mRS-relevant FIV	0.72 (0.62, 0.83)	322	0.74	0.66 (0.54, 0.81)
Model 4	Low mRS-relevant FIV	0.50 (0.38, 0.66)	309	0.70	0.45 (0.31, 0.65)
Multivariable					
Model 5	High mRS-relevant FIV	0.67 (0.53, 0.84)	298	0.76	0.56 (0.41, 0.76)
	Moderate mRS-relevant FIV	1.00 (0.80, 1.25)			0.87 (0.66, 1.16)
	Low mRS-relevant FIV	0.86 (0.54, 1.35)			1.12 (0.65, 1.95)
Ordinal logistic regression (shift towards better outcome)					
Univariable					
Model 6	Total FIV	0.84 (0.81, 0.88)	830	0.72	0.83 (0.79, 0.87)
Model 7	High mRS-relevant FIV	0.70 (0.64, 0.77)	837	0.72	0.67 (0.60, 0.78)
Model 8	Moderate mRS-relevant FIV	0.72 (0.65, 0.80)	859	0.71	0.69 (0.61, 0.78)
Model 9	Low mRS-relevant FIV	0.52 (0.44, 0.62)	841	0.69	0.51 (0.42, 0.62)

Continued

Table 8.2: *Continued*

		OR (95% CI)	AIC	c-stat	aOR (95% CI)
Ordinal logistic regression (shift towards better outcome)					
Multivariable					
Model 10	High mRS-relevant FIV	0.79 (0.69, 0.91)	832	0.72	0.76 (0.65, 0.89)
	Moderate mRS-relevant FIV	0.89 (0.77, 1.04)			0.83 (0.67, 1.37)
	Low mRS-relevant FIV	0.86 (0.62, 1.21)			0.96 (0.67, 1.37)

† Adjusted for age, sex, diabetes mellitus, atrial fibrillation, previous stroke or pre-stroke mRS>0, treatment allocation, occlusion site, time from stroke onset to treatment and the collateral score.

Discussion

For patients with AIS caused by an anterior large vessel occlusion, our results did not show significant differences between models, and therefore no differences in strength of associations between infarct volume and outcome were observed when lesion location was taken into account.

Lesions within low mRS-relevant regions were only present in patients with higher total FIV. The results suggest that lesions progress from high mRS-relevant regions to less mRS-relevant regions when a stroke worsens. This agrees with the concept that leptomeningeal collaterals are relevant only to cortical MCA or ICA tissue and do not compensate for perfusion deficits in subcortical structures, such as the basal ganglia [22], and that ischemia progresses in case of late or inadequate reperfusion.

Our results did not correspond with the results presented by Ernst et al. [2], for which infarct lesion volume was quantified based on NCCT images. Their total FIV and high mRS-relevant FIV were overall larger compared to our study. Also, they showed a larger difference in volume between high mRS-relevant FIV and total FIV. The reason for discrepancy in our results was likely the difference in study populations. Ernst et al. only included patients from the MR CLEAN trial. The MR

8

CLEAN trial included a relatively unselected group of patients with an anterior circulation large vessel occlusion (ICA, middle cerebral artery M1 and M2 segments, anterior cerebral artery A1 and A2 segments) within 6 h after stroke onset and a National Institutes of Health Stroke Scale (NIHSS) score above 2. No other imaging selection criteria as ASPECTS, collateral score or core and/or penumbra size on CTP were used. The inclusion criteria differed between trials and were more selective in some trials: patients were included if occlusions were present in only the intracranial carotid artery or middle cerebral artery (M1 segment) [13], [14], [23], [24], or only with more severe deficits [13], or with good collateral score [24], a core/penumbra mismatch [14] or smaller core [13] or a broader inclusion window [24]

Multiple studies have presented a voxel-based approach, studying the relation between specific anatomy and functional outcome [3], [4], [25],[26],[27]. For example, Cheng et al. [3] used voxel-based lesion symptom mapping to study the relation of infarct lesion measured on fluid-attenuated inversion recovery imaging and functional outcome. They presented statistical maps which show the relation between the spatial distribution of ischemic lesions and mRS at 1-month follow-up. Their results showed that the corona radiata, internal capsule and insula were of highest influence for mRS at 1 month. Laredo et al. [25] showed that large lesions strongly predict poor mRS, especially for insular lesions. Munsch et al. [4] studied the voxel-specific relation between infarct, measured on DWI, and mRS and cognitive function. Their results showed that infarct location is a significant predictor for cognitive function. However, they were not able to show a significant relation between location and dichotomous mRS. Wu et al.[5] showed that the posterior limb of the internal capsule, corona radiata and especially the white matter tracts were associated with greater severity of AIS and poor long-term outcome.

In the study population, lesions were most present in the right lentiform nucleus, which consist of the putamen and globus pallidus. These regions are responsible for the sensory and motor function, and learning processes. Russmann et al. [28]

studied the effect of isolated lentiform nucleus infarcts. Infarcts in this region were related with sensory deficits, aphasia and hemineglect.

The current and previously presented moderate association of infarct volume and functional outcome is possibly explained by Goyal et al. in their recent publication [29]. They state that the variability of tissue vulnerability causes heterogeneity in ischemic tissue. More specific, even though tissue appears infarcted on imaging, it is possible that this tissue is still (partially) salvageable and recovers over time. The heterogeneity of ischemia has previously been studied in small studies. Nagesh et al. [30] showed in 9 patients that within 10 h after stroke onset ischemic lesions consisted of multiple heterogenic zones of ADC values. Guadagno et al. [31] showed, based on PET images of 5 patients, heterogeneity in blood flow and metabolism in regions that appeared hyperintense on DWI. Considering these insights, previously and current presented infarct volumes probably do not correctly represent true infarct.

This study suffers from some limitations. First, even though the HERMES collaboration combined multiple large randomized controlled trials with a heterogeneous population, our substudy population was relatively small and consists of highly selected patients. FU MRI is often not included within standard imaging protocol for FU stroke imaging. As a result, our study population only contained patients from the HERMES centers that included 24-h FU MRI within their study protocol. Moreover, the HERMES trials included only patients without prior disability, with proximal anterior circulation large vessel occlusions who were eligible for EVT. Since all patients had anterior circulation large vessel occlusions, the spectrum of patient deficits was more similar than occurs in an unselected stroke patient population that would include a majority with medium and small vessel occlusions in more locations, including patients with posterior circulation occlusions. Strategic location effects are likely to be more marked when overall lesion volumes are smaller and more varied. Also, our study population does not represent minor or severe cases of stroke. It is expected that patients with infarcts that affect low-mRS relevant regions experience fewer symptoms and are therefore less likely to present acutely in time window for acute interventions (IVT or EVT).

8

Patients who did not meet the inclusion criteria for the trials due to contraindications, such as late presentation or high NIHSS score, were also not included. In addition, the majority of trials selected patients according to imaging characteristics such as the extent of changes on non-contrast CT or MRI, perfusion characteristics or collateral vessel quality. It is also plausible that MRI scans were only acquired for patients that had a better early outcome and were therefore able to tolerate MRI acquisition. Since patients with clinically or radiologically severe presentations are expected to have worse outcome than those included in the HERMES trials, future studies should assess the influence of lesion location and outcome for this population. Also, our study did not take hemispheric dominance into account. Finally, in this study, the mRS score was used for defining functional outcome. This score is a common endpoint in acute ischemic stroke trials and measures the degree of dependence in daily activities. The score is mainly focused on motor function (particularly walking) and is less sensitive for the evaluation of complex or cognitive functions such as memory or emotional processing [24]. Lack of association of radiologically defined tissue volumes weighted by relevance to the mRS therefore is strongly biased towards motor function and does not cover regions such as the cingulate gyrus (which is involved in emotional processing) or parahippocampal gyrus (which is involved in memory processing). In addition, simplifying the mRS outcome into an arbitrary dichotomy of "good" and "poor" may obscure structure–function relationships. Future studies should focus on the relation between the NIHSS in combination of the Montreal cognitive assessment score and infarct location. We expect a stronger relation between neurological impairment found with these scores and specific brain regions.

According to our results, information on the specific post-treatment infarct location depicted on DWI does not contribute to better estimation of treatment outcome. Probably, this is because the high mRS-relevant regions are always included within the infarct.

Conclusion

Our results confirm the association between FIV as depicted on follow-up DWI and favorable functional outcome. We have shown that for patients with an infarct resulting from an ICA/MCA occlusion, the association between FIV quantified on follow-up DWI and functional outcome according to the modified Rankin scale (mRS) is not strengthened when lesion location is taken into account.

References

[1]   A.M.M. Boers, I.G.H. Jansen, L.F.M. Beenen *et al.* "Association of follow-up infarct volume with functional outcome in acute ischemic stroke: a pooled analysis of seven randomized trials.", *J Neurointerv Surg 2018,* vol. 10 (12), pp. 1137–1142, doi: 10.1136/neurintsurg-2017-013724.

[2]   M. Ernst, A.M.M. Boers, A. Aigner *et al.* "Association of computed tomography ischemic lesion location with functional outcome in acute large vessel occlusion ischemic stroke." *Stroke* 2017, vol. 48(9), pp. 2426–2433, doi: 10.1161/STROKEAHA.117.017513

[3]   B. Cheng, N.D. Forkert, M. Zavaglia *et al.* "Influence of stroke infarct location on functional outcome measured by the modified Rankin scale." *Stroke* 2014, vol. 45(6), pp. 1695–1702, doi: 10.1161/STROKEAHA.114.005152.

[4]   F. Munsch, S. Sagnier, J. Asselineau *et al.* "Stroke location is an independent predictor of cognitive outcome." *Stroke* 2016, vol. 47(1), pp. 66–73, doi: 10.1161/STROKEAHA.115.011242.

[5]   O. Wu, L. Cloonan, S.J.R. Mocking *et al.* "Role of acute lesion topography in initial ischemic stroke severity and long-term functional outcomes." *Stroke* 2015, vol. 46(9), pp. 2438–2444, doi: 10.1161/STROKEAHA.115.009643.

[6]   S.A. Sheth *et al.* "Regional contributions to post-stroke disability in endovascular therapy." *Interv Neurol.* 2018, vol. 7(6), pp. 533–543

[7]   S.J. Warach, M. Luby, G.W. Albers *et al.* "Acute stroke imaging research roadmap III imaging selection and outcomes in acute stroke reperfusion clinical

8

trials: consensus recommendations and further research priorities. *Stroke* 2016, vol. 47(5), pp. 1389–1398, doi: 10.1161/STROKEAHA.115.012364.

[8]   S. Rudkin, R. Cerejo, A. Tayal, M.F. Goldberg "Imaging of acute ischemic stroke." *Emerg Radiol* 2018, vol. 25(6), pp. 659–672

[9]   M. Goyal, B.K. Menon, W.H. van Zwam *et al.* (2016) "Endovascular thrombectomy after large-vessel ischaemic stroke: a meta-analysis of individual patient data from five randomised trials." *Lancet* 2016 vol. 387(10029), pp. 1723–1731, doi: 10.1016/S0140-6736(16)00163-X.

[10]   S. Bracard, X. Ducrocq, J.L. Mas *et al.* "Mechanical thrombectomy after intravenous alteplase versus alteplase alone after stroke (THRACE): a randomised controlled trial." *Lancet Neurol* 2016, vol. 15(11), pp. 1138–1147

[11]   K.W. Muir, G.A. Ford, C. Messow *et al.* "Endovascular therapy for acute ischaemic stroke: the Pragmatic Ischaemic Stroke Thrombectomy Evaluation (PISTE) randomised, controlled trial." *J Neurol Neurosurg Psychiatry* 2017, vol. 88(1), pp. 38–44, doi: 10.1136/jnnp-2016-314117.

[12]   O.A. Berkhemer, P.S.S. Fransen, D. Beumer *et al.* "A randomized trial of intraarterial treatment for acute ischemic stroke." *N Engl J Med* 2014, vol. 372(1), pp. 11-20, doi: 10.1056/NEJMoa1411587

[13]   T.G. Jovin, A. Chamorro, E. Cobo *et al.* "Thrombectomy within 8 hours after symptom onset in ischemic stroke." *N Engl J Med* 2015, vol. 372(24), pp. 2296–2306, doi: 10.1056/NEJMoa1503780.

[14]   J.L. Saver, M. Goyal, A. Bonafe *et al.* "Stent-retriever thrombectomy after intravenous t-PA vs. t-PA alone in stroke." *N Engl J Med* 2015, vol. 372(24), pp. 2285–2295, doi: 10.1056/NEJMoa1415061.

[15]   D.W. Shattuck, M. Mirza, V. Adisetiyo *et al.* "Construction of a 3D probabilistic atlas of human cortical structures." *Neuroimage* 2018, vol. 39(3), pp. 1064–1080

[16]   S. Mori, S. Wakana, P.C.M. van Zijl, L.M. Nagae-Poetscher "MRI atlas of human white matter." *Elsevier* 2015*,* Amsterdam, The Netherlands

[17]   N. Makris, J.M. Goldstein, D. Kennedy *et al*. (2006) "Decreased volume of left and total anterior insular lobule in schizophrenia." *Schizophr Res.* 2006, vol. 83(2–3), pp. 155–171, doi: 10.1016/j.schres.2005.11.020.

[18]   J.A. Frazier, S. Chiu, J.L. Breeze *et al* "Structural brain magnetic resonance imaging of limbic and thalamic volumes in pediatric bipolar disorder." *Am J Psychiatry* 2005, Vol. 162(7), pp. 1256–1265, doi: 10.1176/appi.ajp.162.7.1256

[19]   R.S. Desikan , F. Ségonne, B. Fischl *et al*. "An automated labeling system for subdividing the human cerebral cortex on MRI scans into gyral based regions of interest. *Neuroimage* 2006, vol. 31(3), pp. 968–980, doi: 10.1016/j.neuroimage.2006.01.021

[20]   J.M. Goldstein, L.J. Seidman, N. Makris *et al*. "Hypothalamic abnormalities in schizophrenia: sex effects and genetic vulnerability." *Biol Psychiatry* 2007, vol. 61(8), pp. 935–945, doi: 10.1016/j.biopsych.2006.06.027

[21]   E.R. Delong, D.M. Delong and D.L. Clarke-Pearson "Comparing the areas under two or more correlated receiver operating characteristic curves : a nonparametric approach" *International Biometric Society* 2016, vol. 44(3), pp. 837–845, doi: 10.2307/2531595

[22]   D.S. Liebeskind "Collaterals in acute stroke: beyond the clot." *Neuroimaging Clin N Am* 2005, vol. 15(3), pp. 553–573, doi: 10.1016/j.nic.2005.08.012

[23]   B.C.V. Campbell, P.J. Mitchell, T.J. Kleining *et al.* "Endovascular therapy for ischemic stroke with perfusion-imaging selection." *N Engl J Med* 2015, vol. 372(11), pp. 1009–1018\, doi: 10.1056/NEJMoa1414792

[24]   M. Goyal, A.M. Demchuck, B.K. Menon *et al*. "Randomized assessment of rapid endovascular treatment of ischemic stroke." *N Engl J Med* 2015, vol. 372(11), pp. 1019–1030, doi: 10.1056/NEJMoa1414905

[25]   C. Laredo, Y. Zao, S. Rudilosso *et al*. "Prognostic significance of infarct size and location: the case of insular stroke." *Sci Rep* 2018, vol. 8(1), pp. 1–10, doi: 10.1038/s41598-018-27883-3

8

[26]   J.S. Siegel, L.E. Ramsey, A.Z. Snyder *et al.* (2016) "Disruptions of network connectivity predict impairment in multiple behavioral domains after stroke." *Proc Natl Acad Sci* 2016, vol. 113(30), pp. E4367–E4376, doi: 10.1073/pnas.1521083113

[27]   D. Agis, M.B. Goggins, K. Oishi *et al.* "Picturing the size and site of stroke with an expanded national institutes of health stroke scale." *Stroke* 2016, vol. 47(6), pp. 1459–1465, 10.1161/STROKEAHA.115.012324

[28]   H. Russmann, F. Vingerhoets, J. Ghika *et al.* "Acute infarction limited to the lenticular nucleus." *Arch Neurol* 2003, vol. 60(3), pp. 351, doi: 10.1001/archneur.60.3.351

[29]   M. Goyal, M. J.M. Ospel, B. Menon *et al.* "Challenging the ischemic core concept in acute ischemic stroke imaging." *Stroke* 2020, vol. 51(10):3147–3155, doi: 10.1161/STROKEAHA.120.030620

[30]   V. Nagesh, K.M.A. Welch, J.P. Windham *et al.* "Time course of ADC changes in ischemic stroke: beyond the human eye!" *Stroke* 1998, vol. 29(9), pp. 1778–1782, doi: 10.1161/01.STR.29.9.1778

[31]   J.V. Guadagno, E.A. Warburton, P.S. Jones *et al.* "The diffusion-weighted lesion in acute stroke: heterogeneous patterns of flow/metabolism uncoupling as assessed by quantitative positron emission tomography." *Cerebrovasc Dis* 2005, vol. 19(4), pp. 239–246, doi: 10.1159/000084087

8

Chapter 9
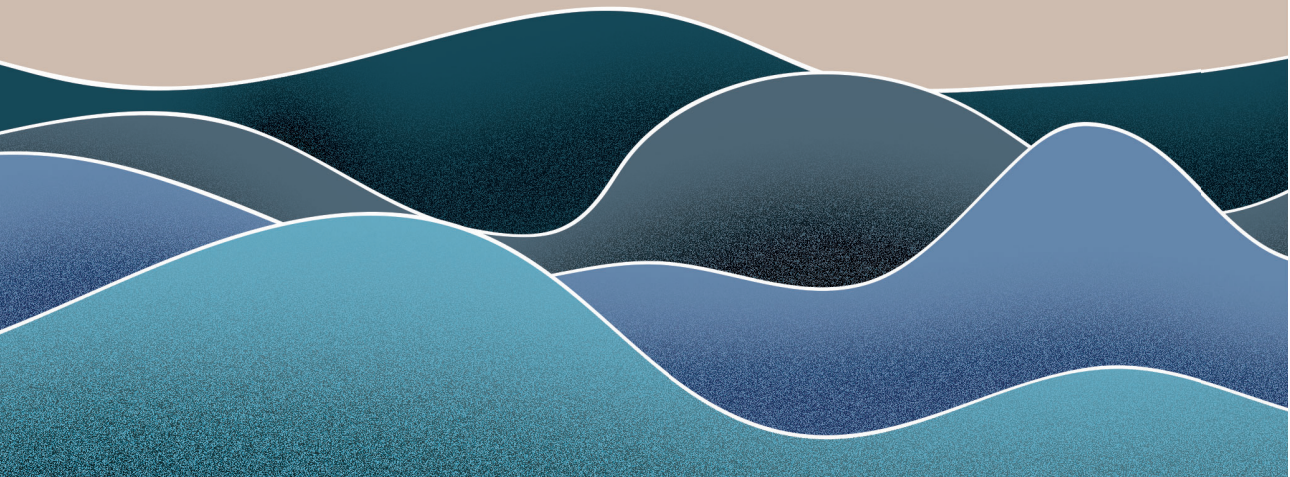
Outcome prediction based on automatically extracted infarct core image features in patients with acute ischemic stroke

M.L. Tolhuisen, J.W. Hoving, M.S. Koopman, M. Kappelhof, H. van Voorst, A.E. Bruggeman, A.M. Demchuck, D.W.J. Dippel, B.J. Emmer, S. Bracard, F. Guillemin, R. van Oostenbrugge, P.J. Mitchell, W. van Zwam, M. Hill, Y.B.W.E.M. Roos, T.G. Jovin, O.A. Berkhemer, B.C.V. Campbell, J. Saver, P. White, K.W. Muir, M. Goyal, H.A. Marquering, C.B. Majoie, M.W.A. Caan, for the MR CLEAN-NO IV and HERMES investigators

9
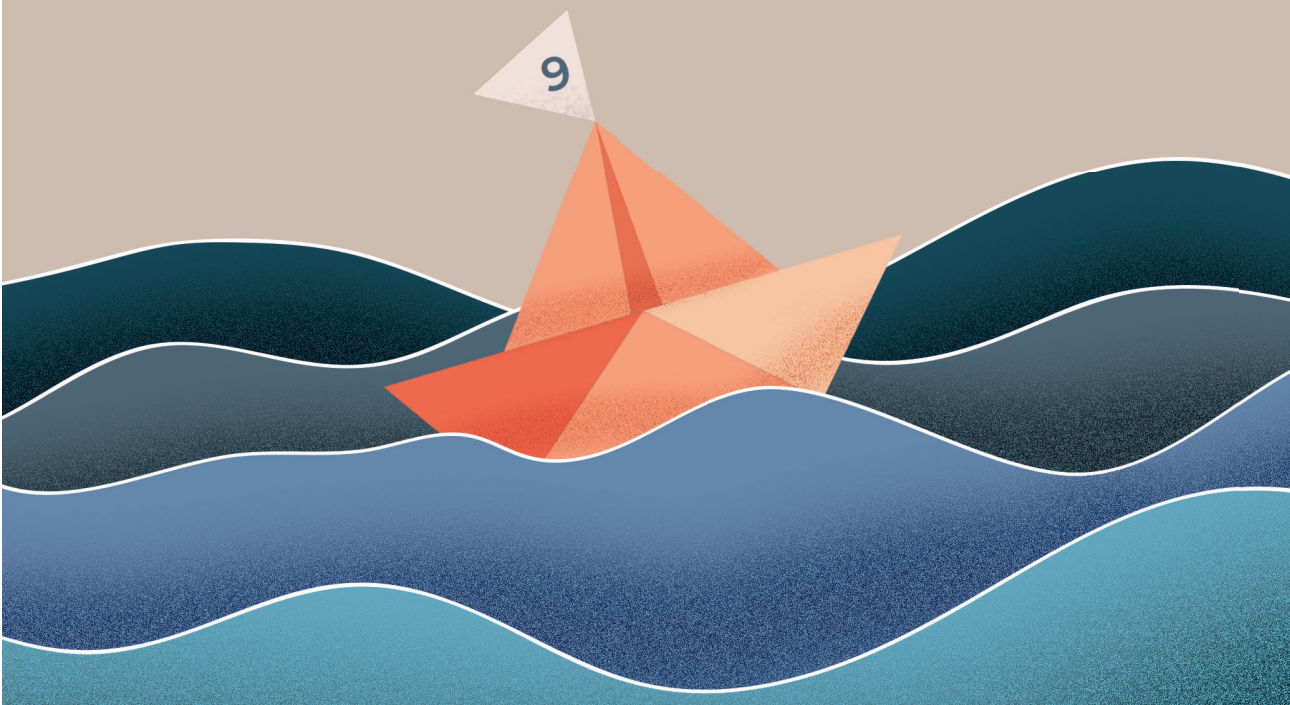
Abstract

Background— Infarct volume (FIV) on follow-up diffusion-weighted imaging (FU-DWI) is only moderately associated with functional outcome in acute ischemic stroke patients. However, FU-DWI may contain other imaging biomarkers which could aid in improving outcome prediction models for acute ischemic stroke.

Methods— We included FU-DWI data from the HERMES, ISLES, and MR CLEAN-NO IV databases. In a first step, lesions were segmented using a deep learning model trained on the HERMES and ISLES datasets. Then, we assessed the predictive performance of three classifiers in the MR CLEAN-NO IV trial cohort, based on: (1) FIV alone, (2) the most important features obtained from a trained convolutional autoencoder (CAE), and (3) radiomics features. In all models, a Support Vector Machine (SVM) was trained to predict functional independence (modified Rankin Scale: 0-2). Furthermore, we investigated feature importance in the radiomics feature-based model.

Results— For the outcome prediction, we included 206 patients, from which 144 scans were included in the training set, 21 in the validation set and 41 in the test set. The classifiers including the CAE and the radiomics features showed an AUC of 0.81 and 0.88 respectively, while the model based on FIV had an AUC of 0.79. This difference was not found to be statistically significant in independent data. Feature importance results from the radiomics model showed that lesion intensity heterogeneity received more weight than lesion volume in outcome prediction by the classifier.

Conclusion— This study suggests that predictions of functional outcome should not be based on FIV alone and that FU-DWI images capture additional prognostic information.

Introduction

Acute ischemic stroke (AIS) has a major impact on patients' lives: the majority of AIS patients do not return to functional independence or their functional status before experiencing AIS – even with adequate treatment [1]. Accurate estimation of functional outcome after treatment could aid to guide patients in setting realistic expectations and deciding on the focus of the rehabilitation process [2].

Follow-up infarct volume (FIV) as measured on radiological follow-up imaging has been suggested as a prognostic marker for functional outcome [3]. However, previous studies have indicated that FIV is only moderately associated with functional outcome: only 12% of functional outcome is explained by FIV [3]. It has been suggested that current imaging techniques – such as computed tomography (CT), CT perfusion, and diffusion-weighted imaging (DWI) – are not able to accurately predict or measure infarcted tissue [4]. A complicating factor is that progression from severely ischemic tissue to actual infarction is likely not constant over time and not always clearly visible on CT or DWI. Also, cells within the ischemic region could potentially remain viable depending on their tolerance to ischemia [4]. A previous study has shown that ischemic lesions may still evolve in the subacute phase even after successful treatment, resulting in smaller or larger lesions after 1 week follow-up [5].

Previous studies have suggested that tissue estimated as infarcted on radiological imaging may contain additional prognostic information which could improve outcome prediction for AIS. For example, intensity heterogeneity on images in infarcted regions might reflect the variance in tissue vulnerability to ischemia and may represent the degree of ischemia [6]. Also, Wang et al. showed that textural features, including heterogeneity, assessed on T2 FLAIR and ADC images are associated with follow-up NIHSS and modified Rankin Scale (mRS) [7]. Moreover, the shape of the lesion may contain important information on the potential progression from ischemia to infarcted tissue [8].

Previous studies have demonstrated the potential of machine learning (ML) to use automatically extracted imaging biomarkers for outcome prediction in AIS. For example, Qiu et al. [9] trained a support vector machine (SVM) to show that

9

thrombus radiomics features were more predictive for recanalization in patients treated with intravenous alteplase compared to manually extracted thrombus features. Also, Hilbert et al. [10] showed that features automatically extracted by an autoencoder combined with a dense layer outperformed ML models trained on handcrafted imaging biomarkers in predicting successful reperfusion and functional outcome at 90 days after stroke onset.

We hypothesized that infarct volume alone as measured on DWI is not sufficient to represent the pathological changes in the ischemic brain region and that DWI data may contain additional prognostic information that is still unknown. We compared the performance of an ML model based on FIV alone with a radiomics features-based model and a model based on features obtained from a deep-learning autoencoder network in the prediction of favorable functional outcome.

Materials and Methods
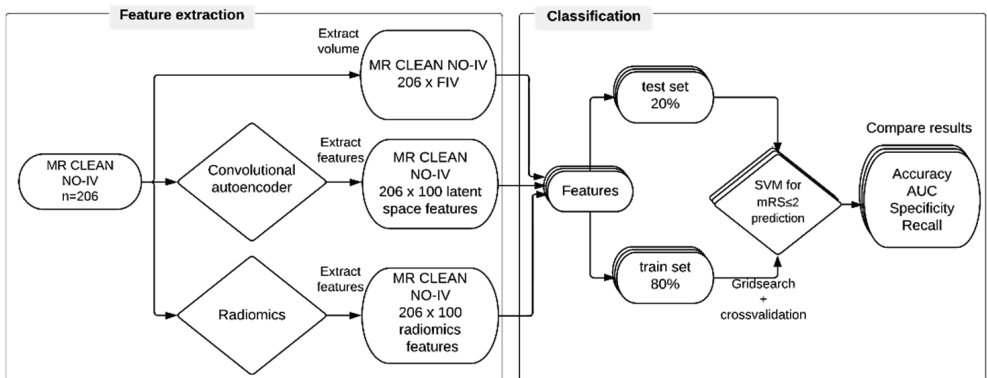
Figure 9.1: *Study workflow for functional outcome prediction. Three different feature sets were extracted: follow-up infarct volume, features extracted by a convolutional autoencoder, and radiomics features. Each feature set was split into a train (80%) and test (20%) set. A support vector machine (SVM) was trained on the train set to classify favorable outcome. The SVMs were tested on the test set. The results were evaluated for each SVM.*

Figure 9.1 shows the workflow of this study, which can be split up into two stages: feature extraction and outcome classification. Before we were able to extract features from the study dataset, we used an external dataset to train the CAE and a deep learning network for the delineation of the infarct lesions.

Datasets

The external dataset included patients from the HERMES collaboration [11] with available diffusion-weighted images (DWI) at 24 hours and DWI images from patients with subacute lesions from SISS ISLES 2015 [12]. The HERMES collaboration was formed to pool patient-level data from seven clinical randomized controlled trials which showed the efficacy of endovascular treatment (EVT) over best medical management alone for patients with an occlusion of arteries of the proximal anterior circulation (ICA, M1 and M2) [11]. Each trial in the HERMES collaboration was approved by the relevant national or local medical ethical committee. All imaging data and clinical reports were anonymized and informed consent was obtained for each patient according to each trial protocol. Patients included in these trials consented to participation in the individual trials as well as the use of their data for future research.

The study dataset included patients from the MR CLEAN-NO IV trial with available DWI at 24 hours post-treatment. The MR CLEAN-NO IV trial was a randomized clinical trial in which the effect of immediate endovascular treatment (EVT) is compared to intravenous treatment with alteplase (IVT) followed by endovascular treatment on 90-day functional outcome in patients with AIS [13]. Patients were included if they were eligible for IVT and EVT, over the age of 18 with a proximal occlusion of the anterior circulation, who were directly admitted to an EVT-capable hospital. Informed consent was obtained following a deferred consent procedure, in accordance with national legislation in the three participating countries[14].

Since imaging was acquired in a multi-center and international setting, scanner types and image acquisition parameters varied. Images were acquired with a field of strength 1.5 or 3 Tesla. The slice thickness ranged from 3 to 6 mm. For this

9

study, patients were excluded if DWI contained motion artifacts or in case of unsolvable registration errors.

Pre-processing and image analysis

Image registration

All DWI images were transformed to standard MNI space via non-rigid registration using the SPM8 toolbox [15], resulting in isotropic voxel dimensions of 1 mm. Intensities were normalized using the white stripe normalization toolbox [16]. Images processed by the CAE were additionally subsampled to an isotropic voxel spacing of 3 mm before analysis.

Lesion segmentation

To delineate the infarct lesions for the MR CLEAN-NO IV population, we trained a Deepmedic network [17]. Deepmedic is a multi-scale 3D convolutional neural network with a fully connected Conditional Random Field and has shown to be computationally efficient and performed best for brain lesion segmentation in the ISLES 2015 challenge [12]. We trained the network on the HERMES DWI images for which lesion segmentations were available [3]. Images were split into a training set (70%), a validation set (10%) and a test set (20%). The trained network was applied to the MR CLEAN NO-IV image dataset. Each resulting segmentation was checked by one of two experienced observers [JWH and MLT] and manually adjusted in case of erroneous segmentation using ITK-SNAP [18]. Hemorrhagic transformation was included within the lesion. For cases where no consensus could be reached, the segmentations were assessed by two expert neuroradiologists [CBLMM and MSK, with >20 and >5 years of experience, respectively] to reach a consensus.

Feature extraction

Convolutional autoencoder

We developed and optimized a CAE for the reconstruction of DWI images (Figure 9.2) using the Keras libraries [19]. By learning how to reduce the dimensions of the feature space and reconstruct images from this low-dimensional
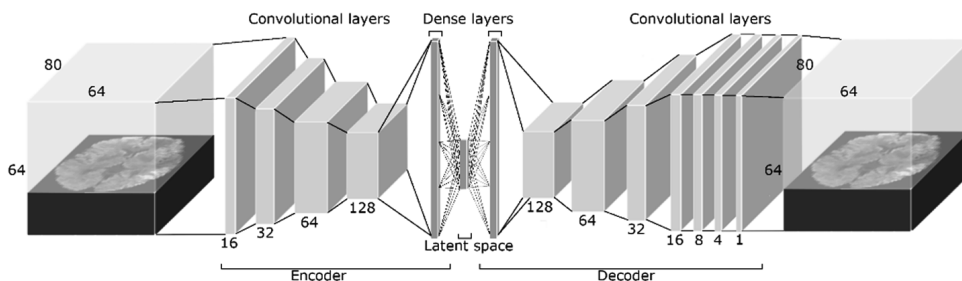
Figure 9.2: The convolutional autoencoder architecture. The dimension of the input image is 64x80x64. The encoder consists of four 4x4x4 convolutional layers with stride 2 and Rectified Linear Unit activation. For each subsequent convolutional layer, the number of filters is doubled, starting at 16. Each convolutional layer is followed by group normalization. After the final convolutional layer of the encoder the feature space is flattened, and a dense layer is added. The decoder contains the same components as the encoder in opposite direction, only the feature space is upsampled first by factor 2 and the stride of the convolutional layers is kept at 1. After the fourth convolutional layer, three additional convolutional layers reduce the fourth dimension of feature space to 1, resulting in the original image dimensions.

feature space (latent space), the CAE learns the most important features that describe the source image. A CAE consists of several layers that downsample an image (encoder) to a compressed feature space (latent space) followed by several upsampling layers (decoder) that inverse the downsampling by upsampling the image to original image dimensions. The encoder consisted of four 4x4x4 convolutional layers with stride 2 and Rectified Linear Unit activation. Since each convolutional layer divides the feature space dimensions in half it was favorable to use input dimensions of powers of 2. Therefore, we have first zero padded the input image to the dimensions of 64x80x64. For each subsequent convolutional layer, the number of filters was doubled, starting at 16. Each convolutional layer was followed by group normalization to reduce the chance of overfitting. After the final convolutional layer of the encoder, the feature space was flattened, and a dense layer was added to reduce the number of features in the latent space to 100. The decoder inversed the encoder by first upsampling the feature space by a factor 2 followed by a convolutional layer with stride 1 to keep feature space dimensions.

9

The number of filters of the first four convolutional layers of the decoder was equal to the encoder, but in opposite direction. Again, each convolutional layer was followed by group normalization. After the fourth convolutional layer, three additional convolutional layers were added to gradually reduce the fourth dimension of feature space to 1 resulting in the input image dimensions. After the last convolutional layer, the output image was cropped to establish the original image dimensions. The loss function of the CAE was the mean squared error (MSE) between the source image and the resulting image.

For the development and optimization of the CAE, the data from HERMES and ISLES challenge were combined and divided into a training (80%) and validation set (20%). To increase the number of training samples available, we performed data augmentation for the training set by flipping the images over the z-axis. The network was trained for 200 epochs with a batch size of 2. We used the validation set to optimize the CAE. After optimization, we extracted features from the MR CLEAN-NO IV DWI dataset.

Radiomics

Radiomics features extracted from medical images aim to identify and quantify pathological effects that might be invisible to the human eye [20]. Radiomics features are extracted from a region of interest (ROI), in our case the infarct lesion, and include first order statistics, shape, and textural features (Figure 9.3). Examples of first-order statistics are minimum, maximum, and mean intensity within the lesion. Shape features contain both 2D metrics such as the maximum diameter within a slice of the ROI, and 3D metrics, including the 3D volume of the ROI. Textural features are computed using filtering methods and matrices that capture the relationship between multiple voxels. An example of these matrices is the gray level size zone matrix (GLSZM), which represents the number of neighboring pixels with the same intensity. Metrics computed from this matrix represent coarseness and homogeneity within the lesion. In total 100 radiomics features were extracted using the PyRadiomic Toolkit [20].
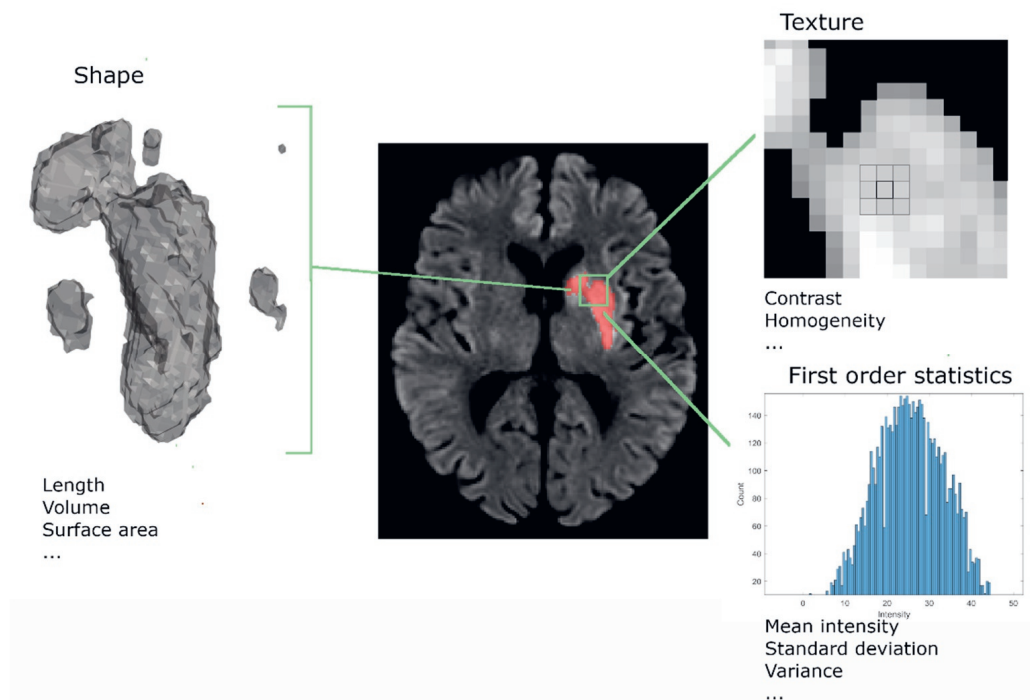
Figure 9.3: *Illustration of the three radiomics feature classes. Radiomics features consist of shape, texture and first order statistics features. Shape features describe the 2D and 3D size and shape of the lesion. Textural features describe the intensity distribution and relations between neighbouring voxels. First order statistics describe the intensity distributions of the lesion.*

Classification

A SVM classifier was optimized based on FIV, radiomics and CAE features, respectively. The SVM classifier separates different outcome groups by optimizing a hyperplane that describes the boundary with maximal distance between the features that belong to the different outcome groups. We assessed its performance for accurately predicting functional independence defined as mRS 0-2 at 90 days. For the implementation of the SVM, we used the scikit-learn toolkits [21]. The optimization and testing were performed similarly for both feature sets. From the MR CLEAN NO-IV DWI dataset, 80% of the DWI images were used for 5-fold cross-validation. The remaining 20% of the images were used to test the

9

performance of the final classifier. Before optimizing the SVMs, all features were normalized with the scikit-learn 'RobustScaler' function, which scales each feature based on its median and interquartile range. To optimize the SVM, we performed a grid search to find the most optimal kernel type and coefficient (gamma), and regularization parameter (C). The following options were used: linear kernel type, radial basis function, polynomial or sigmoid; gamma: 1e-2 to 1e3 per order of magnitude. The performance of the classifiers was evaluated based on the area under the receiver operating characteristic curve (AUC) computed for the test set. The AUCs were pairwise compared and tested for statistically significant differences with the highest AUC as reference using deLong's test [22]. Classification accuracy, precision and recall were also reported. For the radiomics-based classifier, we investigated feature importance based on the Shapley additive explanation (SHAP) values [23]. For the CAE, we visualized a representative predicted validation image and compared it to the original validation image.

Results

Study population

From the 307 patients with FU-DWI imaging in the HERMES dataset, we excluded 55 patients due to poor image quality. No images were excluded from the ISLES dataset (n=64), which resulted in a total dataset of 316 images. From these images, 253 were included in the training set and 63 DWI images in the validation set.

The MR CLEAN-NO IV dataset contained 220 patients with available FU-DWI scans. We excluded 11 patients due to poor image quality and 3 patients due to uncorrectable registration errors. This resulted in 206 patients in the study population from which 144 scans were included in the training set, 21 in the validation set and 41 in the test set. Baseline and follow-up characteristics for the MR CLEAN-NO IV subpopulation and the overall study population are provided in the supplemental material at the end of this chapter, Table A1.

Autoencoder image reconstruction

The training MSE of the CAE was 2.0 e^{-3} (arbitrary units) and the validation error was 5.1e^{-3}. Figure 9.4 shows the reconstruction of a validation image established by the CAE (middle) and the corresponding difference map (right). The difference map shows small intensity differences in most of the healthy brain regions. The largest differences in intensities were present at the transition between brain tissue and cerebral spinal fluid. Of note, some predicted voxels within the lesion and ventricles also differed in intensity from the original. The CAE was able to reconstruct the lesion at a similar location as the original image.
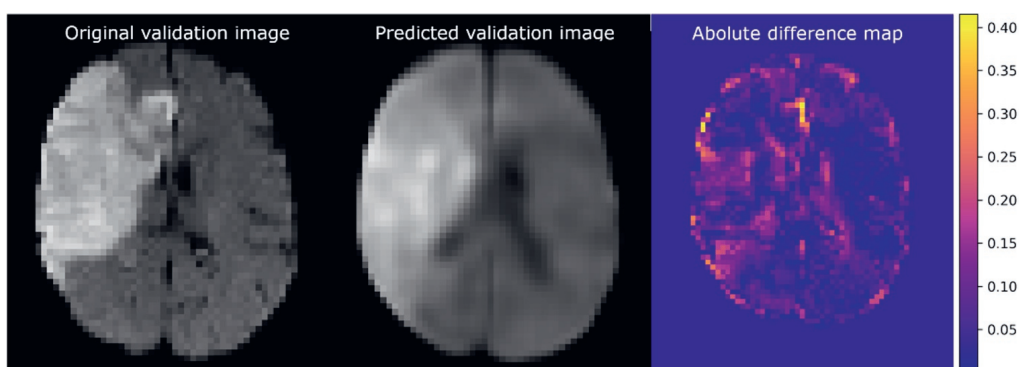
Figure 9.4: Example of imaging reconstruction using a trained convolutional autoencoder. (Left) An axial slice of the original validation image; (Middle) The corresponding slice of the predicted image; (Right) The absolute difference between the normalized original and predicted image.

Functional outcome prediction

Table 9.1 shows the results of the best performing classifiers that were trained on FIV, the CAE, and radiomics features. We found the highest test accuracy for the FIV-based SVM classifier (0.74). The precision was highest for the radiomics features-based SVM classifier (0.80) while the recall was highest for the SVM classifier based on FIV (0.73). Based on the AUC (Figure 9.5), the SVM classifier trained on radiomics features showed the best performance (0.88). Yet, this improved outcome prediction was not statistically significant compared to the

model based on FIV (p=0.15) or the model based on the CAE-trained SVM classifier (p=0.37).

Radiomics feature importance

Figure 9.6 lists the top 15 radiomics features with the largest impact on the outcome prediction by the SVM classifier based on SHAP values. The majority of these features consisted of textural features [24]. The two most important features were 'large area of high gray level emphasis' and 'large area of low gray level emphasis', which are based on the GLSZM matrix. These features represent the presence of large areas with high or low intensities within the lesion and steered the classifier towards unfavorable functional outcome classification. The lesion volume features with the most impact on the classification were mesh volume (volume based on the reconstructed 3D mesh based on the delineation) and voxel volume (lesion volume based on voxel volume). These features were in 9th and 10th place.

Table 9.1 Train and test accuracy, AUC, precision and recall for the best performing SVM classifier based on FIV, the autoencoder features and the radiomics features. The p-values resulting from deLong's tests against the radiomics features are presented in the last column.

| Feature extraction method	Train accuracy (n=144)	Test accuracy (n=41)	AUC (n=41)	Precision (n=41)	Recall (n=41)	deLong's test p-value
FIV only*	0.73	0.74	0.79	0.78	0.73	0.15
Autoencoder**	0.76	0.71	0.81	0.70	0.71	0.37
Radiomics***	0.75	0.71	0.88	0.80	0.65	

*SVM parameters: {C: 1000, gamma: 0.01, kernel: rbf}
** SVM parameters: {C: 0.1, gamma: 0.01, kernel: linear}
*** SVM parameters: {C: 1, gamma : 0.001, kernel: sigmoid}
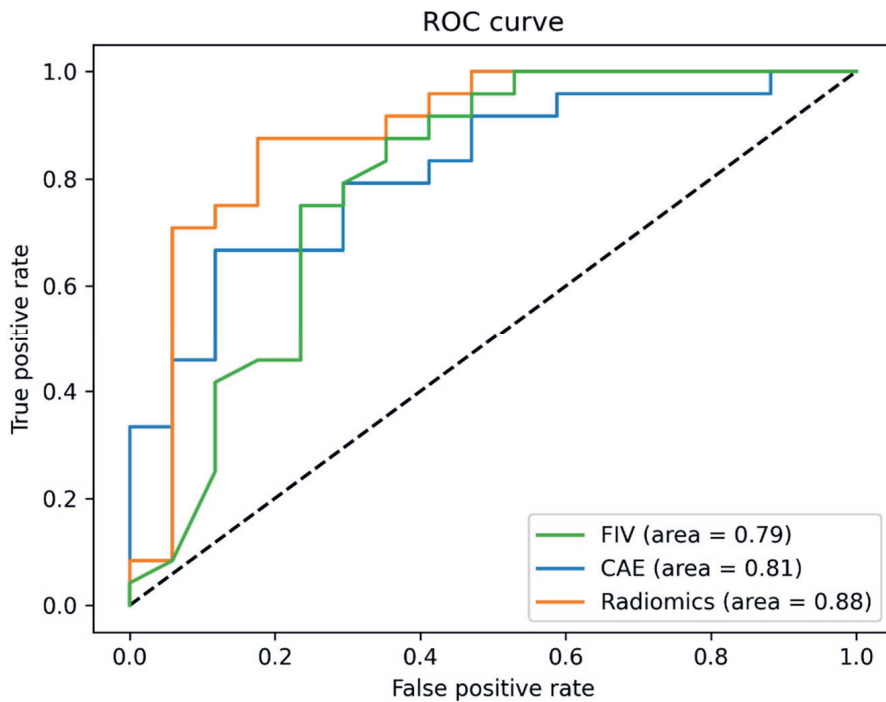
Figure 9.5: *Receiver operating curves for the best performing support vector machine model based on three different inputs: features extracted by the convolutional autoencoder, radiomics features and follow-up infarct volume.*
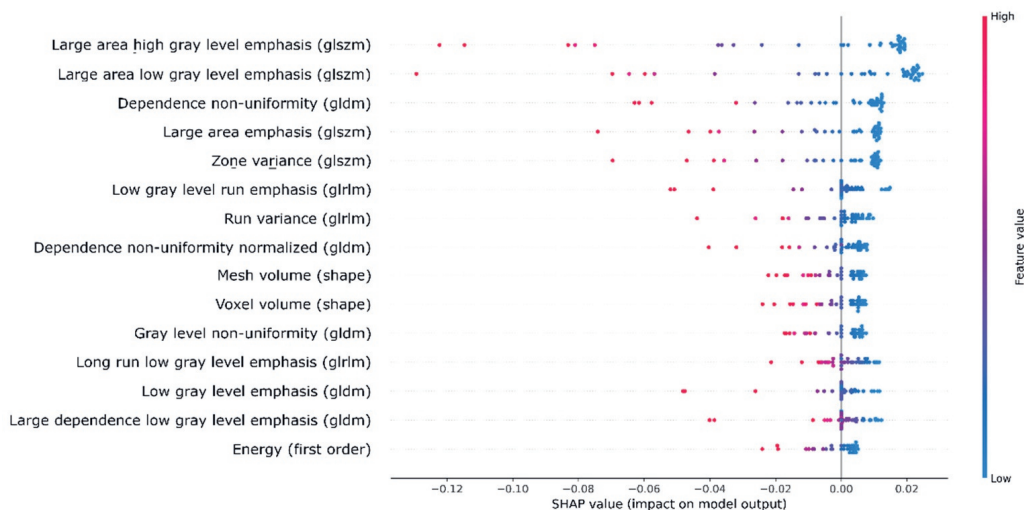
Figure 9.6: *SHAP summary plot showing the top 15 radiomics features and their feature classes with the largest impact on the classification based on the SHAP values. Negative and positive SHAP values represent unfavorable and favorable outcome classification, respectively. The feature values are represented by a color map, ranging from blue (low value) to red (high value). Abbreviations of second order radiomics feature classes in gray level matrices: size zone (glszm), dependence (gldm), run length (glrlm).*

Discussion

We compared the predictive performance of ML models based on three different feature sets: FIV, radiomics, and CAE features. We showed that favorable outcome prediction based on radiological imaging characteristics was improved when using automatically extracted imaging biomarkers from FU-DWI images. However, we were unable to show statistically significant differences in independent data. We found that the intensity heterogeneity in the FU-DWI lesion was most important for functional outcome prediction.

The model based on radiomics features most accurately predicted favorable functional outcome, and our SHAP-analysis showed that its most important features are related to textural information. Thus, the SVM classifier weighted the decision for predicted outcome mostly on texture and to a lesser extent on lesion volume. The most important textural features relate to intensity heterogeneity. This

corresponds with the current literature [7] and might reflect the heterogeneity in tissue vulnerability. Possibly, intensity heterogeneity in our study population relates to the presence of hemorrhage, which is negatively associated with functional outcome [25]. We performed an explorative analysis to study if hemorrhage was present within patients with heterogeneous lesions. Together with an expert neuroradiologist (C.B.L.M.) we visually inspected the DWI and T2* images of patients with high values for heterogeneity and negative SHAP values (which corresponds to the prediction of unfavorable outcome). Information about treatment outcome was not provided. Hemorrhage could not be observed in these patients. This study suggests that functional outcome prediction should not be based on FIV alone as an imaging biomarker and FU-DWI images capture additional prognostic information about the ischemic tissue in patients with an LVO.

The radiomics feature-based SVM outperformed the CAE feature-based SVM and was best at correctly classifying patients with favorable outcome: 20% of the patients for whom the favorable outcome was predicted did not achieve functional independence, while for CAE feature-based SVM this was 25%. However, the recall for the radiomics feature based classifier was only 65%, while for the CAE feature-based SVM 73% of patients with favorable outcome were selected. Considering these results, we think that the CAE feature based SVM is more appropriate for clinical decision making, since patients with the potential for favorable outcome should not be missed.

An advantage of the use of CAE features over radiomics features is that no lesion delineations are required for feature extraction. In this study, lesion delineation required manual annotations which is time consuming and introduces user dependency. Also, since the CAE features are based on the entire brain volume, information on surrounding tissue relative to the lesion is incorporated. A disadvantage of using the CAE is that features are less interpretable. Future studies could potentially perform activation visualization to study which information of the brain was most important for the classifier [26]. Also, ischemic lesion location could be a feature of interest for predicting functional outcome [27].

This study suffers from some limitations. First, selection bias might have occurred since for functional outcome prediction we only included patients who complied with the inclusion criteria of the MR CLEAN NO-IV. Consequently, our results cannot be generalized to ischemic stroke patients with more distal occlusions or posterior circulation occlusions or a stroke with minor symptoms. In addition, our results are not generalizable to patients who were not eligible for IVT and/or EVT, or who were presented outside the treatment window or with a baseline NIHSS <2. Also, in our healthcare system, follow-up MRI for AIS patients is mostly only acquired in a research setting. We therefore only included patients from centers who participated in the NO-IV trial in whom follow-up MRI was performed as a secondary outcome measure as required per trial protocol. Second, the mRS score was used since it is a common endpoint in AIS trials for the assessment of independence in daily activities. However, it is coarse and mainly focuses on motor function, with less attention to the assessment of cognitive function or emotional processing. Third, the performance of the CAE might be hampered due to the optimization process of the CAE itself. Improving the CAE, by for example adding more data to the training set, might improve the classification of functional independence by the SVM based on CAE features.

References

[1]   I.G.H. Jansen, M.J.H.L. Mulder, R.J.B. Goldhoorn *et al.* "Endovascular treatment for acute ischaemic stroke in routine clinical practice: Prospective, observational cohort study (MR CLEAN Registry)," *BMJ* 2018, vol. 360, pp. 360, doi: 10.1136/bmj.k949

[2]   B. Langhammer, K.S. Sunnerhagen, Å. Lundgren-Nilsson *et al.* "Factors enhancing activities of daily living after stroke in specialized rehabilitation: an observational multicenter study within the Sunnaas International Network," *Eur. J. Phys. Rehabil. Med.* 2017, vol. 53(5), pp. 725–734, doi: 10.23736/S1973-9087.17.04489-6

[3]   A.M.M. Boers, I.G.H. Jansen, L.F.M. Beenen *et al.*, "Association of follow-up infarct volume with functional outcome in acute ischemic stroke: a pooled

9

analysis of seven randomized trials," *J. Neurointerv. Surg.* 2018, vol. 10(12), pp. 1137-1142, doi: 10.1136/neurintsurg-2017-013724

[4]   M. Goyal, J.M. Ospel, B. Menon *et al.*, "Challenging the Ischemic Core Concept in Acute Ischemic Stroke Imaging," *Stroke* 2020, vol. 51, pp. 3147-3155, doi: 10.1161/STROKEAHA.120.030620

[5]   P. Konduri, K. van Kranendonk, A.M.M. Boers *et al.*, "The Role of Edema in Subacute Lesion Progression After Treatment of Acute Ischemic Stroke," *Front. Neurol.* 2021, vol. 12, pp. 1–11, doi: 10.3389/fneur.2021.705221

[6]   O. Wu, S. Christensen, N. Hjort *et al.*, "Characterizing physiological heterogeneity of infarction risk in acute human ischaemic stroke using MRI," *Brain* 2016, vol. 129(9), pp. 2384–2393, doi: 10.1093/brain/awl183

[7]   H. Wang, J. Lin, L. Zheng, *et al.*, "Texture analysis based on ADC maps and T2-FLAIR images for the assessment of the severity and prognosis of ischaemic stroke," *Clin. Imaging* 2020, vol. 67, pp. 152–159, doi: 10.1016/j.clinimag.2020.06.013

[8]   C. Frindel, A. Rouanet, M. Giacalone *et al.*, "Validity of Shape as a Predictive Biomarker of Final Infarct Volume in Acute Ischemic Stroke," *Stroke* 2015, vol. 46(4), pp. 976–981, doi: 10.1161/STROKEAHA.114.008046

[9]   W. Qiu, H. Kuang, J. Nair *et al.*, "Radiomics-based intracranial thrombus features on CT and CTA predict recanalization with intravenous alteplase in patients with acute ischemic stroke," *Am. J. Neuroradiol.* 2019, vol. 40(1), pp. 39–44, doi: 10.3174/ajnr.A5918

[10]   A. Hilbert, L.A. Ramos, H.J.A. van Os *et al.*, "Data-efficient deep learning of radiological image data for outcome prediction after endovascular treatment of patients with acute ischemic stroke," *Comput. Biol. Med.* 2019, vol. 115, pp. 103516, doi: 10.1016/j.compbiomed.2019.103516

[11]   M. Goyal, B.K. Menon, W.H. van Zwam *et al.*, "Endovascular thrombectomy after large-vessel ischaemic stroke: A meta-analysis of individual patient data from five randomised trials," *Lancet* 2016, vol. 387(10029), pp. 1723–1731, doi: 10.1016/S0140-6736(16)00163-X

[12]   O. Maier, B.H. Menze, J. von der Gablentz *et al.*, "ISLES 2015 - A public evaluation benchmark for ischemic stroke lesion segmentation from multispectral MRI," *Med. Image Anal.* 2017, vol. 35, pp. 250–269, doi: 10.1016/j.media.2016.07.009

[13]   N.E. LeCouffe, M. Kappelhof, K.M. Treurniet *et al.*, "A Randomized Trial of Intravenous Alteplase before Endovascular Treatment for Stroke.," *N. Engl. J. Med.* 2021, vol. 385(20), pp. 1833–1844, doi: 10.1056/NEJMoa2107727

[14]   E.J.O. Kompanje, J.T.J.M. van Dijck, V. Chalos *et al.*, "Informed consent procedures for emergency interventional research in patients with traumatic brain injury and ischaemic stroke," *Lancet Neurol.* 2020, vol. 19(12), pp. 1033–1042, doi: 10.1016/S1474-4422(20)30276-3

[15]   K.J. Friston, J.T. Ashburner, S.Kiebel *et al.* Eds., "Statistical Parametric Mapping: The Analysis of Functional Brain Images", 1st ed. Amsterdam: Elsevier/Academic Press: Amsterdam, 2007.

[16]   R.T. Shinohara, E.M. Sweeney, J. Goldsmith *et al.*, "Statistical normalization techniques for magnetic resonance imaging," *NeuroImage Clin*. 2014, vol. 6, pp. 9–19, doi: 10.1016/j.nicl.2014.08.008

[17]   K. Kamnitsas, C. Ledig, V.F.J. Newcombe *et al.*, "Efficient multi-scale 3D CNN with fully connected CRF for accurate brain lesion segmentation," *Med. Image Anal.* 2017, vol. 36, pp. 61–78, doi: 10.1016/j.media.2016.10.004

[18]   P. A. Yushkevich, J. Piven, H.C. Hazlett *et al.*, "User-guided 3D active contour segmentation of anatomical structures: Significantly improved efficiency and reliability," *Neuroimage* 2006, vol. 31(3), pp. 1116–1128, doi: 10.1016/j.neuroimage.2006.01.015

[19]   F. Chollet and others, "Keras." 2015. GitHub. https://github.com/fchollet/keras

[20]   J. J. M. Van Griethuysen, A. Fedorov, C. Parmar *et al.*, "Computational radiomics system to decode the radiographic phenotype," *Cancer Res.* 2017, vol. 77(21), pp. e104–e107, doi: 10.1158/0008-5472.CAN-17-0339

[21]   F. Pedregosa, G. Varoquaux, A. Gramfort *et al.*, "Scikit-learn: Machine Learning in {P}ython," *J. Mach. Learn. Res.* 2011, vol. 12, pp. 2825–2830.

9

[22]   E.R. Delon, N. Carolina and D.L. Clarke-Pearson, "Comparing the Areas under Two or More Correlated Receiver Operating Characteristic Curves : A Nonparametric Approach" *Biometrics* 2016, vol. 44(3), pp. 837–845, doi: 10.2307/2531595

[23]   S. M. Lundberg and S.-I. Lee, "A Unified Approach to Interpreting Model Predictions," in *NeurIPS Proceedings* 2017, vol. 32(2), pp. 4765–4774, doi: 10.48550/arXiv.1705.07874

[24]   A. Zwanenburg, M. Vallières, M.A. Abdalah *et al.* 2016, "Image biomarker standardisation initiative: Standardized Quantitative Radiomics for High-Throughput Image-based Phenotyping", *Radiology* 2016, vol. 295(2), doi: 10.1148/radiol.2020191145

[25]   K.R. Van Kranendonk, K.M. Treurniet, A.M.M. Boers *et al.*, "Hemorrhagic transformation is associated with poor functional outcome in patients with acute ischemic stroke due to a large vessel occlusion," *J. Neurointerv. Surg.* 2019, vol. 11(5), pp. 464–468, doi: 10.1136/neurintsurg-2018-014141

[26]   T. Rios, B. Van Stein, S. Menzel, *et al.* "Feature Visualization for 3D Point Cloud Autoencoders," *Proc. Int. Jt. Conf. Neural Networks*, 2020, pp. 1-9, doi: 10.1109/IJCNN48605.2020.9207326

[27]   Y. Xie, J. Oster, E. Micard *et al.*, "Impact of Pretreatment Ischemic Location on Functional Outcome after Thrombectomy," *MDPI* 2021, vol. 11(11), pp. 1–9, doi: 10.3390/diagnostics11112038

Supplementary materials

Figure A1: Baseline and follow-up characteristics of the selected study and total population of the MR CLEAN NO-IV trial

Characteristic	Study population MR CLEAN NO-IV (n = 206)	Total population MR CLEAN NO-IV (n = 539)
Male sex, n (%)	111 (54)	305 (57)
Age, mean (SD)	69 (13)	70 (13)
Pre-stroke mRS >0, n (%)	46 (22)	164 (30)
EVT allocation, n (%)	97 (47)	273 (41)
Left sided stroke, n (%)	115 (56)	290 (54)
Thrombus location, n (%)		
ICA	48 (23)	118 (22) (n=539)
M1	123 (60)	330 (61) (n=539)
M2	34 (17)	85 (16) (n=539)
Other	1 (0.5)	5 (0.9) (n=539)
Follow-up infarct volume (mL), median (IQR)	17 (7.3 to 67)	11 (6 to 74)
mRS≤2, n (%)	115 (56%)	270 (50%)

9

Chapter 10

General Discussion

10
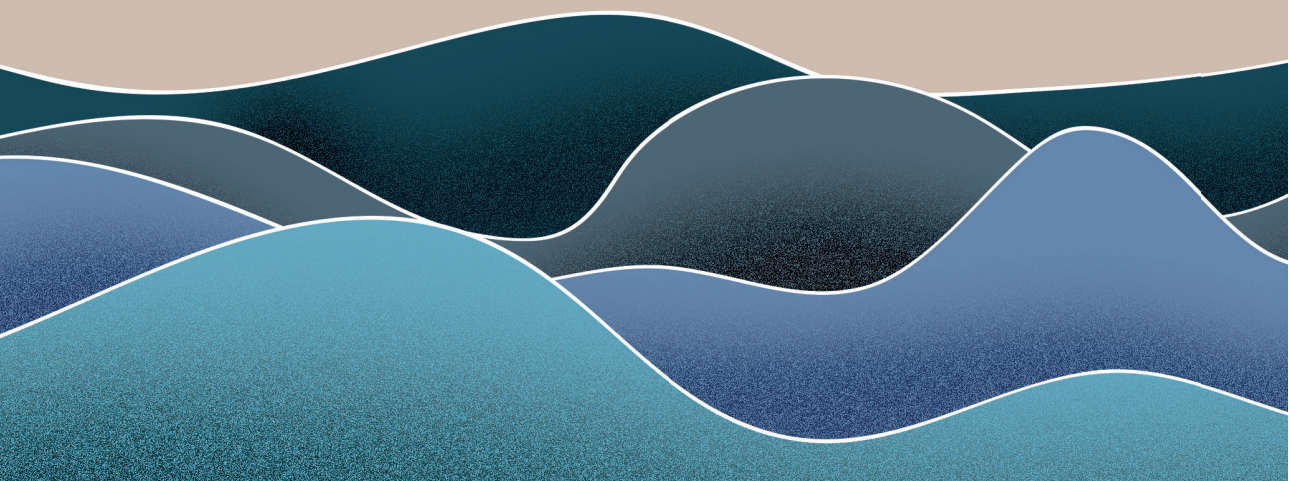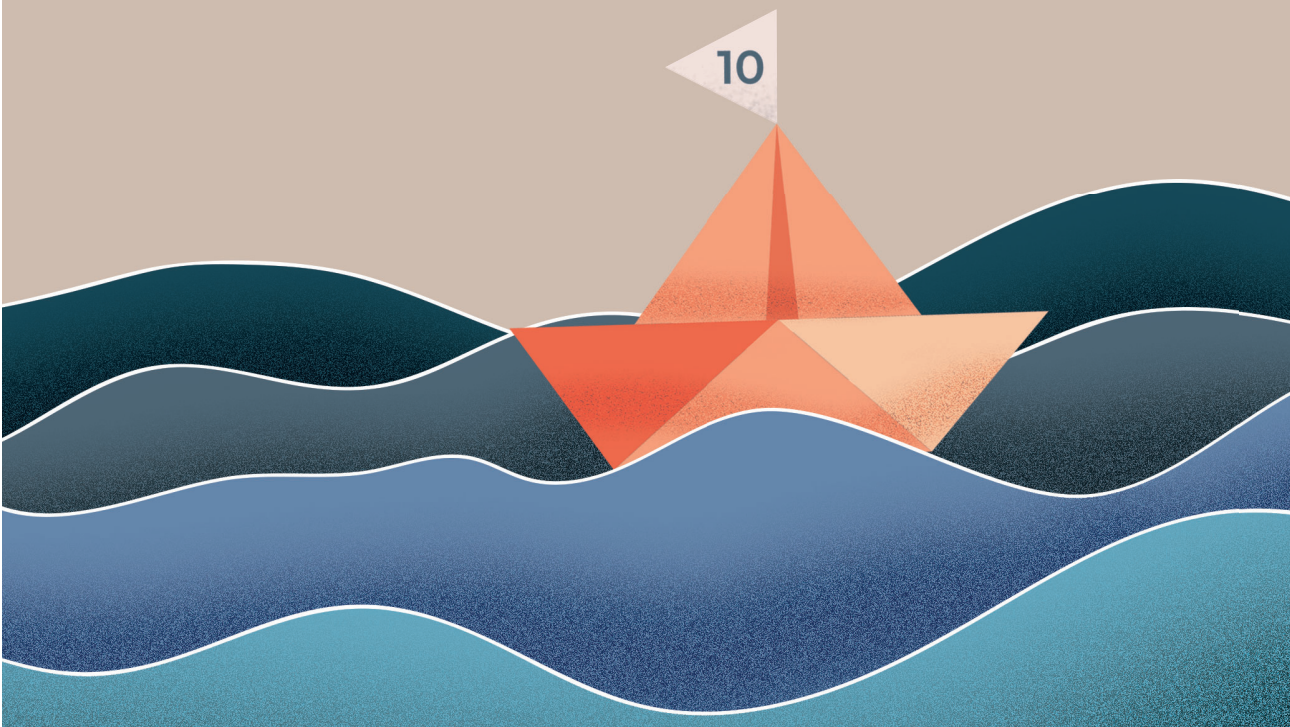
The main goal of this thesis was to extend our knowledge of thrombus and infarct core imaging characteristics and their relation to clinical outcome in patients with AIS. For this, we have studied the effect of image quality and timing on thrombus imaging characteristics. To this end, we have developed machine learning based methods for automated thrombus and infarct core segmentation and studied the association between thrombus and follow-up infarct core image characteristics and clinical outcome.

Thrombus imaging characteristics and treatment outcomes

In part I we have first shown in **chapter 2** that thick slice NCCT can lead to underestimation of thrombus density and overestimation of thrombus perviousness. Our work shows that results on the association between thrombus density and perviousness and functional outcome assessed on thin-slice images cannot be extrapolated to thick-slice NCCT measurements. Therefore, our study emphasizes the importance of understanding the negative consequences of data reduction. In most studies, thin-slice NCCT images are selected for thrombus imaging characteristics assessment [1]–[4], including the studies presented in this thesis. However, in daily clinical practice often only thick-slice NCCT images derived from thin slices are stored to minimize data storage. If thrombus perviousness and density measurements would be included as parameters for AIS treatment decision making based on currently available research, measurements should be performed on the thin slice images before they are disposed of. In the other case, if thick slice images would be used, further research should focus on the association between thrombus density and perviousness measurements assessed on thick slice images and treatment outcome.

Secondly, in **chapter 3** we have studied the association between onset to imaging time and thrombus imaging characteristics. Previous studies have suggested that the thrombus architecture is subjected to clot contraction, natural lysis, and stasis [5]–[11]. Our study was based on the hypothesis that the dynamic behavior of thrombi may influence treatment success. However, the results of our study did not show an association between onset to imaging time and thrombus

length, density, and perviousness. It is expected that future onset to baseline imaging times will only further decrease due to efforts by clinicians to optimize the clinical workflow for patients with AIS [12]. Our study suggests that onset to imaging time only plays a limited role in the interpretation of baseline thrombus imaging characteristics. Hereby, it should be noted that our study only included patients who were treated within an early time window and with a proximal occlusion. The effect of onset to imaging time on thrombus imaging characteristics for patients with prolonged treatment windows or with a more distal occlusion remains unclear.

Third, in **chapters 4 and 5** we have studied the relation between thrombus imaging characteristics and treatment outcomes. In **chapter 4**, we showed that for patients receiving EVT the chance of better functional outcome was higher if the thrombus was shorter, at a more distal location and if the thrombus burden was low. This association was also shown for favorable functional outcome. Thrombus perviousness was positively associated with better functional outcome, but only after adjusting for confounders. Moreover, the study showed that patients with an occlusion within the M1 had a higher chance of successful reperfusion. Additional analysis showed that shorter thrombi were associated with more distal locations, high CBS, high perviousness, and low attenuation. Previous results showed contradicting results for the association between thrombus imaging characteristics and treatment outcomes [13]–[16]. Our study is a step further towards better insight in the relation between thrombus imaging characteristics and treatment outcome of patients treated with EVT.

The study in **chapter 5** focused on the association between thrombus perviousness and treatment outcome. The results of the study showed that, for patients who received best medical care alone, higher thrombus perviousness was significantly associated with better functional outcome and a lower chance for mortality, and higher infarct volume. This positive effect of higher thrombus perviousness on better treatment outcome diminished with EVT treatment.

It has been suggested that the positive effect of thrombus perviousness on treatment outcome after IVT is caused by residual flow through the thrombus.

10

Thrombus perviousness is used as estimation for thrombus permeability. Thrombus permeability possibly facilitates residual blood flow through the thrombus, allowing for alteplase to penetrate more into the thrombus, resulting in more contact of alteplase with fibrin and therefore benefitting lysis.[17], [18] Even though we have shown that some thrombi are pervious, studies have never quantified thrombus permeability. In order to do this, we need to know the pressure drop over the length of the thrombus.

Finally, in **chapter 6** we have developed a CNN for automated thrombus detection and segmentation on baseline NCCT. The CNN showed similar sensitivity and specificity for the detection of thrombi compared to expert neuroradiologists. However, the perviousness and density measurements computed from the segmentations were less accurate than the measurements made by the expert neuroradiologists. Therefore, our suggested method provides a promising tool for thrombus detection but is less suitable for thrombus segmentation.

An automatic thrombus detection tool for NCCT could support less experienced radiologists in recognizing acute ischemic stroke and potentially speed up the clinical workup. In most countries, patients with suspicion of AIS are first brought to the nearest hospital. These are often primary stroke centers with less experience in diagnosing AIS. Since an NCCT scan is the first image acquired within the imaging protocol, the detection of a thrombus on NCCT could allow for faster referral to a comprehensive treatment center, compared to the situation where an additional CTA needs to be acquired first before definite diagnosis.

An automatic thrombus segmentation tool would also benefit the analysis of thrombus imaging characteristics. Currently, the majority of studies that study the relation between thrombus image characteristics and treatment outcomes for patients with AIS are based on manual assessment. The results of these studies include uncertainty introduced due to user dependency. Also, Santos et al. [19] showed that density measurements based on full thrombus segmentation result in a better representation of the thrombus density heterogeneity and allow for accurate volume and length measurements, compared to manual measurements.

Manual segmentation of the entire thrombus is very time-consuming and labor-intensive. Even if studies would show an association between thrombus imaging characteristics and treatment outcomes, based on manually acquired full thrombus segmentations, the manual segmentation of thrombi within daily clinical practice is infeasible since it would cause delays in the clinical workflow.

Infarct core imaging characteristics and treatment outcomes

Part II focused on the relation between infarct core imaging characteristics and treatment outcome. In **chapter 7** we have proposed a CNN for automatic segmentation of cerebral infarcts in follow-up NCCT images. We have shown that the segmentation of infarct lesions based on the union of the results from three different CNNs, each specialized in segmenting lesions of different densities, outperformed a single CNN that was trained to segment the entire lesion regardless of lesion age. The agreement between the results from the best performing CNN and the manual delineations was excellent. Similar to automatic thrombus segmentation, automatic lesion segmentation allows for the exclusion of user dependency and reduces workload in the delineation of the lesions. Therefore, it makes the assessment of lesion imaging characteristics in large image datasets and within clinical practice more feasible.

In **chapter 8** we have studied the added value of including the infarct location in the prediction of functional outcome based on follow-up infarct volume. The results showed no significant difference in the strength of association between infarct volume and functional outcome when the lesion location was taken into account. The results of the study also showed that low mRS-relevant regions were only affected in patients with relatively high lesion volumes. This suggests that with an occlusion of the anterior circulation, high mRS-relevant regions are initially affected and lesions progress into less mRS-relevant regions when the lesion volume increases. Our results were in contradiction with the results presented by Ernst et al. [20] They showed a strengthened association between follow-up infarct volume, measured on NCCT, and functional outcome when lesion location was taken into account.

10

Chapter 9 was based on the hypothesis that lesions shown on follow-up DWI images may contain additional prognostic information, other than lesion volume alone. The results of this study showed better performance by a machine learning model based on radiomics features or features learned by a convolutional autoencoder in predicting favorable functional outcome, compared to a machine learning model based on follow-up infarct volume alone. However, this difference was not statistically significant. Moreover, results showed that the radiomics-based model put more weight on intensity heterogeneity compared to volumetric-based features. The results of this study suggest that future studies should not only focus on follow-up lesion volume when studying the relation between the lesion and functional outcome, but should also include additional information such as heterogeneity within the lesion.

The studies in this thesis benefited from the availability of the HERMES collaboration, including the MR CLEAN trial, the MR CLEAN Registry, and MR CLEAN-NO IV. Earlier studies were performed in the early phase of AIS research, and therefore only included small study groups. The bundling of the HERMES trials allowed us to study a large heterogenic population. The MR CLEAN Registry had the additional advantage of only including patients who were treated within daily clinical care. Specifically, their treatment was not subject to strict clinical trial protocols, which could benefit treatment outcome, and results from the MR CLEAN Registry population provide a more realistic representation of the patient group. Moreover, the MR CLEAN-NO IV study protocol included final lesion volume on MRI at 24 hours as trial endpoint. Consequently, the lesion delineation on follow-up MR was available for a large number of patients within the MR CLEAN-NO IV population.

Despite the available large trial populations, our study populations were still selective. By design, all study populations only included patients over 18 years old, with an occlusion within the proximal anterior circulation, and who received treatment within an early time window. Moreover, patients with poor quality images

were excluded. Considering the small size of thrombi, especially in diameter, thick slice images would miss detailed information on thrombus density and length due to averaging effect. For that reason, our studies focusing on thrombus imaging characteristics only included patients who had thin-slice CT images available. As a side effect of this design of the studies, a majority of patients were excluded since most medical centers only store thick slice images. The studies including DWI images had a selective study population since MR imaging is not part of the standard imaging protocol in most centers. Also, MR imaging is not a suitable image modality for patients who are poorly conditioned and therefore not able to lay still for a long time or patients who are claustrophobic. Nonetheless, MRI images were the modality of choice since it has the highest sensitivity for infarct.

Within this thesis, we have proposed multiple machine learning approaches. Machine learning based approaches have shown to be promising in the assessment of medical imaging, including the detection and segmentation of lesions and classification of outcomes[21], [22]. The advantage of machine learning over conventional rule-based artificial intelligence approaches is that machine learning models can learn complex relations between features and labels from examples. However, it should be noted that most machine learning models are incapable of extrapolating to data domains different from the training data domain. Therefore, it is expected that the accuracy of the models presented within this thesis, for the segmentation of thrombi and infarct lesions and the classification of outcome, would be much lower for patients that do not fit within the inclusion criteria of our studies. As a solution, models can be trained again on new datasets or possibly, transfer learning can be applied since it allows the learning of the predicting functions of a new target domain, with the function learned from our current datasets as background knowledge.

In conclusion, within this thesis, we first emphasized the importance of being aware of the effect of image quality reduction on thrombus imaging characteristics measurements. Secondly, we showed that the time between stroke onset and

10

baseline imaging has a limited effect on thrombus length, density, and perviousness measurements within the early time window. Third, we have shown that a shorter thrombus, with a more distal location or a low thrombus burden, increased the chance for better functional outcome for patients treated with EVT. For patients treated with IVT, we showed a positive association between thrombus perviousness and functional outcome. Fourth, we proposed two ML-based segmentation methods, one for segmenting thrombi and the other segmenting infarct lesions. These methods are a step forward in facilitating user-independent image analysis within large trials and daily clinical practice. Fifth, we showed that taking the lesion location into account does not strengthen the association between lesion volume and functional outcome. And finally, we showed better performance in the prediction of favorable outcome by a machine learning model that was based on radiomics features, compared to a model that was based on lesion volume alone. Hereby, we also showed that, for the best performing model, lesion heterogeneity received more weight than lesion volume for the decision made by the model.

References

[1]   E. M. M. Santos *et al.*, "Permeable Thrombi Are Associated with Higher Intravenous Recombinant Tissue-Type Plasminogen Activator Treatment Success in Patients with Acute Ischemic Stroke," *Stroke*, vol. 47, no. 8, pp. 2058–2065, 2016.

[2]   L. Bouchez *et al.*, "Can clot density predict recanalization in acute ischemic stroke treated with intravenous tPA?," *Clin. Transl. Neurosci.*, vol. 1, no. 1, p. 2514183X1771831, 2017.

[3]   A. B. Bilgic, R. Gocmen, E. M. Arsava, and M. A. Topcuoglu, "The Effect of Clot Volume and Permeability on Response to Intravenous Tissue Plasminogen Activator in Acute Ischemic Stroke," *J. Stroke Cerebrovasc. Dis.*, vol. 29, no. 2, p. 104541, 2020.

[4]   P. Moftakhar *et al.*, "Density of Thrombus on Admission CT Predicts Revascularization Efficacy in Large Vessel Occlusion Acute Ischemic Stroke," vol. 44, pp. 243–246, 2013.

[5]   V. Tutwiler, A. D. Peshkova, I. A. Andrianova, D. R. Khasanova, J. W. Weisel, and R. I. Litvinov, "Contraction of blood clots is impaired in acute ischemic stroke," *Arterioscler. Thromb. Vasc. Biol.*, vol. 37, no. 2, pp. 271–279, 2017.

[6]   D. B. Cines *et al.*, "Clot contraction: Compression of erythrocytes into tightly packed polyhedra and redistribution of platelets and fibrin," *Blood*, vol. 123, no. 10, pp. 1596–1603, 2014.

[7]   E. M. Qazi *et al.*, "Thrombus Characteristics Are Related to Collaterals and Angioarchitecture in Acute Stroke.," *Can. J. Neurol. Sci.*, vol. 42, no. 6, pp. 381–8, 2015.

[8]   F. Docagne, J. Parcq, R. Lijnen, C. Ali, and D. Vivien, "Understanding the functions of endogenous and exogenous tissue-type plasminogen activator during stroke," *Stroke*, vol. 46, no. 1, pp. 314–320, 2015.

[9]   J. Zhu, Y. Wan, H. Xu, Y. Wu, B. Hu, and H. Jin, "The role of endogenous tissue-type plasminogen activator in neuronal survival after ischemic stroke: friend or foe?," *Cell. Mol. Life Sci.*, vol. 76, no. 8, pp. 1489–1506, 2019.

[10]   I. B. Kovacs and J. Yamamoto, "Spontaneous thrombolysis: A forgotten determinant of life or death," *Clin. Appl. Thromb.*, vol. 12, no. 3, pp. 358–363, 2006.

[11]   J. Minnerup and C. Kleinschnitz, "Visualization of clot composition in ischemic stroke: Do we get what we see?," *Stroke*, vol. 42, no. 5, pp. 1193–1194, 2011.

[12]   I. G. H. Jansen, M. J. H. L. Mulder, and R. J. B. Goldhoorn, "Endovascular treatment for acute ischaemic stroke in routine clinical practice: Prospective, observational cohort study (MR CLEAN Registry)," *BMJ*, vol. 360, 2018.

[13]   J. Borst *et al.*, "Value of thrombus CT CHARACTERISTICS in PATIENTS with ACUTE ISCHEMIC STROKE," *Am. J. Neuroradiol.*, vol. 38, no. 9, pp. 1758–1764, 2017.

[14]   F. Seker *et al.*, "Impact of thrombus length on recanalization and clinical outcome following mechanical thrombectomy in acute ischemic stroke," *J. Neurointerv. Surg.*, vol. 9, no. 10, pp. 937–939, 2017.

[15]   B. K. Menon *et al.*, "Association of clinical, imaging, and thrombus characteristics with recanalization of visible intracranial occlusion in patients with acute ischemic stroke," *JAMA - J. Am. Med. Assoc.*, vol. 320, no. 10, pp. 1017–1026, 2018.

[16]   A. M. Spiotta *et al.*, "Hounsfield unit value and clot length in the acutely occluded vessel and time required to achieve thrombectomy, complications and outcome," *J. Neurointerv. Surg.*, vol. 6, no. 6, pp. 423–427, 2014.

[17]   L. A. Labiche, M. Malkoff, and A. V. Alexandrov, "Residual Flow Signals Predict Complete Recanalization in Stroke Patients Treated with TPA," *J. Neuroimaging*, vol. 13, no. 1, pp. 28–33, 2006.

[18]   S. L. Diamond and S. Anand, "Inner clot diffusion and permeation during fibrinolysis," *Biophys. J.*, vol. 65, no. 6, pp. 2622–2643, 1993.

[19]   E. M. M. Santos, W. J. Niessen, A. J. Yoo, and O. A. Berkhemer, "Automated Entire Thrombus Density Measurements for Robust and Comprehensive Thrombus Characterization in Patients with Acute Ischemic Stroke," *PLoS One*, vol. 11, no. 1, pp. 1–16, 2016.

[20]   M. Ernst *et al.*, "Association of Computed Tomography Ischemic Lesion Location with Functional Outcome in Acute Large Vessel Occlusion Ischemic Stroke," *Stroke*, vol. 48, no. 9, pp. 2426–2433, 2017.

[21]   G. Litjens *et al.*, "A survey on deep learning in medical image analysis," *Med. Image Anal.*, vol. 42, no. October, pp. 60–88, 2017.

[22]   A. Kalantari, A. Kamsin, S. Shamshirband, A. Gani, H. Alinejad-Rokny, and A. T. Chronopoulos, "Computational intelligence approaches for classification of medical data: State-of-the-art, future challenges and research directions," *Neurocomputing*, vol. 276, pp. 2–22, 2018.

Appendices

Summary

Radiological imaging characteristics of thrombus and infarct core in acute ischemic stroke and their association with clinical outcome

Acute ischemic stroke (AIS) is caused by an occlusion of an intracranial artery by a thrombus. The occlusion leads to oxygen and nutrient deprivation and disruption of the drainage of waste products in the cerebral tissue distal from the occlusion. Since the brain's low capacity for storing nutrients and oxygen and its high metabolism, deprivation of blood supply quickly leads to tissue death. Therefore, the main focus of AIS treatment is to establish reperfusion as rapidly as possible. Reperfusion therapy includes the intravenous administration of alteplase (IVT) and endovascular thrombectomy (EVT).

Treatment outcomes have improved significantly since multiple randomized controlled trials proved the efficacy of EVT in addition to IVT. However, still only a minority of patients end up independent from care or with minor disability. Therefore, researchers focus on to further improve the understanding of the relation between AIS pathogenesis and treatment efficacy. In this thesis we study the association between radiological thrombus and ischemic core imaging characteristic and their relation to functional outcome.

In **chapter 2** we studied the effect of non-contract CT slice thickness on thrombus density and perviousness measurements. We included 50 patients with an M1 occlusion from the MR CLEAN trial. For each patient, baseline thin-slice non-contrast computed tomography (NCCT) and CT angiography (CTA) were aligned through rigid registration. From the thin-slice NCCT images, thicker slice images were reconstructed by supersampling 1 or multiple slices. The thrombus density and perviousness measurements were acquired for NCCT images with slice thickness ranging between 0.45 mm to 4.95 mm. Results showed that thrombus density values significantly decreased and perviousness measurements significantly increasing with increasing slice thickness. In conclusion, this study suggests previous associations made between thrombus density or perviousness

and favorable prognostics, based on thin slice NCCT images, cannot be extrapolated for thick slice NCCT measurements.

In **chapter 3** we studied if the onset to imaging time is of influence on thrombus length, density and perviousness measurements. We included 245 patients with an M1 occlusion who underwent EVT from the MR CLEAN Registry with available baseline thin-slice NCCT and CTA. After rigid registration, we manually obtained length, density and perviousness measurements. We studied the association between onset or last seen well to NCCT acquisition time per 5 minutes and the thrombus imaging characteristics. Results showed no significant associations, which suggests that that onset to imaging time only plays a limited in the interpretation of baseline thrombus imaging characteristics.

In the study in **chapter 4** we studied the association between thrombus imaging characteristics and treatment outcomes. We included 408 patients from the MR CLEAN Registry, which only included patients who received EVT. We performed manual thrombus characteristics measurements on baseline thin-slice NCCT and CTA images. We evaluated thrombus location, clot burden score (CBS), absolute and relative attenuation, perviousness, length and distance from the internal carotid artery to the thrombus. Results showed that a more distal occlusion, shorter thrombus length and a higher CBS was significantly associated with better functional outcome and a faster EVT procedure. Patients with a thrombus within the proximal and distal M1 had higher chance of reperfusion. Thrombus perviousness was significantly associated with better functional outcome.

In **chapter 5** we performed a similar study as in chapter 4. However, in this study we focused on the association between thrombus perviousness and treatment outcomes. We included 443 patients from the HERMES population with available thin-slice baseline NCCT and CTA. The HERMES population included both patients who were randomized to best medical management (BMM) only, including IVT, or BMM and EVT. Perviousness measurements were performed manually. Results showed that higher perviousness was significantly associated with better functional outcome in patients who only received best medical management. In this patient group, perviousness was also positively associated

with favorable functional outcome. These associations were not seen in the intervention group.

In **chapter 6** we proposed a machine learning (ML) based method for the automatic segmentation of thrombi on baseline NCCT. Our method combined two convolutional neural networks (CNN), one for asymmetry detection and the other for hyperdense artery sign detection. The network was trained and tested on 129 baseline thin-slice NCCT images of patients from the MR CLEAN trial. The results of the CNN were compared to annotation results from two expert neuroradiologists. For this we included additional 58 NCCT scans from patients with a proven occlusion and 45 NCCT scans from patients with stroke mimics. Ground truth was established by two expert observers, who also had the CTA image available. Results showed that the CNN had comparable performance in the correct detecting of the thrombus and quantification of the thrombus volume, compared to the experts. The CNN was less accurate in thrombus density measurements.

In **chapter 7** we developed a ML based method for the segmentation of infarct on follow-up NCCT images. In this study we compared the results of a model that included the combination of three CNNs, each focused on the segmentation of infarct of different density (mild, intermediate and high), with the results of a model that included a single CNN for the segmentation of the entire infarcted region. We included patients from the HERMES collaboration dataset. The CNNs were trained on 570 and tested on 396 NCCT follow-up images, acquired between 12 hours and 2 weeks follow-up. Ground truth included manual delineations from two expert observers. Results showed that the three-CNN approach outperformed the single-CNN approach.

In **Chapter 8** we studied if accounting for infarct location would strengthen the association between follow-up infarct volume (FIV) and functional outcome. For this, we defined low, moderate and high mRS-relevant brain regions. We included 252 patients with available follow-up diffusion weighted imaging from the HERMES collaboration dataset. The infarct lesions were semi-automatically delineated and allocated to the different mRS-relevant regions. We compared the results from a univariable logistic model, which included the total FIV, with a multivariable logistic

model that included the different mRS-relevant infarct volumes in the prediction of favorable functional outcome. The quality assessment of the models was based on the c-statistic and the Akaike information criterion. The results showed no significant strengthening in the association between FIV and functional outcome if lesion location was taken into account. The results additionally showed that lesions were only present within lower mRS-relevant regions in patients with higher total FIV, suggesting that lesions progress from high mRS-relevant regions to lower mRS-relevant regions.

In **chapter 9** we hypothesized follow-up infarct lesions shown on medical images contain prognostic information, additional to infarct volume. To study this, we compared the performance of three ML models in the prediction of favorable functional outcome: a model based on FIV alone, a model based on radiomics features and a model based on features extracted from the latent space of a convolutional autoencoder (CAE). We used the same HERMES dataset as chapter 8 and additional images from the SISS ISLES 2015 challenge to pre-train the CAE and a deep learning network for the segmentation of lesions on DWI images. For the favorable functional outcome prediction by the ML models we included follow-up DWI images of 206 patients from MR CLEAN NO-IV. The model based on the radiomics features showed best performance in predicting favorable outcome, followed by the CAE based model. However, the difference in performance was not statistically significant. For the radiomics based model we additionally performed a feature importance analysis, which showed that texture heterogeneity was most important in the prediction of functional outcome.

In conclusion, in this thesis we emphasized the importance of understanding the negative effect of lower image quality on radiological thrombus image characteristics measurements. We also showed that in the early time window (up to 6 hours), onset to baseline imaging time has limited influence on thrombus imaging characteristics. Furthermore, we showed that thrombus perviousness is associated with better functional outcome in patients who receive best medical management. Results on this association were not consistent for patients who received EVT. However, for patients receiving EVT we did show a positive

association with better functional outcome if the thrombus had a proximal location, was short or for high CBS. We also proposed a ML-based method for automatic thrombus segmentation to make the analysis of radiological thrombus imaging characteristics feasible within routine clinical practice. Similarly, we designed a ML based method for the segmentation of infarct on follow-up NCCT images. Moreover, we showed that accounting for infarct lesion location does not strengthen the association between follow-up infarct volume and functional outcome. And finally we suggested that infarct lesion on follow-up DWI contains prognostic information, additional to FIV, in particular information about texture heterogeneity.

Nederlandse samenvatting

Radiologische beeldkarakteristieken van trombus en infarct bij acute herseninfarcten en hun relatie tot klinische uitkomst

Een acuut herseninfarct wordt veroorzaakt door een occlusie van een intracraniële arterie door een trombus. De occlusie leidt tot een zuurstof en voedingstekort en verstoring van het afvoeren van afvalproducten in het cerebrale weefsel distaal van de occlusie. Door de lage opslagcapaciteit voor voedingsstoffen en zuurstof en het hoge metabolisme van de hersenen, leidt het gebrek aan bloedtoevoer al snel tot necrose. Daarom is het hoofddoel van de behandeling van een herseninfarct het zo snel mogelijk herstellen van de weefselperfusie. De reperfusietherapie bestaat uit de intraveneuze toediening van alteplase (IVT) en endovasculaire trombectomie (EVT).

De uitkomst van behandelingen is aanzienlijk verbeterd nadat meerdere gerandomiseerde klinische studies de veiligheid en effectiviteit van EVT als aanvulling op IVT hadden bewezen. Desondanks is er maar een klein deel van de patiënten die uiteindelijk medisch onafhankelijk zijn, zonder of alleen met lichte handicap. Daarom proberen onderzoekers hun kennis te verbreden over de relatie tussen de pathogenese van acute herseninfarcten en de doeltreffendheid van de behandeling. In dit proefschrift onderzoeken we de relatie tussen de radiologische beeldkarakteristieken van de trombus en het infarct en hun relatie tot klinische uitkomst.

In **hoofdstuk 2** onderzochten we het effect van de plakdikte van CT scans zonder contrast (NCCT) op de gemeten trombus densiteit en perviousness. We includeerden 50 patiënten vanuit de MR CLEAN studie met een occlusie in het M1 segment. Voor elke patiënt gebruikten we de baseline dunne plak NCCT en CT angiografie (CTA) en legden deze op elkaar door middel van rigide registratie. Dikke plakken werden van de dunne plakken gereconstrueerd door middel van de supersampling van 1 of meerdere plakken. De trombus densiteit en perviousness werden daarna gemeten op NCCT met plakdiktes tussen de 0.45 en 4.95 millimeter. De resultaten lieten zien dat de waarden van de gemeten trombus

densiteit significant lager en de gemeten perviousness significant hoger waren met toenemende plakdikte. De conclusie van deze studie is dat eerder aangetoonde relaties tussen trombus densiteit of perviousness en goede prognose, gebaseerd op dunne plak NCCT, niet geëxtrapoleerd kunnen worden naar metingen op basis van dikke plak NCCT.

In **hoofdstuk 3** hebben we onderzocht of de tijd tussen het begin van een acuut herseninfarct en de eerste beeldvorming invloed heeft op de lengte, densiteit en perviousness van de trombus. We includeerden 245 patiënten met een M1 occlusie die EVT zijn ondergaan vanuit de MR CLEAN Registry, waarvan de dunne plak NCCT en CTA van voor de behandeling beschikbaar waren. Na de rigide registratie, verkregen we de trombus lengte, densiteit en perviousness via manuele metingen. We onderzochten de relatie tussen de tijd van het begin van een infarct, of de tijd waarop een patiënt voor het laatste in goede gezondheid is gezien, tot de eerste NCCT (per 5 minuten) en de trombus beeld karakteristieken. De resultaten lieten geen significante relatie zien, wat suggereert dat de tijd tussen het begin van het infarct en de eerste beeldvorming maar in beperkte mate invloed heeft op de trombus beeld karakteristieken gemeten voor behandeling.

In **hoofdstuk 4** onderzochten we de relatie tussen trombus beeld karakteristieken en de uitkomst van behandeling. We includeerden 408 patiënten vanuit de MR CLEAN Registry, waarin alle patiënten behandeld zijn met EVT. De trombus karakteristieken werden manueel gemeten op baseline dunne plak NCCT en CTA. We evalueerden de locatie, clot burden score (CBS), de absolute en relatieve attenuatie, perviousness en lengte van de trombus en de afstand tussen de arteria carotis interna en trombus. De resultaten toonden dat een meer distale occlusie, korte trombus en een hogere clot burden score significant was gerelateerd met een betere uitkomst en een snellere EVT behandeling. Patiënten met een trombus in de proximale en distale M1 hadden een hogere kans op reperfusie. Trombus perviousness was significant gerelateerd met een betere functionele uitkomst.

In **hoofdstuk 5** voerden we een soortgelijke studie uit als in hoofdstuk 4. De focus van deze studie lag echter alleen op de relatie tussen trombus perviousness

en de uitkomst van behandeling. We includeerden 443 patiënten van de HERMES populatie waarvan de baseline dunne plak CT scan en CT angiografie beschikbaar was. De HERMES populatie bevat zowel patiënten die gerandomiseerd waren voor alleen zo goed mogelijke medische management, waaronder IVT, en patiënten die daarop aanvullend EVT behandeling kregen. De perviousness metingen werden manueel verricht. Resultaten lieten zien dat een hogere perviousness significant was gerelateerd aan een betere functionele uitkomst voor patiënten die alleen zo goed mogelijke medische management ontvingen. In deze patiënten groep was perviousness ook positief gerelateerd aan gunstige functionele uitkomst. Dezelfde relaties werden niet gezien in de interventiegroep.

In **hoofdstuk 6** stellen we een op machine learning (ML) gebaseerde methode voor, voor het automatisch segmenteren van trombi op baseline NCCT. Onze methode combineert twee convolutional neural networks (CNN's), de één voor asymmetrie-detectie en de ander voor hyperdense artery sign detectie. Het netwerk is getraind en getest op 129 baseline dunne plak NCCT beelden van patiënten in uit de MR CLEAN trial. De resultaten van de CNN werden vergeleken met annotaties van twee expert neuroradiologen. Hiervoor includeerden we aanvullend 58 NCCT scans van patiënten met een bewezen occlusie en 45 NCCT scan van patiënten met symptomen die lijken of een herseninfarct. De gouden standaard was verkregen door twee expert waarnemers, die ook de CTA scan tot hun beschikking hadden. De resultaten lieten zien dat de CNN vergelijkbaar met de experts in staat was om de trombus te detecteren en het volume van de trombus te bepalen. De CNN was minder precies in de trombus densiteit metingen.

In **hoofdstuk 7** ontwikkelden we een op ML gebaseerde methode voor het segmenteren van infarct op follow-up NCCT beelden. In deze studie vergeleken we de resultaten van een model dat bestond uit de combinatie van drie CNN's, ieder gefocust op de segmentatie van infarct met verschillende intensiteit (mild, gemiddeld, en hoog), met een model dat uit een enkel CNN bestond voor het segmenteren van de gehele infarct regio. We includeerden patiënten uit de database van de HERMES collaboratie. De CNN's werden getraind op 570 en getest op 396 follow-up NCCT beelden die verkregen waren tussen 12 uur en 2

weken follow-up. De gouden standaard bestond uit manuele segmentaties gemaakt door twee expert waarnemers. Het resultaat van het model gebaseerd op de 3 CNN's was beter dan het resultaat van het model gebaseerd op 1 CNN.

In **hoofdstuk 8** onderzochten we of de relatie tussen follow-up infarct volume (FIV) en functionele uitkomst wordt versterkt als de infarct locatie wordt meegewogen. Hiervoor definieerden we lage, gemiddeld en hoge mRS-relevante brein regio's. We includeerden 252 patiënten vanuit de database van de HERMES collaboratie waarvan de follow-up diffusie gewogen MRI beelden (DWI) beschikbaar waren. De infarct laesies werden semiautomatisch gesegmenteerd en verdeeld onder de verschillende mRS-relevante regio's. We vergeleken de resultaten van een univariabel logistisch model, gebaseerd op het totale FIV, met een multivariabel logistisch model dat gebaseerd was op de verschillende mRS-relevante gebieden voor het voorspellen van gunstige functionele uitkomst. De kwaliteit van de beoordelingen van het model werd bepaald met behulp van de c-statistiek en de Akaike informatiecriterium. De resultaten lieten geen significante versterking van de relatie tussen FIV en functionele uitkomst zien wanneer de locatie van de laesie werd meegenomen. Daarbij lieten de resultaten zien dat laesies zich alleen in de lagere mRS-relevante regio's bevonden bij patiënten met een hoger totaal FIV, wat suggereert dat laesies zich vanuit hogere mRS-relevante regio's uitbreiden naar lagere mRS-relevante regio's.

In **hoofdstuk 9** stelden we de hypothese dat follow-up infarct laesies weergegeven op medische beeldvorming prognostische informatie bevatten, aanvullend op infarct volume. Om dit te onderzoeken vergeleken we drie ML modellen voor de predictie van gunstige functionele uitkomst: een model gebaseerd op alleen FIV, een model gebaseerd op radiomics features en een model gebaseerd op features die vanuit de latent space van een convolutional autoencoder (CAE) verkregen zijn. We gebruikten dezelfde HERMES dataset als in hoofdstuk 8 met aanvullend beelden uit de SISS ISLES 2015 challange om de CAE van te voren te trainen en een deep learning network te trainen ter behoeve van het segmenteren van laesies op DWI beelden. Voor het voorspellen van gunstige door de ML modellen includeerden we follow-up DWI beelden van 206

patiënten vanuit de MR CLEAN NO-IV. Het model dat gebaseerd was op de radiomics features presteerde het best in het voorspellen van gunstige uitkomst, gevolgd door het model gebaseerd op de CAE features. Maar de resultaten lieten geen statistisch significant verschil zien. Voor het op radiomics gebaseerde model deden we een extra analyse waarbij we keken naar de weging van features in de predictie. Deze analyse liet zien voor het voorspellen van functionele uitkomst de hoogste weging werd gegeven aan features die betrekking hadden op textuur heterogeniteit.

Concluderend, in dit proefschrift benadrukten we dat het belangrijk is om de negatieve gevolgen van een verlaagde beeldkwaliteit op gemeten radiologische trombus beeldkarakteristieken te begrijpen. We lieten ook zien dat in de eerste uren (tot en met 6 uur), de tijd tussen het begin van een infarct tot aan de baseline beeldvorming maar van beperkte invloed is op gemeten trombus beeldkarakteristieken. Ook lieten we zien dat trombus perviousness gerelateerd is aan betere functionele uitkomst voor patiënten behandeld met zo goed mogelijke medische management. De resultaten voor deze relatie waren niet consistent voor patiënten die behandeld werden door middel van EVT. Maar binnen de interventiegroep werd wel een positieve relatie met betere functionele uitkomst gezien als de trombus een proximale locatie had, kort was of bij een hoge CBS. We stelden ook een op ML gebaseerde methode voor, voor het automatisch segmenteren van trombi om de analyse van trombus beeldkarakteristieken binnen de dagelijkse klinische praktijk mogelijk te maken. Vergelijkbaar ontwikkelden we een op ML gebaseerd model voor het segmenteren van infarct op follow-up NCCT beelden. Daarbij lieten we zien dat de relatie tussen FIV en functionele uitkomst niet werd versterkt wanneer de locatie van de laesie werd meegewogen. En tot slot suggereerden we dat infarct laesies op follow-up DWI beelden prognostische informatie bevatten als aanvulling op FIV, met name informatie over textuur heterogeniteit.

List of contributors and affiliations

MR CLEAN Registry Investigators

Executive committee*:* Diederik W.J. Dippel[1]; Aad van der Lugt[2]; Charles B.L.M. Majoie[3]; Yvo B.W.E.M. Roos[4]; Robert J. van Oostenbrugge[5]; Wim H. van Zwam[6]; Jelis Boiten[14]; Jan Albert Vos[8]

Study coordinators: Ivo G.H. Jansen[3]; Maxim J.H.L. Mulder[1,2]; Robert- Jan B. Goldhoorn[5,6]; Kars C.J. Compagne[2]; Manon Kappelhof[3]; Josje Brouwer[4]; Sanne J. den Hartog[1,2,40]; Wouter H. Hinsenveld [5,6]

Local principal investigators: Diederik W.J. Dippel[1]; Bob Roozenbeek[1]; Aad van der Lugt[2]; Adriaan C.G.M. van Es[2]; Charles B.L.M. Majoie[3]; Yvo B.W.E.M. Roos[4]; Bart J. Emmer[3]; Jonathan M. Coutinho[4]; Wouter J. Schonewille[7]; Jan Albert Vos[8]; Marieke J.H. Wermer[9]; Marianne A.A. van Walderveen[10]; Julie Staals[5]; Robert J. van Oostenbrugge[5]; Wim H. van Zwam[6]; Jeannette Hofmeijer[11];- Jasper M. Martens[12]; Geert J. Lycklama à Nijeholt[13]; Jelis Boiten[14]; Sebastiaan F. de Bruijn[15]; Lukas C. van Dijk[16]; H. Bart van der Worp[17]; Rob H. Lo[18]; Ewoud J. van Dijk[19]; Hieronymus D. Boogaarts[20]; J. de Vries[22]; Paul L.M. de Kort[21]; Julia van Tuijl[21]; Jo P. Peluso[26]; Puck Fransen[22]; Jan S.P. van den Berg[22]; Boudewijn A.A.M. van Hasselt[23]; Leo A.M. Aerden[24]; René J. Dallinga[25]; Maarten Uyttenboogaart[28]; Omid Eschgi[29]; Reinoud P.H. Bokkers[29]; Tobien H.C.M.L. Schreuder[30]; Roel J.J. Heijboer[31];Koos Keizer[32]; Lonneke S.F. Yo[33]; Heleen M. den Hertog[22]; Tomas Bulut[35]; Paul J.A.M. Brouwers[34]

Imaging assessment committee: Charles B.L.M. Majoie[3] (chair); Wim H. van Zwam[6]; Aad van der Lugt[2]; Geert J. Lycklama à Nijeholt[13]; Marianne A.A. van Walderveen[10]; Marieke E.S. Sprengers[3]; Sjoerd F.M. Jenniskens[27]; René van den Berg[3]; Albert J. Yoo[38]; Ludo F.M. Beenen[3]; Alida A. Postma[6]; Stefan D. Roosendaal[3]; Bas F.W. van der Kallen[13]; Ido R. van den Wijngaard[13]; Adriaan C.G.M. van Es[2]; Bart J. Emmer[3]; Jasper M. Martens[12]; Lonneke S.F. Yo[33]; Jan Albert Vos[8]; Joost Bot[36]; Pieter-Jan van Doormaal[2]; Anton Meijer[27]; Elyas Ghariq[13]; Reinoud P.H. Bokkers[29]; Marc P. van Proosdij[37]; G. Menno Krietemeijer[33]; Jo P. Peluso[26]; Hieronymus D. Boogaarts[20]; Rob Lo[18]; Dick Gerrits[35]; Wouter Dinkelaar[2] Auke P.A. Appelman[29]; Bas Hammer[16]; Sjoert Pegge[27]; Anouk van der Hoorn[29]; Saman Vinke[20].

Writing committee: Diederik W.J. Dippel[1] (chair); Aad van der Lugt[2]; Charles B.L.M. Majoie[3]; Yvo B.W.E.M. Roos[4]; Robert J. van Oostenbrugge[5]; Wim H. van Zwam[6]; Geert J. Lycklama à Nijeholt[13]; Jelis Boiten[14]; Jan Albert Vos[8]; Wouter J. Schonewille[7]; Jeannette Hofmeijer[11]; Jasper M. Martens[12]; H. Bart van der Worp[17]; Rob H. Lo[18]

Adverse event committee: Robert J. van Oostenbrugge[5] (chair); Jeannette Hofmeijer[11]; H. Zwenneke Flach[23]

Trial methodologist: Hester F. Lingsma[40]

Research nurses / local trial coordinators: Naziha el Ghannouti[1]; Martin Sterrenberg[1]; Wilma Pellikaan[7]; Rita Sprengers[4]; Marjan Elfrink[11]; Michelle Simons[11]; Marjolein Vossers[12]; Joke de Meris[14]; Tamara Vermeulen[14]; Annet Geerlings[19]; Gina van Vemde[22]; Tiny Simons[30]; Gert Messchendorp[28]; Nynke Nicolaij[28]; Hester Bongenaar[32]; Karin Bodde[24]; Sandra Kleijn[34]; Jasmijn Lodico[34]; Hanneke Droste[34]; Maureen Wollaert[5]; Sabrina Verheesen[5]; D. Jeurrissen[5]; Erna Bos[9]; Yvonne Drabbe[15]; Michelle Sandiman[15]; Nicoline Aaldering[11]; Berber Zweedijk[17]; Jocova Vervoort[21]; Eva Ponjee[22]; Sharon Romviel[19]; Karin Kanselaar[19]; Denn Barning[10].

PhD / Medical students: Esmee Venema[40]; Vicky Chalos[1,40]; Ralph R. Geuskens[3]; Tim van Straaten[19]; Saliha Ergezen[1]; Roger R.M. Harmsma[1]; Daan Muijres[1]; Anouk de Jong[1]; Olvert A. Berkhemer[1,3,6]; Anna M.M. Boers[3,39]; J. Huguet[3]; P.F.C. Groot[3]; Marieke A. Mens[3]; Katinka R. van Kranendonk[3]; Kilian M. Treurniet[3]; Manon L. Tolhuisen[3,39]; Heitor Alves[3]; Annick J. Weterings[3]; Eleonora L.F. Kirkels[3;] Eva J.H.F. Voogd[11]; Lieve M. Schupp[3]; Sabine L. Collette[28,29] ; Adrien E.D. Groot[4]; Natalie E. LeCouffe[4]; Praneeta R. Konduri[39]; Haryadi Prasetya[39]; Nerea Arrarte-Terreros[39]; Lucas A. Ramos[39].

Affiliations
Department of Neurology[1] , Radiology[2] , Public Health[40], Erasmus MC University Medical Center;
Department of Radiology and Nuclear Medicine[3] , Neurology[4] , Biomedical Engineering & Physics[39], Amsterdam UMC, University of Amsterdam, Amsterdam;
Department of Neurology[5] , Radiology[6] , Maastricht University Medical Center and Cardiovascular Research Institute Maastricht (CARIM)

Department of Neurology[7] , Radiology[8] , Sint Antonius Hospital, Nieuwegein;

Department of Neurology[9] , Radiology[10], Leiden University Medical Center;

Department of Neurology[11], Radiology[12], Rijnstate Hospital, Arnhem; Department of Radiology[13], Neurology[14], Haaglanden MC, the Hague;

Department of Neurology[15], Radiology[16], HAGA Hospital, the Hague;

Department of Neurology[17], Radiology[18], University Medical Center Utrecht;

Department of Neurology[19], Neurosurgery[20], Radiology[27], Radboud University Medical Center, Nijmegen;

Department of Neurology[21], Radiology[26], Elisabeth-TweeSteden ziekenhuis, Tilburg;

Department of Neurology[22], Radiology[23], Isala Klinieken, Zwolle;

Department of Neurology[24], Radiology[25], Reinier de Graaf Gasthuis, Delft;

Department of Neurology[28], Radiology[29], University Medical Center Groningen; Department of Neurology[30], Radiology[31], Atrium Medical Center, Heerlen;

Department of Neurology[32], Radiology[33], Catharina Hospital, Eindhoven;

Department of Neurology[34], Radiology[35], Medical Spectrum Twente, Enschede;

Department of Radiology[36], Amsterdam UMC, Vrije Universiteit van Amsterdam, Amsterdam;

Department of Radiology[37], Noordwest Ziekenhuisgroep, Alkmaar;

Department of Radiology[38], Texas Stroke Institute, Texas, United States of America

MR CLEAN-NO IV Investigators, Collaborators, and Affiliations

Principal investigators: Yvo Roos (MD, PhD),[1] Charles Majoie (MD, PhD)[1]

Study coordinators: Kilian Treurniet (MD),[1] Jonathan Coutinho (MD, PhD),[1] Bart Emmer (MD, PhD),[1] Natalie LeCouffe (MD),[1] Manon Kappelhof (MD),[1] Leon Rinkel (MD),[1] Agnetha Bruggeman (MD)[1]

Local principal investigators: Bob Roozenbeek (MD, PhD),[2] Adriaan van Es (MD, PhD),[26] Inger de Ridder (MD, PhD),[4] Wim van Zwam (MD, PhD),[4] Bart van der Worp (MD, PhD),[5] Rob Lo (MD, PhD),[5] Koos Keizer (MD, PhD),[6] Rob Gons (MD, PhD),[6] Lonneke Yo (MD, PhD),[6] Jelis Boiten (MD, PhD),[7] Ido van den Wijngaard (MD, PhD),[7] Geert Lycklama à Nijeholt (MD, PhD),[7] Jeannette Hofmeijer (MD, PhD),[8] Jasper Martens (MD),[8] Wouter Schonewille (MD, PhD),[9] Jan Albert Vos, (MD, PhD),[9] Anil Tuladhar (MD, PhD),[10] Floris Schreuder (MD, PhD),[10] Jeroen Boogaarts (MD, PhD)[10], Sjoerd Jenniskens (MD),[10] Karlijn de Laat (MD, PhD),[11] Lukas van Dijk (MD, PhD),[11] Heleen den Hertog (MD, PhD),[12] Boudewijn van Hasselt (MD),[12] Paul Brouwers (MD, PhD),[13] Emiel Sturm (MD),[13] Tomas Bulut (MD),[13] Michel Remmers (MD),[14] Anouk van Norden (MD),[14] Thijs de Jong (MD),[14] Anouk Rozeman (MD),[15] Otto Elgersma (MD, PhD),[15] Maarten Uyttenboogaart (MD, PhD),[16] Reinoud Bokkers (MD, PhD),[16] Julia van Tuijl (MD, PhD),[17] Issam Boukrab (MD),[17] Hans Kortman (MD),[17] Vincent Costalat (MD, PhD),[18] Caroline Arquizan (MD),[18] Robin Lemmens (MD, PhD),[19] Jelle Demeestere (MD),[19] Philippe Desfontaines (MD),[20] Denis Brisbois (MD),[20] Frédéric Clarençon (MD, PhD),[21] Yves Samson (MD)[21]

Local trial collaborators

Executive and writing committee: Yvo Roos (MD, PhD),[1] Charles Majoie (MD, PhD),[1] Adriaan van Es (MD, PhD),[26] Diederik Dippel (MD, PhD),[2] Aad van der Lugt (MD, PhD),[2] Wim van Zwam (MD, PhD),[4] Jelis Boiten (MD, PhD),[7] Geert Lycklama à Nijeholt (MD, PhD),[7] Lonneke Yo (MD, PhD),[6] Koos Keizer (MD, PhD),[6] Jonathan Coutinho (MD, PhD)[1], Bart Emmer (MD, PhD),[1] Kilian Treurniet (MD),[1] Natalie LeCouffe (MD),[1] Manon Kappelhof (MD),[1] Leon Rinkel (MD),[1] Agnetha Bruggeman (MD)[1]

Data Safety Monitoring Board: Martin Brown (MD) – *Chair*,[22] Phil White (MD, PhD)[23], John Gregson (MD, PhD)[24]

Independent trial statistician: Daan Nieboer (MSc)[2]

CONTRAST clinical trial collaborators

Research leaders: Diederik Dippel (MD, PhD),[2] Charles Majoie (MD, PhD)[1]

Consortium coordinator: Rick van Nuland (PhD)[3]

Imaging assessment committee: Charles Majoie (MD, PhD) – *Chair*,[1] Aad van der Lugt (MD, PhD) – *Chair*,[2] Wim van Zwam (MD, PhD),[4] Alida Postma (MD, PhD),[4] René van den Berg, (MD, PhD),[1] Ludo Beenen (MD),[1] Bart Emmer (MD, PhD),[1] Adriaan van Es, (MD, PhD),[26] Pieter Jan van Doormaal (MD),[2] Geert Lycklama (MD, PhD),[7] Ido van den Wijngaard (MD, PhD),[7] Albert Yoo (MD, PhD),[25] Lonneke Yo (MD, PhD),[6] Jasper Martens (MD, PhD),[8] Bas Hammer (MD, PhD)[11], Stefan Roosendaal (MD, PhD),[2] Anton Meijer (MD, PhD),[10] Menno Krietemeijer (MD)[6], Reinoud Bokkers (MD, PhD)[16], Anouk van der Hoorn (MD, PhD)[16], Dick Gerrits (MD)[13]

Adverse event committee: Robert van Oostenbrugge (MD, PhD) – *Chair*,[4] Bart Emmer (MD, PhD),[1] Jonathan Coutinho (MD, PhD),[1] Ben Jansen (MD, PhD)[17], Bart van der Worp (MD, PhD)[5]

Outcome assessment committee: Yvo Roos (MD, PhD) – *Chair*,[1] Sanne Manschot (MD, PhD),[7] Diederik Dippel (MD, PhD),[2]
Henk Kerkhof (MD, PhD),[15] Ido van den Wijngaard (MD, PhD),[7] Jonathan Coutinho (MD, PhD),[1] Peter Koudstaal (MD, PhD),[1] Koos Keizer (MD, PhD),[6] Jelis Boiten (MD, PhD)[7]

Data management group: Hester Lingsma (PhD),[2] Diederik Dippel (MD, PhD)[2], Vicky Chalos (MD),[2] Olvert Berkhemer (MD, PhD),[1,2]

Imaging data management: Aad van der Lugt (MD, PhD),[2] Charles Majoie (MD, PhD),[1] Adriaan Versteeg,[2] Lennard Wolff (MD),[2] Jiahang Su (MSc)[2], Manon Tolhuisen (MSc)[1], Henk van Voorst (MD)[1]

Biomaterials and translational group: Hugo ten Cate (MD, PhD),[4] Moniek de Maat (PhD)[2], Samantha Donse-Donkel (MD),[2] Heleen van Beusekom (PhD),[2] Aladdin Taha (MD)[2]

Local collaborators: Vicky Chalos (MD),[2] Kilian Treurniet (MD),[1] Sophie van den Berg (MD),[1] Natalie LeCouffe (MD),[1] Rob van de Graaf (MD),[2] Robert-Jan Goldhoorn (MD),[4] Aladdin Taha (MD),[2] Samantha Donse-Donkel (MD),[2] Wouter Hinsenveld (MD),[4] Anne Pirson (MD),[4] Lotte Sondag (MD),[10] Manon Kappelhof (MD),[1] Rik Reinink (MD),[5] Manon Tolhuisen (MD),[1] Josje Brouwer (MD),[1] Lennard Wolff (MD),[2] Matthijs van der Sluijs (MD),[2] Sabine Collette,[16] Wouter van der Steen (MD),[2] Miou Koopman (MD)[1]

Research nurses: Rita Sprengers,[1] Martin Sterrenberg,[2] Naziha El Ghannouti,[2] Sabrina Verheesen,[4] Wilma Pellikaan,[9] Kitty Blauwendraat,[9] Yvonne Drabbe,[11] Joke de Meris,[7] Michelle Simons,[8] Hester Bongenaar,[6] Anja van Loon,[14] Eva Ponjee,[12] Rieke Eilander,[12] Jasmijn Lodico[13], Hanneke Droste[13], Suze Kooij,[15] Marieke de Jong,[16] Esther Santegoets,[17] Suze Roodenburg[15], Ayla van Ahee,[1,5] Marinette Moynier,[18] Annemie Devroye,[19] Evelyn Marcelis,[19] Ingrid Iezzi,[20] Annie David,[20] Atika Talbi [21]

Study monitors: Leontien Heiligers[2], Yvonne Martens[2] Affiliations

[1]   Amsterdam UMC, University of Amsterdam, Amsterdam, the Netherlands;

[2]   Erasmus MC University Medical Center, Rotterdam, the Netherlands;

[3]   Lygature, Utrecht, the Netherlands;

[4]   Cardiovascular Research Institute Maastricht (CARIM), Maastricht University Medical Center,

Maastricht, The Netherlands;

[5]   University Medical Center Utrecht, Brain Center, Utrecht, the Netherlands;

[6]   Catharina Hospital, Eindhoven, the Netherlands;

[7]   Haaglanden Medical Center, the Hague, the Netherlands;

[8]   Rijnstate Hospital, Arnhem, the Netherlands;

[9]   St. Antonius Hospital, Nieuwegein, the Netherlands;

[10]   Radboud University Medical Center, Nijmegen, the Netherlands;

[11]   HagaZiekenhuis, the Hague, the Netherlands;

[12]   Isala Klinieken, Zwolle, the Netherlands;

[13]   Medisch Spectrum Twente, Enschede, the Netherlands;

[14]   Amphia Hospital, Breda, the Netherlands;

[15]   Albert Schweitzer Hospital, Dordrecht, the Netherlands;

16	University Medical Center Groningen, the Netherlands;
17	Elisabeth-TweeSteden Hospital, Tilburg, the Netherlands;
18	Centre Hospitalier Universitaire de Montpellier, Montpellier, France;
19	University Hospitals Leuven, Leuven, Belgium;
20	Centre Hospitalier Chrétien, Liège, Belgium;
21	Pitié-Salpêtrière hospital APHP-Sorbonne Université Paris France, Paris, France;
22	National Hospital for Neurology and Neurosurgery, London, United Kingdom;
23	Institute of Neuroscience and Newcastle University Institute for Ageing, Newcastle University, Newcastle, UK;
24	London School of Hygiene & Tropical Medicine, London, United Kingdom;
25	Texas Stroke Institute, Plano, Texas, United States of America
26	Leiden Universitair Medisch Centrum, Leiden, the Netherlands

List of publications

Within this thesis

M.L. Tolhuisen, M. Ernst, A.M.M. Boers, S. Brown, L.F.M. Beenen, F. Guillemin, Y.B.W.E.M. Roos, J.L. Saver, R. van Oostenbrugge, A.M. Demchuck, W. van Zwam, T.G. Jovin, O.A. Berkhemer, K.W. Muir, S. Bracard, B. C. V. Campbell, A.van der Lugt, P. White, M.D. Hill, D.W.J. Dippel, P.J. Mitchell, M. Goyal, M.W.A. Caan, H.A. Marquering and C.B.L.M. Majoie on behalf of the HERMES collaborators "Value of infarct location in the prediction of functional outcome in patients with an anterior large vessel occlusion: results from the HERMES study" *Neuroradiology.* 2022, vol. 64, pp. 521-530, doi: 10.1007/s00234-021-02784-x

M.L. Tolhuisen, M. Kappelhof, B.G. Dutra, I.G.H. Jansen, V. Guglielmi, D.W.J. Dippel, W.H. van Zwam, R.J. van Oostenbrugge, A. van der Lugt, Y.B.W.E.M. Roos, C.B.L.M. Majoie, M.W.A. Caan, H.A. Marquering, MR CLEAN Registry Investigators "Influence of Onset to Imaging Time on Radiological Thrombus Characteristics in Acute Ischemic Stroke" *Front Neurol.* 2021, vol. 18(12), pp. 693427, doi: 10.3389/fneur.2021.693427

M. Kappelhof, **M.L. Tolhuisen**, K.M. Treurniet, B.G. Dutra, H. Alves, G. Zhang, S. Brown, K.W. Muir, A. Dávalos, Y.B.W.E.M. Roos, J.L. Saver, A.M. Demchuk, T.G Jovin, S. Bracard, B.C.V. Campbell, A. van der Lugt, F. Guillemin, P. White, M.D. Hill, D.W.J. Dippel, P.J. Mitchell, M. Goyal, H.A. Marquering, C.B.L.M. Majoie, HERMES Collaborators. "Endovascular treatment effect diminishes with increasing thrombus perviousness: Pooled data from 7 trials on acute ischemic stroke" *Stroke.* 2021, vol. 52(11), pp. 3633-3641, doi: 10.1161/STROKEAHA.120.033124

R. Sales Barros, **M.L. Tolhuisen**, A.M.M. Boers, I. Jansen, E. Ponomareva, D.W J Dippel, A. van der Lugt, R.J van Oostenbrugge, W.H van Zwam, O.A Berkhemer, M. Goyal, A.M Demchuk, B.K Menon, P. Mitchell, M.D. Hill, T.G. Jovin, A. Davalos, B.C.V. Campbell, J.L. Saver, Y.B.W.E.M. Roos, K.W. Muir, P. White, S. Bracard, F.

Guillemin, S. Delgado Olabarriaga, C.B.L.M Majoie, H.A. Marquering "Automatic segmentation of cerebral infarcts in follow-up computed tomography images with convolutional neural networks" *J NeuroIntSurg*. 2020, vol. 12, pp. 848-852, doi: 10.1136/neurintsurg-2019-015471

M.L. Tolhuisen, E. Ponomareva, A.M.M. Boers, I.G.H. Jansen M.S. Koopman, R. Sales Barros, O.A. Berkhemer, W.H. van Zwam, A. van der Lugt,C.B. L. M. Majoie and H.A. Marquering "A Convolutional Neural Network for Anterior Intra-Arterial Thrombus Detection and Segmentation on Non-Contrast Computed Tomography of Patients with Acute Ischemic Stroke" *Appl. Sci.* 2020, vol. 10, pp. 4861, doi: 10.3390/app10144861

B.G. Dutra*, **M.L. Tolhuisen***, C.B.R.H. Alves, K.M. Treurniet, M. Kappelhof, A.J. Yoo, *et al.* "Thrombus imaging characteristics and outcomes in acute ischemic stroke patients undergoing endovascular treatment." *Stroke*. 2019, vol. 50, pp. 2057– 64. doi: 10.1161/STROKEAHA.118.024247

M.L. Tolhuisen, J. Enthoven, E.M.M. Santos, W.J. Niessen, L.F.M. Beenen, D.W.J. Dippel, A. van der Lugt, W.H. van Zwam, Y.B.W.E.M. Roos, R.J. van Oostenbrugge, C.B.L.M. Majoie and H.A. Marquering, "The effect of non-contrast CT slice thickness on thrombus density and perviousness assessment." *Lect Notes Comput Sci.* 2017, vol. 10555, pp. 105–115, doi: 10.1007/978-3-319-67564-0_17

Other publications

N. Arrarte Terreros, A.A.E. Bruggeman, H. van Voorst, P.R. Konduri, I.G.H. Jansen, M. Kappelhof, **M.L. Tolhuisen**, N. Boodt, D.W.J. Dippel, A. van der Lugt, W.H. van Zwam, R.J. van Oostenbrugge, H.B. van der Worp, B.J. Emmer, F.J.A. Meijer, Y.B.W.E.M. Roos, E. van Bavel, H.A. Marquering, C.B.L.M Majoie; MR CLEAN Registry investigators "Bifurcation occlusions and endovascular treatment outcome in acute ischemic stroke" *J NeuroIntSurg* 2022, vol. 0, pp. 1-9, doi: 10.1136/neurintsurg-2021-018560

A.A.E. Bruggeman, N. Aberson, M. Kappelhof, B.G. Dutra, J.W. Hoving, J. Brouwer, **M.L. Tolhuisen**, N.A. Terreros, P.R. Konduri, N. Boodt, Y.B.W.E.M. Roos, W.H. van Zwam, R. Bokkers, J. Martens, H.A. Marquering, B.J. Emmer, C.B.L.M. Majoie; MR CLEAN Registry investigators. "Association of thrombus density and endovascular treatment outcomes in patients with acute ischemic stroke due to M1 occlusions." *Neurorad.* 2022,. doi: 10.1007/s00234-022-02971-4

M. Mojtahedi,M. Kappelhof, E. Ponomareva, **M.L. Tolhuisen**, I. Jansen, A.E. Bruggeman, B.G. Dutra, L. Yo, N. LeCouffe, J. W. Hoving, H. van Voorst, J. Brouwer, N. Arrarte Terreros, P. Konduri, F.J. A. Meijer, A. Appelman, K. M. Treurniet, J.M. Coutinho, Y.B.W.E.M. Roos, W. van Zwam, D. Dippel, E. Gavves , B.J. Emmer, C.B.L.M. Majoie and H.A. Marquering "Fully Automated Thrombus Segmentation on CT Images of Patients with Acute Ischemic Stroke" *MDPI* 2022, vol. 12(3), pp. 698, doi: 10.3390/diagnostics12030698

N.E. LeCouffe, M. Kappelhof, K.M. Treurniet, L.A. Rinkel, A.E. Bruggeman, O.A. Berkhemer, L. Wolff, H. van Voorst, **M.L. Tolhuisen**, D.W.J. Dippel, A. van der Lugt, A.C.G.M. van Es, J. Boiten, G.J. Lycklama À Nijeholt, K. Keizer, R.A.R. Gons, L.S.F. Yo, R.J. van Oostenbrugge, W.H. van Zwam, B. Roozenbeek, H.B. van der Worp, R.T.H. Lo, I.R. van den Wijngaard, I.R. de Ridder, V. Costalat, C. Arquizan, R. Lemmens, J. Demeestere, J. Hofmeijer, J.M. Martens, W.J. Schonewille, J.A. Vos, M. Uyttenboogaart, R.P.H. Bokkers, J.H. van Tuijl, H. Kortman, F.H.B.M. Schreuder, H.D. Boogaarts, K.F. de Laat, L.C. van Dijk, H.M. den Hertog, B.A.A.M. van Hasselt, P.J.A.M. Brouwers, T. Bulut, M.J.M. Remmers, A. van Norden, F. Imani, A.D. Rozeman, O.E.H. Elgersma, P. Desfontaines, D. Brisbois, Y. Samson, F. Clarençon, G.M. Krietemeijer, A.A. Postma, P.J. van Doormaal, R. van den Berg, A. van der Hoorn, L.F.M. Beenen, D. Nieboer, H.F. Lingsma, B.J. Emmer, J.M. Coutinho, C.B.L.M. Majoie, Y.B.W.E.M. Roos; MR CLEAN–NO IV Investigators. "A Randomized Trial of Intravenous Alteplase before Endovascular Treatment for Stroke." *N Engl J Med.* 2021, vol. 385(20), pp.1833-1844. doi: 10.1056/NEJMoa2107727

A.A.E. Bruggeman, M. Kappelhof, N. Arrarte Terreros, **M.L. Tolhuisen**, P.R. Konduri, N. Boodt, H.M.M. van Beusekom, H.M. Hund, A. Taha, A. van der Lugt, Y.B.W.E.M. Roos, A.C.G.M. van Es, W.H. van Zwam, A.A. Postma, D.W.J. Dippel, H.F. Lingsma, H.A. Marquering, B.J. Emmer, C.B.L.M. Majoie; MR CLEAN Registry Investigators. "Endovascular treatment for calcified cerebral emboli in patients with acute ischemic stroke." *J Neurosurg.* 2021, vol. 2, pp. 1-11. doi: 10.3171/2020.9.JNS201798.

N. Arrarte Terreros, **M.L. Tolhuisen**, E. Bennink, H.W.A.M. de Jong, L.F.M. Beenen, C.B.L.M. Majoie, E. van Bavel, and H.A. Marquering, "From perviousness to permeability, modelling and measuring intra-thrombus flow in acute ischemic stroke" *J. Biomech.* 2020, vol. 111, pp.110001, doi: 10.1016/j.jbiomech.2020.110001

N. Boodt, K.C.J. Compagne, B.G. Dutra, N. Samuels, **M.L. Tolhuisen**, H.C.B.R. Alves, M. Kappelhof, G.J. Lycklama À Nijeholt, H.A. Marquering, C.B.L.M. Majoie, et al.; Coinvestigators MR CLEAN Registry. "Stroke etiology and thrombus computed tomography characteristics in patients with acute ischemic stroke: a MR CLEAN registry substudy." *Stroke.* 2020, vol. 51, pp. 1727–1735. doi: 10.1161/STROKEAHA.119.027749

A. Hilbert, L.A. Ramos, H.J.A. van Os, S.D. Olabarriaga, **M.L. Tolhuisen**, M.J.H. Wermer, R.S. Barros, I. van der Schaaf, D. Dippel, Y.B.W.E.M. Roos, W.H. van Zwam, A.J. Yoo, B.J. Emmer, G.J. Lycklama à Nijeholt, A.H. Zwinderman, G.J. Strijkers, C.B.L.M. Majoie and H.A. Marquering, "Data-efficient deep learning of radiological image data for outcome prediction after endovascular treatment of patients with acute ischemic stroke" *Comp. bio. Med.* 2019, vol. 115, pp. 103516, doi: 10.1016/j.compbiomed.2019.103516

Portfolio

Name PhD student: Manon Louise Tolhuisen

PhD period: November 2016 – November 2022

Names of PhD supervisor(s) & co-supervisor(s): C.B.L.M. Majoie

H.A. Marquering

M.W.A. Caan

1. PhD training

	Year	ECTS
General courses		
— Practical biostatistics	2017	1.1
— The AMC world of Science	2017	0.7
— Clinical Epidemiology: Randomized Clinical Trials	2018	0.6
— Scientific Writing in English for Publication	2018	1.5
— E-BROK	2018	1.0
— Writing a Data Management Plan	2019	1.0
Specific courses		
— Advanced Pattern Recognition	2017	1.5
— NFBIA – Summer School on Medical Image Analysis	2017	1.5
— MISS – Summer school – Medical Imaging meets Deep Learning	2018	1.0

	Year	ECTS
— 'Workshop mediation modelling in causal inference: a single-model approach' by Jeffrey D. Blume	2019	0.1

Seminars, workshops and master classes

	Year	ECTS
— Weekly Cardiovascular Engineering Meeting	2016–2020	4.0
— Bi-weekly Machine Learning meeting	2017–2020	1.0
— Monthly Stroke Research Meeting	2016–2020	2.0
— Masterclass Prof. Dr. Goyal, Amsterdamumc	2016	0.2
— Masterclass Prof. Dr. Goyal, Amsterdamumc	2018	0.2
— Contrast consortium meeting	2018	0.2
— Ischemic stroke meeting (monthly)	2016–2020	2.0

(Inter)national conferences

	Year	ECTS
— Institute Quantivision Conference	2018	0.25
— MICCAI	2018	0.75
— European Stroke Organization Conference	2018	0.75
— MISP – Medical Imaging Symposium for PhD students	2018	0.25
— European Stroke Organization Conference	2019	0.75
— World AI Summit	2018	0.5
— MISP – Medical Imaging Symposium for PhD students	2019	0.25
— MIDL – Medical Imaging with Deep Learning	2019	0.75

	Year	ECTS
— Institute QuantiVision Conference	2019	0.25

2. Teaching

Lecturing and Tutoring

	Year	ECTS
— MIK – Advanced Medical Imaging Processing	2016	1.5

Supervising

	Year	ECTS
— José van Enthoven (Master student Technical medicine)	2017	1.0
— Nora Hagopian (Bachelor student MIK)	2017	1.0
— Augustin Grisel (Bachelor student Télécom Physique Strasbourg engineering)	2016	1.0
— Nerea Arrarte Terreros (Master student Physics and Astronomy)	2018	1.0
— Douwe Bos (Bachelor student MIK)	2018	1.0
— Niels Daen and Maaike Straathof (Orientation internship for physics students)	2018	0.1
— Luuk Geelen (Master student Medical Natural Sciences)	2019	1.0

	Year	ECTS
— Milan Herczog & Vito Seinen		
— (Orientation internship for physics students)		
— Furkan Altay	2019	0.5
(Bachelor student Medical Natural Sciences)		

Acknowledgements

Tijdens mijn promotietraject heb ik het enorme voorrecht gehad om samen te werken met en in grote consortia die gedraaid werden door zeer intelligente en gedreven (medische) wetenschappers. Aan het begin van mijn promotie werd ik ontvangen in een omgeving waar het wereldwijde succes van de MR CLEAN trial en de andere HERMES trials nog fris in het geheugen zat. Iedereen was erg gedreven om als vervolg via substudies zoveel mogelijk extra informatie uit de beschikbare (beeld)data te verkrijgen. Daarbij werd het verzamelen van data voorgezet in de MR CLEAN Registry, met als doel om de conclusies uit de trials nog eens te bevestigen in de normale dagelijkse klinische setting. Ook werden de vervolgtrials al opgezet, gebundeld in het CONTRAST consortium. Ik heb dit allemaal van dichtbij mee mogen maken en samen met vele collega's een deel aan bij mogen dragen. De studies in mijn thesis zouden nooit tot stand zijn gekomen zonder de enorme inzet en doorzettingskracht van een heleboel collega's die de trials en Registry tot succes hebben gebracht. Ik wil daarom veel dank uitspreken naar alle mensen die betrokken zijn geweest in de MR CLEAN trial, HERMES collaboratie, MR CLEAN Registry en de CONTRAST trials.

Uiteraard wil ik ook graag mijn promotiecommissie bedanken, waarbij ik mijn (co)promotoren graag specifiek wil benoemen:

Als eerste natuurlijk mijn eerste promotor, **Charles Majoie**. Charles, ik ben heel erg blij dat jij mijn promotor was. Ik kon altijd bij je terecht en heb veel van je geleerd. Je had altijd een lijst klaar met nieuwe ideeën, verwees mij door naar de juiste mensen en riep me tijdig terug wanneer ik wat afdwaalde. Je hebt mij de mogelijkheid gegeven om heel veel gave ervaringen op te doen, waaronder een trip naar Cerenovus, wat eigenlijk niet bij mijn project hoorde. Je hebt mij ook ruimte gegeven om uit te zoeken waar mijn interesses lagen en mijn kennis uit te breiden door cursussen te volgen. Ik denk dat weinig andere PhD posities zoveel

privileges met zich mee brengen en ben erg dankbaar dat ik bij jou terecht ben gekomen als onderzoeker in opleiding.

Henk Marquering, aan het einde van mijn master kreeg ik twee PhD posities aangeboden, één in het Radboud en één in het AMC. Wat voor mij de doorslag gaf was ons prettige open gesprek en jouw enthousiasme voor de projecten binnen BMEP en de radiologie. Mijn sollicitatie bleek niet ons laatste open gesprek te zijn. Je deur stond regelmatig open, zodat ik gewoon even langs kon lopen om een vraag te stellen. Je was altijd bereid om in een onderwerp te duiken en samen te zoeken naar de juiste onderzoeksmethodes. Ook toen het niet zo lekker ging had je een luisterend oor en stond je altijd klaar om oplossingen te zoeken. Heel veel dank voor al je begeleiding.

En natuurlijk nog **Matthan Caan**. Aan het begin van mijn PhD kwamen wij elkaar vooral tegen toen ik op de MRI afdeling langs kwam voor een meeting met Paul Groot. Maar halverwege mijn traject kwam jij bij ons op de afdeling zitten en werd jij na overleg met Charles en Henk mijn co-promotor. Het was erg verfrissend om een derde lid in mijn promotiecommissie te hebben. Je bracht veel nieuwe ideeën en was altijd bereid om even met mij mee te kijken of me op toolboxen te wijzen die mijn voortgang zouden bespoedigen. Je nam zelfs de moeite om even te buurten in Amersfoort om Lauren te bewonderen toen ze net geboren was. Ook in de laatste periode, waar ik mijn promotie in vrije tijd af heb afgerond, stond je altijd klaar om taken (zoals de proofread van mijn laatste paper) op te vangen om mij zo wat te verlichten. Ik ben erg blij dat jij mijn co-promotor was.

I would also like to thank the other members of my PhD committee, **Prof. dr. van Bavel, dr. Emmer, Prof. dr. ir. de Jong, dr. Coutinho, Prof. dr. Niessen** and **Prof. dr. Išgum**, for reading my thesis and taking the time to participate in my PhD defense.

Next, this thesis would not have succeeded without my great colleagues. The bond between colleagues within the BMEP department is very strong and I see many of them as very good friends. I have so many good memories, not only during work hours, but also outside work hours. From scientific discussions,

escalating lunch breaks to holidays in Spain. I would love to thank all my colleagues within BMEP, with special thanks to: **Praneeta, Nerea, Marcela, Lucas, Henkie, Bruce, Haryadi, Ricardo, Bart, Wessel, and Marit**.

I would also like to thank **Nico.lab** for the great collaboration. It is great to see that some of our colleagues are able to build a business to a great success. Special thanks to Merel, Renan and Elena for the great collaboration.

From the international **HERMES collaborators**: Prof. Goyal, Mayank, thank you for your workshops and all our interesting conversations. Thank you for taking the time and help me make the HERMES studies within this thesis a success. Scott Brown, for performing the statistical tests focused on the HERMES population. Michael Hill, thank you for your supportive emails. And to all other collaborators, thank you for reading the endless stream of draft manuscripts, including some of the papers within this thesis, and taking the time to give useful feedback.

Graag dank ik ook de leden van workpackage 7 binnen het CONTRAST consortium: **Aad, Charles, Henk, Adriaan, Lennard, Matthijs,** en **Jiahang**. Het was een hele uitdaging om alle beelden te verzamelen, te sorteren en te annoteren. Een nog grotere uitdaging was om alle ziekenhuizen met XNAT te verbinden. Grote doelen behaal je met kleine stapjes en veel geduld. Ik denk dat we toch best trots mogen zijn op wat we hebben behaald!

Paul Groot, heel veel dank voor het mogelijk maken van het verzamelen van de medische beelden vanuit het AMC. Zonder jou waren we niet zo ver gekomen met onze databases, je hebt ons werk enorm verlicht.

Terwijl de voorbereidingen voor de CONTRAST trials werden getroffen, mocht ik tijdelijk aansluiten bij het ITEA3 project Medolution. Veel dank aan onze partners voor de fijne samenwerking, waaronder **Philips, Sopheon** en **Technolution**.

Graag noem ik ook even mijn nieuwe collega's van het Thales human behaviour analytics lab: **Johan, Thomas, Rafal, Tije** en **Daria**. Ik ben erg blij dat ik bij jullie terecht ben gekomen en vind het heel erg fijn om met jullie samen te werken. Ik heb in de afgelopen tijd weer heel veel nieuwe dingen geleerd en kijk uit

naar alle uitdagingen die we nog samen tegemoet gaan. Rafal, heel erg veel dank voor de hulp ten aanzien van de lay-out van mijn thesis.

Als laatste zijn er een paar mensen die ik graag persoonlijk wil bedanken:

Als eerste **Manon**, en dan bedoel ik natuurlijk niet mijzelf maar MK. Ik heb zo vaak moeten lachen om de verwarring die wij veroorzaakten. Allebei blond, ongeveer even lang, altijd vrolijk, sportief, houden van reizen en zeilen. Jij de klinische Manon (MK) en ik de technische Manon (MT), allebei deden we onderzoek naar ischemische beroertes en we stonden geregeld samen op papers. Vooral voor onze internationale collega's waren we af en toe moeilijk uit elkaar te houden. Ik vermoed eigenlijk nog steeds dat sommige HERMES collaborators naar aanleiding van mijn studies met mij mailden terwijl ze eigenlijk het idee hadden met jou te mailen. Dat zal mij zeker niet ten nadele zijn gekomen. Ik heb erg genoten van al onze samenwerkingen, waaronder het af en toe motiveren van collega's om toch nog even een zetje extra te zetten om dingen voor elkaar te krijgen. Heel veel dank voor alle leuke en interessante gesprekken, discussies, reisjes, congressen, diners, feestjes en zeilwedstrijden. Ik ben erg blij dat wij ons samen door onze phd hebben mogen ploeteren en hoop dat wij elkaar niet uit het oog zullen verliezen. Ik wens jou heel veel succes met het afronden van je opleiding.

Lieve **Lucas**, jij was de eerste collega die ik ontmoette. Wij mochten op mijn eerste dag, samen met Henk, direct naar Philips en het klikte meteen. We werden daarna kantoorgenootje, huisgenoten en vervolgens dikke vrienden. Ik ben zo blij dat ik jou heb leren kennen en ben heel trots op hoe je van een stille collega tot een vloeiend Nederlands sprekende avonturier bent gegroeid. Tijdens onze promotie ben je er altijd voor mij geweest, ook in tijden dat het niet lekker ging. We hebben heel veel dingen van elkaar geleerd en ben eeuwig dankbaar dat jij mijn collega mocht zijn. Het is fantastisch om te zien hoe je met Lauren omgaat en ik hoop echt dat we nog veel samen op pad zullen blijven gaan. Love you!

Lieve **Wim**, de afgelopen jaren, met name de afgelopen 2 jaar, waren niet gemakkelijk. Er is heel erg veel gebeurd, waaronder ook veel leuke dingen zoals

onze trouwerij, de geboorte van Lauren en de verhuizing naar Deventer. Ondertussen moest ik een thesis afronden terwijl ik al een nieuwe baan had aangenomen. Ik was fysiek altijd thuis, maar mentaal nooit aanwezig. Deze thesis was er niet geweest zonder jouw oneindige geduld. Ik hou zielsveel van jou en kijk erg uit naar de aankomende periode. We kunnen eindelijk gaan genieten van onze vrije tijd.

Lieve **Lauren**, vanaf dag 1 heb je mijn hart veroverd. Je bent een prachtige meid, dapper en nu al enorm pienter. Ik kan alleen maar trots op je zijn en ik kijk heel erg uit naar al jouw avonturen.

En als laatste wil ik natuurlijk mijn **ouders** bedanken. Zonder hen was ik nooit geweest waar ik nu was. Ma, heel erg bedankt voor het oppassen en onze gezellige uitjes. Pa, heel erg bedankt voor al het klus en zeilplezier. Ik hoop dat we nog veel zeiltripjes zullen maken.

About the author

Manon Tolhuisen was born in Almere on the 24th of April, 1991. She grew up in Ede, which is a town located in the largest nature reserve in the Netherlands ('de Veluwe'). Starting at 6 years old, she spent most of the weekends and holidays sailing. She also sailed competitions in her own little sailing boat "Little queen". After graduating from her secondary school, Pallas Athene College, in 2009, she started her technical Medicine course at the University of Twente. After finishing her Bachelor's degree, she moved to England to work as au pair for a lovely British family. In 2013, she started her Master's degree in Medical Imaging and Intervention at the University of Twente. In the second year of her master's, she was able to gain clinical and scientific experience as an intern in 4 different hospitals. One of the internships included the development of a method for automated and user-independent planning of skull reconstruction in infants with craniosynostosis. She continued on this topic in the 6th year of her degree as a graduation project and graduated in September 2016.

In the following years, she worked on her PhD thesis at the AMC and was part of the Biomedical and Engineering department (BMEP) and the department of Radiology and Nuclear Medicine. During her PhD she gained interest in artificial intelligence, specifically the use of machine learning for the analysis and semantic segmentation of medical images. To improve her knowledge on machine learning, she followed multiple courses, joined conferences and summer schools. She also initiated meetings within the BMEP department to discuss new innovations focused on machine learning.

Next to her own research, she has put effort in developing scripts for the automatic organization of the already existing large image databases, including the MR CLEAN Registry. She also took initiative to organize the collection of 4DCTA images within the AMC to create a database for new research topics. Furthermore, she was part of work package 7 within the CONTRAST consortium, which was responsible for the collection and analysis of the medical images within the CONTRAST trials.

Next to working on her PhD, she picked up sailing by buying a J24 sailing boat and sailed competitions on every Wednesday night. In 2019 she married Wim Hoek and in 2020 her daughter Lauren was born, just before the Corona crisis started.

Currently, Manon is working for Thales and is part of the human behavior analytics lab. Together with her collegues, she is focusing on developing a human state monitoring tool.